Volume 66C
Number 1
Jan.–Mar. 1962

# Engineering and Instrumentation

U.S. DEPARTMENT OF COMMERCE

SECTION C

JOURNAL OF RESEARCH

NATIONAL BUREAU OF STANDARDS

**Journal of Research**

**of the**

**National Bureau of Standards**

**C. Engineering and Instrumentation**

JAN.–MAR. • 1962

VOLUME • 66C

NUMBER • 1

Editor: W. A. Wildhack

Associate Editors: G. F. Montgomery, R. B. Jacobs

Publication dates:
Feb. 15, May 15, Aug. 15, Nov. 15, 1962

JOURNAL OF RESEARCH

The National Bureau of Standards Journal of Research reports research and development in the fields of activity shown at right. Also included from time to time are survey articles on topics closely related to the Bureau's scientific and technical program.

The Journal is published in four separate sections as follows:

**A. Physics and Chemistry**

Contains papers of interest primarily to scientists working in these fields. Issued six times a year. Annual subscription: domestic, $4.00; foreign, $4.75.

**B. Mathematics and Mathematical Physics**

Presents studies and compilations designed mainly for the mathematician and the theoretical physicist. Issued quarterly. Annual subscription: domestic, $2.25; foreign, $2.75.

**C. Engineering and Instrumentation**

Reports research and development results of interest chiefly to the engineer and the applied scientist. Issued quarterly. Annual subscription: domestic, $2.25; foreign, $2.75.

**D. Radio Propagation**

Reports work in radio propagation physics and upper atmospheric research. Issued six times a year. Annual subscription: domestic, $4.00; foreign, $4.75.

U.S. DEPARTMENT OF COMMERCE
Luther H. Hodges, Secretary

NATIONAL BUREAU OF STANDARDS
A. V. Astin, Director

**Functions and Activities**

The functions of the National Bureau of Standards are set forth in the Act of Congress, March 3, 1901, as amended. These include the development and maintenance of the national standards of measurement and the provision of means and methods for making measurements consistent with these standards; the determination of physical constants and properties of materials; the development of methods and instruments for testing materials, devices, and structures; advisory services to government agencies on scientific and technical problems; invention and development of devices to serve special needs of the Government; and the development of standard practices, codes, and specifications. The work includes basic and applied research, development, engineering, instrumentation, testing, evaluation, calibration services, and various consultation and information services. The Bureau also serves as the Federal technical research center in a number of specialized fields. The scope of activities of the National Bureau of Standards is suggested in the following listing of the divisions and sections engaged in technical work.

**Washington, D.C.**

**Electricity.** Resistance and Reactance. Electrochemistry. Electrical Instruments. Magnetic Measurements. Dielectrics. High Voltage.
**Metrology.** Photometry and Colorimetry. Refractometry. Photographic Research. Length. Engineering Metrology. Mass and Scale. Volumetry and Densimetry.
**Heat.** Temperature Physics. Heat Measurements. Cryogenic Physics. Equation of State. Statistical Physics.
**Radiation Physics.** X-Ray. Radioactivity. Radiation Theory. High Energy Radiation. Radiological Equipment. Nucleonic Instrumentation. Neutron Physics.
**Analytical and Inorganic Chemistry.** Pure Substances. Spectrochemistry. Solution Chemistry. Standard Reference Materials. Applied Analytical Research.
**Mechanics.** Sound. Pressure and Vacuum. Fluid Mechanics. Engineering Mechanics. Rheology. Combustion Controls.
**Organic and Fibrous Materials.** Rubber. Textiles. Paper. Leather. Testing and Specifications. Polymer Structure. Plastics. Dental Research.
**Metallurgy.** Thermal Metallurgy. Chemical Metallurgy. Mechanical Metallurgy. Corrosion. Metal Physics. Electrolysis and Metal Deposition.
**Mineral Products.** Engineering Ceramics. Glass. Refractories. Enameled Metals. Crystal Growth. Physical Properties. Constitution and Microstructure.
**Building Research.** Structural Engineering. Fire Research. Mechanical Systems. Organic Building Materials. Codes and Safety Standards. Heat Transfer. Inorganic Building Materials.
**Applied Mathematics.** Numerical Analysis. Computation. Statistical Engineering. Mathematical Physics. Operations Research.
**Data Processing Systems.** Components and Techniques. Digital Circuitry. Digital Systems. Analog Systems. Applications Engineering.
**Atomic Physics.** Spectroscopy. Infrared Spectroscopy. Solid State Physics. Electron Physics. Atomic Physics.
**Instrumentation.** Engineering Electronics. Electron Devices. Electronic Instrumentation. Mechanical Instruments. Basic Instrumentation.
**Physical Chemistry.** Thermochemistry. Surface Chemistry. Organic Chemistry. Molecular Spectroscopy. Molecular Kinetics. Mass Spectrometry.

**Office of Weights and Measures.**

**Boulder, Colo.**

**Cryogenic Engineering.** Cryogenic Equipment. Cryogenic Processes. Properties of Materials. Gas Liquefaction.
**Ionosphere Research and Propagation.** Low Frequency and Very Low Frequency Research. Ionosphere Research. Prediction Services. Sun-Earth Relationships. Field Engineering. Radio Warning Service.
**Radio Propagation Engineering.** Data Reduction Instrumentation. Radio Noise. Tropospheric Measurements. Tropospheric Analysis. Propagation-Terrain Effects. Radio-Meteorology. Lower Atmosphere Physics.
**Radio Standards.** High Frequency Electrical Standards. Radio Broadcast Service. Radio and Microwave Materials. Atomic Frequency and Time Interval Standards. Electronic Calibration Center. Millimeter-Wave Research. Microwave Circuit Standards.
**Radio Systems.** Applied Electromagnetic Theory. High Frequency and Very High Frequency Research. Modulation Research. Antenna Research. Navigation Systems. Space Telecommunications.
**Upper Atmosphere and Space Physics.** Upper Atmosphere and Plasma Physics. Ionosphere and Exosphere Scatter. Airglow and Aurora. Ionospheric Radio Astronomy.

Order all publications from the Superintendent of Documents
U.S. Government Printing Office, Washington 25, D.C.

Use of funds for printing this publication approved by the Director of the Bureau of the Budget (June 19, 1961).

JOURNAL OF RESEARCH of the National Bureau of Standards—C. Engineering and Instrumentation
Vol. 66C, No. 1, January–March 1962

# Reference Tables for 40 Percent Iridium-60 Percent Rhodium Versus Iridium Thermocouples*

G. F. Blackburn and F. R. Caldwell

(June 6, 1961)

In a program to establish reference tables for several alloys of iridium and rhodium against iridium, the work has been completed on 40 percent iridium-60 percent rhodium. Tables have been prepared giving emfs for temperatures in degrees Fahrenheit from 32 °F to 3,800 °F and in degrees Celsius (centigrade) from 0 °C to 2,100 °C, and temperatures in these units with emf in millivolts as the argument.

The emf is 11.6 millivolts at 3,800 °F. The thermoelectric power averages 3.1 microvolts per °F, and is within 0.1 microvolt of this value between 500 °F and 3,000 °F. It increases somewhat at temperatures above 3,000 °F.

Measurements at temperatures 32 °F to 2,500 °F were made in a platinum-wound furnace of conventional design, using a Pt-10 percent Rh versus Pt thermocouple to measure temperature. From 1,950 °F to 3,800 °F (thus overlapping the upper end of the lower range), the furnace used was an iridium block heated by electric induction. Blackbody conditions prevailed in the cavity in which the test thermocouple was inserted, and enabled measurement of the temperature with an optical pyrometer.

Good agreement between the data obtained in the overlapping parts of the platinum and optical pyrometer ranges (1,950 °F to 2,500 °F) established confidence in the temperature measurements with the optical pyrometer above 2,500 °F.

In both furnaces, helium surrounded the thermocouple junctions. The gas was dried by passing it through a trap immersed in liquid nitrogen.

Thoria and beryllia were used as thermal and electrical insulation in the high temperature range. While the electrical resistivity of these materials becomes relatively low at high temperatures, it did not become so low as to cause appreciable error in emf measurements. More serious was the introduction into the measuring circuit of a spurious emf, associated with the strong rf field and believed to be due to a rectifying property possessed by the insulators at high temperature. It was present in varying degrees, sometimes not at all. Its magnitude was determined by observing the (instantaneous) change in emf when the rf power was turned off, and the appropriate correction was made in the thermocouple emf measured with the power on.

The accuracy of the measurements is largely that associated with the measurement of temperature using an optical pyrometer. For the present work the maximum uncertainties in the range 2,500 °F to 3,800 °F are believed to range from about 8 °F to 12 °F.

## 1. Introduction

One of the earliest investigations of thermocouples of alloys of iridium and rhodium versus iridium was that made by Feussner [1].[1] His studies led him to suggest the alloy 40 percent iridium-60 percent rhodium for use with iridium. The increasing need in recent years for thermocouples capable of measuring temperatures higher than those at which platinum-rhodium versus platinum thermocouples can be used has led to further work on this combination [2], along with improvements in the metallurgy of these metals. In turn, the gradually increasing use of this and other iridium-rhodium alloys as thermoelements has given rise to the need for reference tables of the type available for platinum-rhodium versus platinum and other thermocouples [3].

The work reported here evolved from a project at the National Bureau of Standards originally sponsored by the United States Air Force, to examine thermocouples of alloys of iridium with 10 percent to 90 percent rhodium versus iridium. The tables (Appendix, I–A to IV–A) give the temperature-electromotive force values for 40 percent iridium-60 percent rhodium versus iridium, the first of the series to be completed.

## 2. Apparatus

Calibration up to 2,500 °F is accomplished in a high-temperature porcelain tube furnace having a bifilar platinum heating coil. The temperature is measured with a platinum-10 percent rhodium versus platinum thermocouple, calibrated prior to each run.

A blackbody is used to calibrate at higher temperatures. It is an iridium cylinder $1\frac{7}{16}$ in. in diameter and $4\frac{5}{16}$ in. long, with cavities as shown in figure 1.

*This paper was presented at the Fourth Symposium on Temperature, Its Measurement and Control in Science and Industry, Columbus, Ohio, March 27–31, 1961, sponsored by the American Institute of Physics, the Instrument Society of America, and the National Bureau of Standards. The proceedings will be published in book form by the Reinhold Publishing Corporation, New York, N.Y.

[1] Figures in brackets indicate the literature references at the end of this paper.

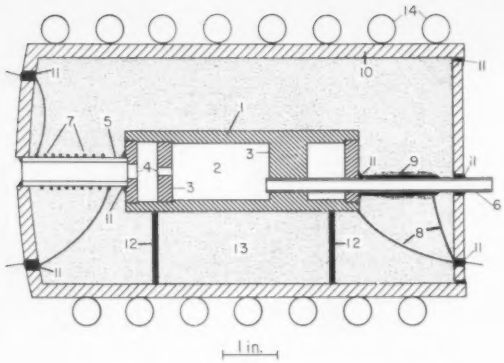


FIGURE 1. *Cross section of induction furnace.*

1, blackbody; 2, central cavity; 3, partitions; 4, sighting holes; 5, sighting tube; 6, thermocouple entrance tube; 7, heater winding; 8, ground wires; 9, iridium shield; 10, porcelain can; 11, thoria cement; 12, thoria supports; 13, thoria powder; 14, copper tubing.

Alined holes are provided in one end and the adjacent partition for inserting the thermocouple into the central cavity, and in the other end for sighting with the optical pyrometer which is used to measure the temperature. The area sighted upon is on the cavity wall opposite the ⅛-in. diameter hole in the partition at this end.

It is assumed that, owing to the design and method of heating the blackbody, the only departure from uniform temperature over the wall of the central cavity is that due to loss of heat by radiation through holes. This loss as calculated by a formula due to Gouffé [4] is about 0.2 percent, which is so small that it is unnecessary to correct observed temperatures on this account.

The blackbody is heated by electric induction with a 20 kw radiofrequency generator. A coil of iridium wire surrounds the sight tube and is connected externally to an rf ammeter and rheostat. The heat produced by rf current in the coil reduces the loss of heat from that end of the blackbody. A similar arrangement could be used at the thermocouple end; however, in an effort to provide shielding for the thermocouple wires and supporting tube, iridium wire was wound in a tight coil that formed a shield over the protection tube. Being heated by induction, this shield also serves to reduce the loss of heat by conduction along the thermocouple wires and supporting tube.

Preliminary experiments showed that it is necessary to ground the blackbody; this is done through an iridium wire welded to it. The shield just described is also grounded, but the thermocouple is not.

Thoria powder insulates the blackbody, which is supported centrally in a porcelain can 4 in. in diameter and 8 in. long by semicircular thoria disks. A coil of ⅜-in. copper tubing surrounding the porcelain can conducts the rf current and carries cooling water.

This assembly is placed with its axis horizontal on Pyrex glass supports in a box made of Transite and Plexiglas and having close fitting but not air tight joints. In use, helium flows into the box continuously at a rate judged sufficient to keep air out. The helium is cooled to the temperature of liquid nitrogen before it enters the furnace enclosure in order to remove water vapor and any other condensable impurities which may be present.

The emf is measured with Leeds and Northrop potentiometers, Models K2 and K3. An L. and N. No. 8622 optical pyrometer is used to measure temperature. Instead of using the temperature scale of the instrument, the temperature is obtained from calibration tables giving the temperature as a function of the current through the pyrometer lamp. A 2-ohm rheostat connected in series with the slide wire of the pyrometer increases the precision with which the lamp current can be adjusted to match the filament brightness with that of the blackbody. The lamp current is determined by measuring the voltage across a 1-ohm precision resistor in series with the lamp.

## 3. Thermocouples

The thermocouple wire was made by Sigmund Cohn Corporation. The first lot (A), obtained in 1955, was 0.035 in. in diameter. The second (B), obtained in 1959, consisted of 0.020- and 0.035-in. diam. wire. A third lot (D) of alloy wire only, acquired in 1960, consisted of wire sizes 0.020 in. and 0.030 in.

The data used in compiling the tables were obtained from a total of eight thermocouples—two from lot A, two from each wire size in lot B, and one from each size wire in lot D. The alloy wire of lot D was joined to iridium wire of lot B. The 0.030-in. alloy joined to 0.035-in. iridium wire formed one thermocouple, and the two 0.020-in. wires the other.

Each thermocouple was identified by a number indicating the lot of wire from which it was made, the percentage of rhodium in the alloy leg ("6," signifying 60 percent rhodium, is the only composition considered in this report), the wire diameter, and its order in a series of similar thermocouples. Thus A635a was thermocouple (a) from wire of lot A, 60 percent rhodium, 0.035 in. in diameter. Thermocouple (b) from the same coils of wire was A635b. The other six thermocouples were B620a, B620b, B635a, B635b, D620B, and D630B. In the last two, "B" signifies that the iridium leg was made from wire of lot B. In the remainder of this report, a particular thermocouple will be referred to by its number.

## 4. Experimental Procedure

In preparing a thermocouple the wires were annealed by heating them electrically in air. The manufacturer recommended annealing for about 1 min. at approximately 200 °C (360 °F) below the melting point. The temperature to be reached as observed with an optical pyrometer was estimated, taking the emissivity as 0.3, to be 3,460 °F for the iridium and 3,180 °F for the alloy wire [5]. In approaching these temperatures it was necessary to increase the current gradually, so that it was not unusual for several minutes to elapse while the temperature was

being raised and pyrometric observations made. Measurement errors were comparatively large under these conditions, due in part to "smoke" that frequently appeared around the wires when they were heated to high temperature in air. For this and other reasons the actual temperature probably differed from those desired by as much as 100 °F.

The junction was welded in an oxyacetylene flame.

Each thermocouple wire joined a copper wire in a bath of melting ice. The copper wires led to a potentiometer through a selector switch.

In working with the induction furnace an undesirably large rf voltage was induced on the thermocouple wires. Most of this was prevented from reaching the potentiometer by inserting a 1-mh choke in each lead between the reference junction and the potentiometer, and a 1-μf capacitor from the low potential end of each choke to ground.

Except for a few readings at intervals of 25 °F on lot A thermocouples at temperatures under 300 °F, the measurements were made at intervals of 50 °F.

The thermocouples were run first in the 2,500 °F furnace. They were supported in high-temperature porcelain tubes and immersed about 8 in. For these runs the test and the reference thermocouples were welded to form a common junction. This made it possible to compare one thermoelement with another, and the readings regularly included measurements of the emf between the iridium and platinum, and between the iridium-rhodium and platinum elements. Each reading consisted of two measurements of each desired emf, made in such sequence that the mean values were very nearly free from error due to the slight change in temperature which unavoidably occurred while the measurements were being made.

Thermocouples A635a and A635b were each run twice, both times at ascending temperatures. The others were each run once, readings being obtained first at ascending, then descending temperatures. The means of the two readings were taken as the experimentally determined temperature-emf relationship for the thermocouple. This applies also to measurements made in the induction furnace.

For calibrating in the induction furnace a thermocouple was supported in an insulating tube of thoria or beryllia. Experiments on the effect of depth of immersion showed that, to be free of error due to conduction of heat away from the junction, the thermocouple should extend not less than ¾ in. into the central cavity. The immersion was at least twice this distance.

In making a single observation, the heating rate was adjusted so as to maintain as nearly as possible constant temperature. Then one observer adjusted the current in the pyrometer lamp until the brightness of the filament was the same as that of the blackbody. Simultaneously another observer measured the thermocouple emf. A "reading" at a given temperature was taken as the mean of two observed values of filament current and corresponding emf.

Readings were made from 1,950 °F to 3,800 °F at intervals of 50 °F, and repeated in descending order.

## 5. Computations

The observed temperatures seldom differed more than 5 °F from the nearest integral multiple of 50 °F. For each observed temperature the emf was "normalized"—that is, it was computed for the nearest integral multiple of 50 °F. The rate of change of emf with temperature ($dE/dT$) required in normalizing was obtained either by direct calculation from observed differences or by plotting these differences and hand fitting a curve through the points.

The emf for lot A wire was taken as the mean of the normalized emfs for the two thermocouples made of that wire. Similarly, the emf for each of the two wire sizes in lot B was computed as the mean of the normalized emfs of the two thermocouples made from each of the two sizes of wires. To these emfs were added the normalized emfs obtained from lot D (one thermocouple from each of the two wire sizes). The average of these five sets of normalized emfs constituted the basic data for constructing temperature-emf tables.

These data, comprising 78 temperatures and the corresponding emfs, were processed by the Computation Section of the NBS Applied Mathematics Division using its IBM 704 Computer. It was found by trial that an equation of the fifth degree with coefficients computed to give a least-square fit to the data gave calculated emfs from which the experimental values differed by not more than 4 μv at temperatures up to 2,700 °F, and not more than 10 μv at temperatures between 2,800° F and 3,800 °F. These deviations were considered satisfactorily small; hence, using the equation so derived, the computer calculated emfs for temperatures in integral multiples of 10 °F from 40 °F to 3,800 °F. The machine-computed deviations were plotted and a smooth curve fitted to them by hand. From this curve the deviations for the 10 °F points were taken, and added to the emfs computed by machine to give table IV-A.

The table of emfs for temperature in integral multiples of 10 °C (table II-A) was interpolated by hand from the Fahrenheit table.

By hand interpolation the temperatures in degrees C and degrees F were obtained for emfs in steps of 0.1 mv from 0 to 11.6 mv. The computer interpolated within the 0.1-mv intervals to obtain temperatures at 0.01-mv intervals (tables I-A and III-A).

Thermal emfs for iridium versus platinum up to 2,500 °F were computed from measurements made in the course of the runs on the iridium-rhodium versus iridium thermocouples. The iridium came from three coils, viz, lot A and the two wire sizes of lot B. By applying corrections obtained from data on the emf of the platinum working standard versus platinum 27, the iridium versus platinum 27 values given in table V-A were obtained.

Thermal emfs for 40 percent iridium-60 percent rhodium versus copper and for copper versus iridium are given in table VI-A. This table may be used to

correct for emfs generated at the junctions of the thermocouple legs with copper lead wires when these junctions are not at the same temperature.

## 6. Discussion

Not surprisingly, the emfs for a given temperature differed appreciably within the three lots of wire. One way of expressing the difference is to compare the individual emfs with the average, at a given temperature. For example, at 3,000 °F the emfs were as shown in table 1.

TABLE 1. *Deviation of the thermal emf of different lots of wire from the average, at 3000 °F*

| Lot | Wire diam | emf E | Difference, $E-E_{av}$ |
|---|---|---|---|
| | *in.* | *mv* | *μv* |
| A | 0.035 | 8.830 | −31 |
| B | .020 | 8.909 | 48 |
| B | .035 | 8.862 | 1 |
| D | .020 | 8.864 | 3 |
| D | .030 | 8.842 | −19 |
| Average | | 8.861 | |

Here the lowest emf was for lot A and the highest the 0.020-in. wire of lot B. The difference is 79 μv, which corresponds to about 24 °F.

Similar data are plotted for the entire range of temperatures in figure 2. Differences shown there are not wholly attributable to the different sources of wire involved, since there were naturally differences in emf between thermocouples made of wire from the same coil. In most cases these differences were only a few microvolts, but in one case, the 0.20-in. wire of lot B, the two thermocouples gave emfs differing by as much as 36 μv, corresponding to about 12 °F.

Figure 3 is a plot, for iridium wire from the three sources (lot A, and the two sizes in lot B) versus platinum 27, of the differences between individual values and the adjusted [6] average of the three. An emf on this graph is a measure of the contribution of the iridium in question to the analagous difference shown in figure 2 for the iridium-rhodium versus iridium thermocouple of which it is an element. For if, of two iridium wires making a common junction with an iridium-rhodium and a platinum wire, one has a higher emf to platinum than the other, its emf to the alloy wire must be lower by the same amount numerically. The reasoning can easily be extended to apply to the difference from the average (the ordinates of figs. 2 and 3). Thus it is evident that the lower emf of a thermocouple of lot A as compared with one from another lot is largely accounted for by the fact that the iridium wire of

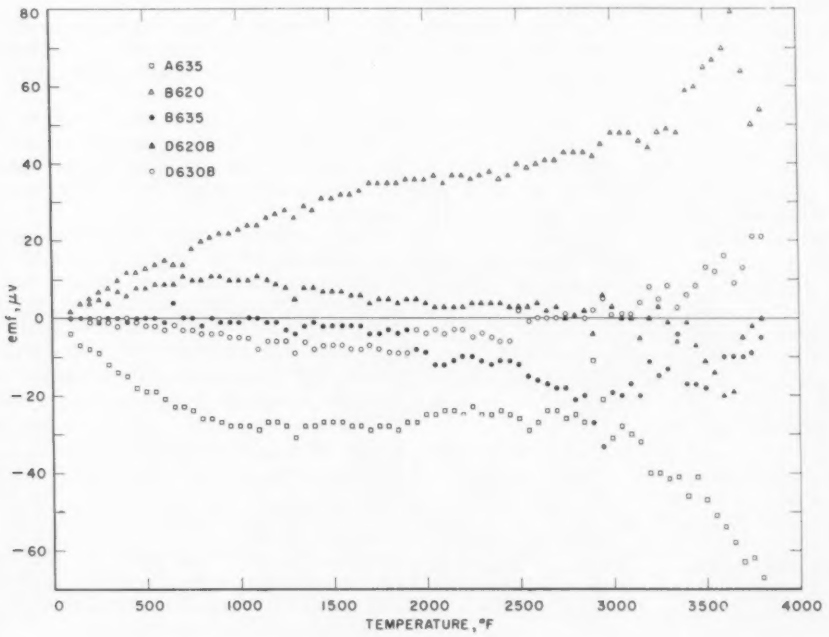


FIGURE 2. *Difference between the emf of each thermocouple and the average emf for 40% Ir 60% Rh versus Ir thermocouples.*

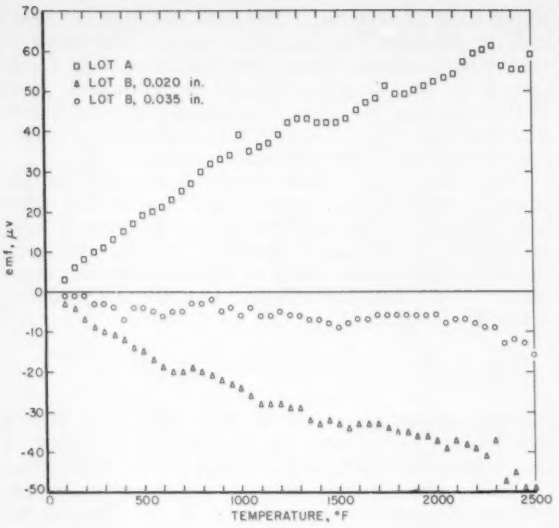


FIGURE 3. *Difference between the emf of each lot and size of Ir wire and the average emf for Ir versus Pt 27.*

this lot had a higher emf to platinum than did either of the other two coils of iridium wire. A similar situation prevails with respect to the 0.020-in. iridium wire of lot B. However, this wire was also used in D620B, and the differences between the emfs of figure 2 for thermocouples B620 and D620B are of course due to the differences between the two alloy wires used. These differences can be, and were, measured directly.

In the range 1,950 °F to 2,500 °F, where temperatures were measured both with the platinum-10 percent rhodium thermocouple (in the platinum-wound furnace) and with the optical pyrometer (in the induction furnace), the difference between emfs of the test thermocouples did not exceed 6 μv in most cases. This is little if any larger than the errors of observation, and gave added assurance that the measurements were free from significantly large systematic errors. The largest difference occurred on thermocouple B635b: The emfs with the optical pyrometer averaged 21 μv higher than with the platinum thermocouple. This corresponds to about 7 °F, and is larger than the reading error. The data yielded no clue as to what caused the difference.

The thermoelectric power is nearly constant over a wide range of temperature, having a value of 3.0 to 3.2 μv per degree from about 600 °F to 3,200 °F. Below 600 °F it decreases to about 2 μv per degree at 100 °F, and above 3,200 °F it increases to about 3.6 μv per degree at 3,800 °F.

The uncertainty in the temperature-emf values is partly that associated with measuring the temperature with a thermocouple and with an optical pyrometer. For the platinum-10 percent rhodium versus platinum thermocouple the uncertainty is about one degree at 2,000 °F and 3 degrees at 2,500 °F [7]. For the optical pyrometer the uncertainty was minimized by carefully calibrating the instrument in terms of lamp current and by adjusting this current precisely in the photometric matching. This procedure together with favorable blackbody conditions probably limited the uncertainty to 5 or 6 degrees at 3,800 ° F.

The increased electrical conductivity of insulators at high temperature contributes to the uncertainty of the emf measurements at temperatures above about 3,200 °F. When the thoria tubes which were used at first to support the wires in the induction furnace exhibited lowered resistance they were replaced with beryllia, which has higher resistivity than thoria [8]. Even so, the resistance between thermocouple wires (as determined in a test made with the wires unjoined) decreased to a few tens of ohms at 3,800 °F. The magnitude of error due to insulator conduction depends on the resistance of the insulator as compared with the resistance of the thermocouple wires between points where they effectively make electrical contact with the insulator. For example, for wire resistance 0.1 ohm between points of contact, an insulator resistance of 100 ohms would cause the observed emf of the thermocouple to be 0.1 percent lower than the actual emf. The available data yield an estimated uncertainty of this order, which at the highest temperature would amount to about 4 °F. Since this conductivity effect is believed to have occurred in a largely fortuitous manner, no correction has been made for it.

An effect was associated with the electrical conduction in the ceramic insulation which manifested itself in the superposition of a spurious emf on the thermal emf due to the presence of the strong rf field. This was thought to result from a rectifying process. It was not always present, but when it was, readings were obtained that were larger or smaller than the thermal emf by as much as 100 μv. Its magnitude was ascertained by turning off the power and observing the instantaneous change in galvanometer deflection, which occurred before an appreciable change due to cooling took place. The readings were corrected by the appropriate amount. We believe that loss in precision arising from this effect was held to a few microvolts by the means adopted to correct for it.

The combined uncertainties are believed not to exceed 12 °F.

The wires were discolored somewhat after a test. Although they were embrittled as a result of heating, and evidently had undergone considerable recrystallization, their thermoelectric properties were not changed appreciably. This was evidenced by good agreement of emfs measured in the low temperature range after a high temperature calibration.

The temperature-emf relationship for 40 percent iridium-60 percent rhodium versus iridium thermocouples is plotted in figure 4 for temperatures 2,000 °F to 3,800 °F, along with the thermal emfs of several other thermocouples useful in this range, all having

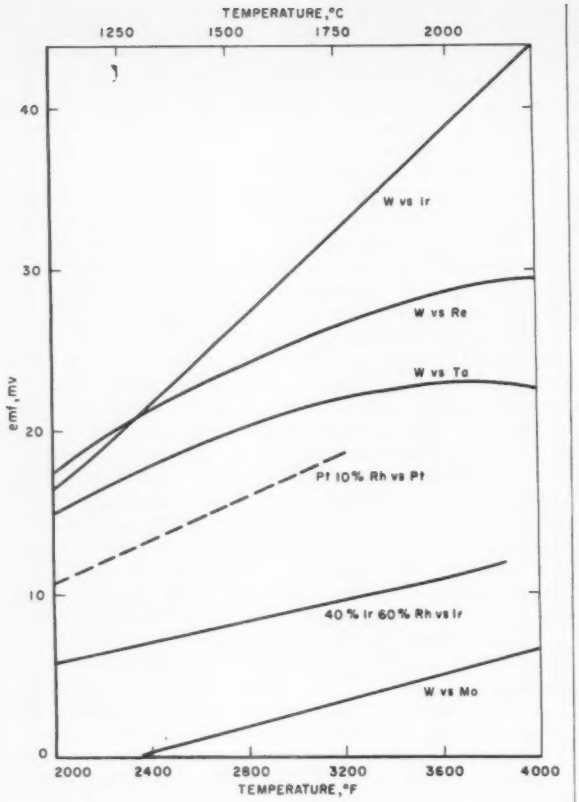


FIGURE 4. *Thermal emf of several thermocouples in the range 2,000 °F to 4,000 °F.*

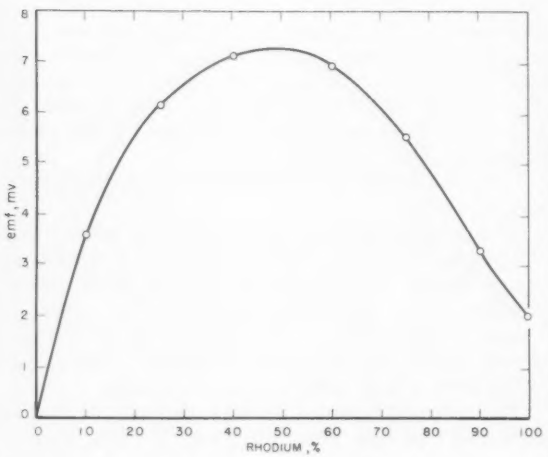


FIGURE 5. *Change of thermal emf of Ir-Rh versus Ir thermocouples with composition of the alloy, at 2,400 °F.*

tungsten as an element. The data on tungsten versus iridium are from Troy and Steven [9]. For tungsten versus rhenium the data were obtained from Lachman [10], for tungsten versus molybdenum from Potter and Grant [11], and tungsten versus tantalum from Sanders [12]. The emf is also plotted for platinum-10 percent rhodium versus platinum [3].

Some data have been obtained at NBS on the effect of varying the percent rhodium in the alloy leg. They have thus far been limited to temperatures at which a platimun-rhodium versus platimun thermocouple can be used to measure the temperature. These data are plotted for one temperature, 2,400 °F, in figure 5.

---

The authors thank J. F. Swindells and Henry Kostkowski for permission to use the facilities of the Temperature Physics Section of the NBS Heat Division, and for their helpful interest in the work; also, to Ronald C. Gordon and D. B. Thomas for calibrating, respectively, the optical pyrometer and platinum-rhodium versus platinum thermocouple used.

They are also indebted to G. M. Galler and B. S. Prush of the Computation Section of the NBS Applied Mathematics Division for their help in arranging the data for processing by the IBM 704 Computer.

## 7. References

[1] O. Feussner, New noble-metal thermoelements for very high temperatures (in German), Elektrotech. Z. **54**, 155 (1933).

[2] C. R. Droms and A. I. Dahl, Iridium vs iridium rhodium thermocouple for gas temperature measurements up to 3500 °F, General Electric Company Report No. R54GL314 (Nov. 19, 1954).

[3] Henry Shenker, John I. Lauritzen, Jr., Robert J. Corruccini, and S. T. Lonberger, Reference tables for thermocouples, Natl. Bur. Standards (U.S.) Circ. **561** (1955).

[4] A. Gouffé, Opening corrections of artificial blackbodies computed on the basis of multiple internal diffusion (in French), Rev. optique **24**, 1 (1945).

[5] Paul D. Foote, C. O. Fairchild, and T. R. Harrison, Pyrometric practice, Tech. Pap. BS **14** (1921).

[6] The averages as computed were adjusted by inspection to smooth the differences corresponding to 50 °F. The change did not exceed 3 microvolts in most cases.

[7] W. F. Roeser and S. T. Lonberger, Methods of testing thermocouples and thermocouple materials, Natl. Bur. Standards (U.S.) Circ. 590 (1958).

[8] I. E. Campbell, High temperature technology (Wiley, 1956), p. 58.

[9] W. C. Troy and Gary Steven, The tungsten iridium thermocouple for very high temperatures, Trans. Am. Soc. Metals **42**, 1131 (1950).

[10] J. C. Lachman, Calibration of rhenium molybdenum and rhenium tungsten thermocouples to 4000 °F, Report APEX 365, General Electric Company, Atomic Products Division (1958).

[11] R. D. Potter and N. J. Grant, Tungsten molybdenum thermocouples, Iron Age **163**, 65 (March 31, 1949).

[12] V. D. Sanders, Review of high-temperature immersion thermal sensing devices for in-flight engine control, Rev. Sci. Instr. **29**, 917 (1958).

# 8. Appendix

TABLE I–A. *Forty percent iridium-60 percent rhodium versus iridium thermocouples*

Electromotive force in absolute millivolts. Temperature in degrees C (Int. 1948). Reference junction at 0 °C.

| *Millivolts* | .000 | .010 | .020 | .030 | .040 | .050 | .060 | .070 | .080 | .090 | .100 | *Millivolts* |
|---|---|---|---|---|---|---|---|---|---|---|---|---|
| 0.000 | 0 | 3.2 | 6.3 | 9.4 | 12.5 | 15.5 | 18.6 | 21.6 | 24.5 | 27.5 | 30.4 | 0.000 |
| .100 | 30.4 | 33.3 | 36.2 | 39.0 | 41.8 | 44.6 | 47.4 | 50.2 | 52.9 | 55.6 | 58.3 | .100 |
| .200 | 58.3 | 61.0 | 63.6 | 66.2 | 68.8 | 71.4 | 73.9 | 76.5 | 79.0 | 81.5 | 84.0 | .200 |
| .300 | 84.0 | 86.5 | 89.0 | 91.5 | 94.0 | 96.5 | 98.9 | 101.4 | 103.8 | 106.2 | 108.6 | .300 |
| .400 | 108.6 | 111.0 | 113.3 | 115.7 | 118.0 | 120.3 | 122.7 | 125.0 | 127.3 | 129.5 | 131.8 | .400 |
| .500 | 131.8 | 134.1 | 136.3 | 138.6 | 140.8 | 143.0 | 145.2 | 147.4 | 149.6 | 151.8 | 154.0 | .500 |
| .600 | 154.0 | 156.2 | 158.3 | 160.5 | 162.6 | 164.8 | 166.9 | 169.1 | 171.2 | 173.3 | 175.4 | .600 |
| .700 | 175.4 | 177.5 | 179.6 | 181.7 | 183.8 | 185.9 | 187.9 | 190.0 | 192.1 | 194.1 | 196.2 | .700 |
| .800 | 196.2 | 198.3 | 200.3 | 202.4 | 204.4 | 206.5 | 208.5 | 210.5 | 212.6 | 214.6 | 216.6 | .800 |
| .900 | 216.6 | 218.6 | 220.6 | 222.6 | 224.6 | 226.6 | 228.5 | 230.5 | 232.5 | 234.4 | 236.4 | .900 |
| 1.000 | 236.4 | 238.4 | 240.3 | 242.3 | 244.2 | 246.1 | 248.1 | 250.0 | 251.9 | 253.9 | 255.8 | 1.000 |
| 1.100 | 255.8 | 257.7 | 259.6 | 261.6 | 263.5 | 265.4 | 267.3 | 269.2 | 271.1 | 273.0 | 274.9 | 1.100 |
| 1.200 | 274.9 | 276.8 | 278.7 | 280.6 | 282.5 | 284.3 | 286.2 | 288.1 | 290.0 | 291.8 | 293.7 | 1.200 |
| 1.300 | 293.7 | 295.6 | 297.4 | 299.3 | 301.1 | 303.0 | 304.8 | 306.7 | 308.5 | 310.4 | 312.2 | 1.300 |
| 1.400 | 312.2 | 314.0 | 315.9 | 317.7 | 319.5 | 321.3 | 323.1 | 325.0 | 326.8 | 328.6 | 330.4 | 1.400 |
| 1.500 | 330.4 | 332.2 | 334.1 | 335.9 | 337.7 | 339.5 | 341.3 | 343.2 | 345.0 | 346.8 | 348.6 | 1.500 |
| 1.600 | 348.6 | 350.4 | 352.2 | 354.0 | 355.7 | 357.5 | 359.3 | 361.1 | 362.8 | 364.6 | 366.4 | 1.600 |
| 1.700 | 366.4 | 368.2 | 370.0 | 371.8 | 373.6 | 375.4 | 377.2 | 378.9 | 380.7 | 382.5 | 384.3 | 1.700 |
| 1.800 | 384.3 | 386.1 | 387.8 | 389.6 | 391.3 | 393.1 | 394.8 | 396.6 | 398.3 | 400.1 | 401.8 | 1.800 |
| 1.900 | 401.8 | 403.6 | 405.3 | 407.1 | 408.9 | 410.7 | 412.4 | 414.2 | 416.0 | 417.7 | 419.5 | 1.900 |
| 2.000 | 419.5 | 421.2 | 423.0 | 424.7 | 426.5 | 428.2 | 430.0 | 431.7 | 433.4 | 435.2 | 436.9 | 2.000 |
| 2.100 | 436.9 | 438.6 | 440.4 | 442.1 | 443.9 | 445.6 | 447.3 | 449.1 | 450.8 | 452.6 | 454.3 | 2.100 |
| 2.200 | 454.3 | 456.0 | 457.8 | 459.5 | 461.2 | 462.9 | 464.7 | 466.4 | 468.1 | 469.9 | 471.6 | 2.200 |
| 2.300 | 471.6 | 473.3 | 475.1 | 476.8 | 478.6 | 480.3 | 482.0 | 483.8 | 485.5 | 487.3 | 489.0 | 2.300 |
| 2.400 | 489.0 | 490.7 | 492.4 | 494.2 | 495.9 | 497.6 | 499.3 | 501.0 | 502.8 | 504.5 | 506.2 | 2.400 |
| 2.500 | 506.2 | 507.9 | 509.6 | 511.4 | 513.1 | 514.8 | 516.5 | 518.2 | 520.0 | 521.7 | 523.4 | 2.500 |
| 2.600 | 523.4 | 525.1 | 526.8 | 528.5 | 530.2 | 531.9 | 533.7 | 535.4 | 537.1 | 538.8 | 540.5 | 2.600 |
| 2.700 | 540.5 | 542.2 | 543.9 | 545.7 | 547.4 | 549.1 | 550.8 | 552.5 | 554.3 | 556.0 | 557.7 | 2.700 |
| 2.800 | 557.7 | 559.4 | 561.1 | 562.8 | 564.6 | 566.3 | 568.0 | 569.7 | 571.4 | 573.1 | 574.8 | 2.800 |
| 2.900 | 574.8 | 576.5 | 578.2 | 579.9 | 581.6 | 583.3 | 585.0 | 586.7 | 588.4 | 590.1 | 591.8 | 2.900 |
| 3.000 | 591.8 | 593.5 | 595.2 | 596.9 | 598.7 | 600.4 | 602.1 | 603.8 | 605.6 | 607.3 | 609.0 | 3.000 |
| 3.100 | 609.0 | 610.7 | 612.4 | 614.2 | 615.9 | 617.6 | 619.3 | 621.0 | 622.8 | 624.5 | 626.2 | 3.100 |
| 3.200 | 626.2 | 627.9 | 629.7 | 631.4 | 633.1 | 634.9 | 636.6 | 638.3 | 640.1 | 641.8 | 643.5 | 3.200 |
| 3.300 | 643.5 | 645.2 | 646.9 | 648.6 | 650.3 | 652.0 | 653.7 | 655.4 | 657.1 | 658.8 | 660.5 | 3.300 |
| 3.400 | 660.5 | 662.2 | 663.9 | 665.6 | 667.4 | 669.1 | 670.8 | 672.5 | 674.2 | 676.0 | 677.7 | 3.400 |
| 3.500 | 677.7 | 679.4 | 681.1 | 682.9 | 684.6 | 686.3 | 688.1 | 689.8 | 691.5 | 693.3 | 695.0 | 3.500 |
| 3.600 | 695.0 | 696.7 | 698.5 | 700.2 | 702.0 | 703.7 | 705.4 | 707.2 | 708.9 | 710.7 | 712.4 | 3.600 |
| 3.700 | 712.4 | 714.1 | 715.9 | 717.6 | 719.4 | 721.1 | 722.8 | 724.6 | 726.3 | 728.1 | 729.8 | 3.700 |
| 3.800 | 729.8 | 731.5 | 733.3 | 735.0 | 736.7 | 738.5 | 740.2 | 742.0 | 743.7 | 745.5 | 747.2 | 3.800 |
| 3.900 | 747.2 | 749.0 | 750.7 | 752.5 | 754.2 | 756.0 | 757.7 | 759.5 | 761.3 | 763.0 | 764.8 | 3.900 |
| 4.000 | 764.8 | 766.6 | 768.3 | 770.1 | 771.9 | 773.6 | 775.4 | 777.2 | 779.0 | 780.7 | 782.5 | 4.000 |
| 4.100 | 782.5 | 784.3 | 786.0 | 787.8 | 789.5 | 791.3 | 793.1 | 794.8 | 796.6 | 798.3 | 800.1 | 4.100 |
| 4.200 | 800.1 | 801.9 | 803.7 | 805.4 | 807.2 | 809.0 | 810.8 | 812.6 | 814.3 | 816.1 | 817.9 | 4.200 |
| 4.300 | 817.9 | 819.7 | 821.4 | 823.2 | 825.0 | 826.7 | 828.5 | 830.3 | 832.1 | 833.8 | 835.6 | 4.300 |
| 4.400 | 835.6 | 837.4 | 839.2 | 840.9 | 842.7 | 844.5 | 846.3 | 848.0 | 849.8 | 851.6 | 853.4 | 4.400 |
| 4.500 | 853.4 | 855.2 | 857.0 | 858.8 | 860.5 | 862.3 | 864.1 | 865.9 | 867.7 | 869.5 | 871.3 | 4.500 |
| 4.600 | 871.3 | 873.1 | 874.9 | 876.7 | 878.5 | 880.3 | 882.2 | 884.0 | 885.8 | 887.6 | 889.4 | 4.600 |
| 4.700 | 889.4 | 891.2 | 893.0 | 894.8 | 896.6 | 898.3 | 900.1 | 901.9 | 903.7 | 905.5 | 907.3 | 4.700 |
| 4.800 | 907.3 | 909.1 | 910.9 | 912.7 | 914.5 | 916.3 | 918.1 | 919.9 | 921.8 | 923.6 | 925.4 | 4.800 |
| 4.900 | 925.4 | 927.2 | 929.1 | 930.9 | 932.7 | 934.5 | 936.4 | 938.2 | 940.0 | 941.9 | 943.7 | 4.900 |
| 5.000 | 943.7 | 945.5 | 947.3 | 949.1 | 950.9 | 952.7 | 954.6 | 956.4 | 958.2 | 960.0 | 961.8 | 5.000 |
| 5.100 | 961.8 | 963.6 | 965.5 | 967.3 | 969.1 | 971.0 | 972.8 | 974.7 | 976.5 | 978.4 | 980.2 | 5.100 |
| 5.200 | 980.2 | 982.0 | 983.9 | 985.7 | 987.5 | 989.3 | 991.2 | 993.0 | 994.8 | 996.7 | 998.5 | 5.200 |
| 5.300 | 998.5 | 1000.3 | 1002.2 | 1004.0 | 1005.9 | 1007.7 | 1009.6 | 1011.4 | 1013.3 | 1015.1 | 1017.0 | 5.300 |
| 5.400 | 1017.0 | 1018.8 | 1020.7 | 1022.5 | 1024.4 | 1026.2 | 1028.1 | 1029.9 | 1031.7 | 1033.6 | 1035.4 | 5.400 |
| 5.500 | 1035.4 | 1037.2 | 1039.1 | 1040.9 | 1042.7 | 1044.5 | 1046.4 | 1048.2 | 1050.0 | 1051.9 | 1053.7 | 5.500 |
| 5.600 | 1053.7 | 1055.5 | 1057.4 | 1059.2 | 1061.1 | 1062.9 | 1064.8 | 1066.6 | 1068.5 | 1070.3 | 1072.2 | 5.600 |
| 5.700 | 1072.2 | 1074.0 | 1075.9 | 1077.7 | 1079.6 | 1081.4 | 1083.3 | 1085.1 | 1087.0 | 1088.8 | 1090.7 | 5.700 |
| 5.800 | 1090.7 | 1092.6 | 1094.4 | 1096.3 | 1098.1 | 1100.0 | 1101.9 | 1103.7 | 1105.6 | 1107.4 | 1109.3 | 5.800 |
| 5.900 | 1109.3 | 1111.2 | 1113.0 | 1114.9 | 1116.7 | 1118.6 | 1120.4 | 1122.3 | 1124.1 | 1126.0 | 1127.8 | 5.900 |
| 6.000 | 1127.8 | 1129.6 | 1131.5 | 1133.3 | 1135.2 | 1137.0 | 1138.9 | 1140.7 | 1142.6 | 1144.4 | 1146.3 | 6.000 |
| *Millivolts* | .000 | .010 | .020 | .030 | .040 | .050 | .060 | .070 | .080 | .090 | .100 | *Millivolts* |

TABLE I–A. *Forty percent iridium-60 percent rhodium versus iridium thermocouples*—Continued

Electromotive force in absolute millivolts. Temperature in degrees C (Int. 1948). Reference junction at 0 °C.

| *Millivolts* | .000 | .010 | .020 | .030 | .040 | .050 | .060 | .070 | .080 | .090 | .100 | *Millivolts* |
|---|---|---|---|---|---|---|---|---|---|---|---|---|
| 6.000 | 1127.8 | 1129.6 | 1131.5 | 1133.3 | 1135.2 | 1137.0 | 1138.9 | 1140.7 | 1142.6 | 1144.4 | 1146.3 | 6.000 |
| 6.100 | 1146.3 | 1148.2 | 1150.0 | 1151.9 | 1153.8 | 1155.6 | 1157.5 | 1159.4 | 1161.3 | 1163.1 | 1165.0 | 6.100 |
| 6.200 | 1165.0 | 1166.9 | 1168.7 | 1170.6 | 1172.5 | 1174.4 | 1176.2 | 1178.1 | 1180.0 | 1181.8 | 1183.7 | 6.200 |
| 6.300 | 1183.7 | 1185.6 | 1187.4 | 1189.3 | 1191.1 | 1193.0 | 1194.9 | 1196.7 | 1198.6 | 1200.4 | 1202.3 | 6.300 |
| 6.400 | 1202.3 | 1204.2 | 1206.0 | 1207.9 | 1209.7 | 1211.6 | 1213.4 | 1215.3 | 1217.2 | 1219.0 | 1220.9 | 6.400 |
| 6.500 | 1220.9 | 1222.8 | 1224.7 | 1226.6 | 1228.5 | 1230.3 | 1222.2 | 1234.1 | 1236.0 | 1237.9 | 1239.8 | 6.500 |
| 6.600 | 1239.8 | 1241.7 | 1243.5 | 1245.4 | 1247.3 | 1249.2 | 1251.0 | 1252.9 | 1254.8 | 1256.6 | 1258.5 | 6.600 |
| 6.700 | 1258.5 | 1260.4 | 1262.2 | 1264.1 | 1266.0 | 1267.8 | 1269.7 | 1271.6 | 1273.5 | 1275.3 | 1277.2 | 6.700 |
| 6.800 | 1277.2 | 1279.1 | 1280.9 | 1282.8 | 1284.7 | 1286.5 | 1288.4 | 1290.3 | 1292.2 | 1294.0 | 1295.9 | 6.800 |
| 6.900 | 1295.9 | 1297.8 | 1299.7 | 1301.5 | 1303.4 | 1305.2 | 1307.1 | 1369.0 | 1310.9 | 1312.7 | 1314.6 | 6.900 |
| 7.000 | 1314.6 | 1316.5 | 1318.3 | 1320.2 | 1322.1 | 1324.0 | 1325.8 | 1327.7 | 1329.6 | 1331.4 | 1333.3 | 7.000 |
| 7.100 | 1333.3 | 1335.2 | 1337.0 | 1338.9 | 1340.7 | 1342.6 | 1344.4 | 1346.3 | 1348.1 | 1350.0 | 1351.8 | 7.100 |
| 7.200 | 1351.8 | 1353.7 | 1355.5 | 1357.4 | 1359.2 | 1361.1 | 1363.0 | 1364.8 | 1366.7 | 1368.5 | 1370.4 | 7.200 |
| 7.300 | 1370.4 | 1372.2 | 1374.1 | 1375.9 | 1377.7 | 1379.6 | 1381.4 | 1383.2 | 1385.0 | 1386.9 | 1388.7 | 7.300 |
| 7.400 | 1388.7 | 1390.5 | 1392.4 | 1394.2 | 1396.0 | 1397.8 | 1399.7 | 1401.5 | 1403.3 | 1405.2 | 1407.0 | 7.400 |
| 7.500 | 1407.0 | 1408.8 | 1410.7 | 1412.5 | 1414.4 | 1416.2 | 1418.1 | 1419.9 | 1421.7 | 1423.6 | 1425.4 | 7.500 |
| 7.600 | 1425.4 | 1427.2 | 1429.0 | 1430.8 | 1432.7 | 1434.5 | 1436.3 | 1438.1 | 1439.9 | 1441.7 | 1443.5 | 7.600 |
| 7.700 | 1443.5 | 1445.3 | 1447.1 | 1448.9 | 1450.7 | 1452.5 | 1454.4 | 1456.2 | 1458.0 | 1459.8 | 1461.6 | 7.700 |
| 7.800 | 1461.6 | 1463.4 | 1465.2 | 1467.0 | 1468.9 | 1470.7 | 1472.5 | 1474.3 | 1476.1 | 1477.9 | 1479.7 | 7.800 |
| 7.900 | 1479.7 | 1481.5 | 1483.3 | 1485.1 | 1486.9 | 1488.7 | 1490.5 | 1492.2 | 1494.0 | 1495.8 | 1497.6 | 7.900 |
| 8.000 | 1497.6 | 1499.4 | 1501.2 | 1503.0 | 1504.7 | 1506.5 | 1508.3 | 1510.1 | 1511.9 | 1513.6 | 1515.4 | 8.000 |
| 8.100 | 1515.4 | 1517.2 | 1518.9 | 1520.7 | 1522.4 | 1524.2 | 1525.9 | 1527.7 | 1529.4 | 1531.2 | 1532.9 | 8.100 |
| 8.200 | 1532.9 | 1534.6 | 1536.4 | 1538.1 | 1539.9 | 1541.6 | 1543.3 | 1545.1 | 1546.8 | 1548.6 | 1550.3 | 8.200 |
| 8.300 | 1550.3 | 1552.0 | 1553.8 | 1555.5 | 1557.2 | 1559.0 | 1560.7 | 1562.5 | 1564.2 | 1566.0 | 1567.7 | 8.300 |
| 8.400 | 1567.7 | 1569.5 | 1571.2 | 1573.0 | 1574.7 | 1576.5 | 1578.3 | 1580.0 | 1581.8 | 1583.5 | 1585.3 | 8.400 |
| 8.500 | 1585.3 | 1587.0 | 1588.8 | 1590.5 | 1592.3 | 1594.0 | 1595.8 | 1597.5 | 1599.3 | 1601.0 | 1602.8 | 8.500 |
| 8.600 | 1602.8 | 1604.6 | 1606.3 | 1608.1 | 1609.9 | 1611.6 | 1613.4 | 1615.2 | 1617.0 | 1618.7 | 1620.5 | 8.600 |
| 8.700 | 1620.5 | 1622.3 | 1624.0 | 1625.8 | 1627.5 | 1629.3 | 1631.1 | 1632.8 | 1634.6 | 1636.3 | 1638.1 | 8.700 |
| 8.800 | 1638.1 | 1639.9 | 1641.6 | 1643.4 | 1645.2 | 1646.9 | 1648.7 | 1650.4 | 1652.2 | 1653.9 | 1655.7 | 8.800 |
| 8.900 | 1655.7 | 1657.4 | 1659.2 | 1660.9 | 1662.6 | 1664.4 | 1666.1 | 1667.8 | 1669.5 | 1671.3 | 1673.0 | 8.900 |
| 9.000 | 1673.0 | 1674.7 | 1676.5 | 1678.2 | 1680.0 | 1681.7 | 1683.5 | 1685.2 | 1686.9 | 1688.7 | 1690.4 | 9.000 |
| 9.100 | 1690.4 | 1692.1 | 1693.8 | 1695.5 | 1697.2 | 1699.0 | 1700.7 | 1702.4 | 1704.1 | 1705.8 | 1707.5 | 9.100 |
| 9.200 | 1707.5 | 1709.2 | 1711.0 | 1712.7 | 1714.4 | 1716.2 | 1717.9 | 1719.6 | 1721.3 | 1723.1 | 1724.8 | 9.200 |
| 9.300 | 1724.8 | 1726.5 | 1728.2 | 1729.9 | 1731.6 | 1733.3 | 1735.0 | 1736.7 | 1738.4 | 1740.1 | 1741.8 | 9.300 |
| 9.400 | 1741.8 | 1743.5 | 1745.2 | 1746.8 | 1748.5 | 1750.2 | 1751.9 | 1753.6 | 1755.2 | 1756.9 | 1758.6 | 9.400 |
| 9.500 | 1758.6 | 1760.3 | 1762.0 | 1763.7 | 1765.4 | 1767.0 | 1768.7 | 1770.4 | 1772.1 | 1773.8 | 1775.5 | 9.500 |
| 9.600 | 1775.5 | 1777.2 | 1778.9 | 1780.5 | 1782.2 | 1783.9 | 1785.6 | 1787.3 | 1788.9 | 1790.6 | 1792.3 | 9.600 |
| 9.700 | 1792.3 | 1794.0 | 1795.7 | 1797.4 | 1799.0 | 1800.7 | 1802.4 | 1804.1 | 1805.8 | 1807.4 | 1809.1 | 9.700 |
| 9.800 | 1809.1 | 1810.8 | 1812.4 | 1814.1 | 1815.7 | 1817.4 | 1819.0 | 1820.7 | 1822.3 | 1824.0 | 1825.6 | 9.800 |
| 9.900 | 1825.6 | 1827.2 | 1828.9 | 1830.5 | 1832.2 | 1833.8 | 1835.5 | 1837.1 | 1838.8 | 1840.4 | 1842.1 | 9.900 |
| 10.000 | 1842.1 | 1843.8 | 1845.4 | 1847.1 | 1848.7 | 1850.4 | 1852.0 | 1853.7 | 1855.3 | 1857.0 | 1858.6 | 10.000 |
| 10.100 | 1858.6 | 1860.2 | 1861.9 | 1863.5 | 1865.2 | 1866.8 | 1868.5 | 1870.1 | 1871.7 | 1873.4 | 1875.0 | 10.100 |
| 10.200 | 1875.0 | 1876.6 | 1878.3 | 1879.9 | 1881.5 | 1883.2 | 1884.8 | 1886.4 | 1888.1 | 1889.7 | 1891.3 | 10.200 |
| 10.300 | 1891.3 | 1892.9 | 1894.5 | 1896.1 | 1897.7 | 1899.3 | 1900.9 | 1902.4 | 1904.0 | 1905.6 | 1907.2 | 10.300 |
| 10.400 | 1907.2 | 1908.8 | 1910.4 | 1912.0 | 1913.6 | 1915.1 | 1916.7 | 1918.3 | 1919.9 | 1921.5 | 1923.1 | 10.400 |
| 10.500 | 1923.1 | 1924.7 | 1926.3 | 1927.9 | 1929.5 | 1931.1 | 1932.7 | 1934.2 | 1935.8 | 1937.4 | 1939.0 | 10.500 |
| 10.600 | 1939.0 | 1940.6 | 1942.1 | 1943.7 | 1945.3 | 1946.8 | 1948.4 | 1949.9 | 1951.5 | 1953.1 | 1954.6 | 10.600 |
| 10.700 | 1954.6 | 1956.2 | 1957.7 | 1959.3 | 1960.8 | 1962.3 | 1963.9 | 1965.4 | 1967.0 | 1968.5 | 1970.0 | 10.700 |
| 10.800 | 1970.0 | 1971.5 | 1973.0 | 1974.4 | 1975.9 | 1977.4 | 1978.9 | 1980.4 | 1981.9 | 1983.4 | 1984.9 | 10.800 |
| 10.900 | 1984.9 | 1986.5 | 1988.0 | 1989.6 | 1991.2 | 1992.8 | 1994.4 | 1995.9 | 1997.5 | 1999.1 | 2000.7 | 10.900 |
| 11.000 | 2000.7 | 2002.2 | 2003.8 | 2005.3 | 2006.9 | 2008.4 | 2009.9 | 2011.4 | 2013.0 | 2014.5 | 2016.0 | 11.000 |
| 11.100 | 2016.0 | 2017.5 | 2019.1 | 2020.6 | 2022.1 | 2023.7 | 2025.2 | 2026.7 | 2028.3 | 2029.8 | 2031.3 | 11.100 |
| 11.200 | 2031.3 | 2032.8 | 2034.3 | 2035.8 | 2037.3 | 2038.8 | 2040.3 | 2041.8 | 2043.3 | 2044.8 | 2046.3 | 11.200 |
| 11.300 | 2046.3 | 2047.8 | 2049.3 | 2050.9 | 2052.4 | 2053.9 | 2055.5 | 2057.0 | 2058.5 | 2060.1 | 2061.6 | 11.300 |
| 11.400 | 2061.6 | 2063.1 | 2064.7 | 2066.2 | 2067.7 | 2069.2 | 2070.7 | 2072.3 | 2073.8 | 2075.3 | 2076.8 | 11.400 |
| 11.500 | 2076.8 | 2078.3 | 2079.8 | 2081.3 | 2082.8 | 2084.3 | 2085.8 | 2087.3 | 2088.8 | 2090.3 | 2091.8 | 11.500 |
| 11.600 | 2091.8 | 2093.3 | 2094.8 | | | | | | | | | |
| *Millivolts* | .000 | .010 | .020 | .030 | .040 | .050 | .060 | .070 | .080 | .090 | .100 | *Millivolts* |

TABLE II–A. *Forty percent iridium-60 percent rhodium versus iridium thermocouples*

Electromotive force in absolute millivolts. Temperature in degrees C (Int. 1948). Reference junction at 0 °C.

| °C | 0 | 10 | 20 | 30 | 40 | 50 | 60 | 70 | 80 | 90 | 100 | °C |
|---|---|---|---|---|---|---|---|---|---|---|---|---|
| 0 | 0.000 | 0.032 | 0.064 | 0.098 | 0.134 | 0.170 | 0.206 | 0.245 | 0.284 | 0.324 | 0.365 | 0 |
| 100 | .365 | .406 | .449 | .492 | .536 | .581 | .627 | .674 | .722 | .770 | .818 | 100 |
| 200 | .818 | .868 | .917 | .968 | 1.019 | 1.070 | 1.122 | 1.174 | 1.227 | 1.280 | 1.334 | 200 |
| 300 | 1.334 | 1.388 | 1.443 | 1.498 | 1.553 | 1.608 | 1.664 | 1.720 | 1.776 | 1.832 | 1.889 | 300 |
| 400 | 1.889 | 1.946 | 2.003 | 2.060 | 2.118 | 2.175 | 2.233 | 2.291 | 2.348 | 2.406 | 2.464 | 400 |
| 500 | 2.464 | 2.522 | 2.580 | 2.639 | 2.697 | 2.755 | 2.814 | 2.872 | 2.930 | 2.989 | 3.047 | 500 |
| 600 | 3.047 | 3.106 | 3.164 | 3.222 | 3.280 | 3.339 | 3.397 | 3.455 | 3.513 | 3.571 | 3.628 | 600 |
| 700 | 3.628 | 3.686 | 3.744 | 3.801 | 3.859 | 3.916 | 3.973 | 4.030 | 4.086 | 4.143 | 4.199 | 700 |
| 800 | 4.199 | 4.256 | 4.312 | 4.368 | 4.424 | 4.480 | 4.537 | 4.593 | 4.648 | 4.703 | 4.759 | 800 |
| 900 | 4.759 | 4.815 | 4.870 | 4.925 | 4.980 | 5.035 | 5.090 | 5.144 | 5.199 | 5.254 | 5.308 | 900 |
| 1000 | 5.308 | 5.362 | 5.417 | 5.471 | 5.525 | 5.580 | 5.634 | 5.688 | 5.742 | 5.796 | 5.850 | 1000 |
| 1100 | 5.850 | 5.904 | 5.958 | 6.012 | 6.066 | 6.120 | 6.173 | 6.227 | 6.280 | 6.334 | 6.388 | 1100 |
| 1200 | 6.388 | 6.441 | 6.493 | 6.548 | 6.601 | 6.654 | 6.708 | 6.761 | 6.815 | 6.869 | 6.922 | 1200 |
| 1300 | 6.922 | 6.976 | 7.029 | 7.082 | 7.136 | 7.190 | 7.244 | 7.298 | 7.352 | 7.407 | 7.461 | 1300 |
| 1400 | 7.461 | 7.516 | 7.571 | 7.626 | 7.681 | 7.736 | 7.791 | 7.847 | 7.902 | 7.957 | 8.013 | 1400 |
| 1500 | 8.013 | 8.070 | 8.127 | 8.183 | 8.241 | 8.298 | 8.356 | 8.413 | 8.470 | 8.526 | 8.583 | 1500 |
| 1600 | 8.583 | 8.640 | 8.697 | 8.754 | 8.811 | 8.868 | 8.925 | 8.983 | 9.040 | 9.098 | 9.156 | 1600 |
| 1700 | 9.156 | 9.214 | 9.272 | 9.331 | 9.390 | 9.449 | 9.508 | 9.567 | 9.627 | 9.686 | 9.745 | 1700 |
| 1800 | 9.745 | 9.805 | 9.866 | 9.926 | 9.987 | 10.048 | 10.108 | 10.169 | 10.230 | 10.292 | 10.355 | 1800 |
| 1900 | 10.355 | 10.417 | 10.480 | 10.543 | 10.606 | 10.670 | 10.735 | 10.800 | 10.865 | 10.930 | 10.995 | 1900 |
| 2000 | 10.995 | 11.061 | 11.126 | 11.192 | 11.258 | 11.324 | 11.389 | 11.455 | 11.521 | 11.588 | 11.654 | 2000 |
| 2100 | 11.654 | | | | | | | | | | | |
| °C | 0 | 10 | 20 | 30 | 40 | 50 | 60 | 70 | 80 | 90 | 100 | °C |

TABLE III–A. *Forty percent iridium-60 percent rhodium versus iridium thermocouples*

Electromotive force in absolute millivolts. Temperature in degrees F (Int. 1948). Reference junction at 32 °F.

| *Millivolts* | .000 | 010 | .020 | .030 | .040 | .050 | 060 | .070 | .080 | .090 | .100 | *Millivolts* |
|---|---|---|---|---|---|---|---|---|---|---|---|---|
| 0.000 | 32.0 | 37.7 | 43.4 | 49.0 | 54.5 | 60.0 | 65.5 | 70.9 | 76.2 | 81.5 | 86.8 | 0.000 |
| .100 | 86.8 | 92.0 | 97.2 | 102.3 | 107.4 | 112.4 | 117.4 | 122.4 | 127.3 | 132.2 | 137.0 | .100 |
| .200 | 137.0 | 141.8 | 146.5 | 151.2 | 155.8 | 160.5 | 165.1 | 169.6 | 174.2 | 178.7 | 183.2 | .200 |
| .300 | 183.2 | 187.7 | 192.2 | 196.7 | 201.1 | 205.6 | 210.0 | 214.4 | 218.7 | 223.1 | 227.4 | .300 |
| .400 | 227.4 | 231.7 | 235.9 | 240.2 | 244.4 | 248.6 | 252.7 | 256.9 | 261.0 | 265.1 | 269.2 | .400 |
| .500 | 269.2 | 273.3 | 277.3 | 281.4 | 285.4 | 289.4 | 293.4 | 297.4 | 301.3 | 305.3 | 309.2 | .500 |
| .600 | 309.2 | 313.1 | 317.0 | 320.9 | 324.8 | 328.7 | 332.5 | 336.4 | 340.2 | 344.0 | 347.8 | .600 |
| .700 | 347.8 | 351.6 | 355.4 | 359.1 | 362.9 | 366.6 | 370.4 | 374.1 | 377.8 | 381.5 | 385.2 | .700 |
| .800 | 385.2 | 388.9 | 392.6 | 396.3 | 399.9 | 403.6 | 407.3 | 410.9 | 414.5 | 418.2 | 421.8 | .800 |
| .900 | 421.8 | 425.4 | 429.0 | 432.6 | 436.2 | 439.8 | 443.3 | 446.9 | 450.4 | 454.0 | 457.5 | .900 |
| 1.000 | 457.5 | 461.0 | 464.5 | 468.0 | 471.5 | 475.0 | 478.5 | 482.0 | 485.5 | 488.9 | 492.4 | 1.000 |
| 1.100 | 492.4 | 495.9 | 499.3 | 502.8 | 506.3 | 509.7 | 513.2 | 516.6 | 520.0 | 523.5 | 526.9 | 1.100 |
| 1.200 | 526.9 | 530.3 | 533.7 | 537.1 | 540.5 | 543.9 | 547.3 | 550.6 | 554.0 | 557.3 | 560.7 | 1.200 |
| 1.300 | 560.7 | 564.0 | 567.4 | 570.7 | 574.1 | 577.4 | 580.7 | 584.1 | 587.4 | 590.7 | 594.0 | 1.300 |
| 1.400 | 594.0 | 597.3 | 600.6 | 603.8 | 607.1 | 610.4 | 613.7 | 616.9 | 620.2 | 623.4 | 626.7 | 1.400 |
| 1.500 | 626.7 | 630.0 | 633.3 | 636.5 | 639.8 | 643.1 | 646.4 | 649.6 | 652.9 | 656.1 | 659.4 | 1.500 |
| 1.600 | 659.4 | 662.6 | 665.9 | 669.1 | 672.3 | 675.5 | 678.7 | 682.0 | 685.2 | 688.4 | 691.6 | 1.600 |
| 1.700 | 691.6 | 694.8 | 698.1 | 701.3 | 704.5 | 707.7 | 711.0 | 714.2 | 717.4 | 720.6 | 723.8 | 1.700 |
| 1.800 | 723.8 | 727.0 | 730.1 | 733.3 | 736.4 | 739.6 | 742.7 | 745.9 | 749.0 | 752.2 | 755.3 | 1.800 |
| 1.900 | 755.3 | 758.5 | 761.7 | 764.8 | 768.0 | 771.2 | 774.4 | 777.6 | 780.8 | 783.9 | 787.1 | 1.900 |
| 2.000 | 787.1 | 790.2 | 793.4 | 796.5 | 799.7 | 802.8 | 805.9 | 809.0 | 812.2 | 815.3 | 818.4 | 2.000 |
| 2.100 | 818.4 | 821.5 | 824.7 | 827.8 | 830.9 | 834.1 | 837.2 | 840.3 | 843.4 | 846.6 | 849.7 | 2.100 |
| 2.200 | 849.7 | 852.8 | 855.9 | 859.1 | 862.2 | 865.3 | 868.4 | 871.5 | 874.7 | 877.8 | 880.9 | 2.200 |
| 2.300 | 880.9 | 884.0 | 887.2 | 890.3 | 893.4 | 896.6 | 899.7 | 902.8 | 906.0 | 909.1 | 912.2 | 2.300 |
| 2.400 | 912.2 | 915.3 | 918.4 | 921.5 | 924.6 | 927.7 | 930.8 | 933.8 | 936.9 | 940.0 | 943.1 | 2.400 |
| 2.500 | 943.1 | 946.2 | 949.3 | 952.4 | 955.5 | 958.6 | 961.7 | 964.8 | 967.9 | 971.0 | 974.1 | 2.500 |
| 2.600 | 974.1 | 977.2 | 980.3 | 983.3 | 986.4 | 989.5 | 992.6 | 995.7 | 998.7 | 1001.8 | 1004.9 | 2.600 |
| 2.700 | 1004.9 | 1008.0 | 1011.1 | 1014.2 | 1017.3 | 1020.3 | 1023.4 | 1026.5 | 1029.6 | 1032.7 | 1035.8 | 2.700 |
| 2.800 | 1035.8 | 1038.9 | 1042.0 | 1045.1 | 1048.2 | 1051.3 | 1054.4 | 1057.4 | 1060.5 | 1063.6 | 1066.7 | 2.800 |
| 2.900 | 1066.7 | 1069.8 | 1072.8 | 1075.9 | 1078.9 | 1082.0 | 1085.1 | 1088.1 | 1091.2 | 1094.2 | 1097.3 | 2.900 |
| 3.000 | 1097.3 | 1100.4 | 1103.4 | 1106.5 | 1109.6 | 1112.7 | 1115.8 | 1118.9 | 1122.0 | 1125.1 | 1128.2 | 3.000 |
| 3.100 | 1128.2 | 1131.3 | 1134.4 | 1137.5 | 1140.6 | 1143.7 | 1146.8 | 1149.9 | 1153.0 | 1156.1 | 1159.2 | 3.100 |
| 3.200 | 1159.2 | 1162.3 | 1165.4 | 1168.5 | 1171.6 | 1174.7 | 1177.8 | 1180.9 | 1184.1 | 1187.2 | 1190.3 | 3.200 |
| 3.300 | 1190.3 | 1193.4 | 1196.4 | 1199.5 | 1202.5 | 1205.6 | 1208.6 | 1211.7 | 1214.8 | 1217.8 | 1220.9 | 3.300 |
| 3.400 | 1220.9 | 1224.0 | 1227.1 | 1230.2 | 1233.3 | 1236.4 | 1239.5 | 1242.6 | 1245.7 | 1248.8 | 1251.9 | 3.400 |
| 3.500 | 1251.9 | 1255.0 | 1258.1 | 1261.2 | 1264.4 | 1267.5 | 1270.6 | 1273.7 | 1276.8 | 1280.0 | 1283.1 | 3.500 |
| 3.600 | 1283.1 | 1286.2 | 1289.4 | 1292.5 | 1295.6 | 1298.7 | 1301.9 | 1305.0 | 1308.1 | 1311.3 | 1314.4 | 3.600 |
| 3.700 | 1314.4 | 1317.5 | 1320.6 | 1323.8 | 1326.9 | 1330.0 | 1333.1 | 1336.2 | 1339.4 | 1342.5 | 1345.6 | 3.700 |
| 3.800 | 1345.6 | 1348.7 | 1351.8 | 1355.0 | 1358.1 | 1361.2 | 1364.3 | 1367.5 | 1370.6 | 1373.8 | 1376.9 | 3.800 |
| 3.900 | 1376.9 | 1380.1 | 1383.2 | 1386.4 | 1389.6 | 1392.8 | 1395.9 | 1399.1 | 1402.3 | 1405.5 | 1408.7 | 3.900 |
| *Millivolts* | .000 | .010 | .020 | .030 | .040 | .050 | .060 | .070 | .080 | .090 | .100 | *Millivolts* |

TABLE III-A. *Forty percent iridium-60 percent rhodium versus iridium thermocouples*—Continued

Electromotive force in absolute millivolts. Temperature in degrees F (Int. 1948). Reference junction at 32 °F.

| *Millivolts* | .000 | .010 | .020 | .030 | .040 | .050 | .060 | .070 | .080 | .090 | .100 | *Millivolts* |
|---|---|---|---|---|---|---|---|---|---|---|---|---|
| 4.000 | 1408.7 | 1411.9 | 1415.1 | 1418.3 | 1421.5 | 1424.7 | 1427.9 | 1431.0 | 1434.2 | 1437.4 | 1440.6 | 4.000 |
| 4.100 | 1440.6 | 1443.8 | 1446.9 | 1450.1 | 1453.2 | 1456.4 | 1459.6 | 1462.7 | 1465.9 | 1469.0 | 1472.2 | 4.100 |
| 4.200 | 1472.2 | 1475.4 | 1478.6 | 1481.8 | 1485.0 | 1488.2 | 1491.4 | 1494.6 | 1497.8 | 1501.0 | 1504.2 | 4.200 |
| 4.300 | 1504.2 | 1507.4 | 1510.6 | 1513.8 | 1517.0 | 1520.1 | 1523.3 | 1526.5 | 1529.7 | 1532.9 | 1536.1 | 4.300 |
| 4.400 | 1536.1 | 1539.3 | 1542.5 | 1545.7 | 1548.9 | 1552.1 | 1555.3 | 1558.5 | 1561.7 | 1564.9 | 1568.1 | 4.400 |
| 4.500 | 1568.1 | 1571.3 | 1574.5 | 1577.7 | 1580.9 | 1584.2 | 1587.4 | 1590.6 | 1593.8 | 1597.1 | 1600.3 | 3.500 |
| 4.600 | 1600.3 | 1603.6 | 1606.8 | 1610.1 | 1613.3 | 1616.6 | 1619.9 | 1623.1 | 1626.4 | 1629.6 | 1632.9 | 4.600 |
| 4.700 | 1632.9 | 1636.1 | 1639.4 | 1642.6 | 1645.8 | 1649.1 | 1652.3 | 1655.5 | 1658.7 | 1662.0 | 1665.2 | 4.700 |
| 4.800 | 1665.2 | 1668.4 | 1671.7 | 1674.9 | 1678.2 | 1681.4 | 1684.7 | 1687.9 | 1691.1 | 1694.4 | 1697.7 | 4.800 |
| 4.900 | 1697.7 | 1701.1 | 1704.3 | 1707.6 | 1710.8 | 1714.1 | 1717.4 | 1720.7 | 1724.0 | 1727.3 | 1730.6 | 4.900 |
| 5.000 | 1730.6 | 1733.9 | 1737.1 | 1740.4 | 1743.7 | 1746.9 | 1750.2 | 1753.5 | 1756.8 | 1760.0 | 1763.3 | 5.000 |
| 5.100 | 1763.3 | 1766.6 | 1769.9 | 1773.2 | 1776.5 | 1779.8 | 1783.1 | 1786.4 | 1789.7 | 1793.0 | 1796.3 | 5.100 |
| 5.200 | 1796.3 | 1799.6 | 1802.9 | 1806.2 | 1809.5 | 1812.8 | 1816.1 | 1819.4 | 1822.7 | 1826.0 | 1829.3 | 5.200 |
| 5.300 | 1829.3 | 1832.6 | 1836.0 | 1839.3 | 1842.6 | 1845.9 | 1849.3 | 1852.6 | 1855.9 | 1859.3 | 1862.6 | 5.300 |
| 5.400 | 1862.6 | 1865.9 | 1869.2 | 1872.5 | 1875.9 | 1879.2 | 1882.5 | 1885.8 | 1889.1 | 1892.4 | 1895.7 | 5.400 |
| 5.500 | 1895.7 | 1899.0 | 1902.3 | 1905.6 | 1908.9 | 1912.2 | 1915.5 | 1918.8 | 1922.1 | 1925.4 | 1928.7 | 5.500 |
| 5.600 | 1928.7 | 1932.0 | 1935.3 | 1938.7 | 1942.0 | 1945.3 | 1948.7 | 1952.0 | 1955.3 | 1958.7 | 1962.0 | 5.600 |
| 5.700 | 1962.0 | 1965.3 | 1968.7 | 1972.0 | 1975.3 | 1978.6 | 1982.0 | 1985.3 | 1988.6 | 1992.0 | 1995.3 | 5.700 |
| 5.800 | 1995.3 | 1998.6 | 2002.0 | 2005.3 | 2008.7 | 2012.0 | 2015.3 | 2018.7 | 2022.0 | 2025.4 | 2028.7 | 5.800 |
| 5.900 | 2028.7 | 2032.0 | 2035.4 | 2038.7 | 2042.0 | 2045.3 | 2048.7 | 2052.0 | 2055.3 | 2058.7 | 2062.0 | 5.900 |
| 6.000 | 2062.0 | 2065.3 | 2068.6 | 2072.0 | 2075.3 | 2078.6 | 2082.0 | 2085.3 | 2088.6 | 2092.0 | 2095.3 | 6.000 |
| 6.100 | 2095.3 | 2098.7 | 2102.0 | 2105.4 | 2108.8 | 2112.1 | 2115.5 | 2118.9 | 2122.2 | 2125.6 | 2129.0 | 6.100 |
| 6.200 | 2129.0 | 2132.4 | 2135.7 | 2139.1 | 2142.5 | 2145.9 | 2149.2 | 2152.6 | 2156.0 | 2159.3 | 2162.7 | 6.200 |
| 6.300 | 2162.7 | 2166.0 | 2169.4 | 2172.8 | 2176.1 | 2179.5 | 2182.8 | 2186.2 | 2189.5 | 2192.9 | 2196.2 | 6.300 |
| 6.400 | 2196.2 | 2199.5 | 2202.9 | 2206.2 | 2209.6 | 2212.9 | 2216.3 | 2219.6 | 2223.0 | 2226.3 | 2229.7 | 6.400 |
| 6.500 | 2229.7 | 2233.1 | 2236.5 | 2239.2 | 2243.3 | 2246.7 | 2250.1 | 2253.5 | 2256.9 | 2260.3 | 2263.7 | 6.500 |
| 6.600 | 2263.7 | 2267.1 | 2270.4 | 2273.8 | 2277.2 | 2280.5 | 2283.9 | 2287.2 | 2290.6 | 2293.9 | 2297.3 | 6.600 |
| 6.700 | 2297.3 | 2300.7 | 2304.0 | 2307.4 | 2310.8 | 2314.1 | 2317.5 | 2320.9 | 2324.2 | 2327.6 | 2331.0 | 6.700 |
| 6.800 | 2331.0 | 2334.4 | 2337.7 | 2341.1 | 2344.5 | 2347.9 | 2351.2 | 2354.6 | 2358.0 | 2361.3 | 2364.7 | 6.800 |
| 6.900 | 2364.7 | 2368.1 | 2371.4 | 2374.8 | 2378.1 | 2381.5 | 2384.9 | 2388.2 | 2391.6 | 2394.9 | 2398.3 | 6.900 |
| 7.000 | 2398.3 | 2401.7 | 2405.0 | 2408.4 | 2411.8 | 2415.2 | 2418.5 | 2421.9 | 2425.3 | 2428.6 | 2432.0 | 7.000 |
| 7.100 | 2432.0 | 2435.3 | 2438.7 | 2442.0 | 2445.3 | 2448.7 | 2452.0 | 2455.3 | 2458.6 | 2462.0 | 2465.3 | 7.100 |
| 7.200 | 2465.3 | 2468.6 | 2472.0 | 2475.3 | 2478.7 | 2482.0 | 2485.4 | 2488.7 | 2492.0 | 2495.4 | 2498.7 | 7.200 |
| 7.300 | 2498.7 | 2502.0 | 2505.3 | 2508.6 | 2511.9 | 2515.2 | 2518.5 | 2521.8 | 2525.1 | 2528.4 | 2531.7 | 7.300 |
| 7.400 | 2531.7 | 2535.0 | 2538.3 | 2541.6 | 2544.9 | 2548.2 | 2551.5 | 2554.8 | 2558.1 | 2561.4 | 2564.7 | 7.400 |
| 7.500 | 2564.7 | 2568.0 | 2571.3 | 2574.6 | 2577.9 | 2581.2 | 2584.5 | 2587.8 | 2591.1 | 2594.4 | 2597.7 | 7.500 |
| 7.600 | 2597.7 | 2601.0 | 2604.2 | 2607.5 | 2610.8 | 2614.0 | 2617.3 | 2620.5 | 2623.8 | 2627.0 | 2630.3 | 7.600 |
| 7.700 | 2630.3 | 2633.6 | 2636.8 | 2640.0 | 2643.3 | 2646.6 | 2649.9 | 2653.1 | 2656.4 | 2659.6 | 2662.9 | 7.700 |
| 7.800 | 2662.9 | 2666.2 | 2669.4 | 2672.7 | 2676.0 | 2679.2 | 2682.5 | 2685.7 | 2689.0 | 2692.2 | 2695.5 | 7.800 |
| 7.900 | 2695.5 | 2698.7 | 2702.0 | 2705.2 | 2708.4 | 2711.6 | 2714.9 | 2718.1 | 2721.3 | 2724.5 | 2727.7 | 7.900 |
| 8.000 | 2727.7 | 2730.9 | 2734.1 | 2737.3 | 2740.5 | 2743.7 | 2746.9 | 2750.1 | 2753.3 | 2756.5 | 2759.7 | 8.000 |
| 8.100 | 2759.7 | 2762.9 | 2766.0 | 2769.2 | 2772.3 | 2775.5 | 2778.6 | 2781.8 | 2784.9 | 2788.1 | 2791.2 | 8.100 |
| 8.200 | 2791.2 | 2794.3 | 2797.5 | 2800.6 | 2803.7 | 2806.9 | 2810.0 | 2813.1 | 2816.2 | 2819.4 | 2822.5 | 8.200 |
| 8.300 | 2822.5 | 2825.6 | 2828.8 | 2831.9 | 2835.0 | 2838.2 | 2841.3 | 2844.5 | 2847.6 | 2850.7 | 2853.9 | 8.300 |
| 8.400 | 2853.9 | 2857.1 | 2860.2 | 2863.4 | 2866.6 | 2869.7 | 2872.9 | 2876.1 | 2879.3 | 2882.4 | 2885.6 | 8.400 |
| 8.500 | 2885.6 | 2888.7 | 2891.9 | 2895.0 | 2898.2 | 2901.3 | 2904.5 | 2907.6 | 2910.8 | 2913.9 | 2917.1 | 8.500 |
| 8.600 | 2917.1 | 2920.3 | 2923.5 | 2926.7 | 2929.9 | 2933.0 | 2936.2 | 2939.4 | 2942.6 | 2945.8 | 2949.0 | 8.600 |
| 8.700 | 2949.0 | 2952.2 | 2955.3 | 2958.5 | 2961.7 | 2964.8 | 2968.0 | 2971.1 | 2974.3 | 2977.4 | 2980.6 | 8.700 |
| 8.800 | 2980.6 | 2983.8 | 2986.9 | 2990.1 | 2993.3 | 2996.4 | 2999.6 | 3002.7 | 3005.9 | 3009.1 | 3012.2 | 8.800 |
| 8.900 | 3012.2 | 3015.3 | 3018.5 | 3021.6 | 3024.7 | 3027.8 | 3030.9 | 3034.1 | 3037.2 | 3040.3 | 3043.4 | 8.900 |
| 9.000 | 3043.4 | 3046.5 | 3049.7 | 3052.8 | 3055.9 | 3059.1 | 3062.2 | 3065.3 | 3068.5 | 3071.6 | 3074.7 | 9.000 |
| 9.100 | 3074.7 | 3077.8 | 3080.9 | 3084.0 | 3087.1 | 3090.2 | 3093.3 | 3096.3 | 3099.4 | 3102.5 | 3105.6 | 9.100 |
| 9.200 | 3105.6 | 3108.7 | 3111.8 | 3114.9 | 3118.0 | 3121.1 | 3124.2 | 3127.3 | 3130.4 | 3133.5 | 3136.6 | 9.200 |
| 9.300 | 3136.6 | 3139.7 | 3142.7 | 3145.8 | 3148.9 | 3151.9 | 3155.0 | 3158.0 | 3161.1 | 3164.2 | 3167.2 | 9.300 |
| 9.400 | 3167.2 | 3170.2 | 3173.3 | 3176.3 | 3179.4 | 3182.4 | 3185.5 | 3188.5 | 3191.5 | 3194.6 | 3197.6 | 9.400 |
| 9.500 | 3197.6 | 3200.6 | 3203.7 | 3206.7 | 3209.7 | 3212.8 | 3215.8 | 3218.8 | 3221.8 | 3224.9 | 3227.9 | 9.500 |
| 9.600 | 3227.9 | 3230.9 | 3234.0 | 3237.0 | 3240.0 | 3243.0 | 3246.1 | 3249.1 | 3252.1 | 3255.2 | 3258.2 | 9.600 |
| 9.700 | 3258.2 | 3261.2 | 3264.3 | 3267.3 | 3270.4 | 3273.4 | 3276.4 | 3279.4 | 3282.5 | 3285.5 | 3288.5 | 8.700 |
| 9.800 | 3288.5 | 3291.5 | 3294.5 | 3297.4 | 3300.4 | 3303.4 | 3306.4 | 3309.3 | 3312.3 | 3315.2 | 3318.2 | 9.800 |
| 9.900 | 3318.2 | 3321.2 | 3324.1 | 3327.1 | 3330.1 | 3333.0 | 3336.0 | 3339.0 | 3342.0 | 3344.9 | 3347.9 | 9.900 |
| *Millivolts* | .000 | .010 | .020 | .030 | .040 | .050 | .060 | .070 | .080 | .090 | .100 | *Millivolts* |

TABLE III-A. *Forty percent iridium-60 percent rhodium versus iridium thermocouples*—Continued

Electromotive force in absolute millivolts. Temperature in degrees F (Int. 1948). Reference junction at 32 °F.

| Millivolts | .000 | .010 | .020 | .030 | .040 | .050 | .060 | .070 | .080 | .090 | .100 | Millivolts |
|---|---|---|---|---|---|---|---|---|---|---|---|---|
| 10.000 | 3347.9 | 3350.9 | 3353.8 | 3356.8 | 3359.8 | 3362.8 | 3365.7 | 3368.7 | 3371.7 | 3374.6 | 3377.6 | 10.000 |
| 10.100 | 3377.6 | 3380.6 | 3383.5 | 3386.5 | 3389.4 | 3392.4 | 3395.3 | 3398.3 | 3401.2 | 3404.2 | 3407.1 | 10.100 |
| 10.200 | 3407.1 | 3410.0 | 3413.0 | 3415.9 | 3418.8 | 3421.7 | 3424.7 | 3427.6 | 3430.5 | 3433.4 | 3436.3 | 10.200 |
| 10.300 | 3436.3 | 3439.2 | 3442.1 | 3444.9 | 3447.8 | 3450.7 | 3453.5 | 3456.4 | 3459.3 | 3462.1 | 3465.0 | 10.300 |
| 10.400 | 3465.0 | 3467.9 | 3470.7 | 3473.6 | 3476.5 | 3479.4 | 3482.2 | 3485.1 | 3488.0 | 3490.8 | 3493.7 | 10.400 |
| 10.500 | 3493.7 | 3496.6 | 3499.4 | 3502.3 | 3505.1 | 3508.0 | 3510.8 | 3513.7 | 3516.5 | 3519.4 | 3522.2 | 10.500 |
| 10.600 | 3522.2 | 3525.0 | 3527.8 | 3530.7 | 3533.5 | 3536.3 | 3539.1 | 3541.9 | 3544.7 | 3547.5 | 3550.3 | 10.600 |
| 10.700 | 3550.3 | 3553.1 | 3555.9 | 3558.7 | 3561.4 | 3564.2 | 3567.0 | 3569.8 | 3572.6 | 3575.3 | 3578.1 | 10.700 |
| 10.800 | 3578.1 | 3580.9 | 3583.7 | 3586.4 | 3589.2 | 3592.0 | 3594.7 | 3597.5 | 3600.3 | 3603.0 | 3605.8 | 10.800 |
| 10.900 | 3605.8 | 3608.6 | 3611.3 | 3614.1 | 3616.8 | 3619.6 | 3622.3 | 3625.1 | 3627.8 | 3630.6 | 3633.3 | 10.900 |
| 11.000 | 3633.3 | 3636.0 | 3638.8 | 3641.5 | 3644.3 | 3647.0 | 3649.8 | 3652.5 | 3655.3 | 3658.0 | 3660.8 | 11.000 |
| 11.100 | 3660.8 | 3663.6 | 3666.3 | 3669.1 | 3671.8 | 3674.6 | 3677.3 | 3680.1 | 3682.8 | 3685.6 | 3688.3 | 11.100 |
| 11.200 | 3688.3 | 3691.0 | 3693.7 | 3696.4 | 3699.1 | 3701.8 | 3704.5 | 3707.3 | 3710.0 | 3712.7 | 3715.4 | 11.200 |
| 11.300 | 3715.4 | 3718.2 | 3720.9 | 3723.7 | 3726.4 | 3729.2 | 3732.0 | 3734.7 | 3737.5 | 3740.2 | 3743.0 | 11.300 |
| 11.400 | 3743.0 | 3745.7 | 3748.5 | 3751.2 | 3754.0 | 3756.7 | 3759.4 | 3762.1 | 3764.9 | 3767.6 | 3770.3 | 11.400 |
| 11.500 | 3770.3 | 3773.0 | 3775.7 | 3778.4 | 3781.1 | 3783.8 | 3786.5 | 3789.2 | 3791.9 | 3794.6 | 3797.3 | 11.500 |
| 11.600 | 3797.3 | 3800.0 | | | | | | | | | | |
| *Millivolts* | .000 | .010 | .020 | .030 | .040 | .050 | .060 | .070 | .080 | .090 | .100 | *Millivolts* |

TABLE IV-A. *Forty percent iridium-60 percent rhodium versus iridium thermocouples*

Electromotive force in absolute millivolts. Temperature in degrees F (Int. 1948). Reference junction at 32 °F.

| °F | 0 | 10 | 20 | 30 | 40 | 50 | 60 | 70 | 80 | 90 | 100 | °F |
|---|---|---|---|---|---|---|---|---|---|---|---|---|
| 0 | | | | | 0.015 | 0.032 | 0.050 | 0.068 | 0.087 | 0.106 | 0.126 | 0 |
| 100 | 0.126 | 0.146 | 0.166 | 0.186 | .206 | .277 | .249 | .271 | .293 | .315 | .337 | 100 |
| 200 | .337 | .360 | .383 | .406 | .430 | .454 | .478 | .502 | .526 | .551 | .576 | 200 |
| 300 | .576 | .602 | .627 | .653 | .679 | .706 | .732 | .759 | .786 | .813 | .840 | 300 |
| 400 | .840 | .868 | .895 | .923 | .951 | .979 | 1.007 | 1.036 | 1.064 | 1.093 | 1.122 | 400 |
| 500 | 1.122 | 1.151 | 1.180 | 1.209 | 1.239 | 1.268 | 1.298 | 1.328 | 1.358 | 1.388 | 1.418 | 500 |
| 600 | 1.418 | 1.449 | 1.480 | 1.510 | 1.541 | 1.571 | 1.602 | 1.633 | 1.664 | 1.695 | 1.726 | 600 |
| 700 | 1.726 | 1.757 | 1.788 | 1.820 | 1.851 | 1.883 | 1.915 | 1.946 | 1.978 | 2.010 | 2.041 | 700 |
| 800 | 2.041 | 2.073 | 2.105 | 2.137 | 2.169 | 2.201 | 2.233 | 2.265 | 2.297 | 2.329 | 2.361 | 800 |
| 900 | 2.361 | 2.393 | 2.425 | 2.458 | 2.490 | 2.522 | 2.554 | 2.587 | 2.619 | 2.652 | 2.684 | 900 |
| 1000 | 2.684 | 2.717 | 2.749 | 2.781 | 2.814 | 2.846 | 2.878 | 2.911 | 2.943 | 2.976 | 3.009 | 1000 |
| 1100 | 3.009 | 3.041 | 3.073 | 3.106 | 3.138 | 3.170 | 3.203 | 3.235 | 3.267 | 3.299 | 3.332 | 1100 |
| 1200 | 3.332 | 3.365 | 3.397 | 3.429 | 3.461 | 3.494 | 3.526 | 3.558 | 3.590 | 3.622 | 3.654 | 1200 |
| 1300 | 3.654 | 3.686 | 3.718 | 3.750 | 3.782 | 3.814 | 3.846 | 3.878 | 3.910 | 3.941 | 3.973 | 1300 |
| 1400 | 3.973 | 4.004 | 4.036 | 4.067 | 4.098 | 4.130 | 4.162 | 4.193 | 4.225 | 4.256 | 4.287 | 1400 |
| 1500 | 4.287 | 4.318 | 4.349 | 4.381 | 4.412 | 4.443 | 4.474 | 4.506 | 4.537 | 4.568 | 4.599 | 1500 |
| 1600 | 4.599 | 4.629 | 4.660 | 4.691 | 4.722 | 4.753 | 4.784 | 4.815 | 4.846 | 4.876 | 4.907 | 1600 |
| 1700 | 4.907 | 4.937 | 4.968 | 4.998 | 5.029 | 5.060 | 5.090 | 5.120 | 5.150 | 5.181 | 5.211 | 1700 |
| 1800 | 5.211 | 5.242 | 5.272 | 5.302 | 5.332 | 5.362 | 5.392 | 5.423 | 5.453 | 5.483 | 5.513 | 1800 |
| 1900 | 5.513 | 5.543 | 5.574 | 5.604 | 5.634 | 5.664 | 5.694 | 5.724 | 5.754 | 5.784 | 5.814 | 1900 |
| 2000 | 5.814 | 5.844 | 5.874 | 5.904 | 5.934 | 5.964 | 5.994 | 6.024 | 6.054 | 6.084 | 6.114 | 2000 |
| 2100 | 6.114 | 6.143 | 6.173 | 6.203 | 6.233 | 6.263 | 6.292 | 6.322 | 6.352 | 6.382 | 6.411 | 2100 |
| 2200 | 6.411 | 6.441 | 6.471 | 6.501 | 6.530 | 6.560 | 6.589 | 6.619 | 6.648 | 6.678 | 6.708 | 2200 |
| 2300 | 6.708 | 6.738 | 6.767 | 6.797 | 6.827 | 6.857 | 6.886 | 6.916 | 6.946 | 6.976 | 7.005 | 2300 |
| 2400 | 7.005 | 7.035 | 7.064 | 7.094 | 7.124 | 7.154 | 7.184 | 7.214 | 7.244 | 7.274 | 7.304 | 2400 |
| 2500 | 7.304 | 7.334 | 7.364 | 7.395 | 7.425 | 7.455 | 7.486 | 7.516 | 7.547 | 7.577 | 7.607 | 2500 |
| 2600 | 7.607 | 7.638 | 7.669 | 7.699 | 7.730 | 7.760 | 7.791 | 7.822 | 7.853 | 7.883 | 7.914 | 2600 |
| 2700 | 7.914 | 7.945 | 7.976 | 8.007 | 8.039 | 8.070 | 8.101 | 8.133 | 8.164 | 8.196 | 8.228 | 2700 |
| 2800 | 8.228 | 8.260 | 8.292 | 8.324 | 8.356 | 8.388 | 8.419 | 8.451 | 8.482 | 8.514 | 8.545 | 2800 |
| 2900 | 8.545 | 8.577 | 8.608 | 8.640 | 8.672 | 8.703 | 8.735 | 8.767 | 8.798 | 8.830 | 8.862 | 2900 |
| 3000 | 8.862 | 8.893 | 8.925 | 8.957 | 8.989 | 9.021 | 9.053 | 9.085 | 9.117 | 9.149 | 9.182 | 3000 |
| 3100 | 9.182 | 9.214 | 9.246 | 9.279 | 9.311 | 9.344 | 9.377 | 9.409 | 9.442 | 9.475 | 9.508 | 3100 |
| 3200 | 9.508 | 9.541 | 9.574 | 9.607 | 9.640 | 9.673 | 9.706 | 9.739 | 9.772 | 9.805 | 9.839 | 3200 |
| 3300 | 9.839 | 9.873 | 9.906 | 9.940 | 9.973 | 10.007 | 10.041 | 10.075 | 10.108 | 10.142 | 10.176 | 3300 |
| 3400 | 10.176 | 10.210 | 10.244 | 10.278 | 10.313 | 10.348 | 10.383 | 10.417 | 10.452 | 10.487 | 10.522 | 3400 |
| 3500 | 10.522 | 10.557 | 10.592 | 10.628 | 10.663 | 10.699 | 10.735 | 10.771 | 10.807 | 10.843 | 10.879 | 3500 |
| 3600 | 10.879 | 10.915 | 10.951 | 10.988 | 11.024 | 11.061 | 11.097 | 11.133 | 11.170 | 11.206 | 11.243 | 3600 |
| 3700 | 11.243 | 11.280 | 11.317 | 11.353 | 11.389 | 11.426 | 11.462 | 11.499 | 11.536 | 11.573 | 11.610 | 3700 |
| 3800 | 11.610 | | | | | | | | | | | 3800 |
| °F | 0 | 10 | 20 | 30 | 40 | 50 | 60 | 70 | 80 | 90 | 100 | °F |

TABLE V–A. *Thermal emf of iridium versus platinum 27*

Reference junction at 32 °F.

| °F | mv | °F | mv |
|---|---|---|---|
| 32 | 0 | 1300 | 7.729 |
| 100 | 0.227 | 1350 | 8.158 |
| 150 | .413 | 1400 | 8.596 |
| 200 | .616 | 1450 | 9.043 |
| 250 | .834 | 1500 | 9.499 |
| 300 | 1.066 | 1550 | 9.964 |
| 350 | 1.310 | 1600 | 10.437 |
| 400 | 1.565 | 1650 | 10.919 |
| 450 | 1.830 | 1700 | 11.410 |
| 500 | 2.105 | 1750 | 11.910 |
| 550 | 2.390 | 1800 | 12.419 |
| 600 | 2.685 | 1850 | 12.936 |
| 650 | 2.988 | 1900 | 13.460 |
| 700 | 3.299 | 1950 | 13.992 |
| 750 | 3.619 | 2000 | 14.532 |
| 800 | 3.947 | 2050 | 15.079 |
| 850 | 4.284 | 2100 | 15.632 |
| 900 | 4.630 | 2150 | 16.190 |
| 950 | 4.985 | 2200 | 16.753 |
| 1000 | 5.349 | 2250 | 17.321 |
| 1050 | 5.723 | 2300 | 17.893 |
| 1100 | 6.106 | 2350 | 18.469 |
| 1150 | 6.498 | 2400 | 19.048 |
| 1200 | 6.899 | 2450 | 19.629 |
| 1250 | 7.309 | 2500 | 20.211 |

TABLE VI–A. *Thermal emf of 40 percent iridum-60 percent rhodium versus copper and copper versus iridium thermocouples*

Reference junction at 32 °F.

| °F | 40% Ir-60% Rh vs Cu | Cu vs Ir |
|---|---|---|
| | mv | mv |
| 32 | 0.000 | 0.000 |
| 50 | .026 | .006 |
| 75 | .064 | .014 |
| 100 | .103 | .023 |
| 125 | .141 | .035 |
| 150 | .178 | .049 |
| 175 | .217 | .065 |
| 200 | .253 | .084 |
| 225 | .289 | .105 |
| 250 | .325 | .129 |
| 275 | .359 | .155 |
| 300 | .392 | .184 |
| 350 | .459 | .247 |
| 400 | .525 | .315 |
| 450 | .584 | .395 |
| 500 | .637 | .485 |

(Paper 66C1-81)

JOURNAL OF RESEARCH of the National Bureau of Standards—C. Engineering and Instrumentation
Vol. 66C, No. 1, January–March 1962

# A Method for the Self-Calibration of Attenuation-Measuring Systems*

Robert L. Peck

(August 4, 1961)

The theory and experimental procedures are given for the self-calibration of insertion loss or attenuation-measuring systems. Four circuit configurations are developed. The calibrations may be obtained by simple graphical means or by an analytical solution. Experimental results are given which demonstrate that, by using the techniques outlined, attenuation calibrations of high accuracy may be made without reference to any previously calibrated attenuator.

## 1. Introduction

The feasibility of self-calibrating attenuators has been demonstrated previously by Allred [1, 2][1] and by Laverick [3]. They have shown that it is not necessary to use any reference standard and that only a signal source, a signal null indicator, and a suitable arrangement of transmission-line components are required.

Allred has described a three-branch system for obtaining the phase as well as the magnitude of the attenuation coefficients of two piston attenuators operating with the $TE_{11}$ evanescent mode. This is done by obtaining a set of dial readings from the two attenuators, one in series with a fixed phase shifter constituting one branch and the other constituting the second branch. The third branch contains an adjustable phase shifter and a two-position step attenuator. With any initial setting of the adjustable phase shifter, the two attenuators are adjusted for a null. The step attenuator is then changed, and the attenuators are again adjusted for a null. This operation is repeated as the adjustable phase shifter is set successively to different values. From the knowledge that in each case the step attenuator has undergone the same change in attenuation and phase for each set of measurements, a series of equalities of the form

$$K=\frac{e^{-\gamma_y Y_a}+We^{-\gamma_z Z_a}}{e^{-\gamma_y Y_b}+We^{-\gamma_z Z_b}}$$

is obtained, where $K$ is the complex insertion ratio of the step attenuator, $\gamma_y$ and $\gamma_z$ are the propagation constants of each of the two piston attenuators, $W$ is a separately evaluated constant expressing the relative magnitudes and phase angles of the output voltages of the two attenuators, and $Y_a$, $Y_b$, $Z_a$, $Z_b$ are dial readings of the attenuator. These expressions can then be solved for the unknown parameters of the two attenuators.

Laverick's method uses a three-branch system with switches for opening two of the branches. Two of the branches contain phase shifters to set these branches 180° out of phase with the third. The three branches are then adjusted for equal output by successively nulling one branch against one of the other two. All three branches are then connected together, and one of the attenuators is reset for a new null. This corresponds to a 6.02 db change in attenuation. Repeating the operation yields attenuation steps of 3.52 db, 2.50 db, etc.

A new method for the self-calibration of the change in insertion loss of continuously variable attenuation-measuring systems is described in this paper. This method requires two basic operations. The first operation yields the law of attenuation, $A=af(l)$, where $a$ is the attenuation coefficient and $f(l)$ is a function of the adjustment parameter, $l$, which makes $a$ a constant. The second operation yields the attenuation coefficient, $a$. The method is applicable to four different circuit configurations which are described in the order of their decreasing dependency upon component stabilities. Circuit 1 (fig. 1) is a single-channel system using the conventional series-substitution circuit. It requires a reasonably stable generator and monitor. The monitor can be of the differential-voltage type, but must be linear over the range to be used.

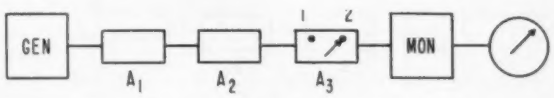


FIGURE 1. *Simple series substitution circuit.*

*Contribution from the Radio Standards Laboratory, National Bureau of Standards, Boulder, Colo.

[1] Figures in brackets indicate the literature references at the end of this paper.

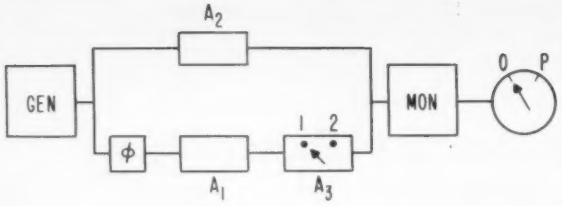


FIGURE 2. *Parallel substitution circuit.*

The second circuit (fig. 2) is the common parallel substitution circuit. It requires a reasonably stable generator and monitor, but the monitor does not need to be linear.

The third circuit (fig. 3) is similar to that used by Laverick, with the exception that only one switch is used. This circuit minimizes the effect of generator-power and monitor-gain variations. The upper branch must be isolated from the other two branches to prevent an impedance change at their junction when the switch is opened or closed (40 db isolation is generally sufficient). The fourth circuit is similar to that in figure 3, but with the switch removed and the attenuator $A_4$ replaced by a step attenuator. It then resembles the circuit used by Allred. The accuracy obtainable with this circuit is limited by the resolution and reproducibility of the attenuator dial, by the sharpness of the voltage null obtainable on the monitor, and by the time stability of components. It is essentially independent of generator and monitor variations. If the phase shift of the unknown attenuator depends upon its setting, the variations in insertion loss of the phase shifters must be known.

The methods of Allred and Laverick have limitations as well as advantages compared to the method described in this paper. Allred's method yields the complex attenuation coefficient, but the equations involved are quite difficult to solve. Laverick's method yields fixed 6.02 db and other smaller steps without calculations. The method described here yields only the magnitude of the attenuation coefficient, but it is easy to apply and is not affected by fixed-impedance mismatches in the system.

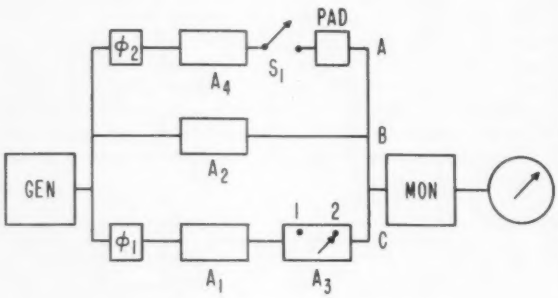


FIGURE 3. *Three-leg substitution circuit.*

It is to be noted that in all three systems the calibration is good only as long as the attenuators are connected to constant-impedance lines. If the impedances are varied, the calibration changes. Also, in the use of any calibrated system for calibrating other attenuators, the unknown attenuator must be matched to its characteristic impedance within the system.

## 2. Theory

The change in attenuation of an adjustable attenuator in a matched system may be defined as $A=20 \log |V_{01}|/|V_{02}|$, where $A$ is in decibels, $V_{01}$ is the output voltage of the network for the initial dial setting $l_0$, and $V_{02}$ is the output voltage corresponding to the dial setting $l_1$. Since the attenuation (or insertion loss) is determined by a ratio, it is dimensionless, and hence no absolute units of voltage or other absolute units of measurement are required for its determination.

The simplest method of calibrating an attenuator would be to connect the attenuator to a voltage source of the proper frequency and to use a monitor which has an output reading proportional to the input voltage for indicating the voltage output of the attenuator. The monitor reading would be recorded as a function of the dial reading, $l$, of the attenuator. In this case the change in attenuation corresponding to two attenuator dial readings would be

$$\Delta A=20 \log \left|\frac{GV_1}{GV_2}\right|=20 \log \left|\frac{V_1}{V_2}\right| \qquad (1)$$

where $V_1$ is the monitor reading for one attenuator dial setting, $l_1$; $V_2$ is the monitor reading for another dial setting, $l_2$; and $G$ is the unknown proportionality factor of the monitor. This method, however, is impractical, since it is difficult to obtain a high-resolution, high-gain linear monitor without a residual voltage output.

One practical monitor, which could be used with the circuit of figure 1, is a linear voltmeter. This type of voltmeter normally has an expanded scale for high resolution, and its indicated voltage, $V$, is equal to $G(V_{in}+V_0)$ where $G$ is the unknown gain, $V_{in}$ is the input voltage, and $V_0$ some constant but unknown equivalent input voltage. Because of the unknown term, $V_0$, the attenuation cannot be calculated directly as in eq (1). However, it will be shown that $V_0$ need not be known.

The monitor reading $V$ can be graphed as a function of the dial reading of the attenuator over any desired range. This plot of voltage as a function of $l$ is then compared to a corresponding plot of attenuation arbitrary units as a function of $l$ over the same range (fig. 4). This curve can be obtained by stepping off some unknown fixed attenuation, $\Delta A$, and by obtaining corresponding dial readings as in section 3. This process yields a series of dial readings with equal but unknown attenuation steps, $\Delta A$, between each set of readings. These readings can be plotted and a smoothed curve drawn.

From the $A$ scale in figure 4, two equal attenuation steps are chosen. For simplicity two adjacent steps

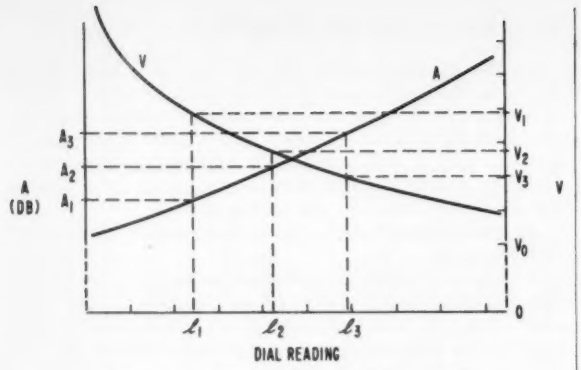


FIGURE 4. *Voltage and attenuation curves.*

are used such that

$$A_3-A_2=A_2-A_1.$$

To $A_1$ there corresponds the dial reading $l_1$, to $A_2$ the dial reading $l_2$, and to $A_3$ the dial reading $l_3$. For each of these dial readings there are corresponding points on the $V$ scale, $V_1$, $V_2$, and $V_3$. Since the two attenuation steps are equal,

$$A_3-A_2=20\log\left[\frac{G(V_3+V_0)}{G(V_2+V_0)}\right]$$

$$=A_2-A_1=20\log\left[\frac{G(V_2+V_0)}{G(V_1+V_0)}\right]. \quad (2)$$

Assuming $G$ constant, eliminating $V_0$, and substituting into the expression for $A_3-A_2$ or $A_2-A_1$ gives

$$A_2-A_1=A_3-A_2=20\log\left(\frac{V_2-V_3}{V_1-V_2}\right). \quad (3)$$

Thus the chosen increments of attenuation can be expressed in terms of the corresponding voltage increments, without regard to the equivalent input voltage, $V_0$, of the monitor. This process may be repeated to give the calibration of the attenuator, over the desired portion of its range, to an accuracy limited only by the accuracy of the experimental data points and the precision with which the graphical analysis is made.

Increased accuracy of data may be obtained by use of the circuits of figures 2 or 3 where $A_2$ and/or $A_1$ are to be calibrated. The plot of attenuation in arbitrary units as a function of dial setting is obtained essentially as before. However, the voltage curve is obtained in a different manner, and the monitor is used only as a null indicator. The principle can be understood by referring to figures 3 and 5. In figure 3, $A_1$ and $A_2$ are continuously variable attenuators, and $A_4$ is a fixed attenuator, the output voltage of which determines the size of the incremental voltage step, $\Delta V$. $A_3$ is a two-position attenuator used only for stepping off equal $\Delta A$ steps for obtaining the $A$ curve. $\phi_1$ and $\phi_2$ are phase shifters, set so that the voltages from branches $A$ and $C$ are

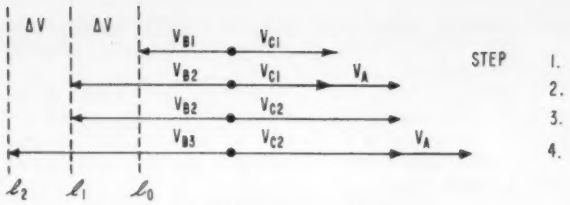


FIGURE 5. *Addition of equal voltage increments.*

continuously in phase but 180° out of phase with the voltage from branch $B$. The process by which the voltage curve is obtained may be clarified by reference to figure 5, which depicts the voltage outputs of the various branches of the circuit. Here, for simplicity, the letters denoting the particular branch are used to denote the voltage output of that branch. Initially branches $B$ and $C$ are nulled with the switch open, and the initial dial reading $l_0$ of $A_2$ is recorded. The switch is then closed, adding the voltage $V_A$ to $V_{C1}$. A new null is achieved by adjusting $\phi_1$ and advancing the dial of $A_2$ to $l_1$ so that the voltage from branch $B$ equals $V_{C1}+V_A$. The voltage increment, $\Delta V$, in the output of branch $B$, is then equal to $V_A$. The switch is then opened, and a null is again obtained by adjusting $\phi_1$ and advancing $A_1$ so that $V_{C2}=V_{B2}$. The switch is closed, $\phi_2$ adjusted, and the dial of $A_2$ advanced to $l_3$, so that again $V_{B3}=V_{C2}+V_A$. Thus another voltage increment, $\Delta V$, has been added to the output of $A_2$. The operation is continued until the desired range of $A_2$ has been covered.

From the data thus obtained, the voltage curve (curve $V$, figure 4) can be plotted. The unit of voltage is the arbitrary voltage step $\Delta V$, and the initial voltage, $V_0$, corresponding to the dial setting $l_0$ of $A_2$ is unknown. However, eq (3) and the discussion of it still apply. Thus, a monitor indicating only a null can be used to obtain voltage ratios, and the calibration of the attenuator, $A_2$, can be obtained as before.

The preceding discussion gave a graphical procedure for calibrating an unknown attenuator. An analysis is now presented in which it is shown that, after the law of attenuation of the attenuator has been obtained, the attenuator can be calibrated by using three dial readings corresponding to two equal steps in the output voltage and by consulting a table which has been computed from a derived equation.

The law of attenuation, $A=af(l)$, can be obtained from comparisons of equal attenuation steps and the corresponding dial readings of the dial of the attenuator to obtain a function of $l$ such that $dA/df(l)=a$, a constant. Integrating this expression gives

$$\Delta A=a\,[f(l_i)-f(l_j)], \quad (4)$$

where $a$ is the attenuation coefficient yet to be determined. This function of $l$ will then yield a straight line when plotted against $A$ as in figure 4. The function $f(l)$ depends upon the type of attenuator used. For piston-type attenuators ideally matched, $f(l)=l$ and for unmatched piston-type attenuators

with normal insertion losses $f(l)$ closely approaches $l$. For rotary-vane attenuators in an ideally matched system, $f(l)=\log \cos^2 l$.

When the attenuator dial setting is changed from $l_i$ to $l_j$, the change in attenuation in then given by eq (4). Further, if $V_i$ and $V_j$ are the output voltages of the attenuator corresponding to the dial settings $l_i$ and $l_j$, then also

$$\Delta A=20 \log \left|\frac{V_i}{V_j}\right|. \tag{5}$$

If $l_o$ is the dial setting corresponding to the output voltage $V_0$, $l_1$ is that corresponding to $V_0+\Delta V$, and $l_2$ is that corresponding to $V_0+2\Delta V$, then the following equations hold:

$$\Delta A_1=\alpha[f(l_0)-f(l_2)]=20 \log \frac{|V_0|}{|V_0+2\Delta V|}$$

$$\Delta A_2=\alpha[f(l_1)-f(l_2)]=20 \log \frac{|V_0+\Delta V|}{|V_0+2\Delta V|}.$$

(It may be noted that $\Delta A_1$ and $\Delta A_2$ are not equal, as was true in the graphical procedure.) If for convenience $V_0$ is written as some multiple, $k$, of the voltage increment ($V_0=k\Delta V$), the equations can be rewritten as

$$\Delta A_1=\alpha[f(l_0)-f(l_2)]=20 \log \frac{k}{k+2}, \tag{6}$$

$$\Delta A_2=\alpha[f(l_1)-f(l_2)]=20 \log \frac{k+1}{k+2}. \tag{7}$$

Dividing the second equation by the first yields

$$\frac{f(l_1)-f(l_2)}{f(l_0)-f(l_2)}=\frac{\log \frac{k+1}{k+2}}{\log \frac{k}{k+2}}. \tag{8}$$

The term on the left side of (8) is the experimentally measured constant, determined by the law of attenuation, the chosen initial dial setting, $l_0$, and the magnitude of $\Delta V$.

A series-approximation method may be used to find the value of $k$ to any desired accuracy, or a table may be obtained from National Bureau of Standards, Electronic Calibration Center, Boulder, Colo., for the direct determination of $k$ to 6-place accuracy from experimental data.

Once $k$ is known, eq (6) may be used to determine $\Delta A_1$ in decibels and also $\alpha$. This step results in the final calibration of the attenuator.

## 3. Experimental Procedures

In this section the detailed procedures are described for using the four circuits to obtain equal attenuation and voltage steps as a function of the dial setting of an attenuator.

### 3.1. Circuit 1

In the simple series-substitution circuit of figure 1, $A_2$ is the continuously variable attenuator to be calibrated. $A_3$ is a step attenuator which may be changed by a fixed amount $\Delta A$, which need not be known. $A_1$ is a continuously adjustable attenuator used for power level control and may be an adjustable output control on the power source.

Attenuation as a function of dial setting is obtained as follows:

1. The attenuator to be calibrated, $A_2$, is set at the lowest desired value of attenuation, with dial reading $l_0$; $A_3$ is set at its higher attenuation, position 2, and $A_1$ is adjusted to give any desired fiducial reading on the output meter.

2. $A_3$ is then set at its lower attenuation position 1, $A_2$ is adjusted to bring the meter to the previously chosen fiducial point, and its dial reading $l_1$ is recorded. The attenuation of $A_2$ has now been increased by an amount $\Delta A$ in advancing the dial from $l_0$ to $l_1$.

3. $A_3$ is reset to position 2, and $A_1$ is adjusted so that the meter again returns to the fiducial point.

4. Steps 2 and 3 are repeated until the desired range of $A_2$ is covered.

Each time the dial reading of $A_2$ is changed, its attenuation is increased by an unknown amount $\Delta A$. The resulting data may be used to plot a curve of attenuation, in unknown units, as a function of dial reading.

Voltage as a function of dial setting is obtained from a monitor which is linear over the range of the output voltage of the attenuator under calibration, or which has an output voltage that can be expressed as $V=G(V_{in}+V_0)$, where $G$ is the constant but unknown gain of the monitor, $V_{in}$ is its input voltage, and $GV_0$ is the residual output voltage. In this case the indicated voltage of the monitor is simply plotted as a function of the dial reading of the attenuator. This is a simple procedure, but the monitor may impose undesirable limitations on the accuracy of the voltage measurement.

### 3.2. Circuit 2

Where increased accuracy is required, the parallel-substitution circuit of figure 2 is used. A phase shifter $\phi$, having constant loss independent of phase shift, has been added to the components of circuit 1. This phase shifter adjusts the voltage output of one branch to be 180° out of phase with the other. Hence the system operates on the null principle. For obtaining the attenuation of $A_2$ as a function of dial reading, the following method is used:

1. With the attenuator to be calibrated, $A_2$, set at the lowest desired value of attenuation $l_0$, and with $A_3$ set for its lower attenuation position 1, $A_1$ and $\phi$ are adjusted for a null reading on the monitor.

2. $A_3$ is set to position 2, $A_2$ is advanced and $\phi$ is adjusted until there is again a null reading on the monitor, and the dial reading $l_1$ is recorded.

3. $A_3$ is returned to position 1, and $A_1$ and $\phi$ are adjusted to obtain a null reading.

4. Steps 2 and 3 are repeated until the desired range of the attenuation of $A_2$ is covered.

For obtaining voltage as a function of dial reading, the following procedure is used:

1. With $A_2$ set at any convenient initial setting $l_0$ and $A_3$ set at either position, a null is achieved by adjusting $A_1$ and $\phi$.

2. $A_2$ is advanced until some fiducial reading $P_1$ is obtained and the dial reading $l_1$ is recorded.

3. $A_1$ and $\phi$ are adjusted to obtain a new null.

4. $A_2$ is advanced until the reading $P_1$ is observed, and the dial reading $l_2$ is recorded.

5. Steps 1 through 4 are repeated if additional points are desired.

By following this procedure a series of dial readings $l_0$, $l_1$, $l_2$. . . . . is obtained which corresponds to equal but unknown increments in the output voltage of the attenuator under calibration.

### 3.3. Circuit 3

To eliminate the effects of monitor instabilities, the circuit of figure 3 may be used. This circuit requires the addition of a switch, another phase shifter, $\phi_2$, attenuator, $A_4$, and an isolation pad.

With $S_1$ open, the attenuation of $A_2$ as a function of dial reading is obtained exactly as oulined for figure 2. However, voltage as a function of the dial reading is obtained without relying on the constancy of a fiducial point. This is achieved by introducing from the third branch a voltage 180° out of phase with the output of $A_2$ and of suitable amplitude determined by $A_4$. The procedure is as follows:

1. With $S_1$ open, $A_2$ is set to the highest desired attenuation reading, $l_0$, and $\phi_1$ and $A_1$ are adjusted until a null reading on the monitor is obtained.

2. $A_2$ is set to any lower attenuation reading, $l_1$, as desired; the switch, $S_1$, is closed, and $A_4$ and $\phi_2$ are adjusted until a null reading on the monitor is obtained.

3. $S_1$ is opened, and $A_1$ and $\phi_1$ are adjusted for *nulled* voltage output.

4. $S_1$ is closed, and $A_2$ and $\phi_2$ are adjusted for a null indication. The dial reading $l_2$ of $A_2$ is recorded.

5. Steps 3 through 4 may be repeated if further equal voltage steps are required.

By this procedure, the output voltage of $A_2$ as a function of the dial reading may be obtained using the monitor only as a null indicating device.

### 3.4. Circuit 3 (Modified)

A further modification of the circuit may be made to reduce interaction effects when the switch, $S_1$, is opened and closed.

1. Switch $S_1$ is removed or closed.

2. Attenuator $A_4$ is replaced by a step attenuator which may be set to either of two fixed values of attenuation $A_{41}$ or $A_{42}$.

3. The foregoing procedure is used with the exception that when it is specified that $S_1$ is to be open, $A_4$ is set to the higher attenuation level $A_{42}$, and when it is specified that $S_1$ is to be closed, the lower attenuation level $A_{41}$ should be used.

4. The total attenuation in branch $A$ with $A_4$ set at the higher attenuation level, $A_{42}$, should be adjusted so that a null can be obtained for the preceding second step.

## 4. Experimental Results

The change in attenuation of an $X$-band, rotary-vane attenuator corresponding to two chosen dial readings was measured by the use of circuit 1. This value was found to be 2.10 db. The corresponding value obtained by an $IF$ substitution calibration system was $2.0 \pm 0.1$ db. The linearity of the monitor was not accurately known and may have been the principal cause of error.

A 30 M/cs attenuation-measuring system, using a parallel-branch circuit with a piston attenuator operating in the $TE_{11}$ evanescent mode as the reference standard [2], was calibrated with the circuit of figure 2. To increase resolution of the constant-gain monitor used with this system and to obtain equal voltage steps, the circuit shown in figure 6 was used. In this circuit the d-c output of the monitor, with the switch $S_1$ closed, is bucked out by the emf developed across $P_1$. The resulting signal, which consists of noise and time variations of power and gain, is fed into the RC filter network and then amplified. To obtain equal voltage steps, $P_2$ is adjusted so that the voltage across $S_1$ corresponds to the desired voltage step and then can be switched into or out of the circuit by opening and closing $S_1$. For use with circuit 3, $P_2$ is not used. The d-c amplifier is of high input impedance with variable gain. At the null or zero position the meter reads zero, and when the voltage across $P_2$ is added to the circuit, the meter reading can be returned to zero by increasing the voltage into the monitor by an amount $\Delta V$.

The measured value of the attenuation coefficient of the 30 Mc/s system was found to be 10.006 db/in. with a standard deviation of 0.003 db/in. The value of the attenuation coefficient computed from theoretical considerations is $10.000 \pm 0.002$ db/in. over the measured range.

The circuit of figure 3 was applied to the preceding system, with the third branch coupled to the generator through a 35-db directional coupler. A 30-db attenuator was used for the attenuator $A_4$ and the switch was isolated from the monitor junction by a 20-db attenuator. A correction was necessary for the change in impedance at the junction. This impedance change resulted from the change of

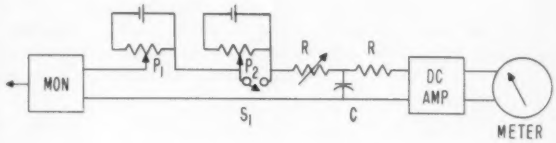


FIGURE 6. *Voltage differential and integrating circuit.*

reflected impedance through the 20-db isolation attenuator to the monitor junction as the switch was opened and closed. The use of a larger attenuator would have effectively eliminated this interaction effect. The measured value of the attenuation coefficient of the system was 10.003, with a standard deviation of 0.003 db/in.

Laverick's method was tried on this setup by inserting a switch in one of the other branches. The measured value of the attenuation coefficient was 10.023 db/in. with a standard deviation of 0.004 db/in. The error is assumed to be due to improper impedance matching of the three branches.

The author thanks H. W. Lance, R. L. Fey, C. M. Allred, and many others of the NBS staff for their constructive criticisms and assistance in the development of the paper. The author also acknowledges the assistance of D. H. Russell and W. Larson in the experimental verification of the method.

## 5. References

[1] C. M. Allred, Self-calibrating method of measuring insertion ratio, NBS Tech. News Bull. 41, 132 (1957).
[2] C. M. Allred and C. C. Cook, A precision RF attenuation calibration system, IRE Transactions I-9, 268 (1960).
[3] E. Laverick, The calibration of microwave attenuators by an absolute method, IRE Transactions MTT–5, 250 (1957).

(Paper 66C1-82)

JOURNAL OF RESEARCH of the National Bureau of Standards—C. Engineering and Instrumentation
Vol. 66C, No. 1, January–March 1962

# Special Shielded Resistor for High-Voltage D-C Measurements

J. H. Park

(September 26, 1961)

A new design for an accurate high-voltage d-c standard resistor has been devised. It is made up of a large number of individually shielded, one-megohm wire-wound resistors connected in series and arranged to form a vertical helix between a ground plate and a high-voltage electrode. The individual shields completely enclose each one-megohm resistor and prevent formation of corona at the surface of the resistance coil no matter how high the potential of the shield is above ground. The vertical helical configuration with a large "hat," or high-voltage electrode, on top serves to prevent concentration of electric field and corona formation at the high-potential end of the resistor. A 200-megohm unit, constructed during 1955 and tried out up to 100 kv in 1956, indicated the design to be free of corona errors but, for the particular one-megohm resistors used, the variation with temperature was quite large (0.01 percent per °C). A 100 megohm unit using low-temperature coefficient resistors has been recently constructed and tested up to 100 kv.

An experimental method of checking for corona or leakage errors at high values of voltage was developed. It consisted of accurately comparing the current "in" at the high voltage end of the resistor with the current "out" at the ground end for several different values of applied voltage. These measurements together with others performed to check temperature and leakage errors indicated that the value of resistance for the 100-megohm unit remains constant to within about 10 ppm for voltages up to 50 kv under ordinary laboratory conditions. At 100 kv the maximum error (caused by heating) was estimated to be about 40 ppm.

## 1. Introduction

Accurate measurements of d-c voltages at values above 10 v are nearly always dependent upon a resistive voltage divider which consists of a high resistance, $R_1$, in series with a low resistance, $R_2$. The voltage to be measured is connected across the series combination with $R_2$ at the ground end. The divider ratio, $(R_1+R_2)/R_2$, is chosen to give about a 1 v drop across $R_2$, which can then be measured with a null potentiometer. This is the well known "volt-box" method and tapped resistors or "volt boxes" are readily available for voltages up to at least 1,500 v. In extending this method to higher voltages the only additional difficulty is in designing a high-voltage resistor with an effective value which does not change with voltage.

A change in effective resistance with voltage may be due to any one or a combination of three factors: (1) heating of the resistance wire due to the $I^2R$ loss—the magnitude of this change will depend upon the temperature coefficient of the entire resistor; (2) current leakage through the volume or over the surface of the insulation used to support the resistor—such leakage usually increases with voltage and in effect decreases the total resistance; (3) corona discharges which may appear at locations of high gradient along the resistor as the voltage is increased—in effect they "leak" part of the resistor current to ground. The heating effect, factor (1) can be quite bothersome unless the overall temperature coefficient is very low. However, a high-voltage resistor is most conveniently made up by connecting a large number of one-megohm units in series. Thus, temperature coefficient can be reduced to a negligible minimum by choosing some resistors with positive and others with negative temperature coefficients. This can readily be done if a large number of one-megohm units made up of either Karma [1] or Evanohm [1] wire are available and their temperature coefficients have been measured. Factors (2) and (3), above, cannot be measured and reduced to a low magnitude in any such simple manner. Thus, the primary design problem is to keep leakage and corona effects as low as possible. Also, some experimental method must be devised to check for these effects with full voltage applied to the complete resistor.

[1] Trade names for special alloys (NiCr+Al+Fe) having high resistivity and low temperature coefficient of resistance.

## 2. Helical Resistor Made in 1955

A special helical design to keep corona effects to a minimum when a large number of 1-megohm resistors are connected in series was first devised in January 1955. It was made up of 200 one-megohm wire-wound resistor units which had been obtained on surplus after World War II. Each unit consisted of wire wound on a cylindrical spool ¾ in. in diameter and 1¼ in. long and connected to screw terminals at each end of the cylinder. Overlapping brass caps with ribbon insulation between them were attached to the screw terminals as indicated in figure 1. These two brass caps form a complete potential shield around the unit and definitely fix the voltage gradient environment immediately surrounding the resistance wire. Such voltage gradients are determined only by the potential difference between the two caps which is equal to the *IR* drop across the resistor. Thus the possibility of corona appearing in the air immediately surrounding the resistance wire is eliminated no matter how high the potential of the resistor and its shields may be with respect to ground.

A jig was made to support the individually shielded units along a circular helical path. They were then soldered together in this position and mounted on a lucite tube 4 in. in diameter and 39 in. high as shown in figure 2. The circular helical shape keeps a uniform potential drop per turn along the lucite tube. The 24 inch diameter copper "hat" placed on top of the lucite tube serves to intercept electrostatic lines of force from objects at ground potential and prevents concentration of such lines of force at the top turns of the resistor helix. Thus the gradient at the outside surface of the individual resistor caps is very nearly the same for units near the top as those near the bottom, and the possibility of corona from these shield caps is greatly reduced or eliminated.

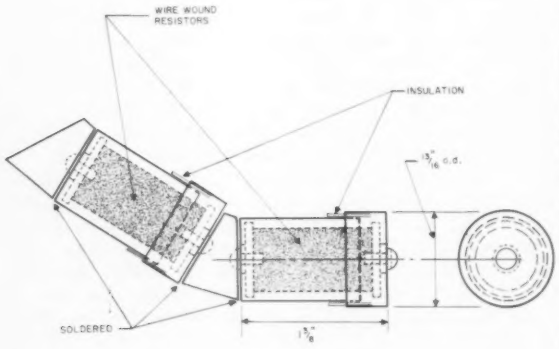


FIGURE 1. *Two one-megohm wire-wound resistors, mounted inside their shield caps, as used in first model of helical resistor.*

Indicates method of connecting resistors in series to form helix.

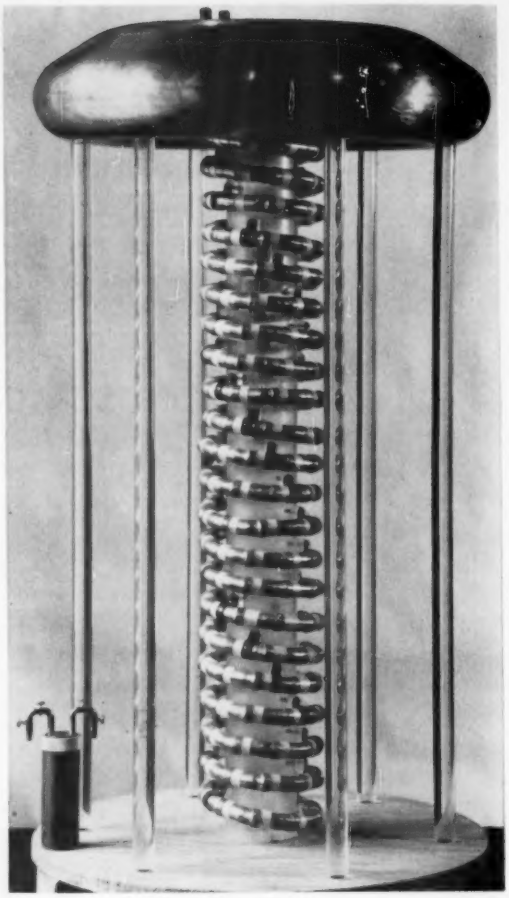

FIGURE 2. *The first model of helical resistor.*

Made during 1955.

If there were any corona discharge or even "dark current" from the resistor at some point between the high-voltage electrode and the low-voltage lead, it would cause the current "out" at the low-voltage lead to be less than the current "in" at the high-voltage electrode. This would introduce a change in the value of effective resistance which is used in voltage measurements. Current leakage through or over the surface of any insulating supports would cause a similar type of error. An experimental check for such errors can be obtained by getting a simultaneous measurement on the current "in" and "out" at various voltages up to the highest which can be used. This was done by adjusting the applied voltage to give a certain fixed value of current "in" under steady conditions and measuring the current "out".

The current "in" was set to a fixed known value by

passing it through a standard resistor and balancing the IR drop to that of a standard cell by use of a reflecting mirror galvanometer. The standard resistor, standard cell, and galvanometer were placed on top of the high-voltage electrode and covered with a 3-gal cylindrical can to prevent corona discharges from them. The resistance of the standard resistor used in this circuit was chosen to give the value of current desired. The current "out" was measured in the usual manner by passing it through a standard resistor and measuring the IR drop with a null potentiometer. The procedure then was to choose a value of standard resistor to give the required current "in" and adjust this current to give a balance on the reflecting galvanometer mounted inside the 3-gal can. When a balance was attained the current "out" was read on the potentiometer at the ground end. Any discrepancy between these two currents indicated either a leakage or corona effect.

Some special precautions taken during these measurements should be noted. The switch closing the galvanometer circuit inside the 3-gal can must not be closed until the current has been approximately adjusted to the correct value. This requires a remotely operated switch because the 3-gal can is at high voltage. A waxed cord was tried first for operating this switch but found to be unsatisfactory because it jarred the galvanometer off scale. A relay operated by a photoelectric cell circuit which could be closed by a beam of light was installed inside the 3-gal can and found to operate satisfactorily. It was also found desirable to place extra filter capacitors across the high-voltage supply, giving high RC time constants on both charge and discharge, thus serving to keep the current steady.

Current measurements were made using 5,000- and 2,000-ohm standard resistors in the 3-gal can giving voltage values of approximately 40 and 100 kv across the 200-megohm resistor. At 40 kv the current "in" and current "out" agreed to within about 20 ppm which was considered the limit of accuracy for this particular test. At 100 kv the agreement could be certain only to within about 70 ppm because of unsteadiness in the supply voltage. No further attempt to minimize these measurement errors was made at that time because the expected accuracy of the first model was about $\pm 0.01$ percent.

Actually the largest error in this model was found to be due to the temperature coefficient of resistance of the 1-megohm resistors. Apparently Nichrome V wire had been used in winding these resistors. The measured change of resistance with room temperature as determined with low voltage applied was $+0.01$ percent per degree C increase in ambient temperature. The increase of resistance with applied voltage followed the square law as expected, and this total change from low to rated voltage of 100 kv was 0.09 percent. Correction curves were derived for changes in applied voltage and room temperature. It was concluded that, with care in applying these corrections, accuracies within 0.02 percent could be expected for applied voltage up to 50 kv.

## 3. Improved Helical Resistor Built in 1961

The first model has been used as a standard for calibrating other high-voltage resistors at the National Bureau of Standards for several years. In most cases the accuracy attainable was sufficient, but in several instances accuracy needs reached 0.01 percent or better. In view of the ever higher accuracy needs as time goes on, especially in experiments involving the accurate measurement of atomic and nuclear constants, it was decided to build another resistor of the same design using 1-megohm units with lower temperature coefficients.

In 1960 it was found that due to improvements in resistor winding techniques and to the development of special alloy wire of low temperature coefficient, it was possible to obtain 1-megohm units guaranteed to have a temperature coefficient less than 5 ppm per degree C. A large number were ordered, and on delivery their temperature coefficients were determined by measurements at three or more temperatures between 20 and 44 °C. They were all well within the 5 ppm per degree C limit—also some resistors increased and others decreased with rising temperature and in general the change was proportional to temperature. Thus it was possible to choose matched pairs of these resistors with nearly zero average temperature coefficient. By connecting such matched pairs in series, a high-voltage resistor with nearly zero change with temperature was made.

To keep corona and leakage errors as low as possible the same spiral type of construction as that in the first model was used. A new technique for making the shields and connecting them in a helix was devised. Each shielded unit contained two resistors and was assembled from brass parts, machined out of tubing, and a 45° brass elbow, as shown in figure 3. Polyethylene sheet insulation was used between the overlapping shields around each resistor as before. Eight of these units, fitted together, constitute a single turn of the helix with an outside diameter of 9½ in. They were fastened to a 7-in.-diam lucite tube (⅛ in. wall thickness) using one nylon clamp and screw for each unit. The pitch of the helix was chosen to prevent any possibility of corona between adjacent turns.

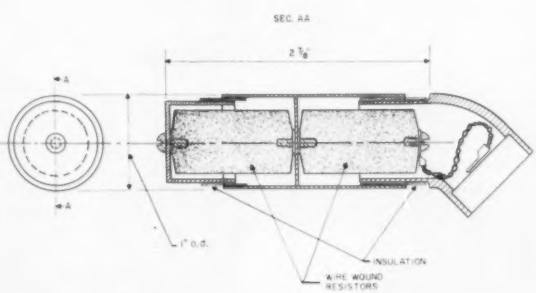


FIGURE 3. *A two-resistor shielded unit as used in the second model of helical resistor.*

First an estimate of required pitch was made based on a maximum rated voltage for each 1-megohm resistor of 1,000 v. This gave 16 kilovolts per turn. A pitch of 2⅜ in. per turn was taken, giving 1⅜ in. between adjacent brass shields from one turn to the next. A 1½-turn resistor (maximum rating 24 kv) was made up using this pitch and its resistance was measured at various voltages up to 27 kv. This was done using a wheatstone bridge with the 1955 model 200-megohm helical resistor as the other high-voltage arm. Only gradual uniform changes in resistance were noted as voltage was increased in steps from 5 to 27 kv, and they could be accounted for by heating effects. There was no evidence of corona effects even at 27 kv, which is 125 percent of the maximum to be used.

On the basis of these preliminary tests a 100-megohm resistor of 6¼ turns was made up with the same pitch. The lucite tube is 16½ in. long and mounted vertically between a brass ground plate and a high-voltage electrode as shown by the photograph in figure 4. The electrode on top of the lucite tube was designed so that another similar resistor could be placed on top of it. By stacking resistors and connecting them in series, voltage ranges in multiples of 100 kv could be obtained. At present only one 100-megohm resistor has been constructed because so far there has been no urgent requirement for very accurate measurements at voltages above 50 kv. However, corona tests on the high-voltage electrode were made up to 200 kv by using two 100 kv power supplies. The normally grounded brass plate was supported on ceramic insulators and connected to the minus 100 kv. The high-voltage electrode was connected to the plus 100 kv. For this test the 100 1-megohm resistors were removed but the same lucite tube was used to separate the electrode from the brass plate. Only a visual test could be made; thus the setup was put inside a completely enclosed dark box large enough to house an observer also. With a total voltage of 200 kv between brass plate and electrode there was no visible or audible evidence of corona. Since this was twice the maximum voltage ever to be used with the resistors in place, it was concluded that there would be no corona current off the middle shield electrode when two units are stacked in series. If more than two units are to be stacked, further corona tests should be made and possibly larger shield electrodes than the one shown in figure 4, which is 22 in. in diameter, would be required.

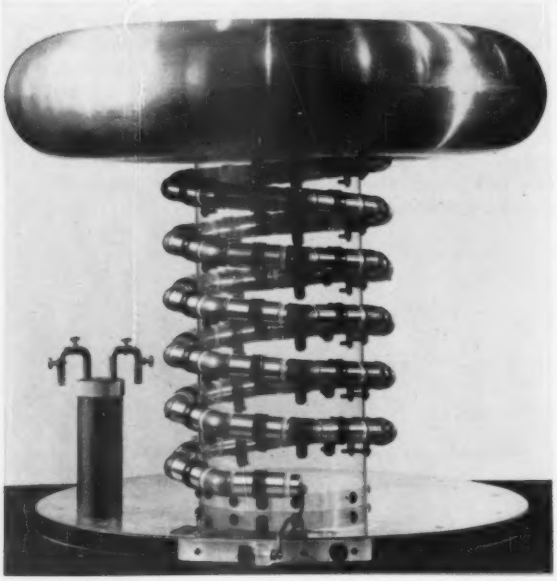

FIGURE 4. *100-megohm, 100 kv, helical resistor constructed in 1961.*

## 4. Accuracy Limits on 1961 Model

Throughout the design and construction of the 1961 model helical resistor, primary consideration was given to eliminating any possible corona or leakage errors. Corona tests were made using voltages much above the expected maximum rating. These precautions by themselves do not eliminate the possibility of corona and leakage errors. The crucial test for detecting such errors is to measure current "in" and current "out" by the method already described and used for the 1955 model.

The accuracy attained was considerably improved over that in the previous tests. In part the higher accuracy was obtained by using somewhat more sensitive galvanometers and reducing the effects of thermal emf's. However, the main improvement was obtained by stabalizing the d-c voltage supply, getting finer control, and using greater patience. Also, by a modified experimental procedure, any constant measurement errors such as might be introduced by the potentiometer, resistance standards, or standard cells were cancelled. This was done by taking current "in" and "out" measurements at low voltage with the 100-megohm resistor shorted, before and after each high-voltage check. Then if the potentiometer reading at balance is the same at high voltage as at low voltage with the resistor shorted, no leakage or corona effects are introduced by the high voltage.

Measurements were made with three different values of current (approximately 0.204, 0.509, and 1.019 ma) giving total voltages across the resistor of about 20.4, 50.9, and 101.9 kv. The odd values resulted from the use of 5,000-, 2,000-, and 1,000-ohm NBS-type resistance standards in conjunction with an unsaturated standard cell for setting current "in." A 5-dial null-type Wolff potentiometer was used to measure the voltage across a similar standard resistor connected between the resistor low-voltage lead and ground, yielding the current "out." The precision obtainable with stable current and fine control was considered to be within 10 ppm. The check of current "in" and "out" with the 100-megohm resistor shorted gave values agreeing within 10 ppm. With the 100-megohm resistor unshorted, requiring high voltage to balance current "in" and "out", settings on the Wolff potentiometer were the same within 10 ppm as with the 100-megohm resistor shorted.

The accuracy of setting the Wolff potentiometer with 20 and 50 kv across the resistor was within 10 ppm, i.e., the same as when the 100-megohm resistor was shorted. With 100 kv across the resistor this accuracy was estimated as within 20 ppm—the small increase being due to greater difficulty in holding current nearly constant at the required value.

Current "in" and "out" data were obtained on several different days over a period of 2 months. Room temperature varied only from 24 to 25 °C and relative humidity from 37 to 50 percent. Most of these data were taken with the brass ground plate connected to ground and tied to the resistor low-voltage terminal through the standard resistor used in measuring current "out" (because that is the way the resistor will normally be used). As a further check on possible leakage current errors when two or more complete units are connected in series, data were also taken with the brass ground plate connected to the resistor low-voltage lead and insulated from ground. On all of these tests the current "out" was found to be equal to the current "in" to within the accuracy of measurement. This shows that corona and leakage errors for this helical resistor are less than 10 ppm for voltages up to 50 kv and are not greater than 20 ppm for 100 kv.

The only other source of error is that due to the overall temperature coefficient of resistance of the 1-megohm wire-wound resistors. The temperature coefficient from 20 to 40 °C as measured for each 1-megohm resistor used in this resistor was less than 2 ppm per degree C. Also resistors with approximately equal positive and negative temperature coefficients were mounted as pairs. The overall temperature coefficient is estimated to be less than 0.4 ppm per degree C. Thus no correction for room temperature under normal laboratory conditions need be applied. Heating of the 1-megohm units due to current at the higher voltage values, however, might cause a slight error because the resistors are totally enclosed and attain higher temperature than they would in a free air space. An estimate of the magnitude of such heating errors was obtained as described in the following two paragraphs.

During the corona tests evidence of heating errors were detected (as already mentioned) when the resistance of the 1½-turn, 24-unit, test sample was measured at various voltages. These 24 units were all purposely chosen to have large temperature coefficients of the same sign so that temperature rise could be estimated from change in resistance. The average coefficient for the 24 units was −3 ppm per degree C. The total change in resistance, from a measurement at 9 kv taken immediately after putting voltage on, to a measurement at 12 kv after voltage had been on for about 70 min, was 70 ppm. This indicates a temperature rise of about 23 °C with 0.5 kv applied across each 1-megohm coil. Thus for the complete 100-megohm resistor it would take 50 kv to produce a 23 °C temperature rise; but since the complete resistor is made up of temperature compensated pairs, the 50 kv would cause a resistance change of less than 10 ppm.

Voltages above 12 kv were also applied to the 24-unit special test resistor in order to estimate possible heating errors at higher voltages. After 24 kv had been applied for 2 hrs the shields around the resistor units became noticeable hot to the touch and the total change in resistance was 270 ppm. Based on the −3 ppm temperature coefficient this would mean a 90 °C temperature rise for the resistance wire. Since the final 100-megohm resistor has an estimated temperature coefficient of 0.4 ppm, as compared to 3 ppm for the 24-unit special test resistor, its maximum change with 100 kv applied would be only 36 ppm. However, this voltage does cause considerable heating and should not be held continuously. It was arbitrarily decided that after applying voltages above 70 kv for 30 min a cooling period of 30 min should be allowed with no voltage applied.

## 5. Calibration of 100-Megohm Resistor

As explained in the preceding section, it has been experimentally demonstrated that corona and leakage errors for this 100-megohm resistor remain within certain limits up to 100 kv. Within these limits then it is permissible to calibrate or measure its resistance at low values of voltage and then use this measured resistance at much higher voltages to compute resistor $IR$ drop.

One method of calibration was to measure each 1-megohm unit individually by placing it in the "unknown" arm of a Wheatstone bridge. All other arms of the bridge were made up of sealed NBS-type standard resistors except for a decade resistor box used for fine control by supplying from 0.00 to 10.00 ohms in 0.01-ohm steps. Values of all resistances used in the bridge, except the 1-megohm unit being tested, were carefully determined by the Resistance and Reactance Section of the National Bureau of Standards. Temperature corrections were applied when necessary. These measurements were made before the complete resistor was assembled. The total resistance was taken to be the sum of the measured values for the 100 units comprising the complete resistor.

A question now arises as to a possible change in effective resistance of an individual unit due to its being mounted inside its shield caps and their being mounted in turn on the lucite tube using nylon clamps and screws. Such a change could be caused by leakage current either via the lucite tube and nylon clamps or via the polyethelene between shield caps. Normally any leakage current via the lucite tube would have been detected during the current "in" and "out" tests but leakage via the polyethelene would not. To check for a possible error due to such leakage, the resistances of several matched pairs of the 1-megohm units were measured after they had been mounted inside their shields and on the lucite tube. In every case the resistance thus measured agreed to within 10 ppm with the sum of the resistance of the individual units as measured before assembly.

Another method of calibration was used with the complete resistor assembled. This was to make connections at every fifth brass elbow (every 10th resistor unit) so that the 100-megohm standard could be divided into 10 sections of 10-megohm units. These 10 sections were then connected in parallel and measured as a 1-megohm resistor. The resistances of all 10 sections in series could then be readily computed from the parallel resistance value, provided the resistance of each section is equal to 10 megohms (within 0.1 percent). Values were obtained in this manner on several different days and at room temperatures from 23 to 26 °C. All such values agreed with that obtained by summing individual resistor measurements to within 15 ppm.

## 6. Summary

A special design of high-voltage d-c resistor made up of a large number of individually shielded 1-megohm wire-wound resistors connected in series and arranged in helical form, was investigated and found to be suitable for voltages up to 100 kv.

Measurements on the first helical resistor built in 1955 indicated negligible leakage and corona errors to within the accuracy of the measurements made at that time. However the heating errors were considerable (0.01 percent per degree C) in this resistor because of the temperature coefficient of the wire-wound 1-megohm units.

A second helical resistor, of the same design, was constructed in 1961 using 100 one-megohm, low-temperature coefficient, wire-wound units. By using matched pairs of these units having temperature coefficients equal in magnitude and opposite in sign, the final 100-megohm resistor was estimated to have a temperature coefficient not greater than 0.4 ppm per degree C. Corona and leakage errors for this resistor as determined using improved measurement techniques were found to be less than 10 ppm at 50 kv and less than 20 ppm at 100 kv.

This 100-megohm resistor has a special "hat" or high-voltage electrode designed to give uniform gradients from it to ground. This would allow other similar resistors to be stacked on top of it and connected in series for higher voltages. Corona tests on the electrode indicated the feasibility of such "stacking". Exact limits of accuracy attainable at voltages above 100 kv have not yet been determined.

---

The construction of the two high-voltage resistors described above was carried out almost exclusively by John L. Mills. Harold N. Cones and John L. Mills performed most of the experimental measurements.

(Paper 66C1–83)

JOURNAL OF RESEARCH of the National Bureau of Standards—C. Engineering and Instrumentation
Vol. 66C, No. 1, January–March 1962

# Voltage Ratio Measurements With a Transformer Capacitance Bridge*

(October 23, 1961)

**Thomas L. Zapf**

A bridge having inductively-coupled ratio arms, designed for the calibration of capacitors, is applicable to the accurate measurement of voltage ratio and phase angle of a-c voltage dividers at audiofrequencies. The ability to measure quickly the ratios of certain capacitors in the bridge circuit, and the excellent inherent accuracy of the inductively-coupled ratio arms in the bridge, combine to permit the measurement of ratio of voltage dividers by a method independent of absolute determinations of any of the electrical units. This paper describes equipment now available and procedures developed at the National Bureau of Standards for the accurate calibration of voltage dividers at audiofrequencies by this method.

## 1. Introduction

Equipment commonly used for the establishment of known voltage ratios includes volt boxes, resistive voltage dividers, attenuators, and inductive voltage dividers. With the exception of inductive voltage dividers, these devices are generally constructed of resistive elements, which, if used on alternating current at higher audiofrequencies, cannot be relied upon to the accuracy with which they can be calibrated on direct current, because of the deleterious effects of uncompensated inductance and capacitance.

Variable inductive voltage dividers are now widely used as ratio arms of bridges for the calibration of resistors, capacitors, and inductors as well as other ratio devices throughout a large part of the audiofrequency spectrum. The inherent stability and accuracy of inductively coupled ratio arms, together with excellent resolution of ratio, have challenged the capabilities of equipment and techniques formerly used to measure voltage ratios.

The search for better accuracy in the calibration of inductive voltage dividers has led to the development of several methods [1, 2, 3] for determining corrections to the nominal readings. Another method, capable of determining these corrections with an uncertainty less than $\pm 0.000\ 000\ 2$, has resulted from an investigation of possible other applications of apparatus intended for the accurate measurement of capacitance.

## 2. Capacitance Bridge

The bridge circuit that is used for the voltage ratio measurements has been described [4], and consists of accurate inductively-coupled ratio arms having very low effective series impedances, a group of three-terminal air capacitors, and a conductance balancing circuit. These components and the unknown capacitor, $C_X$, are shown schematically in figure 1. Each of the capacitors, $C_1$, $C_2$, . . . . , $C_8$, has one electrode connected to the detector and the other electrode connected separately to the rotors of eight switches. Each switch has 12 positions, the fixed contacts being connected to 12 taps on the winding of the inductively-coupled ratio arms. The position of the contact arm of each switch is numbered according to its connection to the ratio arms, $-1$, 0, 1, 2, 3, . . . 10, and each switch is identified by the capacitance-per-step that it controls. The corrected reading of the dials associated with these switches represents the capacitance required to balance the bridge and is denoted by $C_A$. A similar arrangement of switches associated with an auxiliary inductive voltage divider and a resistance-capacitance network provides control over the conductance balance. If $C_X$ and $G_X$ are the capacitance and the shunt conductance of the unknown, $G_A$ is the conductance associated with the capacitance complex $C_A$, and $G_B$ is the reading of the conductance balance controls on the bridge, then

$$C_X = C_A \tag{1}$$

and

$$G_X = G_A + G_B \tag{2}$$

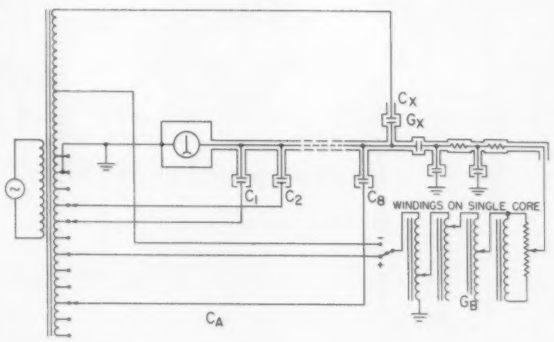


FIGURE 1. *Schematic of a transformer capacitance and conductance bridge used for the accurate measurement of direct capacitance.*

*Contribution from the Radio Standards Laboratory, National Bureau of Standards, Boulder, Colo.

A self-consistent calibration of the capacitance decades in the bridge can be accomplished quickly by an internal step-up method. The accuracy of the bridge for capacitance calibration work is limited by the accuracy of the standard capacitor to which the self-consistent calibration is referred. This does not detract from the ability of the bridge to measure the ratio of the capacitances of two nearly equal capacitors to better than one-tenth part per million.

## 3. Voltage Divider Calibration

In figure 2 a generalized voltage divider having an output-to-input-voltage ratio denoted by $A$ is shown connected to the bridge and to a three-terminal capacitor, $C$. The voltage divider reduces the voltage applied to one electrode of the three-terminal capacitor by a factor $A$ times the voltage that would be applied if the capacitor were connected directly to the upper extremity of the bridge transformer. In general, the voltage at the adjustable tap of a voltage divider will not be exactly in phase with the voltage applied to its input terminals, and the difference in phase can be expressed as a phase angle. A very small phase angle affects the conductance balance to a significant extent but has only a second order effect on the capacitance balance. When the bridge is balanced, the readings of the bridge, corrected for internal errors, yield values for the apparent capacitance and conductance, $C_X$ and $G_X$, connected to the terminals of the bridge.

The capacitance balance of the bridge is a measurement of the ratio of the in-phase (real) components of the complex voltages, and the conductance balance is a measurement of the quadrature (imaginary) component. Because the phase angles involved are very small (see fig. 3) no appreciable error arises from considering that the ratio of the magnitudes of the voltages, $A=A_N[(1+\alpha)^2+\beta^2]^{\frac{1}{2}}$, equals the ratio of the in-phase components, $A_N(1+\alpha)$. Also, no significant error arises by considering that the phase angle, $\gamma$, equals $\beta$ in the equation $\mathbf{A}=\mathbf{A}_N(1+\alpha+j\beta)$. Because of the somewhat independent nature of the capacitance and the conductance balance, they will be considered separately.

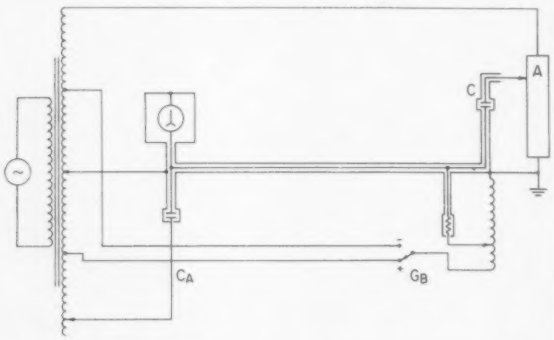


FIGURE 2. *Simplified schematic of a transformer capacitance bridge used to measure the complex voltage ratio of voltage dividers.*

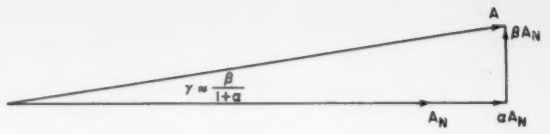


FIGURE 3. *The phasor diagram defines the true ratio,* **A**, *and phase angle,* $\gamma$, *in terms of the nominal ratio,* $\mathbf{A}_N$, *the ratio error,* $\alpha$, *and the quadrature component,* $\beta$.

The phase angle and ratio errors are grossly exaggerated for clarity.

## 4. Voltage Ratio Measurement

The voltage ratio of a generalized divider is indicated primarily by the capacitance balance of the bridge. The reduced voltage applied to capacitor $C$ is equivalent to the full voltage applied to the measured capacitance, $C_X$. In figure 4 it is evident that the relationship between $C_X$ and $C$ is

$$C_X=AC. \tag{3}$$

Therefore, the scalar voltage ratio of the generalized voltage divider is

$$A=\frac{C_X}{C}. \tag{4}$$

The resolution of the capacitance balance of the bridge often approaches 1 part in $10^5$; hence, excellent accuracy in ratio measurements is easily achieved if care is taken to eliminate the effect of environmental disturbances such as changes of temperature.

The actual ratio measured by this procedure may differ, both in magnitude and phase angle, from the ratio that would be obtained if no current were withdrawn from the divider at the adjustable tap. The

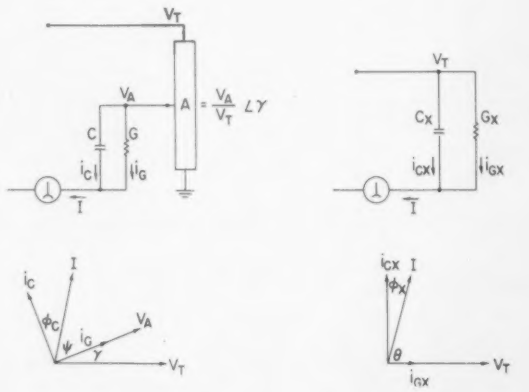


FIGURE 4. *The equivalent circuit and phasor diagram on the right represents the capacitance and parallel conductance equivalent to the actual circuit with voltage divider shown on the left.*

effect of loading on the voltage ratio of resistive and inductive voltage dividers is considered in sections 7 and 8 of this paper. In general, this effect may be expressed as a magnitude error and a phase angle error. Corrections, $\mu$ and $\rho$, to the measured ratio, **A**, may be defined by the following equation:

$$\mathbf{A}_0=\mathbf{A}(1+\mu+j\rho) \tag{5}$$

where $\mathbf{A}_0$ is the voltage ratio when no load is connected.

## 5. Phase Angle Measurement

The conductance balance of the bridge is related to the phase angle associated with the voltage divider as well as to the conductances of capacitors $C$ and $C_A$ (fig. 2). The relationship among these parameters is such that the phase angle of the divider may be calculated from the difference between certain conductance balances of the bridge. In this paper the phase angle, $\gamma$, of the voltage divider is defined as the angle between the phasors $V_A$ and $V_T$, where $V_A$ is the voltage at the adjustable tap and $V_T$ is the voltage at one extremity of the divider, both referred to a common point at the other extremity unless otherwise noted. The phase angle is considered positive if $V_A$ leads $V_T$ and negative if $V_A$ lags $V_T$. These phasors and the circuits to which they refer are depicted in figure 4. The right half of the figure represents the equivalent circuit, as measured by the bridge, of the more complex actual circuit shown on the left. It is evident that

$$\theta=\frac{\pi}{2}-\phi_x, \qquad \psi=\frac{\pi}{2}-\phi_c \tag{6}$$

and

$$\theta=\psi+\gamma. \tag{7}$$

Then

$$\gamma=\theta-\psi=\phi_c-\phi_x, \tag{8}$$

and at any frequency, $f$, if $\phi_c$ and $\phi_x$ are very small angles, it can be shown that

$$\phi_c=\frac{G}{C}T, \tag{9}$$

and

$$\phi_x=\frac{G_X}{C_X}T \tag{10}$$

where $T=\frac{1}{2\pi f}$. Combining eqs. (8), (9), and (10) yields

$$\gamma=T\left(\frac{G}{C}-\frac{G_x}{C_x}\right). \tag{11}$$

It has been found convenient to express the phase angle of voltage dividers in fractions of a radian. If $T$ is expressed in microseconds, $G$ and $G_X$ in picomhos, $C$ and $C_X$ in picofarads, eq (11) yields $\gamma$ in microradians.

The phase angle correction for loading is significant and is discussed in section 7.

## 6. Three-Terminal and Four-Terminal Dividers

The excellent resolution obtained by this method led to the consideration of errors resulting from the impedance in the leads and connectors that are used to connect voltage dividers to other circuit elements, as well as the errors resulting from undesirable losses within the ratio apparatus itself.

In order that the calibration of ratio devices be useful, the conditions under which the equipment is used must be duplicated at the time of calibration, or corrections must be made for any significant differences. One source of significant difference is the manner in which connections are made to the input and output terminals. Many ratio devices, both resistive and inductive, are constructed with four terminals, so that a source may be connected to two "input" terminals, and a load connected to the two "output" terminals. Often one input terminal and one output terminal are connected together internally by a wire of low, but not infinitesimal, impedance. Nevertheless, such a device may be described as "four-terminal," and the internal branch-point may be considered the lower extremity of the output of the divider.

On the other hand, one of the common terminals may be ignored and the divider connected to a circuit as a three-terminal device. Current in the wires between the terminals and the internal branch-points produces voltage drops that can cause a three-terminal calibration to differ significantly from a four-terminal calibration. In figure 5 the input voltage, $E_I$, of the divider is the potential difference between the input terminals 3 and 1. If $v_n$ represents the magnitude of the in-phase component[1] of potential at terminal $n$ relative to terminal 0,

$$E'_I=v_3-v_1. \tag{12}$$

The output voltage, $E_H$, of the divider, considered as a four-terminal network, is

$$E'_H=v_4-v_2, \tag{13}$$

and the output voltage, $E_T$, of the divider, considered as a three-terminal network, is

$$E'_T=v_4-v_1. \tag{14}$$

Now certain ratios of the in-phase component of potential, relative to the 0 terminal, may be defined as follows (see fig. 6):

$$A_1=\frac{v_1}{v_5},\ A_2=\frac{v_2}{v_5},\ A_3=\frac{v_3}{v_5},\ \text{and}\ A_4=\frac{v_4}{v_5}, \tag{15}$$

from which

$$v_1=A_1v_5,\ v_2=A_2v_5,\ v_3=A_3v_5,\ \text{and}\ v_4=A_4v_5. \tag{16}$$

[1] The term "in-phase component" and the prime notation here denotes components in phase with the reference voltage phasor, $E_3$ (or reference voltage ratio phasor, $A_3$). As indicated previously, these in-phase components are very nearly equal to the absolute values because the quadrature components are comparatively very small.

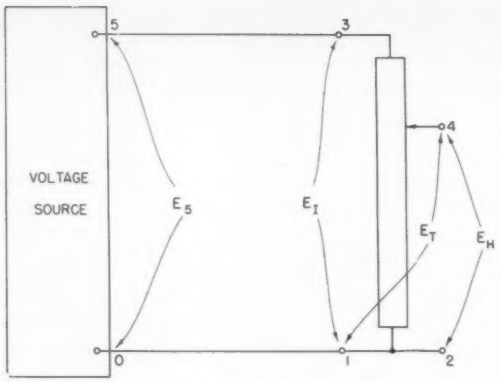


FIGURE 5. *A generalized four-terminal voltage divider connected to a source of voltage.*

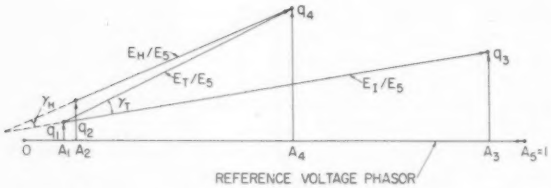


FIGURE 6. *Phasor relationships of the voltages shown in figure 5.* $A_1$, $A_2$, $A_3$, and $A_4$ *are the in-phase components of the voltage-ratio phasors along the reference voltage phasor.*

E here denotes the magnitude of the phasor **E**s.
The angles have been grossly exaggerated for clarity.

It is apparent that the in-phase component of voltage ratio for the four-terminal network is

$$A_H=\frac{E'_H}{E'_I}=\frac{v_4-v_2}{v_3-v_1}=\frac{A_4-A_2}{A_3-A_1}, \tag{17}$$

and the corresponding ratio for the three-terminal network is

$$A_T=\frac{E'_T}{E'_I}=\frac{v_4-v_1}{v_3-v_1}=\frac{A_4-A_1}{A_3-A_1}. \tag{18}$$

These equations show that the desired ratios, $A_H$ or $A_T$, may be computed from measurements of certain other elementary ratios. It can be shown that $A_T$ and $A_H$ are related by the equation

$$A_T=A_H+\delta, \tag{19}$$

where

$$\delta=\frac{A_2-A_1}{A_3-A_1}. \tag{20}$$

In the calibration of the decade ratio apparatus now in use as a standard at NBS Electronic Calibration Center it was unnecessary to measure $A_1$, $A_2$, and $A_3$ more than once because these ratios are primarily dependent upon impedances which remain essentially constant during the calibration. The ratio $A_4$ was measured for each dial setting of interest, and the ratio $A_H$ or $A_T$, or both, was computed according to eqs (17), (18), or (19). It is evident from eq (20) that $\delta$ in eq (19) is independent of ratio setting $A_4$. In the calibration of other decade dividers, $\delta$ may not be truly independent of $A_4$. A redistribution of internal stray impedances or large external loading impedance, as $A_4$ is varied, may cause a significant change in $A_1$, $A_2$, $A_3$, and it may be necessary to measure these for each value of $A_4$.

Turning now to the consideration of phase angle measurements, it will be convenient to express the phase angle, $\gamma$, in terms of the in-phase and quadrature components of the complex voltage ratio. Here $\gamma$ is intended to represent the angle between the output-voltage phasor and the input-voltage phasor, even though the separate phasors may not have a common origin (as in the four-terminal network described).

The quadrature components of the complex voltage ratio at the terminals 1, 2, 3, and 4, are denoted by $q_1$, $q_2$, $q_3$, and $q_4$, as shown in figure 6. At each point of measurement the quadrature component measured from the reference voltage phasor can be obtained from $q=A\gamma$ where $\gamma$ is determined in accordance with eq (11). The phase angle for the four-terminal network is the angle between $E_H$ and $E_I$

$$\gamma_H=\frac{q_4-q_2}{A_4-A_2}-\frac{q_3-q_1}{A_3-A_1}, \tag{21}$$

and since $A_1$ and $A_2$ are very small, and $A_3$ is approximately 1, eq (21) can be simplified for practical computations, giving

$$\gamma_H=\frac{q_4-q_2}{A_4}-(q_3-q_1). \tag{22}$$

Similarly, the phase angle for the three-terminal network is the angle between $E_T$ and $E_I$

$$\gamma_T=\frac{q_4-q_1}{A_4}-(q_3-q_1), \tag{23}$$

hence

$$\gamma_T=\gamma_H+\frac{q_2-q_1}{A_4}. \tag{24}$$

The eqs (22), (23), and (24) provide a useful means by which the phase angles for the four-terminal and three-terminal networks may be computed from the quadrature components of the complex voltage ratio.

## 7. Resistive Divider Calibration

Several sources of error accompany the measurement of ratio of resistive voltage dividers by the method described in this paper. The small voltage drops in the wires connecting the voltage divider to the bridge constitute a source of error for which correction may be made. The resistance in the leads in series with the resistive voltage divider causes a voltage drop affecting the measurement of ratio. This error, if not unduly large, can be eliminated by the procedure described in section 6.

Resistive dividers having low resistance, when connected to the bridge transformer as in figure 2, can burden the transformer to an intolerable extent. If loading on the secondary of the bridge transformer imposes a limitation on the accuracy of the measurement, the transformer may be energized by connecting the a-c source across that part of the secondary in parallel with the resistive divider rather than to the primary winding. When this connection is made, the primary of the bridge transformer is ignored and the secondary serves as an inductive voltage divider, in which the loading from interturn capacitance and leakage inductance becomes a source of error, but of smaller magnitude. Thus, the corrections for the errors in ratio of the transformer would not be expected to be the same as those discussed in section 9, and may be considerably larger. The calibration of resistive voltage dividers by this method has not progressed to the extent that accuracy of measurement was restricted by errors in the transformer. It is more convenient to calibrate resistive voltage dividers by comparison with inductive voltage dividers which have been calibrated by the method described in this paper.

Another source of significant error arises from the loading on the resistive voltage divider, predominantly by the capacitance to ground, $C_g$, from the adjustable tap. Resistive voltage dividers having high resistance are particularly susceptible to loading of this sort. The current from this capacitance in the resistive voltage divider causes ratio and phase angle errors at the adjustable tap of the divider that can be expressed by the equation

$$\mathbf{A}_0=\mathbf{A}\left[1-(A-A^2)\frac{X_L}{X_{Cg}}+j\,(A-A^2)\frac{R}{X_{Cg}}\right] \quad (25)$$

where $\mathbf{A}_0$ is the ratio with no load connected to the output of the divider, $\mathbf{A}$ is the voltage ratio in the presence of loading, $X_{Cg}$ is the reactance of the capacitance $C_g$, and $R+jX_L=Z$, where $Z$ is the total impedance of the voltage divider. In resistive voltage dividers it is expected that $X_L<<R$, so that the most prominent correction term is the last one as shown in eq (25). Thus, the effect of capacitive loading on the real component of the complex ratio is generally negligible, while the effect on the phase angle may be significant. The correction to the phase angle measurement is dependent upon the ratio being measured and is the greatest when $A=0.5$.

It must be noted that eq (25) is applicable only to a resistive divider circuit having a uniformly distributed inductance. Loading errors of decade voltage dividers having the Kelvin-Varley slide are represented only approximately by eq (25). The treatment of loading errors for other, more complex, resistive voltage dividing circuits requires detailed analysis and will not be discussed here. The voltage division associated with resistive attenuators is particularly susceptible to loading, and for this reason attenuators are not usually considered suitable for use as standards of voltage ratio in the audiofrequencies.

For simple resistive voltage dividers it is evident from eq (25) that the corrections, $\mu$ and $\rho$, defined in eq (5) are

$$\mu=-\omega^2(A-A^2)C_gL \quad (26)$$

and

$$\rho=\omega(A-A^2)C_gR. \quad (27)$$

Corrections can be made to reduce these errors, leaving only second order errors to contribute to the overall uncertainty of measurement. In practical measurement work the small second order errors (resulting from the use of certain approximations in the derivations of the above equation) are generally extremely small relative to the accuracy limit imposed by the resolution and stability of the resistive divider being calibrated.

If a reasonably accurate measurement of phase angle is desired, it is evident from eq (27) that $C_g$ should be small in order to reduce to a minimum the quadrature error component for which correction must be made. A practical limit to the reduction of $C_g$ is imposed by the necessity of obtaining sufficient resolution in the ratio measurements as indicated by eq (4), in which the direct capacitance, $C$, is a part of the total capacitive load, $C_g$, on the divider.

In the event that the correction for loading, as described here, is inconvenient or creates intolerable uncertainties, a method is available for reducing the loading to an imperceptible level. A capacitance, $C'=C_g\frac{A}{1-A}$, may be connected from the output terminal of the voltage divider to the upper input terminal (see fig. 2). The capacitances, $C'$ and $C_g$, then form a capacitive voltage divider having approximately the same ratio, $A$, as the divider being calibrated, and the loading effect is much reduced.

## 8. Inductive Divider Calibration

In general, with the method described, less difficulty is encountered in the calibration of inductive voltage dividers than resistive voltage dividers. The close coupling between the sections of inductive voltage dividers results in relatively low effective series output impedance which minimizes the effects of external loading as well as internal variations of impedance. The voltage drop resulting from current in the effective series impedance, $Z_s$, shown in figure 7 produces an actual voltage ratio, $\mathbf{A}$, differing in magnitude and phase angle from the voltage ratio, $\mathbf{A}_0$, without load as indicated by the equation

$$\mathbf{A}_0=\mathbf{A}\left(1-\frac{X_{Ls}}{X_{Cg}}+j\frac{R_s}{X_{Cg}}\right). \quad (28)$$

It must be noted that the effective series impedance generally is not constant, but varies with the setting of the divider. Correction for loading errors usually can be made by measuring the actual voltage ratio and phase angle at the terminals with two known

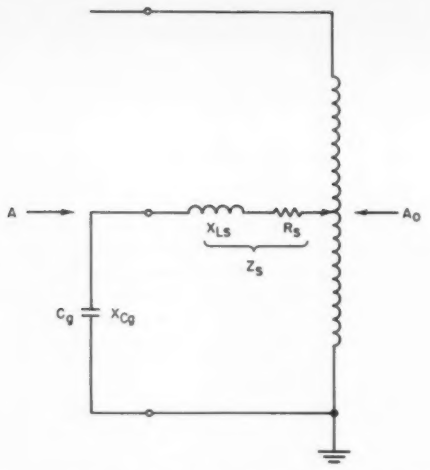


FIGURE 7. *The actual voltage ratio,* **A**, *at the terminals of an inductive voltage divider differs from the ratio,* $\mathbf{A}_0$, *as a result of loading by the capacitance,* $C_g$, *on the effective series output impedance of the divider,* $Z_s$.

capacitive loads and extrapolating to determine the voltage ratio and phase angle at zero load.

Comparison of eqs (5) and (28) shows that for inductive voltage dividers

$$\mu = -\omega^2 C_g L_s \tag{29}$$

and

$$\rho = \omega C_g R_s. \tag{30}$$

At a frequency of 1,000 c/s, if $C_g$=200 pf, $L_s$= 100 μh, and $R_s$=10 ohms, $\mu$ is approximately $0.8\times 10^{-6}$, and $\rho$ is approximately $12\times 10^{-6}$. The method described in section 7 for eliminating these corrections is applicable here also, although the extrapolation to zero load as described above has been found convienient.

## 9. Calibration Techniques and Accuracy

In general, the calibration of adjustable voltage dividers consists of determinations of voltage ratio and phase angle corresponding to certain nominal ratio settings when no load is connected to the output terminals. The expression for voltage ratio for the four-terminal network given by eq (17) can be modified according to eq (5) to yield the voltage ratio under no-load conditions

$$A_{H0} = \frac{A_4 - A_2}{A_3 - A_1}(1+\mu). \tag{31}$$

From eqs (5) and (18) the voltage ratio for the three-terminal network is

$$A_{T0} = \frac{A_4 - A_1}{A_3 - A_1}(1+\mu). \tag{32}$$

The phase angle for the four-terminal network, from eqs (5) and (22), is

$$\gamma_{H0} = \frac{q_4 - q_2}{A_4} - (q_3 - q_1) + \rho, \tag{33}$$

and, from eqs (5) and (23), the phase angle for the three-terminal network is

$$\gamma_{T0} = \frac{q_4 - q_1}{A_4} - (q_3 - q_1) + \rho. \tag{34}$$

The loading corrections, $\mu$ and $\rho$, are usually very small and often can be computed on the basis of measurements involving no great accuracy. The ratios $A_1$, $A_2$, and $A_3$ need be measured only once in the calibration of a voltage divider if the input impedance of the divider remains constant when the divider ratio is changed.

The accuracy of the measurement of voltage ratio and phase angle by this method is dependent upon a relatively few systematic errors and a number of random errors. A satisfactory appraisal of the propagated errors must allow for more or less complete cancellation or certain errors that, if considered independently, are of rather large magnitude. Errors in the values of the capacitors are of this nature, since the ratio of the capacitances and conductances of two capacitors can be measured with much better accuracy by substitution methods than the accuracy with which any one capacitor can be measured.

The precision of the measurements can be enhanced by reducing the effect of temperature changes in the bridge components. In the work described, the temperature of the bridge was regulated by forced warm air. The 100 pf capacitor, $C$, was temperature compensated, and the design of the enclosures of this capacitor, as well as those within the bridge, incorporated a large amount of thermal lagging. The drift of these capacitors with time was a source of error that was reduced by arranging the sequence of work so that the time between critical measurements was minimum. It may be possible to further reduce the effects of drift by a timed program of sandwiched measurements, although this procedure has not yet been necessary. The capacitance ratio, $C/C_A$, can be determined most accurately if $C$ is nominally equal to $C_1$, or $C_2$, or . . . $C_8$, shown in figure 1.

The total estimated maximum error in the establishment of known ratios by the method described in this paper was derived by adding, without regard to sign, the estimated maximum error associated with each step in the measurement and estimated possible residual systematic errors. This method of expressing the accuracy of the measurements was chosen because most of the elementary errors are not completely independent. A number of tests were made to determine the magnitude of errors in the ratios of the secondary taps on the transformer in the capacitance bridge. Although several methods designed to detect ratio errors (departure from

linearity) were used, no errors were found that exceeded twice the propagated uncertainties attributed to resolution of the bridge during these measurements. These methods are discussed below. In general, no error in ratio was found that exceeded 0.000 000 06, and the uncertainty of these errors was about ±0.000 000 03. Accordingly, the estimated uncertainty from this source was considered to be ±0.03 ppm of ratio when the largest capacitor in use ($C_1$, $C_2$, . . . or $C_8$, in fig. 1) spans the entire lower half of the secondary. This estimated uncertainty then increases to ±0.3 ppm of ratio when the largest capacitor in use spans only 0.1 of the lower half of the secondary. The resolution of the equipment, as used for the determination of the ratio $A_4$, was equivalent to a ratio of ±0.000 000 01, i.e., ±0.01 microvolt output voltage per volt input. The estimated maximum uncertainty from this cause was conservatively estimated as equivalent to a ratio of ±0.000 000 02. A similar uncertainty exists in the measurement of $A_1$ or $A_2$. In the measurement of lower ratios these two sources of uncertainty predominate, limiting accuracy to within ±0.000 000 04 at a ratio of 0.001. The determination of capacitance ratio can be accomplished with an estimated uncertainty of ±0.03 ppm of ratio for measurements of voltage ratios from 1 to 0.1; ±0.2 ppm of ratio for ratios from 0.1 to 0.01 wherein two steps are required; and ±2 ppm of ratio for ratios from 0.01 to 0.001 wherein three steps are required. The determination of $A_3-A_1$, as it enters into the computation of ratio, can be accomplished with a relatively small uncertainty of ±0.02 ppm of ratio. The sum of these uncertainties, without regard to sign, and expressed as an additive ratio, is shown in table 1 as the estimated maximum uncertainty in ratio at a frequency of 1,000 c/s.

TABLE 1. *Estimated accuracy at 1,000 cycles per second*

| Nominal ratio | Estimated maximum uncertainty | |
|---|---|---|
| | Ratio | Phase angle |
| | | *Microradians* |
| 1 | ±0.000 000 12 | ±0.5 |
| 0.5 | ±.000 000 10 | ±2.3 |
| .1 | ±.000 000 08 | ±4 |
| .05 | ±.000 000 06 | ±3 |
| .01 | ±.000 000 06 | ±7 |
| .005 | ±.000 000 05 | ±13 |
| .001 | ±.000 000 04 | ±46 |

The estimated maximum uncertainties listed in table 1 do not indicate the actual error in any particular measurement. It is to be expected that actual errors are much smaller than the estimated maximum uncertainties. A separate experiment was conducted to obtain a quantitative appreciation of the actual error in the measured voltage ratio assigned to particular voltage dividers. This utilized two decade voltage dividers, one of which was carefully calibrated as a three-terminal divider by the method described above. This calibrated divider then was used as a standard for the calibration of the highest decade of the other divider by a comparison method in which the input terminals were connected in parallel and the output terminals connected to a phase-sensitive detector. The two dividers formed an a-c bridge in which the true voltage ratios were equal under conditions of balance. The connections to the input terminals of the divider under test were reversed, and a second calibration of the highest decade was obtained. In the first comparison, the readings of the standard and the test dividers were matched, i.e., (0.9, 0.9), (0.8, 0.8), . . ., (0.1, 0.1,), while in the latter comparison, the readings were related in the manner (0.9, 0.1), (0.8, 0.2), . . ., (0.1, 0.9). Additive corrections to each step of the highest decade were thus obtained, based upon two different ratios of the standard divider. The difference between corresponding additive corrections to the nominal ratio in no case exceeded 0.000 000 04, and generally the corrections agreed within 0.000 000 02. Better agreement than this could hardly be expected, because the precision of the initial calibration of the standard was estimated as ±0.000 000 02. Although corrections to the divider under test at the ratio 0.5 can be obtained accurately by the reversed-comparison method independently of the voltage ratios assigned to the standard voltage divider, it should be understood that this method does not reveal residual errors in the calibrated standard that are symmetrical about the ratio 0.5. An investigation to discover such symmetry in the capacitance bridge was conducted by a step-up method in which a fixed capacitance was repeatedly added to one side of the bridge and the differences in readings of the capacitance complex in the lower side of the bridge were noted. Although this investigation suffered from a small drift in the capacitors, and a timed sequence of readings was used to eliminate the effects of this drift, there was no evidence of errors of symmetry greater than 0.000 000 06. The uncertainty of these errors was ±0.000 000 03, which was the limit of uncertainty in the investigation, primarily a result of uncontrolled drift. In this test for symmetry, the differences between 0.1 sections of the lower half of the secondary were adjusted for drift in the capacitor, and added cumulatively to obtain the total error at each tap. The results were averaged over several tests and then adjusted to eliminate the effect of nonsymmetrical errors. The measured, algebraically additive, errors of symmetry were found to have magnitudes of approximately 0.04, 0.06, 0.04, and 0.02 $\times 10^{-6}$ (all with an uncertainty of $\pm 0.03 \times 10^{-6}$), corresponding to the ratios 0.1 and 0.9, 0.2 and 0.8, 0.3 and 0.7, and 0.4 and 0.6, respectively.

The accuracy of position of the centertap on the secondary of the transformer was determined by connecting a 7-decade inductive voltage divider across the entire secondary and adjusting the inductive voltage divider to obtain a balanced condition. Then the connections from the divider to the transformer secondary were interchanged, and the inductive voltage divider again adjusted to obtain balance. Half the difference in readings of the inductive voltage divider is indicative of the error in position of

the centertap. In the experiment, the interpolated readings were equal, with a precision of $\pm 0.\ 000\ 000\text{-}01$. Hence the centertap is believed to be within $\pm 0.\ 000\ 000\ 01$ of true center.

Although great accuracy usually is not required in the measurement of the phase angle, the capacitance bridge method presented in this paper is capable of providing quantitave phase angle measurements on inductive voltage dividers. A similar analysis was made of the errors contributing to the uncertainty of the phase angle. A simple method was developed to eliminate the effect on phase angle of conductance in the capacitors. This is accomplished by measuring the difference in conductances between the external capacitor, $C$, and the capacitor in use within the bridge. It is this difference of conductance that enters into the computation of phase angle. The difference can be measured with an accuracy within 0.3 percent of the difference. In the work described, the differences in conductances were measured quite simply at the times the capacitors were compared. At ratios near 1, the largest uncertainty in phase angle is contributed by the transformer. It is believed that this error is no larger than $\pm 0.3$ microradian when the largest capacitor in use spans the entire lower half of the secondary, and $\pm 3$ microradians when the largest capacitor in use spans only 0.1 of the lower half of the secondary. The largest uncertainties in phase angle at low ratio measurements are contributed by a series of two conductance balances, each contributing about $\pm 0.02 \times 10^{-6}$ uncertainty to the measurement of the quadrature component, part of which is systematic, and another conductance balance that introduces about $\pm 0.003 \times 10^{-6}$ uncertainty, although there is some cancellation of the previously mentioned systematic error. At a ratio of 0.001, the sum of these uncertainties in the quadrature component converted to phase angle is about $\pm 46$ microrodians. The overall maximum estimated error at a frequency of 1,000 c/s is given in table 1.

## 10. Conclusion

The method described has been employed for the very accurate calibration of a few decade inductive voltage dividers that, in turn, serve as standards for the more economical calibration of other dividers by a comparison method.

---

The author thanks Raymond V. Lisle for his assistance during the experimental stages of this development.

## 11. References

[1] W. C. Sze, Trans. AIEE, pt. I, **76,** 444 (1957).
[2] C. B. Pinckney, Trans, AIEE, pt. I, **78,** 182 (1959).
[3] N. E. Morrison, Electro Scientific Industries, AIEE Summer and Pacific General Meeting, Paper 59-997 (1959).
[4] M. C. McGregor, J. F. Hersh, R. D. Cutkosky, F. K. Harris, and F. R. Kotter, Trans. IRE on Instrumentation, **I-7,** 253 (1958).
[5] R. D. Cutkosky and J. Q. Shields, Trans. IRE on Instrumentation, **I-9,** 243 (1960).

(Paper 66C1-84)

JOURNAL OF RESEARCH of the National Bureau of Standards—C. Engineering and Instrumentation
Vol. 66C, No. 1, January–March 1962

# Weight Calibration Schemes for Two Knife-Edge Direct-Reading Balances

H. E. Almer, L. B. Macurdy, H. S. Peiser, and E. A. Weck

(August 11, 1961)

Direct-reading, two knife-edge, single-pan balances of high quality are shown to be well suited for most laboratory weight calibrations. The requirements for the design of good calibration series on such balances include:

1. Series are based on external mass standards rather the dial-operated weights.
2. Balance sensitivity is measured.
3. Substitution differences, not single balance indications, enter into mass determinations.
4. Tests for inadvertent fluctuations in balance indications are included.
5. Every indication entering into the calibration is subject to some check.
6. Known standard weights are calibrated side by side with unknown weights.
7. Series must have sufficient redundancy to permit a study of errors.
8. Buoyancy corrections, when not negligible, are applied.

Three rapid series are described in which drift of the balance indication is liable to introduce some uncertainty. Three other series are described which require more individual weighings, but nearly eliminate the effects of such slow drifts.

When unknown weights are compared with standards of the same denomination simplification is achieved usually associated with a loss of accuracy. Finally, methods for tolerance testing on single-pan balances are given.

## 1. Introduction

### 1.1. Basis for Use of Single-Pan Damped Balances

In recent years a number of well-known balance manufacturers have designed and marketed damped, direct-reading, high-precision laboratory balances. The work here described was carried out with balances which have a single pan, a beam with only two knife-edges, and internal weights that are applied to the pan suspension so as to bring the total applied load to a constant value. This technique of using the same load for all weighings effectively minimizes an important cause of changes in sensitivity. Although the quick-weighing features of such balances currently available may place a limitation on weighing precision somewhat lower than can be obtained by more elaborate weighing methods on the best equal-arm types of balances, the precision attainable under suitable weighing conditions is good enough so that weighings meaningful to a few parts in $10^7$ of the balance capacity can be regularly attained. With a set of suitable balances each used for the calibration of about a decade of weights the largest of which is not much smaller than the balance capacity, it is possible to obtain about 1 part in $10^6$ or better over a wide range of loads to be weighed. Weights adjusted on the customary bulk-buoyancy basis [1, p. 673][1] rather than the true-mass basis are still subject to small variations of bouyancy due to changes in ambient-air density. The errors introduced by neglecting such effects are about 1 part in $10^6$. Consequently higher precisions are attainable only through more detailed bouyancy corrections. Thus the single-pan balances discussed here can provide a precision of weighing that is entirely adequate for the great majority of weight calibrations. The gain in simplicity and speed by their use should dispel any apprehension that weight calibration is too difficult and tedious to be undertaken even in laboratories where accurate weighings are attempted.

### 1.2. Requirements for an Individual Balance for Use in Weight Calibration

The suitability of a balance in weight calibration is easily judged. The sum of the errors due to the imprecision of the balance and the inaccuracy of the standard reference weight must not exceed the acceptable error. The relevant term for describing the imprecision of the balance is its standard deviation for a single observation divided by an appropriate factor to give a limit for the effect of random errors of the measurements. Lashof and Macurdy [2] have described a searching test suitable for single-pan damped balances from which a value of the standard deviation of a single observation is obtained. The other and quite independent uncertainty arises from the inaccuracy of the reference weight. The portion applicable to an unknown weight is the standard deviation of the reference-weight value multiplied by the ratio of the mass of the unknown to that of the standard weight.

### 1.3. General Requirements for the Weighing Series

Having established that a balance is suitable for a weight calibration the following precautions must still be taken.

[1] Figures in brackets indicate the literature references at the end of this paper.

1. The mass values must be determined by comparison with externally applied standard weights (not necessarily of the same nominal value) and must not depend on the accuracy of counterpoise or other built-in balance weights.

2. The sensitivity of the balance must be determined (if only as check of direct-reading characteristics of the balance) by addition of sensitivity weights of known value on the pan and must not be assumed to be constant from day to day or equal to the designed value.

3. The calibration series must be entirely based on substitution differences so that it is not necessary to adjust the balance indication to read any particular value. A weight of zero correction need not produce a zero indication.

4. Tests for the presence of fluctuations in the balance indication by extraneous disturbances must be included in the weighing schemes.

5. There must be some check on each individual balance indication.

6. Each series must include one or more standards, having a known mass value, which are experimentally evaluated with the unknown weights.

7. The series must have sufficient redundancy so that the desired precision is achieved by least squares or similar averaging of independent observations.

8. Buoyancy and standard-weight corrections, when not negligible, are applied as for all precise weight calibrations.

## 2. Pienkowsky Type Weighing Series

Figures 1, 2, and 3,[2] give the actual figures for calibrations by substitution series essentially evolved by A. T. Pienkowsky (unpublished). The aim of these series is to provide simple but sound calibrations with few observations.

In all three series the method of differential weighing is used, in which the indication given by the balance is not used as a measure of the mass of the load on the pan, but in which the difference between indications is taken as the difference in the masses of the loads. In the cases illustrated the sensitivity weighings verify that the scale readings are in milligrams.

In figure 1 the weighings are made in the order shown in the load column. The loads and errors of weights are indicated by a nomenclature which is best illustrated by a few examples:

(50) is the designation of the weight to be calibrated having a nominal value of 50 units.

NH $10_1$ is one of the standard weights whose nominal value is 10 units and which is part of the series NH; there is more than one 10-unit weight in that series and the subscript is a distinguishing mark. All mass standards are identified by the set designation preceding the denomination. A broken line before the denomination calls for the designation of the standard.

$\Sigma(50)$ is a specific group of weights the sum of whose nominal values is 50 units. On this form $\Sigma(50)=(20)+(20)+(10)$

Cr(50) is the "correction" of the (50) weight. The "correction" of a weight or group of weights is by magnitude and sign equal to the difference: actual minus nominal mass values.

The difference between the appropriate scale readings, together with the correction for the sum $(50)+\Sigma(50)$ carried forward from comparisons in the next higher decade are used to compute the corrections for (50) and $\Sigma(50)$ by the sum and difference method. One-half the sum of equations marked (1) and (2) in the margins of figure 1 is the correction for (50) and one-half the difference is the correction for $\Sigma(50)$ denoted $K$. The difference between the second and third scale readings is added to the Cr $\Sigma(50)$ to compute the value of the standard, NH 50, as determined by this calibration. The agreement of this value of the standard with the accepted value previously determined by a more precise method is a measure of the accuracy of the calibration. The third and fourth scale readings are used to verify the sensitivity adjustment of the balance. Their difference $D_s$ should equal the mass $M_s$ of the small added weight within the reproducibility of the balance.

The last eight scale readings together with the Cr $\Sigma(50)$ are used to compute the corrections for $(20)_1$, $(20)_2$, (10), $\Sigma(10)$, and standard 10. The scale readings are taken in the order shown and the indicated computations performed, the end result being the corrections of the weights (the numbers by the arrowheads in the margin). The three differences, denoted $Z_i$, in the right-hand column at the middle of the figure, are three measurements of the difference between $(20)_1$ and $(20)_2$ and their agreement (within 0.03 mg under these particular weighing conditions) is a measure of the precision of the calibration as is the difference between $a$ and $h$ ($h$ is a repetition of $a$). The latter figure is a convenient measure of the net balance drift. The agreement of the value of the standard 10 as determined by this calibration with its accepted value, is a measure of the accuracy of the calibration. The computations indicated in the shaded areas are computational checks and the figures within each box must agree except for errors due to rounding-off. The double framed boxes on the form are observational checks as indicated above.

The sensitivity of the balance was not determined with that series because it had been determined with the calibration of the (50 g) and $\Sigma(50$ g), just prior to this series.

A very approximate estimate of the standard deviation $s_F$ of the final values is obtained from the following formula

$$s_F=\frac{1}{3}[\text{Range in } Z+(a-h)+s_K]$$

[2] The forms shown in these and later figures are in regular use for weight calibrations at the National Bureau of Standards.

| Temperature | FORM NBS-345.03 (REV. 8-31-60) | U.S. DEPARTMENT OF COMMERCE NATIONAL BUREAU OF STANDARDS | Sheet 2 |
|---|---|---|---|
| Humidity | **SUBSTITUTION CALIBRATION (5, 2, 2, 1, Σ1 SERIES)** | | Unit (Wts.) g |
| Barometer | **Single Pan Damped Balances** | | Unit (Cr. and Diff) mg |
| ρ = | $\Sigma(50) = (20)_1 + (20)_2 + (10)$ | | |

| Observer HSP | Balance M-1 | Date 10-7-59 | Set A | NBS Test No. 158575 |
|---|---|---|---|---|

**COMPUTATIONAL CHECKS IN SHADED AREAS** — **OBSERVATIONAL CHECKS IN FRAMED BOXES**

| Load | Dial Setting | Scale Reading | Substitution Differences |
|---|---|---|---|
| (50 ) | 50.0 | 0.50 | (50 ) − NL 50 = +.03 |
| NL 50 | " | 0.47 | (50 ) − Σ(50 ) = −.00 |
| Σ(50 ) | " | 0.50 | NL 50 − Σ(50 ) = −.03 |
| " + L 10 mg | " | 10.49 | Obs $D_s$ = +9.99; $M_s$ = 10.00 |
| (10 ) Σ(10 ) NL $10_1$ | 30.0 | a .54 | a+h = A = 1.07 |
| (20 )$_1$ NL $10_1$ | " | b .55 | b+c = B = 1.09 |
| (20 )$_2$ NL $10_1$ | " | c .54 | |
| (20 )$_2$ (10 ) | " | d .58 | d+e = D = 1.15 |
| (20 )$_1$ (10 ) | " | e .57 | f+g = F = 1.12 |
| (20 )$_1$ Σ(10 ) | " | f .56 | |
| (20 )$_2$ Σ(10 ) | " | g .56 | A+B+D+F = 4.43 |
| (10 ) Σ(10 ) NL $10_1$ | " | h .53 | a+b+c+d+e+f+g+h = 4.43 |
| " + | " | | Obs Ds = Ms = − |

From Sheet 1 $Cr\Sigma(100)$ = Cr[(50 ) + Σ(50 )] = +.04 (1)
(50 ) − Σ(50 ) = −.00 (2)

1/2 Sum = Cr (50 ) = +.02

1/2 Diff. = $Cr\Sigma$(50 ) = +.02 = K

NL 50 − Σ(50 ) = −.03

NL 50 − Σ(50 ) + K = −.01 = Cr NL 50

Acc. Cr NL 50 = −.027

A−B+D−F

Sum = +.01 = C

B−D = −.06 = E

F−D = −.03 = G

C+E+G = −.08

A−D = −.08

K = +.02

Cr[(2)$_1$ + (2)$_2$ + (1)] = +.03

1/2 E = −.03

NL 10 − (10 ) = −.03

1/2 G = −.02

Σ(10 ) − (10 ) = −.02

Obs Ds = Ms = −

Note: Σ(10 ) = (5) + (2)$_1$ + (2)$_2$ + (1)

b−c = $Z_1$ = +.01
e−d = $Z_2$ = −.01
f−g = $Z_3$ = −.00

Mean Z = −.00 = Z'

Total Range in Z's = .02

Net Balance Drift
a−h = +.01

Z' = −.00

(20 )$_1$ − (20 )$_2$ = −.00

Cr NL $10_1$
5E+10 Cr (10 )
0.1 Sum = −.02

Acc Cr = −.011

| Cr (20 )$_1$ | Cr (20 )$_2$ | Cr (10 ) | Cr Σ (10 ) |
|---|---|---|---|
| −C+5Z'+4K | −C−5Z'+4K | 2C + 2K | 5G+10Cr (10 ) |
| 0.1 Sum = +.01 | 0.1 Sum = +.01 | 0.1 Sum = +.01 | 0.1 Sum = −.01 |

USCOMM-DC 24061-P60

FIGURE 1.

| Temperature | FORM NBS-345.02 (1-12-61) | U.S. DEPARTMENT OF COMMERCE NATIONAL BUREAU OF STANDARDS | Sheet 3 |
|---|---|---|---|
| Humidity | **SUBSTITUTION CALIBRATION (5, 2, 2, 1, SERIES)** | | Unit (Wts.) g |
| Barometer | **Single Pan Damped Balances** | | Unit (Cr. and Diff.) mg |
| ρ = | $\Sigma(5) = (2)_1 + (2)_2 + (1)$ | | |

| Observer NBQ | Balance M-2 | Date 10-28-59 | Set I | NBS Test No. 158783 |
|---|---|---|---|---|

**COMPUTATIONAL CHECKS IN SHADED AREAS** — **OBSERVATIONAL CHECKS IN FRAMED BOXES**

| Load | Dial Setting | Scale Reading | Substitution Differences |
|---|---|---|---|
| (5 ) | 5.00 | .129 | (5 ) − NB 5 = +.029 |
| NB 5 | " | .100 | (5 ) − Σ(5 ) = +.030 |
| Σ(5 ) | " | .099 | NB 5 − Σ(5 ) = +.001 |
| " +85mg a | " | 5.099 | Obs $D_s$ = 5.001 <br> $M_s$ = 5.000 |
| (1 ) C1 NB 1 | 3.00 | a .081 | a+h=A = .166 |
| (2 )1 NB 1 | " | b .084 | b+c=B = .184 |
| (2 )2 NB 1 | " | c .100 | |
| (2 )2 (1 ) | " | d .109 | d+e=D = .198 |
| (2 )1 (1 ) | " | e .089 | f+g=F = .144 |
| (2 )1 C1 | " | f .060 | |
| (2 )2 C1 | " | g .084 | A+B+D+F = .692 |
| (1 ) C1 NB 1 | " | h .085 | a+b+c+d+e+f+g+h = .692 |
| " + | | | Obs $D_s$ = . $M_s$ = . |

From Sheet 2 $Cr\Sigma(10\ ) = Cr|(5\ ) + \Sigma(5\ .\ ) | = +.033$ ; $(5\ ) - \Sigma(5\ ) = +.030$

1/2 Sum = Cr (5 ) = +.032

1/2 Diff. = Cr Σ(5 ) = +.002 = K

NB 5 − Σ(5 ) = +.001

NB 5 − Σ(5 ) + K = +.003 = Cr NB 5

Acc. Cr NB 5 = +.003

A−B+D−F

Sum = +.036 = C

B−D = −.014 = E

C−E = +.022

A−F = +.022

K = +.002

$Cr|(2\ )_1 + (2\ )_2 + (1\ )| = +.002$

1/2 E = −.007

NB 1 − (1 ) = −.007

| | | |
|---|---|---|
| $b-c=Z_1$ | = −.016 | |
| $e-d=Z_2$ | = −.020 | |
| $f-g=Z_3$ | = −.024 | |
| Mean Z | = Z′ = −.020 | |
| Total Range in Z′s | = .008 | |
| Net Balance Drift | | |
| a − h | = −.004 | |
| Z′ | = −.020 | |
| (2 )1 − (2 )2 | = −.020 | |

| Cr (2 )1 | Cr (2 )2 | Cr (1 ) | Cr NB 1 |
|---|---|---|---|
| −C+5Z′+4K | −C−5Z′+4K | 2C+2K | 1/2 E + Cr(1 ) |
| 0.1 Sum = −.013 | 0.1 Sum = +.007 | 0.1 Sum = +.008 | Sum = +.001 |
| | | | Acc Cr = −.002 |

USCOMM-DC 24047-P80

FIGURE 2.

| Temperature | FORM NBS-345.01 (REV. 8-29-60) | U.S. DEPARTMENT OF COMMERCE NATIONAL BUREAU OF STANDARDS | Sheet 2 |
|---|---|---|---|
| Humidity | **SUBSTITUTION CALIBRATION (5, 3, 2, 1, Σ1 Series)** | | Unit (Wts.) g |
| Barometer | **Single Pan Damped Balances** | | Unit (Cr. and Diff.) mg |
| ρ = | Σ(10) = (5) + (3) + (2) | | |

| Observer JAW | Balance M-1 | Date 2-6-61 | Set B | NBS Test No. G28462 |
|---|---|---|---|---|

**COMPUTATIONAL CHECKS IN SHADED AREAS**

| Load | Dial Setting | Scale Reading | |
|---|---|---|---|
| NX 50 | 50.0 g | 0.93 | a-b = -.01<br>m-l = -.01 |
| (50) | " | a 0.98 | Mean = A<br>= -.01 |
| (30)<br>(20) | " | b 0.99 | b - g = B<br>= +.01 |
| (30)<br>NX 20 | " | c 0.94 | c - h = C<br>= -.09 |
| (30)<br>(10)<br>Σ(10) | " | d 1.04 | d - i = D<br>= +.12 |
| (20)<br>NX 20<br>(10) | " | e 1.08 | e - j = E<br>= +.18 |
| (20)<br>NX 20<br>Σ(10) | " | f 1.07 | f - k = F<br>= +.16 |
| + (b+c+d+e+f) = + | | 5.12 | B+C+D+E+F |
| - (g+h+i+j+k) = - | | 4.74 | = |
| Sum = 1 | | 0.38 | = +0.38 |
| NX 20<br>(10)<br>Σ(10)<br>C10 | 50.0 | g 0.98 | b + g<br>1.97 |
| (20)<br>(10)<br>Σ(10)<br>C10 | " | h 1.03 | c + h<br>1.97 |
| (20)<br>NX 20<br>C10 | " | i 0.92 | d + i<br>1.94 |
| (30)<br>Σ(10)<br>C10 | " | j 0.90 | e + j<br>1.98 |
| (30)<br>(10)<br>C10 | " | k 0.91 | f + k<br>1.98 |
| (30)<br>(20) | " | l 1.00 | l + g<br>1.98 |
| (50) | " | m 0.99 | Obs $D_s$<br>= 9.99 |
| " | " | m' 10.98 | $M_s$<br>= 10.00 |
| +L10mg | | | |

**OBSERVATIONAL CHECKS IN FRAMED BOXES**

From sheet 1

K = Cr Σ(100)
= +.05

Computed K:
Cr {(5) + (3) + (2)}
= +.05

2 Cr Σ(50)
K - A = +.06 = P

Q=4Cr(30)-6Cr(20)

D=B+2C-E-F

Sum = -.41 = Q

Optional Computational Aids

| | |
|---|---|
| C - B | = -.10 |
| E - C | = +.27 |
| 2Q | = -.82 |
| P | = +.06 |
| F - C | = +.25 |

Total Range in Sums
= .02

Net balance drift
a - m = -.01

-1/2 (C - B) = +.05
(20) - NX 20
= +.05

1/2 (D - B) = +.04
(10) + Σ(10) - (20)
= +.14

1/2 (E - F) = +.01
(10) - Σ(10)
= +.01

Cr (50)
1/2 (K + A) = +.02

Cr NX 50
NX 50 - (50) = -.05
+ Cr(50) = +.02
Cr NX 50 = -.03

Acc Cr NX 50 = -.03

Cr (30)
3P+Q
0.1 Sum = -.02 ←

Cr (20)
2P-Q
0.1 Sum = +.05 ←

Cr NX 20
1/2 (C-B)+Cr(20)
Sum = -.00

Acc Cr = +.01

Cr (10)
5 (E-C)+P+2Q
0.1 Sum = +.06 ←

Cr Σ(10)
5 (F-C)+P+2Q
0.1 Sum = +.05 ←

USCOMM-DC 24088-P60

FIGURE 3.

where $s_K$ is the estimated standard deviation of $K$.

The series illustrated in figure 2 is the same as that in figure 1, except that there is no $\Sigma(1)$ and that in the example given the weights involved are only one-tenth as large. The weighings are taken in the same order. The checks and the computations are the same except that those needed to find the correction for the summation are not made. C 1, a "constant weight," appears where $\Sigma(10)$ appeared in figure 1. The value of this "constant weight" is not computed. Its presence in the series introduces the desired redundancy. Apart from the requirement of adjustment to nominal value within the on-scale range of the balance, the "constant weight" need only remain constant while the observations in one series are taken.

The nomenclature indicating the loads and errors of the weights in figure 3 is the same as in figures 1 and 2. The weighings are made in the order shown. The first scale reading and those designated $a$ through $m$ together with the correction for the $\Sigma(100)$ (from another sheet, not shown, on which the comparisons in the next higher decade, corrected for air buoyancy, are given) are used to determine the corrections for the weights (50), (30), (20), (10), $\Sigma(10)$, NH 50, and NH 20. $\Sigma(50)$ on this form signifies (30)+(20). To obtain the corrections for the weights the indicated computations are performed. Again the checks on computation are in the shaded areas and the figures within each box must agree except for rounding-off errors. The double-framed boxes on the form are observational checks. The agreement of the sums $b+g$, $c+h$, etc., in the lower half of the fourth column from the left, corresponds to the agreement between $Z$'s in figures 1 and 2, and is an indication of the precision of the calibration, as is the agreement between $a$ and $m$ ($m$ is a repetition of $a$). This latter figure is used principally as a measure of the balance drift. The agreement of the values of the standards, NH 50 and NH 20, determined by this calibration with their accepted values provides valuable overall checks.

The last weighings, $m'$ and $m$, are used to determine the sensitivity of the balance. Their difference should equal the mass of the small added weight within the reproducibility of the balance.

Discussion of Pienkowsky-type series would not be complete without reference to the possible adverse effects on precision resulting from drift in balance indication. Over the entire time of completing balance readings at any one load in a series (fig. 1 to 3) such balance drift is liable to introduce an uncertainty in the ultimate mass values. "Trend elimination" therefore becomes an important feature in the design of such series.

The reader can readily convince himself by inspection of figure 3, for example, that the series is so designed that for a steady balance drift proportional to time, under a uniform rate of recording observations, the effects of balance drift on the mass comparison are entirely eliminated. The stated conditions of operation, however, are in practice difficult to achieve within the required limits; nor is the $(a-m)$ test any measure of the nonuniformity of drift. A low value for the $(a-m)$ difference in balance indication may hide a maximum in the extent of drift during the observational period. It is true that some knowledge of the individual characteristics of a balance might help; some designs for instance appear to produce drift periods of the order of an hour. On such instruments an experienced observer will try to complete observations within a quarter of that period. The reader should here notice that a higher value of $(a-m)$ may then actually be indicative of a better set of observations than would be characteristic of a lower $(a-m)$ value! Another feature of balances (except some high-capacity types) is that they are influenced by the thermal disturbance caused by an operator sitting within several feet of the balance. The light illuminating the scale may cause a similar disturbance. Drifts for the first half-hour of observations tend therefore to be far greater than later. Because of these effects an observer should not interrupt his observations within a series.

It is of course true that better tests for drifts could be introduced, leading to superior methods of trend elimination. Such tests achieved by additional observations would, however, detract from the basic aim of the Pienkowsky type of series, to provide extremely simple but sound mass calibration with very few observations. The use of these series should be discouraged for all but experienced observers working with well tested balances in favorable environments.

The examples given in figures 1 to 3 will provide appropriate weighing series for the majority of weight sets. The proper use of these series will usually suggest itself even when the weight set differs slightly from those used for the illustrations. For instance, if in a terminating series involving the smallest weights of a set having the 5321 sequence an extra 1 weight is provided, it will take the place of the weight group $\Sigma 1$ used in figure 3. If, however, the set does not contain an extra weight 1 an additional mass standard $\underset{\sim}{1}$ can be introduced giving another valuable check. An optional but less desirable alternative is to substitute a "constant weight," as defined above, the correction for which is not computed.

A less straightforward example of the use of the series given in the illustrations concerns the 5211 $\Sigma 1$ weight sequences sometimes encountered, for which the 5221 $\Sigma 1$ series (fig. 1) can be applied. A standard 2 weight replaces the second (2) weight to be calibrated and the additional (1) weight in the 5211 $\Sigma 1$ set replaces the standard 1 weight in the illustration. It should be noted that the $\Sigma(10)$ obtained from the next higher decade must have been made up as follows: $(5)+(2)+\underset{\sim}{2}+(1)$. If $\Sigma(10)=(5)+(2)+(1)_1+(1)_2+\Sigma(1)$ is preferred, the algebraic solutions for all the weights must be correspondingly amended. As is discussed below, least squares solutions must be used. The $(5)+(2)+\underset{\sim}{2}+(1)$ summation will probably commend itself, firstly because the form given in the illustration can be employed without much change and, secondly,

because the $(5)+(2)+(1)_1+(1)_2+\Sigma(1)$ summation includes an inconveniently large number of weights. There are circumstances, however, under which the additional handling of the ___ 2 weight in the summation will not be considered justifiable.

For very unusual weight sequences in weight sets the authors would be glad to furnish Pienkowsky-type weighing series on request. However, the reader might wish to devise such series for himself. For this purpose an outline of the principal considerations in devising these series follows:

To the list of denominations of unknown weights in one decade are added one or more denominations for standard weights to be intercompared with the the unknown weights. A "constant weight," as defined above, may also be introduced. A larger denomination for the standard provides a better check on the accuracy than a standard weight of smaller denomination, but more important is the provision of the necessary combinations for weighings with a minimum number of nominal values for the total loads. Often there is difficulty in finding a convenient solution, if the (5) and $\Sigma(5)$ are determined by intercomparison with the smaller denominations. Intercomparison of the (5) and $\Sigma(5)$ with a check on a standard 5 separate from the intercomparison of the smaller denominations may then be the best choice.

In the Pienkowsky-type series each independent balance indication after the first at each particular total load provides one independent observation. (The sensitivity check reading is not counted as an independent observation.) A condition or mathematical restraint is established by some sum of unkown denominations, usually $\Sigma(5)$ or $\Sigma(10)$, the correction for which is determined by comparison with a standard or by a series at the next higher decade. The number of statistical degrees of freedom of the series then equals the number of independent observations plus one (for the restraint imposed by the assumed weight or summation weight), diminished by the number of weights evaluated in the series (including the "constant" weight where used). The computation of all the weight corrections must follow by least-square solutions. It is preferable to design the series so that the coefficients in these solutions do not involve recurring decimals.

The details of the series must be planned to eliminate all types of errors as far as possible. The verification of the direct-reading characteristic of the balance by a sensitivity weighing has already been discussed. Similarly, the need for measurement of the precision of the observations will be understood from previous elucidation. All the algebraic solutions for any one weight, any one sum, or any one difference of weights in the series can be used for determining a statistical range for the evaluation of precision. The choice should be determined by the desirability of having a large number of independent values to compare. This number for some sums will be larger than the number of degrees of freedom as defined above. The second consideration to guide the choice is the need for as many observations as possible to be involved in the range determination. In this way a safeguard is provided against misreadings of the balance indication.

The effect of balance drift has also been discussed above. It is here necessary to stress only the need for designing weighing series so that, firstly, a measure of the drift is obtained by at least one repetition of at least one load at as large an interval as possible; and that, secondly, the observations are grouped for optimum statistical trend elimination. However, it is not always practicable for the various checks on precision to fulfil this trend-elimination requirement. It will then be probable that the calibrated values are not worse than is indicated by the checks.

The series should be planned to detect a false placement of a weight in a combination. In the series, therefore, every weight should be placed on and removed from the balance at least twice. In the opinion of the authors, the designer of the series should leave to the observer the judgment when an individual discrepancy should no longer be accepted as within the precision range of observation.

Finally, every computational step should be subject to at least one check on the form, as a safeguard against computational blunders. Except for rounding-off errors, every discrepancy revealed by these checks points to error in the computation or the check itself.

## 3. Hayford-Benoit Type Weighing Series

The chief weakness of the Pienkowsky-type series lies in the difficulty of recognizing and properly eliminating the effects of slow drifts in balance indications; wherefore the Pienkowsky-type series cannot quite realize the full potentialities of a balance.

Figures 4, 5, and 6, illustrate series which reduce the effect of balance drift by being based on self-consistent pairs of weighings. The figures refer to actual weight sets calibrated by means of a 1-kg balance. The series used are equivalent to those evolved at the National Bureau of Standards for transposition weighings on equal-arm balances [1, p. 661 ff]. The type of weighing series is here named Hayford-Benoit after the two investigators to whom we are indebted for careful analyses of these methods [3, 4]. It should be noted that there is a fundamental distinction between the two types of weighing series: In the Pienkowsky type one additional reading of a balance indication may increase the number of degrees of freedom by one whereas in the Hayford-Benoit type at least two readings are needed.

The nomenclature for the loads and the corrections for the weights is the same as for figures 1, 2, and 3. The differential method of weighing is again used. Therefore, for a given substitution weighing, the dial-operated weights must not be changed. Each of the series is made up of from six to nine equations. Each weighing equation states the observed difference between two weights or groups of weights. These observed differences are denoted $a_1$, $a_2$, $a_3$, etc. First one weight or one group of weights is placed on the balance pan. The dials are then set for the nominal

| Temperature | FORM NBS-347.02 (11-7-60) | U.S. DEPARTMENT OF COMMERCE NATIONAL BUREAU OF STANDARDS | Sheet 2 |
|---|---|---|---|
| Humidity | SUBSTITUTION CALIBRATION (2,1,1,Σ1 Series) | | Unit (Wts.) ozt |
| Barometer | Single Pan Damped Balances | | Unit (Cr. and Diff.) mg |
| ρ= | Σ(1) = Σ(6) = (2)₁ + (2)₂ + (1) + Σ(1) | | |

| Observer W2a | Balance M-3 | Date 10-22-59 | Set B | NBS Test No. G24777 |
|---|---|---|---|---|

COMPUTATIONAL CHECKS IN SHADED AREAS — OBSERVATIONAL CHECKS IN FRAMED BOXES

| Load | Dial Setting | Scale Reading | Computations |
|---|---|---|---|
| (1) + (6) | 186.6g | 25.25 | (1)₁ − (1)₂ = a₁ : (6) − d6 = −0.35 |
| (1)₂ d6 | " | 25.60 | Obs−Cal = −.02 |
| (1)₁ (6) | " | 25.30 | (1)₁ − Σ(1) = a₂ : (6) − Σ(6) = −0.95 |
| Σ(1) Σ(6) | " | 26.25 | Obs−Cal = −.03 |
| (1)₂ d6 | " | 25.80 | (1)₂ − Σ(1) = a₃ : d6 − Σ(6) = −0.60 |
| Σ(1) Σ(6) | " | 26.40 | Obs−Cal = −.01 |
| (1)₁, (1)₂ (6), d6 | 373.2g | 46.70 | (1)₁ + (1)₂ − (2) = a₄ : (6) + d6 − 1lbt₁,₄ = −2.45 |
| (2) 1lbt₁,₄ | " | 49.15 | Obs−Cal = +.05 |
| (1)₂, Σ(1) d6, Σ(6) | " | 47.50 | (1)₂ + Σ(1) − (2) = a₅ : d6 + Σ(6) − 1lbt₁,₄ = −1.65 |
| (2) 1lbt₁,₄ | " | 49.15 | Obs−Cal = −.07 |
| (1)₁, Σ(1) (6), Σ(6) | " | 47.20 | (1)₁ + Σ(1) − (2) = a₆ : (6) + Σ(6) − 1lbt₁,₄ = −1.90 |
| (2) 1lbt₁,₄ | " | 49.10 | Obs−Cal = +.01 |
| " + L20 mg₁ | " | 69.15 | Obs $D_s$ = 20.05 ; L20 mg₁ = $M_s$ = 20.01 |

From Sheet 1 or Below: K = +3.98

Cr|(2) + (1)₁ + (1)₂ + Σ(1)| = Computed K = +3.98

$$\text{Cr}\,\frac{(2) - 1\text{lbt}_{1,4} - a_4 - a_5 - a_6 + 2K}{5} = +2.79$$

$$\text{Cr}\,\frac{(1)_1 (6) + 5a_1 + 5a_2 + 3a_4 - 2a_5 + 3a_6 + 4K}{20} = -0.02$$

$$\text{Cr}\,\frac{(1)_2\, d6 - 5a_1 + 5a_3 + 3a_4 + 3a_5 - 2a_6 + 4K}{20} = +0.31$$

Acc Cr = +0.25

$$\text{Cr}\Sigma\,\frac{(\lambda 6) - 5a_2 - 5a_3 - 2a_4 + 3a_5 + 3a_6 + 4K}{20} = +0.90$$

If Series Based on:

$(2) = ___2; K = \dfrac{5\text{Cr}___2 + a_4 + a_5 + a_6}{2} = -$

$(1)_2 = ___1; K = \dfrac{20\text{Cr}___1 + 5a_1 - 5a_3 - 3a_4 - 3a_5 + 2a_6}{4} = -$

Check Sums

| | |
|---|---|
| $a_1 - a_2 + a_3$ | = 0.00 |
| $a_2 - a_4 + a_5$ | = −.15 |
| $a_3 - a_4 + a_6$ | = −.05 |
| $a_1 + a_5 - a_6$ | = −.10 |

$$s = \sqrt{\frac{\Sigma(\text{Obs}-\text{Cal})^2}{3}}$$

s = 0.06 mg

USCOMM-DC 24101-P60

FIGURE 4.

| Temperature | FORM NBS-347.03 (11-80) U.S. DEPARTMENT OF COMMERCE NATIONAL BUREAU OF STANDARDS | Sheet 5 |
|---|---|---|
| Humidity | **SUBSTITUTION CALIBRATION (2,2,1,Σ1 Series)** **Single Pan Damped Balances** | Unit (Wts.) 9 |
| Barometer | Σ(1 ) = | Unit (Cr. & Diff.) mg |
| ρ = | | |

| Observer H.E.D. | Balance M-3 | Date 11-19-59 | Set | NBS Test No. Comp. No. 3001 |
|---|---|---|---|---|

COMPUTATIONAL CHECKS IN SHADED AREAS | OBSERVATIONAL CHECKS IN FRAMED BOXES

| Load | Dial Setting | Scale Reading | Computations |
|---|---|---|---|
| (1→) [100]* | 100.0 | 2.10 | (1→)−Σ(1→) =$a_1$ |
| Σ(1→) L100g$_1$ | " | 2.35 | [100] − L100g$_1$ = −0.25 |
| | | | Obs−Cal= −0.05 |
| (1→), Σ(1→) [100]* L100g$_1$ | 200.0 | 2.30 | (1 )+Σ(1 )−(2 )$_1$ =$a_2$ |
| (2→)$_1$ V200$_1$ | " | 2.10 | = +0.20 |
| | | | Obs−Cal= −0.01 |
| (1→), Σ(1→) [100]* L100g$_1$ | " | 2.40 | (1 )+Σ(1 )−(2 )$_2$ =$a_3$ |
| (2→)$_2$ V200$_2$ | " | 2.20 | = +0.20 |
| | | | Obs−Cal= +0.01 |
| (2→)$_1$ V200$_1$ | " | 2.20 | (2 )$_1$−(2 )$_2$ =$a_4$ |
| (2→)$_2$ V200$_2$ | " | 2.20 | = −0.00 |
| | | | Obs−Cal= +0.02 |
| (1→), (2→)$_1$ [100]* V200$_1$ | 300.0 | 2.35 | (1 )+(2 )$_1$−Σ(1 )−(2 )$_2$ =$a_5$ |
| Σ(1→), (2→)$_2$ L100g$_1$ V200$_2$ | " | 2.55 | = −0.20 |
| | | | Obs−Cal= +0.02 |
| (1→), (2→)$_2$ [100]* V200$_2$ | " | 2.05 | (1 )+(2 )$_2$−Σ(1 )−(2 )$_1$ =$a_6$ |
| Σ(1→), (2→)$_1$ L100g$_1$ V200$_1$ | " | 2.20 | = −0.15 |
| | | | Obs−Cal= +0.03 |
| " +L20 mg$_1$ | " | 22.20 | Obs $D_s$ = 20.00 |
| | | | $M_s$ = 20.01 |

From Sheet 4 or Below:
K = −0.10

Cr (2 )$_1$+(2 )$_2$+(1 ) =
Computed K = −0.10

S, m, M

$\frac{a_1+a_5+a_6}{3}$ = −0.20 = S

$2S+a_2+a_3$ = −0.00 = m

4K − m = −0.40 = M

N

$-a_2+a_3+2a_4+2a_5-2a_6$

$\frac{5}{7}$ Sum = −0.07 = N

Cr (1→) [100]
2K +2m
0.1 Sum = −0.02 ←

Cr (2→)$_1$ V200$_1$
M + N
0.1 Sum = −0.05 ←

Cr (2→)$_2$ V200$_2$
M − N
0.1 Sum = −0.03 ←

Cr Σ(1→) L100g$_1$
Cr (1 ) − S
Sum = +0.18
Acc. Cr. = +0.16

If Series Based on:
(2)$_1$= 2 and (2)$_2$= 2 ;

5{Cr 2+Cr $\frac{2}{3}$ = = M

$\frac{M+m}{4}$ = = K

Check Sums

| | |
|---|---|
| $a_2-a_3+a_4$ | = 0.00 |
| $a_1+a_4-a_5$ | = −0.05 |
| $a_1-a_4-a_6$ | = −0.10 |
| $a_4+\frac{a_5}{2}+\frac{a_6}{2}$ | = +0.02 |

$s = \sqrt{\frac{\Sigma(\text{Obs}-\text{Cal})^2}{3}}$

s = 0.04

*FROM SET E, 2.6 TEST NO. 105

USCOMM-DC 24108-P80

FIGURE 5.

| Temperature | FORM NBS-347.01 (11-23-60) | U.S. DEPARTMENT OF COMMERCE NATIONAL BUREAU OF STANDARDS | Sheet 3 |
|---|---|---|---|
| Humidity | **SUBSTITUTION CALIBRATION (2, 2, 1, 1, . . 1 Series)** | | Unit (Wts.) lb |
| Barometer | **Single Pan Damped Balances** | | Unit (Cr. and Diff.) mg |
| ρ = | | | |

| Observer HEA | Balance M-3 | Date 10-20-59 | Set A | NBS Test No. 62477 |
|---|---|---|---|---|

COMPUTATIONAL CHECKS IN SHADED AREAS — OBSERVATIONAL CHECKS IN FRAMED BOXES

| Load | Dial Setting | Scale Reading | Computations |
|---|---|---|---|
| (1 )$_1$ | 453 mg | 1.0 | (1 )$_1$−(1 )$_2$ = $a_1$ = −0.70 |
| B1 λ$_2$ | " . | 1.7 | Obs−Cal= −.04 |
| (1 )$_1$ | " . | 1.1 | (1 )$_1$−...1 = $a_2$ = +3.80 |
| ...1 lb$_{II}$ | " . | −2.7 | Obs−Cal= +.01 |
| B1 λ$_2$ | " . | 1.8 | (1 )$_2$−...1 = $a_3$ = +4.40 |
| ...1 lb$_{II}$ | " . | −2.6 | Obs−Cal= −.05 |
| (1 )$_1$,B1 λ$_2$ | 907 mg | 97.2 | (1 )$_1$+(1 )$_2$−(2 )$_1$ = $a_4$ = +4.50 |
| (2 )$_1$ | " . | 92.7 | Obs−Cal= .00 |
| B1 λ$_2$,...1 lb$_{II}$ | " . | 93.4 | (1 )$_2$+...1 −(2 )$_1$ = $a_5$ = +0.70 |
| (2 )$_1$ | " . | 92.7 | Obs−Cal= −.01 |
| (1 )$_1$,...1 lb$_{II}$ | " . | 92.8 | (1 )$_1$+...1 −(2 )$_1$ = $a_6$ = +0.05 |
| (2 )$_1$ | " . | 92.75 | Obs−Cal= +.05 |
| (1 )$_1$,B1 λ$_2$ | " . | 97.0 | (1 )$_1$+(1 )$_2$−(2 )$_2$ = $a_7$ = +3.50 |
| (2 )$_2$ | " . | 93.5 | Obs−Cal= +.04 |
| B1 λ$_2$,...1 lb$_{II}$ | " . | 93.1 | (1 )$_2$+...1 −(2 )$_2$ = $a_8$ = −0.35 |
| (2 )$_2$ | " . | 93.45 | Obs−Cal= −.02 |
| (1 )$_1$,...1 lb$_{II}$ | " . | 92.4 | (1 )$_1$+...1 −(2 )$_2$ = $a_9$ = −1.0 |
| (2 )$_2$ . | " . | 93.4 | Obs−Cal= −.01 |
| " + 1.10 mg | " . | 107.35 | Obs $D_s$ = 9.95, $M_s$ = 10.00 |

From Sheet 2 or Below: K = +7.76

Cr [(2)$_1$+(2)$_2$−(1)$_1$] =

Computed K = +7.76

$a_1+a_2+a_4+a_6+a_7+a_9$ = +10.15 = $B_1$

$-a_1+a_3+a_4+a_5+a_7+a_8$ = +13.45 = $B_2$

$-a_2-a_3+a_5+a_6+a_8+a_9$ = −8.80 = $B_3$

$-a_4-a_5-a_6$ = −5.25 = $B_4$

$-a_7-a_8-a_9$ = −2.15 = $B_5$

$B_1+B_2+B_3+2B_4+2B_5$ = 0 Equal Zero

Cr ...1 lb$_{II}$

$\frac{-B_1+5B_3+B_4+B_5+5K}{25}$ = −0.91

Acc Cr = −0.91

Cr (2lb)$_1$

$\frac{-6B_1+11B_4-14B_5+30K}{75}$ = +1.92

Cr (2lb)$_2$

$\frac{-6B_1-14B_4+11B_5+30K}{75}$ = +2.96

Cr (1lb)$_1$

$\frac{4B_1+B_4+B_5+5K}{25}$ = +2.88

Cr B1lb$_2$

$\frac{-B_1+5B_3+B_4+B_5+5K}{25}$ = +3.54

Acc Cr = +3.6

If Series Based on ...1 ;

$K = \frac{25Cr_{...1}+B_1-5B_3-B_4-B_5}{5}$ = −

Check Sums

$a_1-a_2+a_3$ = −0.1
$a_2-a_4+a_5$ = 0.0
$a_1+a_5-a_6$ = −0.05
$a_3-a_4+a_6$ = −0.05
$a_2-a_7+a_8$ = −0.05
$a_3-a_7+a_9$ = −0.1
$a_1+a_8-a_9$ = −0.05

$s = \sqrt{\frac{\Sigma(\text{Obs}-\text{Cal})^2}{5}}$

s = 0.04 mg

USCOMM-DC 24109-P60

FIGURE 6.

value of the load, and the scale reading observed and recorded. Similarly the other weight or group of weights are compared. In each pair of weighings the sign of the difference between the two weights is the sign that the heavier of the weights has in the observation equation. The scale readings and the differences between the weights are expressed in milligrams.

Figures 4, 5, and 6 show the observations and computations for the 2, 1, 1, Σ1; the 2, 2, 1, Σ1; and the 2, 2, 1, 1, _ _ _1 series respectively. The computations and checks are the same as if the $a$'s had been obtained by transposition weighing. The estimate of the standard deviation of a single observation, $s$, provided by the particular series of weighings, is a measure of the precision of the individual weighings. The agreement of the value of the standard weight, where one is used, obtained by this calibration with its accepted value is a further valuable indication of the accuracy of the calibration. When a standard weight is not included in the series an additional comparison is made. In this comparison a standard weight is evaluated in terms of a weight whose value was determined in the series. The agreement of the value of the standard weight obtained by this comparison with its accepted value will serve as an indication of the accuracy of the calibration.

The Hayford-Benoit type series, of course, can be applied to other groups of weights; the method for developing such weighing series is simpler than for Pienkowsky-type series where an all-important choice of possible comparisons has to be made. For Hayford-Benoit series, however, it is best to make all possible comparisons at all loads. Moreover, the derivation of these series is well described in the literature [4]. The adaptation to single-pan balances presents no difficulty.

## 4. Other Weighing Procedures

When a test weight is compared only once with a standard weight of the same denomination, an acceptable but less accurate procedure is illustrated as follows.

| Load | Scale reading |
|---|---|
| NH 10 $g_1$ | $+0.517=I_1$ |
| (10 g) | $+0.559=I_2$ |
| (10 g)$+\beta$ 10 mg | $+10.565=I_3$ |
| NH 10 $g_1+\beta$ 10 mg | $+10.527=I_4$ |

In this example the balance was adjusted to read about 0.5 mg more than the actual loads so that negative numbers would not be introduced into the record. For the average difference for (10 g)−NH 10 $g_1$, the computation is as follows:

$$(10\text{ g})-\text{NH }10\text{ g}_1=\tfrac{1}{2}\,[(I_2-I_1)+(I_3-I_4)]=+0.040$$

(in scale divisions).

The observed differences in scale divisions are verified to equal corresponding differences in milligrams within the precision of the balance.

$$I_3-I_2=10.006\text{ (in scale divisions)}=10\text{ mg}$$

but $\beta$ 10 mg=10.008 mg (accepted value)

$$\text{hence (10 g)}-\text{NH 10 g}_1=0.040\times\frac{10.008}{10.006}=+0.040\text{ mg}$$

(therefore scale divisions represent milligrams within the accuracy of measurement).
But Cr NH 10 $g_1=-0.011$ mg (accepted value).
Thus Cr (10 g)$=+0.029$ mg.

At the National Bureau of Standards weights whose value is based on this type of weighing are not said to have been "calibrated." That term is reserved for measurements based on at least two mass standards.

In many instances weights for use on less precise balances may be tested on a direct-reading, quick-weighing balance. Weights are accepted if their values fall within some acceptable deviation from nominal value. Such tests may be performed rapidly and without written observations or computations by methods that are practically free from systematic effects.

For such "tolerance tests" a standard weight of the denomination of the test weights is placed on the balance pan; the balance indication is then adjusted to read the actual value of the standard; next a sensitivity weight is added to change the scale reading by a known amount. If the change in scale reading should not agree with the actual value of the sensitivity weight the balance may require adjustment. This should happen only very rarely.

The sensitivity having been proved correct the standard is removed and test weights substituted on the balance pan. The indicated values may then be taken as actual values of test weights for use on balances of lower precision. At the end of the series the standard weight must be replaced on the pan and the reading indicated by the balance must agree within the planned precision of the weighings. If many test weights are involved, the standard must be replaced on the pan after each small group of weights (consisting of say three weights each) has been tested. If the results show that the balance is remaining constant, the size of the group may be increased moderately.

---

Even with the inclusion of four authors, these developments in weighing technique have not been adequately characterized as the team effort upon which they are based. Every member of the National Bureau of Standards Mass Laboratory has contributed significantly. In addition, we have had the benefit of unusually wide discussion and criticism from interested scientists in other laboratories. Above all, we should single out the help we have received on statistical considerations from C. Eisenhart and J. M. Cameron of the Statistical Engineering Section of the National Bureau of Standards.

## 5. References


[1] National Bureau of Standards, Precision measurement and calibration, NBS Handb. 77, Vol. III. Optics, metrology, and radiation (1961).

[2] T. W. Lashof and L. B. Macurdy, Testing a quick-weighing balance, Anal. Chem. **26,** 707 (1954).

[3] John A. Hayford, On the least square adjustment of weighings, U.S. Coast and Geodetic Survey Appendix 10, Report for 1892 (1893).

[4] M. J. R. Benoit, Travaux et Mémoirs du Bureau International des Poids et Mesures **13,** 1, (1907).


(Paper 66C1–85)

JOURNAL OF RESEARCH of the National Bureau of Standards—C. Engineering and Instrumentation
Vol. 66C, No. 1, January–March 1962

# Tunnel Diode Large-Signal Equivalent Circuit Study and the Solutions of Its Nonlinear Differential Equations

Sidney B. Geller and Paul A. Mantek

(October 31, 1961)

A large-signal equivalent circuit for the Esaki or tunnel diode is presented that characterizes the dynamic and static response of this semiconductor device. Nonlinear differential equations are written on the model and a graphical-numerical solution technique is described. Analog computer solutions for the nonlinear equations are also discussed for various modes of operation.

## 1. Introduction

Most of the equivalent circuit models presented for the tunnel diode have been small-signal types. The small-signal operation of this semiconductor device can be correctly characterized by its incremental resistance at a fixed bias point and some associated reactive elements. However, the large-signal departures from this bias point which typify bistable switching and relaxation oscillations make the model inadqeuate. In digital systems the active circuit elements are typically required to operate over extended ranges of their voltage-current characteristics. This paper presents a large-signal equivalent circuit for the tunnel-diode (fig. 1). This circuit characterizes both the static and dynamic responses of the device for all modes of operation. The network enclosed in the dashed box simulates the static V-I characteristic of the tunnel diode.

Nonlinear differential equations are produced from the model and a graphical-numerical solution technique is described that is applicable to driven or self-excited systems. The equations are readily solved by analog computer techniques, particularly when curve following is employed on a monotonic curve that is presented in this paper.

An example of the graphical-numerical solution of the nonlinear equations for the relaxation oscillation case is presented in detail. Some comparisons are made between the graphical and analog computer solutions of bistable switching and sinusoidal oscillation modes of operation.

## 2. Tunnel Diode Large-Signal Equivalent Circuit and Solution Techniques

The validity of the small-signal tunnel diode model [1][1] has been extended over a large-signal range by incorporating the static terminal characteristics of the device into the model shown in figure 1. The lead inductance, $L_s$, the series body resistance, $R_s$, and the barrier capacitance, $C$, are assumed to maintain constant values over the operating range of interest [2]. Measurement techniques for these elements are described in the literature [3].

[1] Figures in brackets indicate the literature references at the end of this paper.

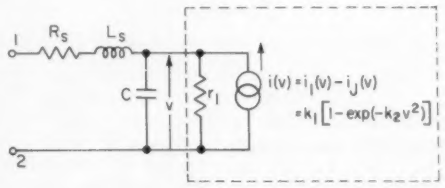


FIGURE 1. *Large-signal tunnel diode equivalent circuit.*

This study was made using the GE ZJ–56 (1 ma peak current) tunnel diodes. Typical values for $L_s$, $R_s$, and $C$ in this device are:

$$L_s = 6.0 \text{ nh}$$

$$R_s = 1.5\ \Omega$$

$$C = 5.0 \text{ pf}$$

Figure 2 shows a static V–I plot of the terminal characteristics of the ZJ–56 tunnel diode. Curve A in figure 3 is a broken-line approximation to this static plot which is simulated by the $i(v)$ current generator and resistance, $r_1$, of figure 1 (dashed box). The output from the $i(v)$ current generator (see appendix) is defined by either

$$i(v) = i_1(v) - i_j(v) \quad \text{(fig. 3 curve B)} \qquad (1)$$

or by an analytic approximation to curve B

$$i(v) = k_1[1 - \exp(-k_2 v^2)] \quad \text{(fig. 3 curve C)}. \qquad (2)$$

$i_1(v)$ is defined by the linear equation relating $v$ and $i$ in region 1 of curve A. $i_j(v)$ is defined by the linear equations relating $v$ and $i$ in each of the $j$ linear regions ($j$=1,2,3,4) of curve A. The resistance $r_1$ is set equal in value to the inverse slope of region 1 of curve A in figure 3.

The following pair of equations can be written on the tunnel diode circuit in figure 4 with which all principal modes of operation such as switching and oscillating can be realized:

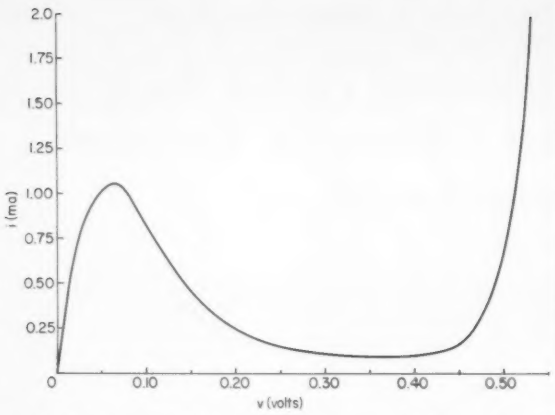


FIGURE 2. *Static V-I characteristic for the GE ZJ-56 tunnel diode.*

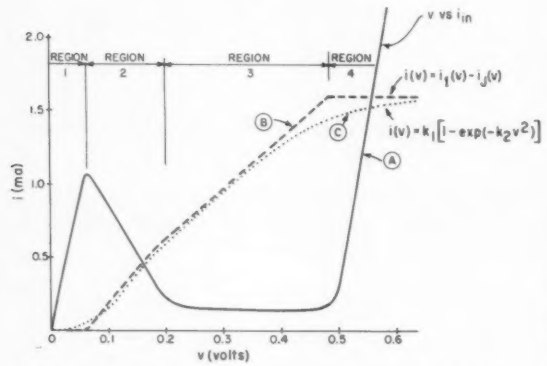


FIGURE 3. *Curve A: Approximation to the GE ZJ-56 tunnel diode static V-I characteristic.*

*Curve B: Broken-line approximation to the current from the* i(v) *generator.*

*Curve C: Analytic approximation to the current from the* i(v) *generator.*

$$\begin{cases} C\dfrac{dv}{dt}+\dfrac{v}{r_1}-k_1[1-\exp(-k_2v^2)]-i_L=0 & (3) \\ L\dfrac{di_L}{dt}+Ri_L=E(t)-v. & (4) \end{cases}$$

$E(t)$ is the applied voltage, $R=R_x+R_s$ and $L=L_x+L_s$.

Combining eqs (3) and (4) produces a nonlinear differential equation whose solution yields the junction voltage, $v$, i.e.,

$$\frac{d^2v}{dt^2}+\frac{1}{C}\left[\left(\frac{1}{r_1}+\frac{RC}{L}\right)-2k_1k_2v\exp(-k_2v^2)\right]\frac{dv}{dt} +\omega_0^2\left[\left(1+\frac{R}{r_1}\right)v-Rk_1[1-\exp(-k_2v^2)]\right] =E(t)\omega_0^2 \quad (5)$$

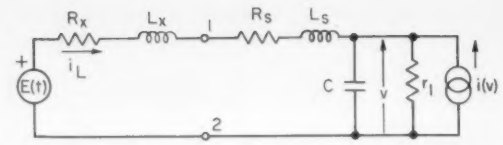


FIGURE 4. *Tunnel diode circuit containing external* $R_x$ *and* $L_x$ *elements.*

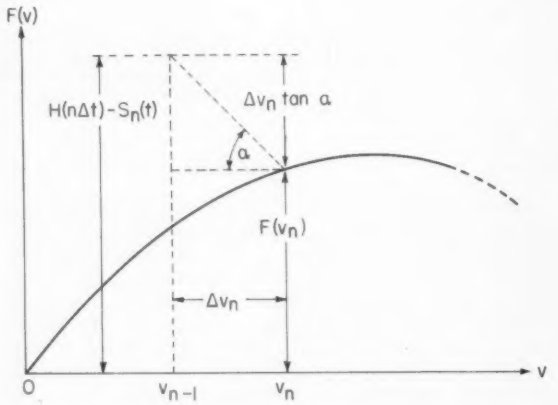


FIGURE 5. *Typical construction increment in the* F(v) *versus* v *plane.*

where $\omega_0^2=\dfrac{1}{LC}$. This equation does not lend itself to a closed form solution. It falls into the class of nonlinear equations of the type [4]

$$\frac{d^2v}{dt^2}+f(v)\frac{dv}{dt}+g(v)=h(t). \quad (6)$$

After some investigation a graphical solution for this form was found and techniques for its application were worked out [5]. The solution process begins with an integration of eq (5) with respect to the time which yields

$$\frac{dv}{dt}+F(v)+\int_0^t g(v)dt=H(t)+K \quad (7)$$

where,

$$F(v)=\frac{1}{C}\int_0^v\left[\left(\frac{1}{r_1}+\frac{RC}{L}\right)-2k_1k_2v\exp(-k_2v^2)\right]dv \quad (8)$$

$$g(v)=\omega_0^2\left[\left(1+\frac{R}{r_1}\right)v-Rk_1[1-\exp(-k_2v^2)]\right] \quad (9)$$

$$H(t)=\omega_0^2\int_0^t E(t)dt \quad (10)$$

$K$=integration constant.

Equation (7) is then converted into incremental form

$$\frac{\Delta v_n}{\Delta t}+F(v_n)+S_n(t)=H(n\Delta t)-K \tag{11}$$

where,

$$S_n(t)=\int_0^t g[v(t)]\,dt. \tag{12}$$

A fixed value of $\Delta t$ is chosen heuristically and an angle

$$\alpha=\arctan\frac{1}{\Delta t} \tag{13}$$

is determined. It may be necessary to multiply equation (11) through by some constant in order to produce useful $\alpha$'s. $\alpha$ is corrected to accommodate the departure of the abscissa-to-ordinate scaling of $F(v)$ versus $v$ from a one-to-one numerical relationship per unit length. Equation (11) is then rewritten into its final form preparatory to graphical solution as

$$\Delta v\tan\alpha+F(v_n)=H(n\Delta t)+K-S_n(t). \tag{14}$$

The angle $\alpha$ is constructed physically on a template. Vertical lines of length $H(n\Delta t)-S_n(t)+K$ are constructed in the $F(v)$ versus $v$ plane as the solution proceeds. The successive $\Delta v_n$'s are determined by the construction technique shown in the typical segment in figure 5. $S_n(t)$ is determined at each step of the process by applying the trapezoidal rule to the values of $g(v_n)$ and $g(v_{n+1})$. This will be further detailed in the following section.

## 3. Example of a Graphical-Numerical Solution of Equation (5), Relaxation Oscillation Case

The circuit parameters were chosen to produce relaxation oscillations, i.e.,

$$R<\frac{L}{|-r|\ C}\text{ and }R<|-r|$$

where $-r$ is the value of the inverse differential slope at each point in the negative resistance region of the V-I characteristic ($|-r|\approx 150\Omega$). A type GE ZJ-56 tunnel diode was employed in the circuit shown in figure 4. The values of the parameters were

$R=20\Omega$
$L=100\mu$h
$C=10$ pf
$E=0.25v$ (step)
$r_1=58.8\Omega$
$k_1=0.008$
$k_2=11.0$
$\omega_0^2=10^{15}$ rad/sec.

These numerical values were put into eq (5) which was then integrated in respect to time. In order to produce angle $\alpha$'s of reasonable size the equation was multiplied through by $30\times10^{-9}$. This yielded (in the form of equation (11))

$$\Delta v_n\left(\frac{30\times10^{-9}}{\Delta t}\right)+30[1.7v-.8[1-\exp(-11.0v^2)]]$$
$$+30\times10^6\int_0^t[1.34v-.16[1-\exp(-11.0v^2)]]\,dt$$
$$=7.5(10^6)(n\Delta t)+K. \tag{15}$$

Since

$$\Delta v_n\tan\alpha=\Delta v_n\left(\frac{30\times10^{-9}}{\Delta t}\right) \tag{16}$$

therefore

$$\alpha=\arctan\left(\frac{30\times10^{-9}}{\Delta t}\right). \tag{17}$$

For example, if $\Delta t=30\times10^{-9}$ sec is chosen as the construction increment then $\alpha=45°$. The $\Delta t$ chosen depends on the predicted response of the device. If $\Delta t$ is too large, the construction will be extremely coarse. If $\Delta t$ is too small, the solution will proceed very slowly. The value of $\Delta t$ may be easily altered during the solution process in order to achieve optimum speed and resolution. The analytical error between the exact solution of eq (7) and its graphical solution is of the order of $-1/2\Delta^2 v_n$ in each interval.

At this point the $F(v)$ versus $v$ and $g(v)$ versus $v$ plots were drawn where

$$F(v)=30[1.7v-.8[1-\exp(-11.0v^2)]] \tag{18}$$

and

$$g(v)=30\times10^6[1.340v-0.16[1-\exp(-11.0v^2)]] \tag{19}$$

Figures 6 and 7A show these plots.

Values of $H(n\Delta t)=7.5(10^6)\ (n\Delta t)\ n=1, 2, 3, \ldots$ were tabulated.

Since the F($v$) versus $v$ curve was found to be reasonably plotted on a 10:1 physical scale, the angle $\alpha$ was adjusted to compensate for this departure from a 1:1 relationship. This resulted in

$\alpha=5°44'$ for $\Delta t=30\times10^{-9}$ sec
$\alpha=71°34'$ for $\Delta t=1\times10^{-9}$ sec
$\alpha=85°15'$ for $\Delta t=0.3\times10^{-9}$ sec.

Three templates were constructed containing these angles.

The integration constant $K$, which is equal to $\dot{v}$ at $t=0$, was set equal to zero. The actual value of $K$ was sufficiently small to make this completely reasonable.

The $S_n(t)$ term is evaluated at each step of the graphical solution by the trapezoidal rule. Values of $v$ as a function of time such as $v(n\Delta t)$ and $v[(n+1)\Delta t]$ are determined by the successive constructions in the $F(v)$ versus $v$ plane. Then the values $g[v(n\Delta t)]$ and $g[v[(n+1)\Delta t]]$ are directly obtained from the g($v$) versus $v$ plot. As the construction proceeds each quantity

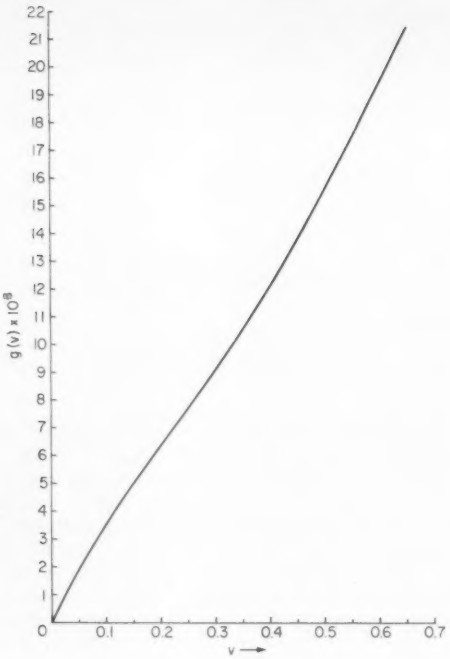


FIGURE 6. g(v) *versus* v *plot employed in graphical solution of relaxation oscillator case.*

$$S_n(t)=\left(\frac{g(v[(n\Delta t)]+g(v[(n+1)\Delta t])}{2}\right)\Delta t \qquad (20)$$

is added on to the preceding total value of $S_n(t)$ and this new total is subtracted from the next applied $H(n\Delta t)$. This gives the length of the vertical construction line, $H(n\Delta t)-S_n(t)$ (as shown in fig. 5).

As each construction is made, the time required for each $\Delta v_n$ to occur is known from the relationship of $\Delta t$ to the angle $\alpha$ employed in the construction. When the $H(n\Delta t)-S_n(t)$ line falls below the $F(v)$ curve the construction reverses direction and proceeds towards the origin.

The angle $\alpha$ was changed during the construction process in order to produce maximum resolution and solution speed. For example, in the jump region the angle $\alpha=85°15'$ (for $\Delta t=0.3\times10^{-9}$ sec) was employed.

Figure 7A displays the $H(n\Delta t)-S_n(t)$ locus in the $F(v)$ versus $v$ plane for the relaxation oscillation case. Figure 7B shows the junction voltage, $v$, versus time that was derived from the graphical construction. A single pulse from the actual ZJ–56 relaxation oscillator pulse train is shown superimposed upon a pulse produced by the graphical method which was based upon the analytic approximation of eq (2). The graphical process will produce a train of similar pulses if it is continued.

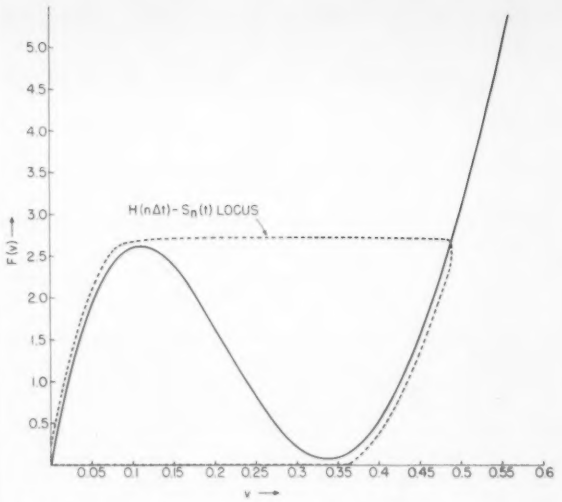


FIGURE 7. (*A*) F(v) *versus* v *plot employed in the graphical solution of the relaxation oscillator case (solid line).*

The dashed line is the locus of $H(n\Delta t)-S_n(t)$ obtained during the graphical construction.

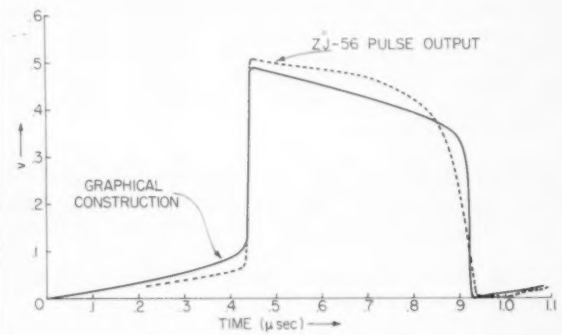


(*B*) *Junction voltage,* v, *versus time obtained from graphical solution (solid line) superimposed upon actual pulse (dashed line).*

## 4. Comparison of Analog and Graphical Results

Equations (3) and (4) were mechanized on the National Bureau of Standards Mid-Century 500 Analog Computer employing curve-following techniques for both the broken-line and analytic $i(v)$'s as defined by eqs (1) and (2). The method of constructing the broken-line $i(v)$ function is described in the appendix. Since these curves were relatively smooth and monotonic, (as compared to curve A, fig. 3) the curve-following operated well. The $R$, $L$, and $C$ elements were adjusted to produce bistable switching and (nearly) sinusoidal oscillations. Graphical solution technigues were then applied for these same operating conditions. Figure 8 displays the response of the system to a ramp driving function

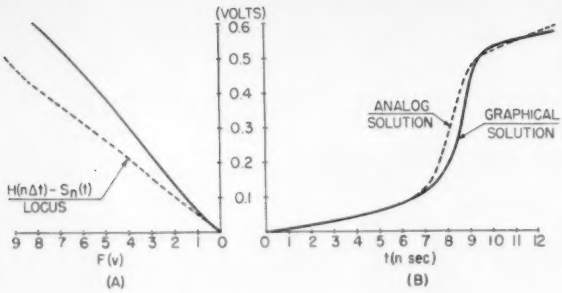


FIGURE 8. *(A) Graphical construction in the* F(v) *versus* v *plane.*
*(B) Analog computer and graphical solution for junction* v *versus time (ramp-driven switching mode).*

FIGURE 9. *(A) Graphical construction in the* F(v) *versus* v *plane.*
*(B) Analog computer and graphical solution for junction* v *versus time (oscillatory mode).*

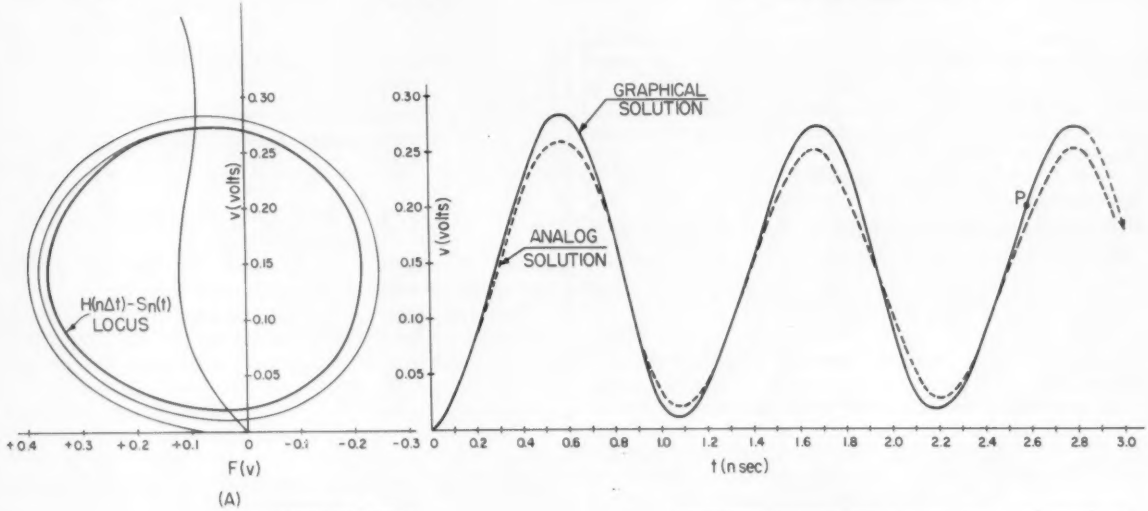


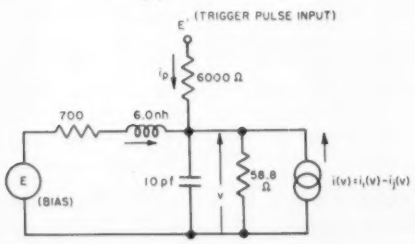


FIGURE 10. *(A) Simulated bistable switching circuit with additional pulse triggering source.*

*(B) Analog computer mechanization for circuit in figure 10A.*

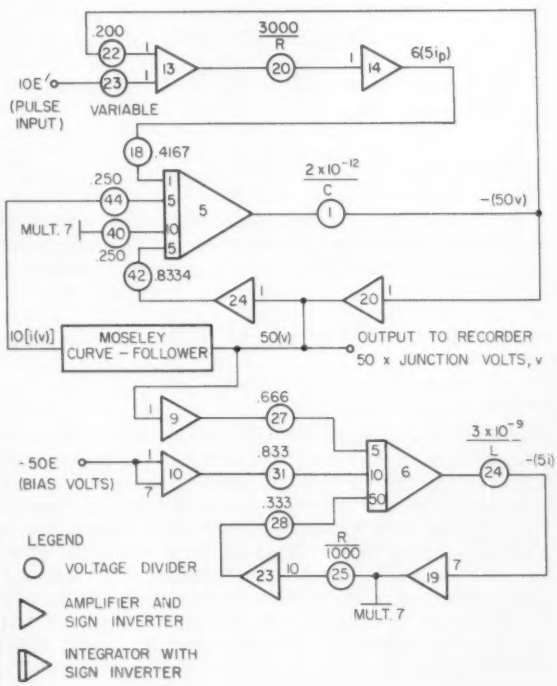


with the circuit operating in the switching mode, i.e., $R>|-r|$, $R=470\Omega$, $L=5.0$ nh and $C=2.0$ pf. Figure 9 shows the sinusoidal response to a voltage step with $R<|-r|$, $R=16\Omega$, $L=7.5$ nh and $C=2.0$ pf.

The bistable switching case was simulated on the analog computer for another circuit configuration (fig. 10A). Here the tunnel diode was steadily biased with a voltage, $E$, that produced a stable singular point near the peak in region 1 (curve A,

fig. 3). The circuit was then triggered over to the second stable singular point in region 4 by an injected current pulse, $i_p$. It was possible to observe the effects of pulses of different duration and amplitudes on the triggering process. This technique can be used to study the optimum trigger requirements for the tunnel diode and other negative resistance devices. Figure 10B shows the analog computer mechanization. The $i(v)$ function eq (1) was plotted with a conducting material and curve-followed during the simulation process.

## 5. Appendix

Crisson [6] has presented a method for producing a voltage-controlled negative resistance at the input terminals of an "ideal amplifier" with feedback. It can be shown that the network enclosed by the dashed line in figure 1 displays the same characteristics as the "ideal amplifier."

The "ideal amplifier" shown in figure 11A can be represented by the circuit shown in figure 11B. The resistance, $r_j$, seen looking into the 1-2 terminals of the circuit is

$$r_j=\frac{R_1R_2}{R_1+R_2-M_j} \quad (j=1,2,3,4.) \tag{21}$$

where $M_j$ is a variable mutual impedance term. When $M_j>R_1+R_2$ then $r_j<0$ which produces a negative resistance at terminals 1–2. $M_j$ can therefore be the basis for the simulation of the tunnel diode static V–I characteristic with its alternating positive and negative regions. Resistance $r_1$ (see fig. 1) is set equal to the inverse slope of region 1 in curve A figure 3. Therefore, if $M_1$ is set equal to zero in this region, then the parallel combination of $R_1$ and $R_2$ is chosen to be equal in value to $r_1$. In any one of the other three regions the variable $M_j$ can be be determined from

$$M_j=(R_1+R_2)\left(1-\frac{r_1}{r_j}\right). \tag{22}$$

A conversion can be made from the circuit in figure 11B to the circuit enclosed in the dashed box in figure 1 in which the current generator output is

$$i(v)|_j=i_1(v)\left(1-\frac{r_1}{r_j}\right) \tag{23}$$

$$=i_1(v)-i_j(v) \tag{24}$$

where, $i_1(v)$ and $i_j(v)$ are defined by the functional relationship of the current to the voltage in each linear region of curve A in figure 3 and each region is bounded by the breakpoints on the curve. Curve B in figure 3 is the monotonic $i(v)$ curve that is produced by eq (24). This curve is easily followed by curve-following analog techniques. An analytic approximation to curve B was also produced for use in obtaining a total differential equation for the junction voltage, $v$, of the tunnel diode. The approximation is

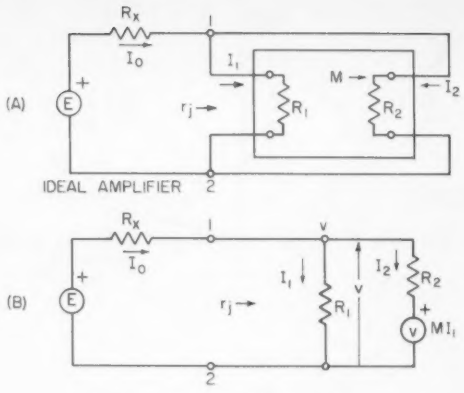


FIGURE 11. *(A) Ideal amplifier.*
*(B) Network equivalent to the "ideal amplifier."*

$$i(v)=k_1[1-\exp(-k_2v^2)] \text{ (fig. 3 curve C)} \tag{25}$$

where, $k_1=0.008$ and $k_2=11.0$ for the GE ZJ–56 tunnel diode type that is used in this study.

The $i(v)$ curve B for use in analog simulation is constructed by differentiating eq (24) in respect to $v$ which gives

$$\left.\frac{di(v)}{dv}\right|_j=\frac{di_1(v)}{dv}-\frac{di_j(v)}{dv}. \tag{26}$$

For each of the $j$ linear regions ($j=1,2,3,4$) of curve B a line with slope $\left.\frac{di(v)}{dv}\right|_j$ is drawn from region breakpoint-to-breakpoint starting at the origin. Note that $\left.\frac{di(v)}{dv}\right|_{j=1}=0$.

---

The authors thank E. S. Sherrard for his assistance with the analog computer mechanization.

## 6. References

[1] M.E. Hines, High-frequency negative-resistance circuit principles for Esaki diode applications, Bell System Tech. J. **39,** 477 (1960).
[2] S. Cohen, Tunnel diode characterization, Elect. Equip. Eng. **8,** 102 (1960).
[3] General Electric, Tunnel diode manual, (1961).
[4] S. Lefshetz, Differential equations: geometric theory, Interscience Publishers, 261 (1957).
[5] P. S. Hsia, A graphical analysis for nonlinear systems, Proc. IEE **99,** 125 (1952).
[6] G. Crisson, Negative impedances in the twin 21 type repeater, Bell System Tech. J. **10,** 485 (1931).

(Paper 66C1–86)

JOURNAL OF RESEARCH of the National Bureau of Standards—C. Engineering and Instrumentation
Vol. 66C, No. 1, January–March 1962

# A Missile Technique for the Study of Detonation Waves[1]

Fillmer W. Ruegg and William W. Dorsey

(October 30, 1961)

Problems and effects of stabilizing combustion and detonation against hypersonic flow were investigated by observation of a 20 millimeter spherical missile in a stoichiometric mixture of hydrogen and air at rest. Combustion produced detectable effects on the shape and position of the shock wave at Mach numbers between 4 and 6.5, and above pressures of one-tenth atmosphere. Chemical equilibrium probably was not reached in the time the gas spent near the front of the sphere. One of the factors in the delayed equilibrium was delayed ignition behind the shock wave, which was observed to be between about one and ten microseconds. Ignition delay is explained in terms of chemical kinetic theory and compared with results of experiments in shock tubes. Strong combustion-driven oscillations originated in front of the sphere, with frequencies up to about one-tenth megacycle per second. These were observed when the Mach number was less than 6 at a pressure of one-half atmosphere, and less than 5 at one-quarter atmosphere. A large reduction of the drag coefficient of the missile was noted in one case of intermittent combustion.

## 1. Introduction

Combustion in hypersonic streams is of considerable theoretical interest, and has a possible application in propulsion of missiles and aircraft. Application would require a knowledge of the problems of stabilizing the combustion against hypersonic flow. Recently some information has become available through the research of Gross [1][2] on shock-induced detonations stabilized on a wedge. Nicholls et al., [2] studied combustion behind a normal shock wave in a free jet. These experiments were limited in range by problems encountered in generating streams of gas having a realistically high total temperature. In addition, the results may have been influenced by the methods used in mixing the fuel and air.

It appeared that these problems could be avoided by using a hypervelocity missile in a combustible gas at rest. This report presents the initial results obtained from a study of combustion near a missile in a mixture of 30 percent by volume of hydrogen in air. Hydrogen was chosen because a substantial theory exists on its combustion, and because it may be useful in propulsion systems. Wave shape and position were studied by high speed photography to determine the conditions required to induce combustion, and to determine the effect of the missile on the combustion. Combustion is induced by the enthalpy rise of the gas in or behind the shock wave which is dependent only on the speed of the missile, and thus it was possible to create over and under driven detonations for study. Since the missile and wave were viewed through a stationary gas, the observations were not influenced by boundary layers and turbulence as in experiments on detonation in tubes. These advantages permitted observations on the spatial structure of detonation waves, which were interpreted in terms of the mechanism of reaction of hydrogen with oxygen. Although temperature changes would have an important effect, temperature was not changed from ambient in these initial experiments. Pressure was varied from 20 mm Hg to atmospheric to learn of its effects.

## 2. Experimental Apparatus

The apparatus is illustrated in figure 1 and is composed of: (a) A gun and range which contains the test gas, (b) an electronic time delay ratio generator which triggers a submicrosecond light source (spark) when the missile is expected at the observation station, (c) two electronic microsecond counters, (d) an optical system to make schlieren or shadow pictures of the missile, and (e) auxiliary equipment such as pressure gages, vacuum pumps, etc.

In the experiments to date nylon spheres, 0.785-in. diam (19.94 mm), have been mounted in an electric-primed case containing a fast burning gun powder. This technique of propelling the missile was borrowed from Eckerman [3]. Other techniques may be used, such as the light gas gun [4]. The missile travels through an evacuated range illustrated in the diagram, and enters the test gas after breaking through a thin diaphragm (8).

Signals from the phototubes and ratio delay generator actuate the two time counters, and the measured time intervals are used to compute the velocity of the missile between light beams and in the test gas. The schlieren optical system is illuminated by a spark of about $10^{-7}$ sec duration, obtained by the discharge of a barium titanate capacitor, and in some early pictures by light from a flash tube of about $0.5\times10^{-6}$ sec duration. These illuminate a piece of ground glass adjacent to four razor blades which outline a rectangular slit $\frac{5}{16}$ by $\frac{1}{8}$ in. This is used as the light source of the schlieren system. A rectangular slit is also used as a schlieren stop to

[1] Sponsored by the Air Force Office of Scientific Research, U.S. Air Force.
[2] Figures in brackets indicate the literature references at the end of this paper.

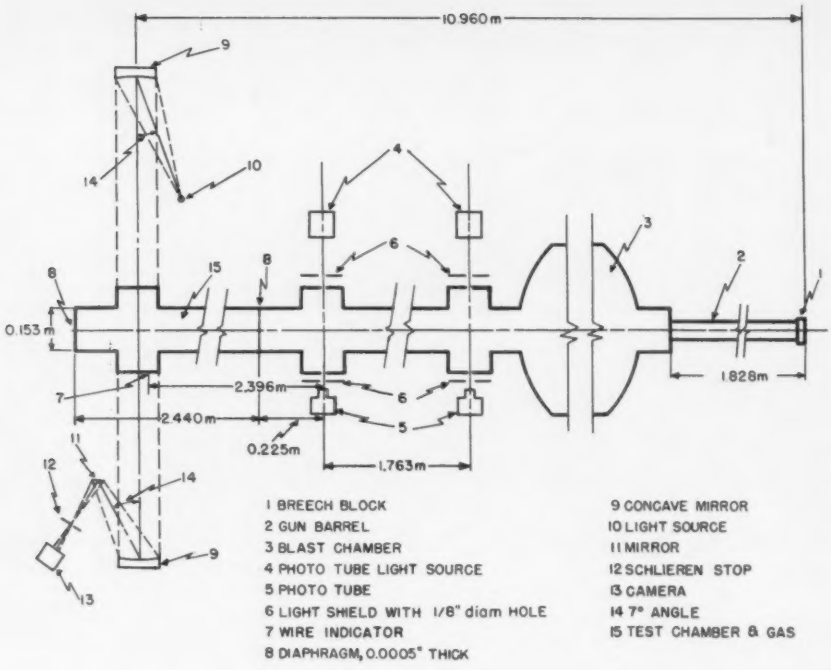


FIGURE 1. *Experimental apparatus.*

reduce effect of light emitted by combustion. Both slits are vertical to measure gradients of index of refraction parallel to the horizontal axis of flight. It was also found necessary to close the shutter of the camera within tenths of a millisecond after taking the schlieren picture to further reduce the effect of emitted light. The apparatus was used to obtain photographs of the missile and the shock and combustion waves that were generated in the combustible gas.

## 3. Experimental Results

All experiments in this report were made in a mixture of 30 volume percent of hydrogen in air. This mixture was chosen because it may be useful in propulsion systems, and because a considerable theoretical and experimental background exists on its combustion. Preliminary tests were made at pressures, $p$, from 0.026 to 1 atm absolute and at Mach numbers, $M$, up to 6.5. These showed that effects of combustion on wave shape and position could be detected at pressures of 0.1 atm and higher, and for a range of $M$ from 4 to 6.5. The upper limit of 6.5 on $M$ was fixed by the gun and missile, while these pressures were selected to partially cover the range that might be found in propulsion systems. Since results between pressures of 0.5 and 1 atm are qualitatively similar, this report describes results at pressures of 0.1, 0.25, and 0.5 atm.

$M$ at the observation point was determined from two speed measurements and the speed of sound, C, where C is 409 m per second in the combustible gas and 347 m per second in air, both at 300 °K. It was estimated from drag coefficient information on spheres, that since the percentage change of velocity of the missile in the test gas was less than 5 percent, the change of deceleration would be less than 10 percent. Therefore, the deceleration was assumed a constant in the derivation of $M$ at the observation point.

### 3.1. Photographic Results

Experimental results are primarily in the form of pictures obtained by schlieren photography of the region surrounding the missile. These are presented in figures 2 and 3. One shadow photograph is presented in figure 2b. Schlieren pictures of the missile in air, 2a, and in a mixture of nitrogen and hydrogen, 3a, are also presented for comparison with those in the combustible gas. All pictures contain two dark heavy lines, one from a horozintal wire (out of focus) to help delineate the line of flight, and one from a wire perpendicular to the latter to give the position of the missile in the test gas. It is evident that in the range of $M$ between 4 and 6.5, combustion takes place in the shocked gas near the missile, and in many instances has an oscillatory or intermittent property.

At $M$=4.3 and 0.5 atm, picture 2b shows a discrete region of flame surrounding the sphere. Schlieren

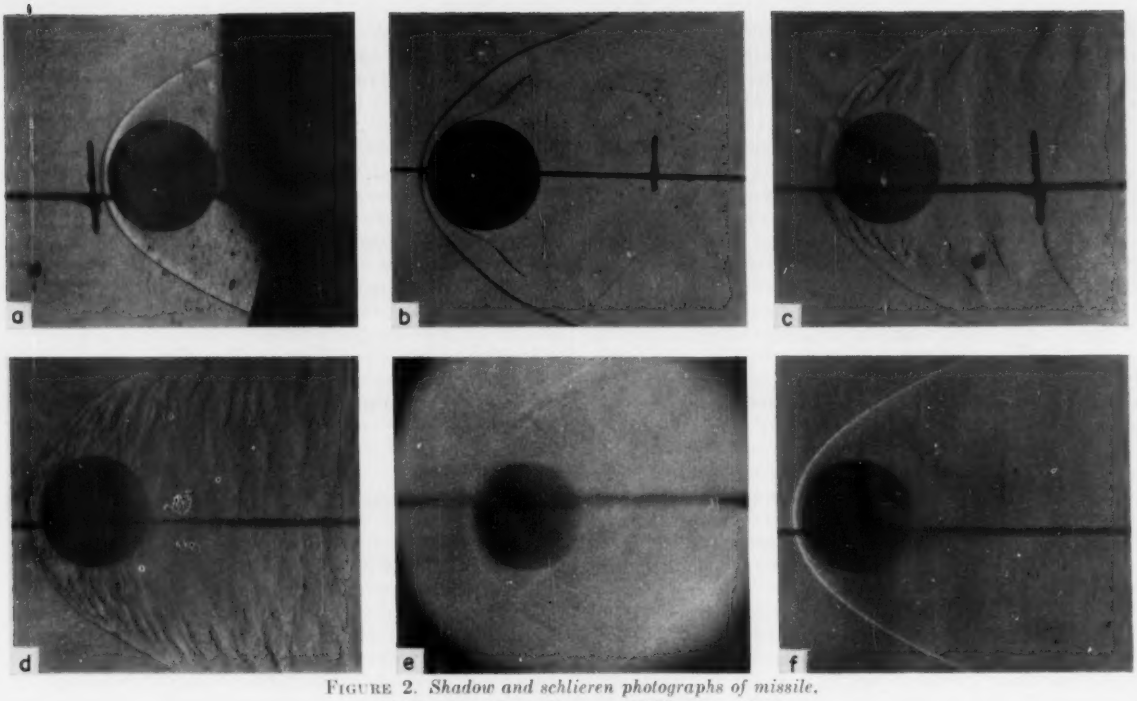


FIGURE 2. *Shadow and schlieren photographs of missile.*

(a) M=5.4; p=0.5 atm; Air
(b) M=4.3; p=0.5 atm
(c) M=4.8; p=0.5 atm
(d) M=5.5; p=0.5 atm
(e) M=6.3; p=0.5 atm
(f) M=5.0; p=0.1 atm

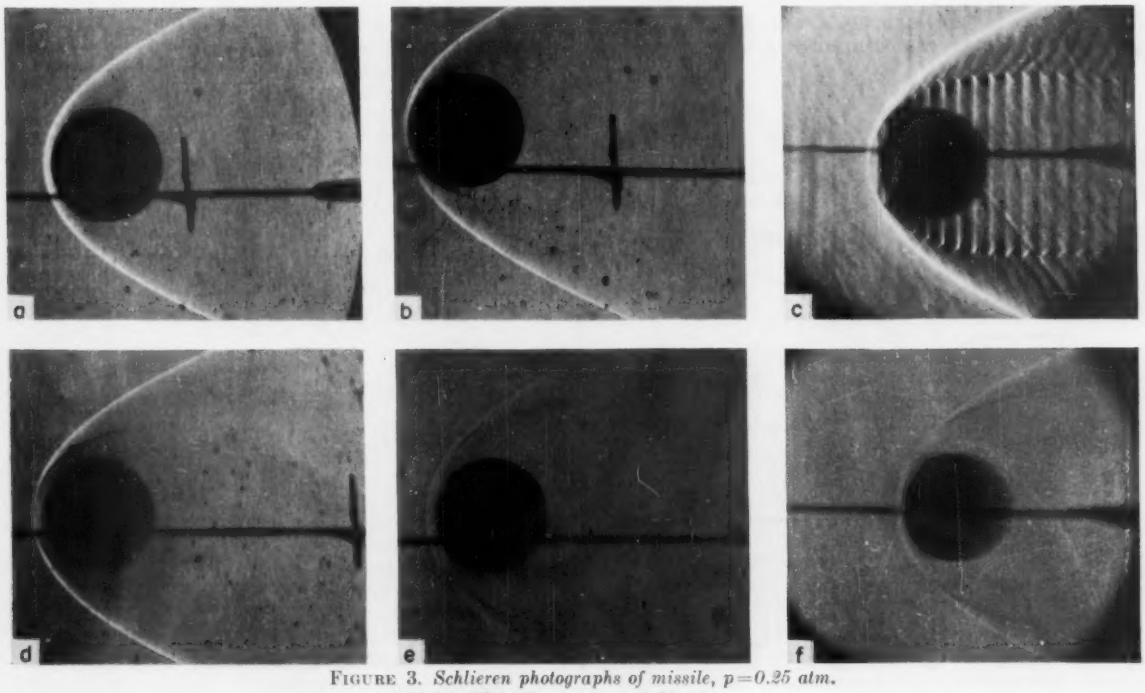


FIGURE 3. *Schlieren photographs of missile, p=0.25 atm.*

(a) M=4.4; $.3H_2+.7N_2$
(b) M=4.5
(c) M=4.9
(d) M=5.1
(e) M=5.9
(f) M=6.5

pictures of the region behind the sphere at this value of $M$ showed discrete regions of burned or burning gas spaced about three sphere radii from center to center and two sphere radii thick along the axis of flight. The regions of combustion overlap at higher $M$, and finally merge to give a continuous flame front at $M$ of about 6, as in picture 2e. Only one picture at 0.1 atm is presented, 2f, in which a combustion wave is demonstrated between the front of the sphere and the shock wave at $M=5.0$. Other pictures above $M=5$ did not demonstrate combustion waves that could be measured.

When the pressure was 0.25 atm, as in figure 3, a dark combustion wave is plainly visible in picture 3b at $M=4.5$, and there is evidence of a weak oscillation in the combustion zone. Amplitude of the oscillation became large enough to be plainly demonstrated by the photography when $M$ was 4.9, picture 3c. Above $M=5$ the combustion zone is enclosed in a smooth flame front as illustrated in pictures 3d to 3f. Picture 3e has additional waves that apparently emanate from the front surface of the missile. Breakage of the missile was troublesome during these experiments, and it is possible that a small chip caused these waves.

There are other differences between the results that should be explained. First, pictures 2e, 3c, and 3f were taken using light from the flash tube with relatively poor picture quality. Second, the shock waves are bright in figure 3 (except 3e) compared to the dark waves of figures 2a to 2d. Large positive density gradients in the shock at 0.5 atm move the image of the light source, to the left as illustrated in part (a) of figure 4, to produce a dark wave. A smaller density gradient at 0.25 atm gives less movement, as shown in part (b), and results in a bright wave. A negative density gradient in a combustion wave would have the effect, as shown in part (c), to produce a dark wave. In air, and in some instances with the combustible gas a black and white shock wave is produced, as illustrated in figures 3e and 4. When the slit was replaced by the ordinary knife stop all shock waves were bright, as in figure 2e. However, the bright wave of figure 2f is a result of the low pressure which caused the effect illustrated in part (b) of figure 4. In all cases it is evident that a substantial part of the total compression in the shock wave takes place before combustion (or detonation) moderates the density rise of the shock wave. Picture 3c appears to have three lines radiating from the sphere; these lines are the results of imperfections present in one of the windows used in early experiments.

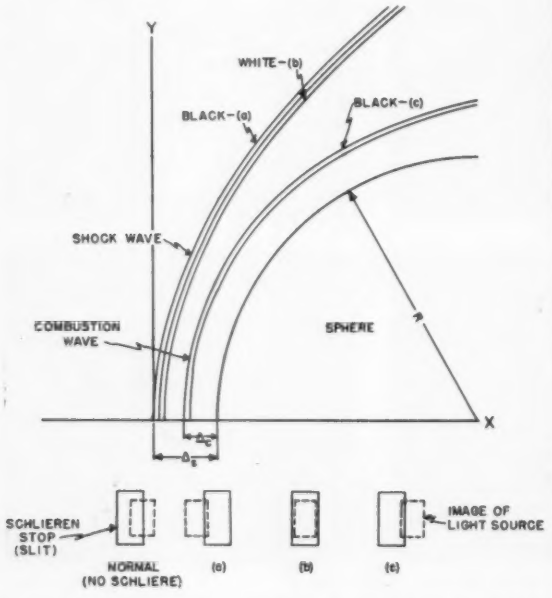


FIGURE 4. *Image position of light source for various regions of the schlieren picture and wave coordinate system.*

### 3.2. Effect of Combustion on Wave Shape and Detachment

Since combustion can be expected to have an appreciable effect on the density of the gas between the wave and sphere, it would also be expected that combustion would affect the shape and detachment of the wave from the sphere. Thus a measure of he extent of combustion in the vicinity of the sphere may be derived from these quantities. A projector was used to enlarge the image on the negatives from one-half to 7.64 times actual size, and the image of the waves and missile were traced on coordinate paper containing ten lines to the inch. Coordinates of the leading edge of the waves were read from the drawings and plotted to determine their shape.

It was found that in the immediate vicinity of the sphere the shock waves could be represented by parabolas, and the combustion waves (at 0.25 atm) by ellipses. No attempt was made to measure the shape of the combustion waves at 0.5 and 0.1 atm. Equations of the waves, in the coordinate system of figure 4, are given below:

$$\text{shock wave: } \left(\frac{y}{R}\right)^2 = m\frac{x}{R}, \quad \frac{x}{R} < 0.5$$

$$\text{combustion wave: } \left(\frac{y}{R}\right)^2 = a\left(\frac{x}{R} - \frac{\Delta_s - \Delta_c}{R}\right) - b\left(\frac{x}{R} - \frac{\Delta_s - \Delta_c}{R}\right)^2, \quad \frac{x}{R} < 0.9.$$

The constants $m$ and $\Delta_s$ were determined and used to specify the shape and detachment of the shock wave, while the constants $a$, $b$ and $\Delta_c$ were determined and used to specify the shape and detachment of the combustion wave. These quantities are plotted in figure 5 for the shock waves at 0.5 and 0.1 atm and in figure 6 for both waves at 0.25 atm, all against $M$. Both figures contain results of these measurements in air and Eckerman's [3] measurements in oxygen which he obtained with an 8mm sphere. His values

of $\Delta_s$ are less than the present results in air, possibly because he used a rotating mirror and a fast spark to provide a stopped image of the sphere and wave.

Results from tests with both light sources are included in the figures. Spark data on $\Delta_s$ are represented by closed circles, and flash tube data by closed triangles. Smaller values of $\Delta_s$ result from the spark data, perhaps for the same reason that Eckerman's results are smaller than ours in air. Values of wave shape $m$ are also differentiated the same way, but values of $\Delta_c$ and constant $a$ are not.

Constant $b$ (not plotted) varied linearly between a value of 0.7 at $M=4.5$ and a value of 0.58 at $M=6.1$ when the spark pictures were evaluated, and was about 0.15 smaller at corresponding $M$ when the flash tube pictures were evaluated. All data at 0.1 atm were obtained with the faster spark.

Inspection of figures 5 and 6 shows that the effect of combustion is to move the shock wave away from the sphere, and that the effect increases as pressure increases. The large effect of pressure, and the maximum in the curve of wave detachment, suggest that chemical reaction is not complete near the wave front. Thus the situation probably can be described as a shock wave followed by chemical reaction with relaxation time comparable to or larger than the time the gas spends near the front of the missile. Duff [5] has calculated the progress of the chemical reaction behind shock waves, and Bird [6] has outlined a graphical-numerical technique of handling the equations of motion of the gas between the wave and sphere. It is theoretically possible to combine these calculations to derive the shape and detachment of the waves. Alternatively, the measured shape and detachment may be used to check the validity of the chemical rate processes. Any computation of this kind would be long and involved. For the time being an estimate of the situation is all that will be given.

Eckerman [3] observed that the shock-detachment distance in air varied approximately inversely with the density ratio $\rho_2/\rho_1$ across the shock wave, where subscript 1 represents the condition before and 2 the condition after the wave. This relation was used to estimate the wave detachment to be expected in these experiments. Therefore, at a given $M$, wave detachment with combustion would be approximated by

$$\Delta_s=\Delta_{s,\text{air}}\frac{\rho_2}{\rho_3},$$

where subscript 3 represents the condition behind the detonation wave. Density ratios $\rho_1/\rho_2$ of adiabatic shock waves in the mixture of air and hydrogen were calculated using real gas properties, and calculated values of $\rho_1/\rho_3$ across detonations at chemical equilibrium were given by Eisen and coworkers [7]. They showed that an initial pressure change from one to $10^{-3}$ atm changed the density ratio across Chapman-Jouguet detonations by about only 6 percent. Thus it seemed that their calculated

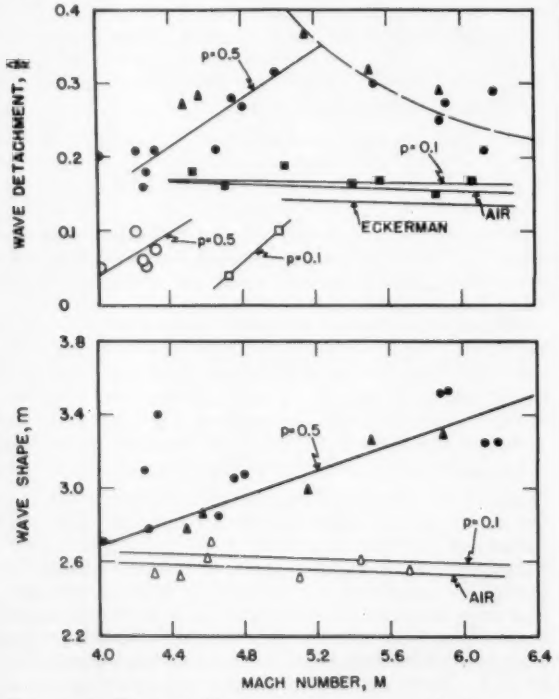


FIGURE 5. *Effect of Mach number on wave detachment and shape for a mixture of 30 volume percent* $H_2$ *in air at pressures of 0.1 and 0.5 atm.*

Shock wave●▲■ for $H_2$ and air;△ for air.
Combustion wave○□.

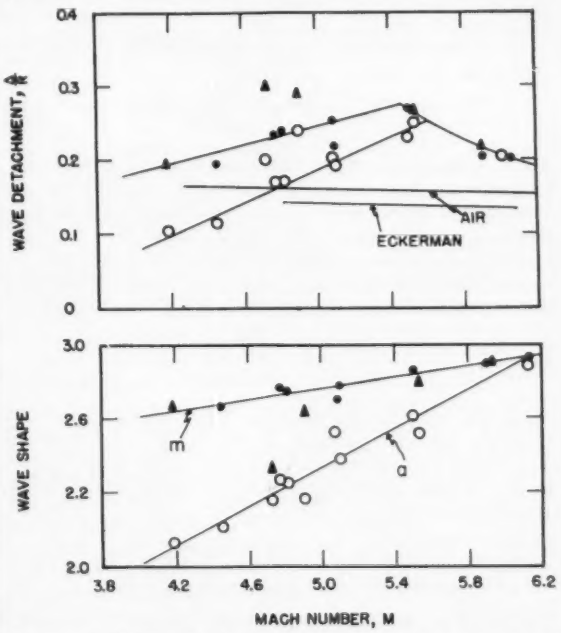


FIGURE 6. *Effect of Mach number on wave detachment and shape for a mixture of 30 volume percent* $H_2$ *in air at a pressure 0.25 atm.*

Shock wave●▲.
Combustion wave○.

values of density ratio across strong detonations at 1 atm could be used for comparison with results of these experiments. These calculated density ratios, and observed values of $\Delta_{s,\,air}$, gave estimates of $\Delta_s$ for detonations which are plotted as a dashed line in figure 5. Agreement between experiment and estimate above $M=5.5$ indicates the possibility that chemical equilibrium was approached near the front of the sphere. However, two experiments at $M=5.3$ and 6.0 at a pressure of 1 atm showed an increase of about 20 percent in $\Delta_s$ over the values at 0.5 atm. This indicates that the estimated curve would probably be corrected to larger values of $\Delta_s$ by an exact fluid-mechanical calculation. Thus, chemical equilibrium is probably not reached under any condition in these experiments near the front of the missile, especially below $M$ about 5.5.

### 3.3. Ignition Delay and Chemical Kinetics

One factor involved in delayed equilibrium is the observed delay in ignition behind the shock wave. A picture such as figure 3d could be used to determine the state of the gas and the time spent between shock and combustion waves along any selected streamline through fluid-mechanical calculations as outlined in reference [6]. Comparison of the time intervals and the state of the gas for different streamlines might furnish information on the factors that control the onset of combustion. In this report we use the observed separation between shock and combustion waves to estimate the state of the gas and the ignition delay time, $\tau$, on the central streamline (axis of flight).

The time spent by the gas between the shock wave and $x$ is

$$t(x)=\int_0^x \frac{dx}{V}$$

where $V$ is velocity on the central streamline, and $x$ is defined as in figure 4. Bird [6] stated that the velocity decay to zero at the sphere is approximately linear. If it is also assumed that the flow between waves is the same as that behind a shock wave of the same Mach number and shape without subsequent combustion, velocity $V$ is given by the equation

$$V=V_2\left(1-\frac{x}{\Delta_{s,\,air}}\frac{m_{air}}{m}\right).$$

$V_2$ is the velocity behind the shock in the real combustible mixture, and $m$ is the shape of the shock wave and is proportional to the radius of curvature at the origin. Insertion in the integral and integration from zero to $x=\Delta_s-\Delta_c$ gives

$$\tau=-\frac{\Delta_{s,\,air}}{V_2}\frac{m}{m_{air}}\ln\left(1-\frac{\Delta_s-\Delta_c}{\Delta_{s,\,air}}\frac{m_{air}}{m}\right).$$

Values of $\Delta_s$, $\Delta_c$, $\Delta_{s,\,air}$ and $m$ were taken from figures 5 and 6, and calculated values of $\tau$, which is considered an ignition delay, are plotted in figure 7. Spark data only are used here since it is considered more accurate than the "slower" flash tube data. Ignition delays cover a range of zero to 10 $\mu$sec. Curves in the figure are derived from a correlation to be described. Portions of the curves are dotted to indicate extrapolations.

An attempt was made to explain these ignition delays through considerations of chemical kinetics, and to compare the results with those of other research workers. Lewis and von Elbe [8], Schott and Kinsey [9], and Duff [5] have discussed the kinetics of the hydrogen-oxygen reaction. Their explanation of the factors that are involved in the initial stage of the reaction is used. Five important reactions, and their contribution to the rate of formation of the hydrogen atom, are listed below:

| | |
|---|---|
| (0) $H_2+I \quad =2H+I$ | $[\dot{H}]_0 \quad =2k_0[H_2][I]$ |
| (1) $H+O_2 \quad =OH+O$ | |
| (2) $O+H_2 \quad =OH+H$ | $[\dot{H}]_{1-3}=2k_1[H][O_2]$ |
| (3) $OH+H_2 \quad =H_2O+H$ | |
| (4) $H+O_2+I=HO_2+I$ | $[\dot{H}]_4 \quad =-k_4[H][O_2][I]$ |

Inert species are indicated by I, concentrations are indicated by brackets, and $k$'s are rates of reaction. Reactions (2) and (3) are considered very fast compared to the others, and their effect is to form three hydrogen atoms for every one consumed by (1). Total rate of formation of [H] is the sum of the three rate equations, if it is assumed that there is no reverse reaction of any significance during the induction period. The temperature behind the shock wave, $T_2$, and therefore $k$, as well as the concentrations of $H_2$, I, $O_2$, are probably unchanged during the induction period. Therefore the rate equation can be integrated to give

$$\ln\frac{[\dot{H}]_t}{[\dot{H}]_{t=0}}=2k_1[O_2]\left(1-\frac{k_4[I]}{2k_1}\right)t.$$

Although the particular chain initiation reaction chosen is open to question, other plausible reactions essentially would modify only the denominator of the left side of the above equation.

Schott and Kinsey [9] tested a part of the above equation over a range of time intervals from 5 to 500 $\mu$sec for combustion behind incident and reflected shock waves in tubes. A straight line was obtained when $\ln[O_2]\,\tau$ was plotted against $T_2^{-1}$, where $T_2^{-1}$ is proportional to $\ln k_1$. This implies that the ratio of $[\dot{H}]$ is always the same at ignition, when $t=\tau$, or that changes of $\ln\ln([\dot{H}]/[\dot{H}]_{t=0})$ were not significant over the range of the experiments. Their intervals were measured to the appearance of the OH radical. Strehlow [10] measured ignition delays behind reflected shocks in tubes over a range of 12 to 880 $\mu$sec. His time intervals were from 20 to 100 percent larger than those observed by [9], possibly for the reason that ignition is that much later than the appearance of OH. Both omitted the effect of reaction (4) in their correlation, possibly due to the low pressures of their experiments.

Ignition delays presented in figure 7 are plotted in figure 8 using the correlation given by the above

equation. $[O_2]$ was calculated from $p_2$ and $T_2$ immediately behind the shock front in the real combustible gas. The temperature rises by about two percent and pressure by about 15 percent between the shock and combustible waves. Therefore the error is less than 15 percent when shock pressure and temperature are used. Information is presented by [8] on the rates of reactions (1) and (4) which can be used to derive the effect of reaction (4). For these experiments it is given by

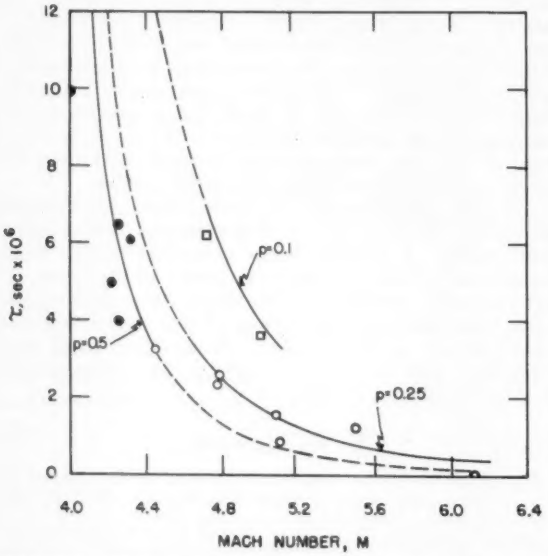


FIGURE 7. *Effect of Mach number on ignition delay behind the shock wave.*

●p=0.50 ○p=0.25 □p=0.10

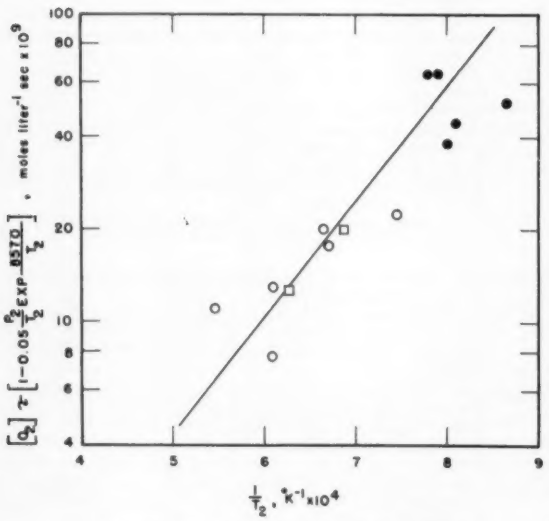


FIGURE 8. *Correlation of ignition delay.*

●p=0.50 ○p=0.25 □p=0.10

$$\frac{k_4[I]}{2k_1}=0.05\,\frac{p_2}{T_2}\exp\frac{8570}{T_2}$$

where 8,570 °K is the activation temperature of reaction (1), and the constant 0.05 °K atm$^{-1}$ is one-quarter of that derived from the information of [8] for this combustible mixture. Since our data are not comprehensive enough to fix the activation temperature, the constant 0.05 was used in order that the data would give an activation temperature of 8,570 °K. This lies between that of 8,300 °K given by [10] and 8,800 °K given by [9]. Inclusion of the effect of reaction (4) in this manner modified only the time results of experiments at 0.5 atm, in which the pressure was high enough and temperature low enough for reaction (4) to be significant.

The equation of the line in figure 8 is

$$2.3\log_{10}\left([O_2]\,\tau\left[1-0.05\,\frac{p_2}{T_2}\exp\frac{8570}{T_2}\right]\right)=\frac{8570}{T_2}-23.49.$$

Since the values of $[O_2]\tau$ are only 10 to 20 percent larger than those given by [10], it appears that this method of correlating ignition delay is valid over a range of time from about $10^3$ to about 1 μsec. Curves in figure 7 were derived from the above equation, and it appears that these experiments have permitted observation of ignition delay behind shock waves with a time resolution of about a microsecond.

### 3.4. Combustion Oscillations and Drag Coefficient

Many of the pictures of figures 2 and 3 exhibit oscillations that are driven by combustion, and in one case (picture 2b) an intermittent combustion as demonstrated. At this Mach number of 4.3 and pressure of 0.5 atm, the data on $\Delta_s$ and $m$ show large variations, which suggests that the oscillations originate at the front of the sphere. These oscillations may contribute to the scatter of the data on ignition delay described in the previous section, since some of the data were taken from pictures showing oscillations. It is likely that oscillations will appear in applications of hypersonic combustion as it does in most other forms of combustion.

In pictures 3b and 3c, the oscillation appears as a regular wave motion, probably originating in the region ahead of the sphere. Longitudinal oscillations in rocket motors also exhibit this characteristic. They can be described approximately as an acoustic oscillation in a tube with both ends closed, since expansion waves cannot be reflected upstream against the sonic flow in the throat of the nozzle [11]. If longitudinal oscillations between the sphere and wave front contribute to the observed oscillation, it would be expected that they would be comparable to those in a tube with one end open, since in this case expansion waves may be reflected from the shock front. The period of acoustic oscillation, $\tau'$, would be given by

$$\tau'=\frac{4\Delta_s}{nC_3}$$

where $C_3$ is the velocity of sound between the wave

and sphere. In picture 3c the velocity of sound would be between 890 and 1,130 m per second. These values are those behind an adiabatic shock wave at $M=4.9$, and behind a detonation at $M=4.8$ at chemical equilibrium, respectively. The latter value was computed by [7]. Using these values and a value of $0.24R$ for $\Delta_s$ gives a period between 8 and $11 \times 10^{-6}$ sec for the fundamental oscillation ($n=1$). This period is, and probably should be, larger than the ignition delay of 2 $\mu$sec at this Mach number of 4.9. An accurate analysis of the motion probably would need to take account of a three-dimensional propagation of waves of finite amplitude with a periodicity in the rate of heat release.

Since deceleration of the missile was computed to determine $M$ at the observation point, the drag coefficient, $C_D$, was also evaluated in each test. Over a period of many tests it became apparent that the time measurements were not reproducible enough to give consistent results. $C_D$ is derived from a small difference between two large velocities, and an error of several microseconds would have a large effect on the difference, but not on the absolute velocity. Since $C_D$ was unusually small in the first test at $M=4.3$, pressure 0.5 atm, a series of eight tests was made to attempt a tentative evaluation of the effect of combustion on the drag coefficient. It was hoped that the system would be reproducible in this short interval of eight tests. At these conditions picture 2b demonstrates intermittent combustion. A rapid lateral expansion of the burning gas at the rear half of the sphere is also evident. This may have delayed the separation of the flow from the rear surface, thereby causing the unusually small value of the drag coefficient.

Four tests at a Mach number of 4.6 showed that the drag coefficient of the missile in air was $0.8 \pm 0.1$, which compares well with results of about 0.9 given by measurements in wind tunnels. Uncertainty of 0.1 in the drag coefficient corresponds to an uncertainty of about 3 $\mu$sec in the time measurements. Drag coefficient changes very slowly with $M$ in this range, and this value of $C_D$ can be compared with results in the combustible gas at $M=4.3$. One test before, and three immediately after the tests in air, all at $M=4.3$, gave $0.4 \pm 0.3$ in the combustible gas. Since there was no known change in the characteristics of the measurement system, the larger uncertainty in the combustible gas may have been caused by variations in the characteristics of the combustion process. Detachment of the shock wave from the sphere was only slightly larger than that in air, and it seems unlikely that reduced pressure on the front of the sphere caused the reduction of $C_D$. Hence the tentative conclusion may be drawn that the pressure on the rear of the sphere was increased. It was estimated that a time average value of $6p$ over the rear of the sphere would be needed to reduce the drag coefficient by the observed one-half. Pressure on the rear of the sphere in air was estimated to be $0.3p$. A missile with a turning angle less than that of the rear of the sphere would probably respond even more favorably to this effect and perhaps a net thrust would be realized. Although this effect on the drag coefficient appeared when combustion was intermittent, it is not necessarily dependent on the intermittent character of the combustion.

## 4. Conclusion

It is concluded that observation of a hypervelocity missile is a technique which may be used to study some of the problems of stabilizing hypersonic combustion. Combustion waves are observed in some instances to follow the shock wave generated by the missile. The spatial separation was converted to ignition delay times, which were between about 1 and 10 $\mu$sec. These were about one order of magnitude smaller than previously observed by experiments in shock tubes. Satisfactory agreement between these and observations in shock tubes was obtained through chemical-kinetic theory. Thus it is concluded that the method may be used to determine some of the properties of detonation waves. As in most all applications of combustion, oscillations driven by combustion are demonstrated under some conditions. A possible large reduction of the drag coefficient of the missile was noted in one case of intermittent combustion in which the combustion may have delayed separation of the flow from the rear surface of the missile. Fluid-mechanical calculations will be used to extend the information derived from this technique.

## 5. References


[1] Robert A. Gross, Exploratory studies of combustion in supersonic flow, AFOSR TN 59, 587, ASTIA AD 216769 (June 1959).

[2] J. A. Nicholls, E. K. Dabora, and R. L. Gealer, Studies in connection with stabilized gaseous detonation waves, 7th Symposium on Combustion. 1958, Butterworths Scientific Publications, London (1959).

[3] Jerome Eckerman, The measurement of the rate of dissociation of oxygen at high temperature, PhD Thesis, Catholic University of America Press (1958).

[4] C. Bioletti and B. E. Cunningham, A high-velocity gun employing a shock-compressed light gas, NASA TN D–307 (Feb. 1960).

[5] R. E. Duff, Calculation of reaction profiles behind steady-state shock waves. I. Application to detonation waves. J. Chem. Phys. 28, 1193 (1958).

[6] G. A. Bird, A simple numerical solution of the flow around a blunt body in a supersonic stream—with application to real gases, Tech. Note HSA 52, Weapon Research Establishment, Australian Defence Scientific Service, Dept. of Supply (Sept. 1959).

[7] Eisen, Gross, and Rivlin, Theoretical calculations in gaseous detonation, Combustion and Flame 4, 137 (1960).

[8] Lewis and von Elbe, Combustion, flames and explosions of gases, Academic Press, N.Y. (1951).

[9] G. L. Schott and J. L. Kinsey, Kinetic studies of hydroxyl radicals in shock waves. II. Induction times in the hydrogen oxygen reaction, J. Chem. Phys. 29, 1177 (1958).

[10] R. A. Strehlow and A. Cohen, A shock tube technique for studying the kinetics of highly exothermic reactions—shock initiated detonations, Am. Chem. Soc., Division of Fuel Chemistry, St. Louis, Mo. (March 1961).

[11] A. O. Tischler, R. V. Massa, and R. L. Mantler, An investigation of high-frequency combustion oscillations in liquid-propellant rocket engines, NACA RM E53B27 (June 1953).


(Paper 66C1–87)

JOURNAL OF RESEARCH of the National Bureau of Standards—C. Engineering and Instrumentation
Vol. 66C, No. 1, January–March 1962

# Creep of Cold-Drawn Nickel, Copper, 70 Percent Nickel-30 Percent Copper, and 30 Percent Nickel-70 Percent Copper Alloys

William D. Jenkins and William A. Willard

(August 17, 1961)

Creep tests were made in tension under constant loads at temperatures of 300, 700, 900, and 1,200 °F on nickel, copper, 70-percent nickel-30-percent copper, and 30-percent-nickel-70-percent copper specimens, initially cold-drawn to 40-percent reduction in area. Conformance to the conventional creep rate laws was obtained only over limited ranges of stresses, temperatures, creep rates, and strains. Metallographic examinations were carried out on some of the fractured specimens to ascertain the effects of temperature and stress on the necking characteristics, internal cracking, subgrain formation and the number and distribution of "etch figures." The relations between cold-drawing and the creep characteristics are discussed.

## 1. Introduction

A comprehensive investigation, designed to evaluate the effects of stress and temperature on the mechanical properties of metals, has been in progress for several years at the National Bureau of Standards. Some of the results of tests made on nickel, copper, and nickel-copper alloys have been published [1 to 9].[1] The present phase of the study was made to evaluate the effects of stress and temperature on the creep characteristics at 300, 700, 900, and 1,200 °F of nickel, copper, 70 percent nickel-30 percent copper, and 30 percent nickel-70 percent copper specimens, as cold-drawn to 40 percent reduction in area. Some creep data, obtained on the annealed metals [8], made from the same heats as those used in the present studies, are included to evaluate the relations between cold-drawing and creep behavior.

Extensive reviews of current literature on theories of solid-solution alloying [10] and of creep [11] have recently been presented. Therefore, only selected references, pertinent to the present data, are listed.

## 2. Materials and Procedures

The chemical compositions of each of four metals used is given in table 1. All the bars of each material were processed from a single heat and they were supplied in the form of $\frac{7}{8}$ or $\frac{13}{16}$-in. rounds. The annealing treatments produced average grain sizes as shown in table 1 and these annealing treatments were used prior to the final cold-drawing of the rods to 40-percent reduction in area. The creep specimens of each metal for each condition were machined from a single bar and had a 0.505-in. diam over a 2-in. reduced section.

Each specimen was heated for 24 hr in air at the desired temperature before loading to a predetermined stress in increments of approximately 5,300 psi, applied at 1-hr intervals. The temperatures of the creep furnaces were controlled to $\pm 1$ °F of the desired values over the specimen length and the probable error in measuring the extension increments was less than 0.00002 in.

## 3. Results and Discussion

The data are summarized in table 2, and in figures 1 to 16 inclusive. The relation between cold-drawing and the creep characteristics of nickel was previously described [9]. Some of these data on the nickel are used in this paper for comparison purposes. The relation of cold-drawing to the creep characteristics of the other metals used were essentially similar when comparisons were made at equal test temperature-recrystallization temperature ratios. These relations are generally illustrated, in this paper, by the data obtained on the 30 percent nickel-70 percent copper alloy specimens.

### 3.1. Effects of Stress and Temperature on Strain-Time Relations

Numerous equations have been proposed to describe the strain-time relations for specimens tested at different temperatures and stresses. However, the equations generally are applicable only to specific stages of creep over limited ranges of stresses within definite temperature limits and in some cases are empirically derived. In spite of the similarity of strain-time curves obtained under various test conditions, it is not feasible to derive another complete strain-time curve by simple transposition even for specimens of the same metal tested at the same tem-

[1] Figures in brackets indicate the literature references at the end of this paper.

TABLE 1. *Chemical composition and grain sizes of metals*

| Metal | Chemical composition, wt% | | | | | | | | | | | | Average[c] grain diameter |
|---|---|---|---|---|---|---|---|---|---|---|---|---|---|
| | C | Cu | Ni | Co | Fe | Mn | Si | S | Zn | $O_2$ | $N_2$ | $H_2$ | |
| | | | | | | | | | | | | | *mm* |
| Copper[a] (OFHC) | | 99.99+ | | | | | | | | | | | 0.025 |
| 30%–Ni–70% Cu | 0.023 | 68.84 | 29.89 | 0.04 | 0.50 | 0.65 | 0.003 | 0.004 | 0.09 | 0.001 | 0.001 | 0.0002 | .040 |
| 70%–Ni–30% Cu | .017 | 29.71 | 70.08 | [b] | .01 | .01 | .12 | .002 | | .001 | .0015 | .0003 | .025 |
| Nickel | .007 | 0.009 | 99.85 | [b] | .04 | .03 | .11 | .002 | | .002 | .001 | .0002 | .045 |

[a] An arc spectrum of the copper was examined for the sensitive lines of Ag, Al, B, Be, Co, Fe, In, Ir, Mg, Mo, Na, Ni, Pb, Sb, Si, Sn, Ti, V, and Zn. The lines for Ag, Al, Mg, and Si were identified and there was some indication of the presence of Fe, Ni, and Pb.
[b] Not detected.
[c] Values obtained on specimens prepared from the annealed bars.

TABLE 2.—*Test conditions and results of creep tests on high-purity nickel, initially cold-drawn to 40-percent reduction in area*

| Specimen | Test temperature | Creep stress | Plastic strain | | Average creep rate, second stage | Beginning of third stage | | End of test | | | | | Remarks |
|---|---|---|---|---|---|---|---|---|---|---|---|---|---|
| | | | 1 hour after application of load | Intercept at zero time | | Time | Plastic stain | Time | Elongation | Reduction of area | True strain at fracture | True stress at fracture | |
| | °F | *lb/in.²* | % | % | %/1,000 hr | *hr* | % | *hr* | % | % | $\log_e(A_o/A)$ | *lb/in.²* | |
| A–17 | 300 | 72,000 | 0.15 | 0.46 | 0 | | | 2,297 | [a] 0.46 | [b] 0.4 | | | Test stopped in second stage. |
| A–19 | 300 | 75,000 | .47 | .37 | 75 | 2.5 | 0.61 | 3.2 | 18.5 | 76.4 | 1.442 | 317,000 | Tested to complete fracture. |
| A–20 | 300 | 75,600 | | .13 | 1,270 | 0.15 | .32 | 0.25 | 18 | 78.1 | 1.518 | 345,000 | Do. |
| A–10 | 700 | 42,670 | 0 | .07 | 0.42 | 425 | .25 | 2,091 | 26.8 | 82.1 | 1.722 | 238,000 | Do. |
| A–4 | 700 | 48,000 | .11 | .17 | 4.12 | 80 | .5 | 164.3 | 23.0 | 83.4 | 1.793 | 288,000 | Do. |
| A–18 | 700 | 51,500 | .26 | .23 | 21.4 | 14 | .56 | 27.8 | 22 | 87.8 | 2.064 | 300,000 | Do. |
| A–8 | 700 | 53,330 | 2.01 | .15 | 670 | 0.6 | .55 | 1.2 | 23.5 | 83.6 | 1.808 | 325,000 | Do. |
| A–15 | 900 | 24,000 | 0.01 | .19 | 0.67 | 1,320 | 1.08 | 3,546 | 42 | 84.5 | 1.863 | 154,000 | Do. |
| A–12 | 900 | 26,670 | .06 | .31 | 1.66 | 800 | 1.62 | 1,746 | 30.0 | 82.2 | 1.721 | 149,000 | Do. |
| A–9 | 900 | 32,000 | .11 | .17 | 6.55 | 165 | 1.25 | 452 | 30.3 | 85.0 | 1.901 | 213,000 | Do. |
| A–5 | 900 | 37,330 | .35 | .30 | 61 | 9 | 0.85 | 44.5 | 33.5 | 89.5 | 2.219 | 343,000 | Do. |
| A–16 | 900 | 40,000 | .51 | .29 | 200 | 3.2 | .93 | 7.5 | 24.5 | 82.8 | 1.761 | 232,000 | Do. |
| A–11 | 1,200 | 2,665 | .15 | 1.2 | 1.24 | 2,100 | 3.8 | 4,853 | [a] 8.5 | [b] 7.5 | | | Test stopped in third stage. |
| A–6 | 1,200 | 4,010 | .40 | 1.75 | 7.9 | 500 | 5.7 | 3,825 | 74.5 | 78.8 | 1.554 | 19,000 | Tested to complete fracture. |
| A–7 | 1,200 | 6,670 | 1.88 | 4.15 | 72.6 | 58.5 | 8.4 | 86 | 97.3 | 97.6 | 3.745 | 281,000 | Do. |
| A–14 | 1,200 | 9,330 | 6.72 | 7.6 | 632 | 21.2 | 21.0 | 28.3 | 62.5 | 97.8 | 3.839 | 433,000 | Do. |

[a] These values are for plastic strain as the specimens did not break.
[b] These values are for contraction of area as the specimens did not break.

TABLE 2a. *Test conditions and results of creep tests on* OFHC *copper, cold-drawn 40-percent reduction in area*

| Specimen | Test temperature | Creep stress | Plastic strain | | Average creep rate, second stage | Beginning of third stage | | End of test | | | | Remarks |
|---|---|---|---|---|---|---|---|---|---|---|---|---|
| | | | 1 hour after application of load | Intercept at zero time | | Time | Plastic strain | Time | Elongation | Reduction of area | True strain at fracture | |
| | °F | *lb/in.²* | % | % | %/1,000 hr | *hr* | % | *hr* | % | % | $\log_e(A_o/A)$ | |
| 9 | 300 | 29,335 | 0.22 | 0.38 | 0.75 | 1,160 | 1.25 | 1,945 | 5.5 | 9 | 0.092 | Tested to complete fracture. |
| 12 | 300 | 40,000 | .57 | .34 | 240 | 1.5 | .7 | 3.4 | 20 | 79.5 | 1.596 | Do. |
| 15 | 300 | 42,670 | | .11 | 2,100 | 0.05 | .37 | .2 | 18.5 | 82 | 1.707 | Do. |
| 14 | 700 | 1,450 | .001 | .1 | .62 | 3,400 | 2.2 | 8,450 | 24 | 9 | .095 | Do. |
| 7 | 700 | 2,100 | .07 | .21 | 2.2 | 600 | 1.52 | 2,505 | 17 | 10.5 | .109 | Do. |
| 6 | 700 | 2,765 | .01 | .3 | 3 | 410 | 1.5 | 1,306 | 15 | 9.5 | .1 | Do. |
| 21 | 700 | 4,010 | .82 | 1.53 | 11.6 | 275 | 4.75 | 575 | 15.5 | 10.5 | .109 | Do. |
| 5 | 700 | 5,330 | 1.52 | 2 | 64 | 80 | 7.1 | 110 | 18.5 | 13 | .139 | Do. |
| 4 | 700 | 10,670 | 11.1 | 7.8 | 3,540 | 1.75 | 14 | 4 | 36.5 | 29 | .343 | Do. |
| 20 | 900 | 725 | .015 | .05 | 2.75 | 960 | 2.7 | 3,146 | 25 | 14.5 | .158 | Do. |
| 8 | 900 | 1,450 | .08 | .17 | 13.3 | 250 | 3.5 | 535 | 13 | 12.5 | .131 | Do. |
| 10 | 900 | 2,100 | .21 | .28 | 50 | 70 | 3.8 | 143 | 17 | 11 | .113 | Do. |
| 11 | 900 | 2,765 | .72 | .7 | 166 | 50 | 9 | 54.5 | 20 | 13.5 | .147 | Do. |
| 16 | 900 | 5,330 | 5.34 | 2.9 | 2,480 | 2.3 | 8.6 | 4.4 | 27 | 22 | .248 | Do. |
| 18 | 1,200 | 365 | .005 | 1.2 | 1.4 | 840 | 2.4 | 1,606 | 7.5 | 16 | .173 | Do. |
| 19 | 1,200 | 725 | .11 | .3 | 50.5 | 120 | 6.4 | 214 | 21 | 17.5 | .190 | Do. |
| 13 | 1,200 | 1,450 | 1.25 | 1.1 | 390 | 20 | 9 | 21 | 16 | 18 | .199 | Do. |
| 17 | 1,200 | 2,100 | 4.53 | 2.2 | 2,300 | 2.5 | 6 | 2.9 | 15 | 25 | .285 | Do. |

TABLE 2b. *Test conditions and results of creep tests on 70 percent* Ni-*30 percent* Cu, *cold-drawn 40-percent reduction in area*

| Specimen | Test temperature | Creep stress | Plastic strain | | Average creep rate, second stage | Beginning of third stage | | End of test | | | | Remarks |
|---|---|---|---|---|---|---|---|---|---|---|---|---|
| | | | 1 hour after application of load | Intercept at zero time | | Time | Plastic strain | Time | Elongation | Reduction of area | True strain at fracture | |
| | °F | lb/in.² | % | % | %/1,000 hr | hr | % | hr | % | % | $\log_e(A_0/A)$ | |
| 23 | 300 | 93,000 | 0.12 | 0.21 | 0 | | | 1,651 | [b] 0.21 | [b] 0.2 | | Test stopped in second stage. |
| 24 | 300 | 93,800 | .49 | .56 | 0 | | | 1,200 | [a] .56 | [b] .5 | | Do. |
| 21A | 300 | 94,300 | .54 | .62 | 0 | | | 814 | [a] .62 | [b] .6 | | Do. |
| 20A | 300 | 94,500 | | .42 | 940 | 0.19 | 0.6 | .25 | 15 | 76 | 1.431 | Tested to complete fracture. |
| 14 | 700 | 69,330 | .06 | 1.8 | .78 | 7,300 | 7.5 | 10,199 | 21 | 48 | .653 | Do. |
| 21B | 700 | 72,000 | .46 | 2.5 | 2.52 | 2,300 | 7.52 | 3,097 | 20 | 54 | .780 | Do. |
| 13 | 700 | 74,670 | .29 | .56 | 11.1 | 265 | 3.45 | 602 | 30 | 62.5 | .979 | Do. |
| 12 | 700 | 80,000 | 1.16 | 1.08 | 76 | 3 | 1.29 | 35 | 24 | 74 | 1.354 | Do. |
| 17 | 700 | 82,670 | 3.15 | 3.03 | 118 | 2.1 | 3.28 | 4.8 | 20 | 71 | 1.230 | Do. |
| 22 | 700 | 84,000 | | | 10,000 | | | 0.2 | 17 | 72.5 | 1.296 | Do. |
| 28 | 900 | 21,330 | .13 | .32 | .90 | 1,400 | 1.6 | 13,839 | 62 | 54.5 | .790 | Do. |
| 30 | 900 | 24,000 | .08 | .46 | 1.4 | 420 | 1.0 | 2,415 | [a] 6.18 | [b] 5.8 | | Test stopped in third stage. |
| 29 | 900 | 24,000 | .17 | | | | | 4,875 | 77 | 59.5 | .901 | Tested to complete fracture. |
| 25 | 900 | 25,670 | .14 | .50 | 2.0 | 1,000 | 2.5 | 4,255 | 55 | 61 | .944 | Do. |
| 16 | 900 | 32,000 | .10 | | | | | 3,570 | 37 | 45 | .596 | Do. |
| 15 | 900 | 37,330 | .23 | .50 | 12.6 | 100 | 1.75 | 507 | 35 | 55.5 | .806 | Do. |
| 10 | 900 | 42,670 | .51 | 1.8 | 24 | 200 | 6.6 | 367 | 31 | 52.5 | .740 | Do. |
| 7 | 900 | 48,000 | .78 | 1.0 | 52 | 125 | 7.5 | 185 | 29 | 53 | .751 | Do. |
| 11 | 900 | 53,330 | 1.0 | .75 | 260 | 13.4 | 4.2 | 29 | 31 | 52.5 | .740 | Do. |
| 20B | 900 | 58,670 | 2.18 | 1.1 | 1,040 | 3.3 | 4.6 | 7.5 | 25 | 59 | .885 | Do. |
| 19 | 1,200 | 2,100 | .04 | .16 | 0 | | | 1,513 | [a] .16 | [b] 0.1 | | Test stopped in second stage. |
| 8 | 1,200 | 2,665 | .02 | .68 | .51 | | | | | | | Do. |
| 27 | 1,200 | 4,010 | .06 | 1.5 | 4.6 | 2,300 | 12 | 4,310 | 31 | 21.5 | .239 | Tested to complete fracture. |
| 9 | 1,200 | 5,330 | | | 7 | | | 2,001 | 31 | 25.5 | .293 | Do. |
| 4 | 1,200 | 6,670 | .08 | .05 | 12.5 | 115 | 1.5 | 960 | 35 | 28.5 | .335 | Do. |
| 5 | 1,200 | 9,330 | .31 | .4 | 43.5 | 110 | 5.2 | 401 | 42 | 32 | .385 | Do. |
| 6 | 1,200 | 16,000 | 3.82 | 2.9 | 1,640 | 10.2 | 13.5 | 18 | 47 | 44 | .579 | Do. |

[a] These values are for plastic strain as specimens did not break.

[b] These values are for contraction of area as specimens did not break.

TABLE 2c. *Test conditions and results of creep tests on 30 percent* Ni-*70 percent* Cu, *cold-drawn 40-percent reduction in area*

| Specimen | Test temperature | Creep stress | Plastic strain | | Average creep rate, second stage | Beginning of third stage | | End of test | | | | Remarks |
|---|---|---|---|---|---|---|---|---|---|---|---|---|
| | | | 1 hour after application of load | Intercept at zero time | | Time | Plastic strain | Time | Elongation | Reduction of area | True strain at fracture | |
| | °F | lb/in.² | % | % | %/1,000 hr | hr | % | hr | % | % | $\log_e(A_0/A)$ | |
| 14 | 300 | 72,000 | 0.23 | 0.28 | 0 | | | 2,011 | [a] 0.28 | [b] 0.3 | | Test stopped in second stage. |
| 16 | 300 | 73,100 | .33 | .40 | 0 | | | 1,652 | [a] .4 | [b] .4 | | Do. |
| 18 | 300 | 75,000 | .40 | .30 | 115 | 1.1 | 0.42 | 1.5 | 15 | 71 | 1.241 | Tested to complete fracture. |
| 13 | 700 | 42,670 | 0.0 | .27 | 0.33 | | | 8,490 | [a] 3 | [b] 3 | | Test stopped in second stage. |
| 15 | 700 | 51,500 | .16 | .50 | 1.7 | 690 | 1.65 | 1,550 | 8 | 31.5 | 0.375 | Tested to complete fracture. |
| 20 | 700 | 53,330 | .31 | .65 | 22.3 | 85 | 2.4 | 165 | 16 | 33 | .399 | Do. |
| 19 | 700 | 56,030 | .69 | .60 | 100 | 13.5 | 1.95 | 28 | 15 | 45.5 | .602 | Do. |
| 21 | 700 | 58,670 | 1.2 | 1.04 | 160 | 5.5 | 1.92 | 10 | 17 | 52.5 | .746 | Do. |
| 17 | 900 | 16,000 | 0.05 | 0.32 | 0.39 | 3,250 | 1.6 | 14,044 | 46 | 36 | .447 | Do. |
| 10 | 900 | 21,330 | .11 | .45 | 1.5 | 1,550 | 2.75 | 4,190 | 23 | 31.5 | .375 | Do. |
| 4 | 900 | 26,670 | .28 | .55 | 11.1 | 275 | 3.6 | 710 | 35 | 42 | .547 | Do. |
| 7 | 900 | 32,000 | .33 | .35 | 33.3 | 70 | 2.7 | 192 | 21 | 31.5 | .375 | Do. |
| 8 | 900 | 37,330 | .46 | .29 | 180 | 4.5 | 1.1 | 20 | 15 | 25.5 | .292 | Do. |
| 11 | 1,200 | 1,450 | 02 | .40 | 2.65 | 1,700 | 4.9 | 5,062 | 28.5 | 25 | .287 | Do. |
| 5 | 1,200 | 2,665 | .02 | .10 | 7.5 | 240 | 1.9 | 1,032 | 16 | 15 | .165 | Do. |
| 6 | 1,200 | 4,010 | .05 | .10 | 26.4 | 75 | 2.1 | 355 | 31 | 21.5 | .240 | Do. |
| 9 | 1,200 | 6,670 | .36 | .10 | 240 | 1.4 | 0.43 | 47.5 | 36 | 28 | .328 | Do. |

[a] These values are for plastic strain as specimens did not break.

[b] These values are for contraction of area as specimens did not break.

perature with different stresses [9]. The creep curves obtained for the metals used in this investigation were essentially similar when the comparisons were made at equal test temperature—recrystallization temperature ratio values.[2] The general shape of the creep curves are illustrated by the log strain-log time data in figure 1 for the 30 percent Ni-70 percent Cu alloy specimens. The general trend of the curves, except for the data at 300 °F, is a positive contour; i.e., an increase in slope of the log-log curves with increase in time; however, linear relations were sometimes observed over limited ranges during the second stage of creep.

In general, this linearity was more apparent at the lower stresses at 700 and 900 than at 300 or 1,700 °F. The ranges of strain, over which a linear relation exists, depends on the strain on loading, the extent of the first stage of creep and the strain at the beginning of the third stage.

Strain-time curves for the cold-drawn specimens of nickel and the nickel alloys tested under identical conditions at 700, 900, and 1,200 °F are shown in figures 2 to 5, inclusive. Tests for the copper could not be made at the stress levels shown in these figures as its creep resistance[3] was too low. The creep stresses used on the 70 percent Ni-30 percent Cu alloy at 700 °F were too high to compare with the other metals under equal test conditions. The resistance of creep of the 30 percent Ni-70 percent Cu alloy was greater than that of the nickel at 700 °F (figs. 2 and 3). The magnitude of the increase was greater for the higher stresses. The creep resistance at 900 (fig. 4) and 1,200 °F (fig. 5) of the nickel is generally intermediate between the 70 percent nickel alloy and the 30 percent nickel alloy. Apparently the solute atoms which act as barriers to the motion of dislocations are less effective as the temperature is raised. Prior cold-drawing tends to decrease the temperature range at which strengthening due to alloying is effective [8]. Furthermore, as indicated by the microstructures obtained after fracture (fig. 21), some recrystallization occurred in some of the 30 percent Ni-70 percent Cu specimens tested at 900 °F. This phenomenon would tend to cause a decrease in the creep resistance of the alloy below that of the unrecrystallized nickel tested under identical conditions.

[2] Approximate recrystallization values for the cold-drawn metals used in this investigation are: Cu, 350 °; Ni, 1,100 °; 70 percent Ni-30 percent Cu, 1,100 °; 30 percent Ni-70 percent Cu, 1,050 °F (1 hr at temperature).

[3] When the test conditions are identical, the more creep-resistant metal may be defined as the one having the smaller strain at a given time.

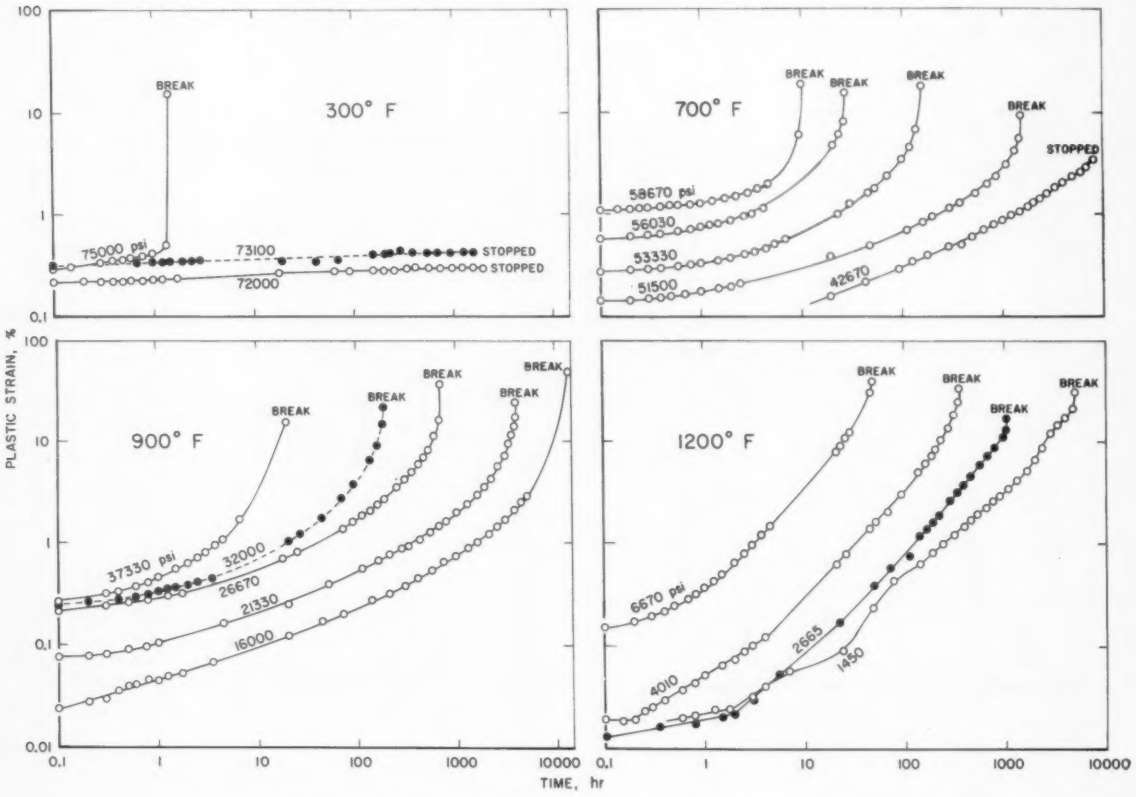


FIGURE 1. *Strain-time curves for the cold-drawn 30% Ni-70% Cu specimens tested in creep.*

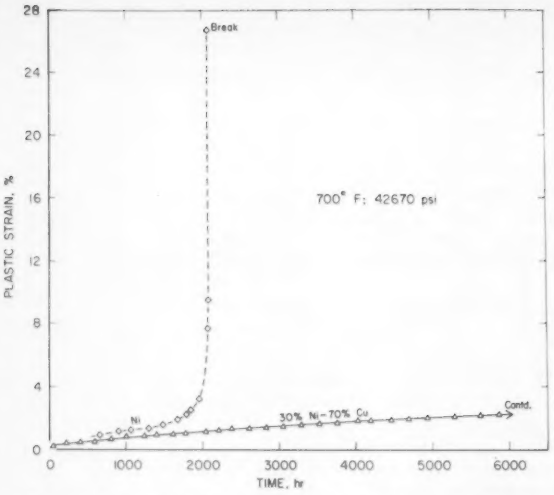


FIGURE 2. *Strain-time relations of cold-drawn specimens tested at 700 °F with a stress of 42,670 psi.*

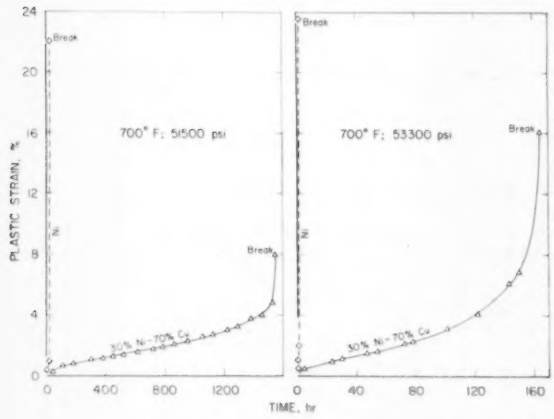


FIGURE 3. *Strain. time relations of cold-drawn specimens tested at 700 °F with different stresses.*

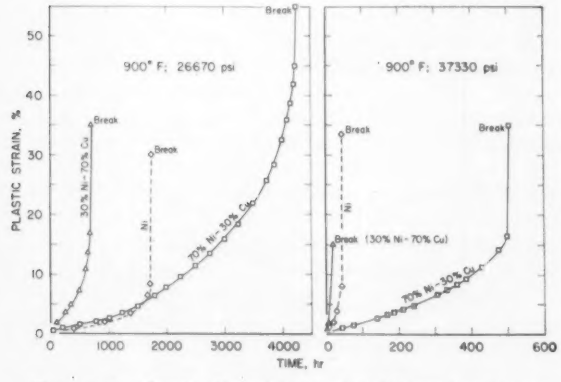


FIGURE 4. *Strain-time relations of cold-drawn specimens tested at 900 °F with different stresses.*

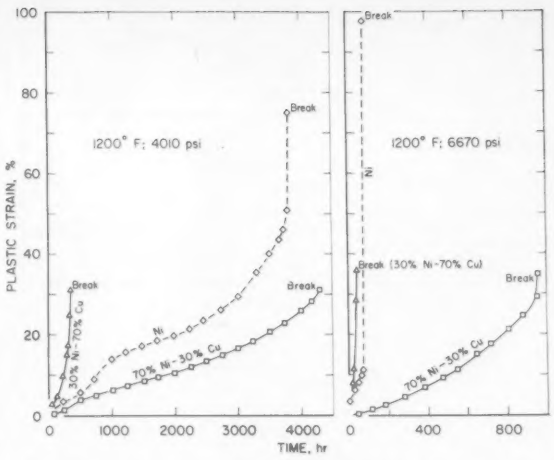


FIGURE 5. *Strain-time relations of cold-drawn specimens tested at 1,200 °F with different stresses.*

### 3.2. Relations of Temperature, Stress, and Composition to Second Stage Creep Rate

During the first stage of creep, the creep rate decreases as the test time increases. Eventually, the creep rate appears to become approximately constant over a period of time, the extent of which depends on the test conditions. This constant rate, which is described as the second stage creep rate, has been used as a strength index for evaluating the properties of different materials at constant or differing test conditions. Furthermore, this constancy of rate has become the basis for much theoretical discussion as the second stage is sometimes considered to be the range in which there is a balance between strain hardening and recovery of metal crystals. Some of the formulas derived from theoretical considerations indicate that either a linear or a power relation exists between the applied stress and second stage creep rate. Others indicate a linear relation between creep rate and the hyperbolic sine of the stress [12]. It has also been postulated that a single curve might describe stress-creep rate parameter relations over a wide range of temperatures and stresses [13].

The degree of success in the application of the formulas to data obtained in creep tests depends on such factors as the models used, the initial condition of the metals, the homologous temperature, the creep stress-tensile strength ratio, the reactions taking place during testing, and the ductility.

The interrelations of stress, second stage creep rate, and temperature, as influenced by composition and cold-drawing, are shown, for the metals used in the present investigation, in figures 6 to 12, inclusive.

The relations of creep stress, and of the creep stress-tensile strength ratio to the second stage creep rate of the annealed and cold-drawn 30 percent Ni–70 percent Cu alloy specimens, are shown in figure 6. At each temperature, the shape of the

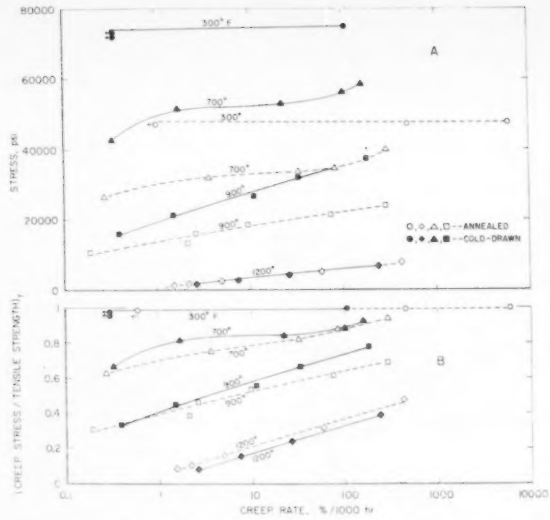


FIGURE 6. *Effect of cold-drawing on (A) the stress-creep rate relations and on (B) the creep stress-tensile strength ratio-creep rate relations for 30% Ni-70% Cu specimens.*

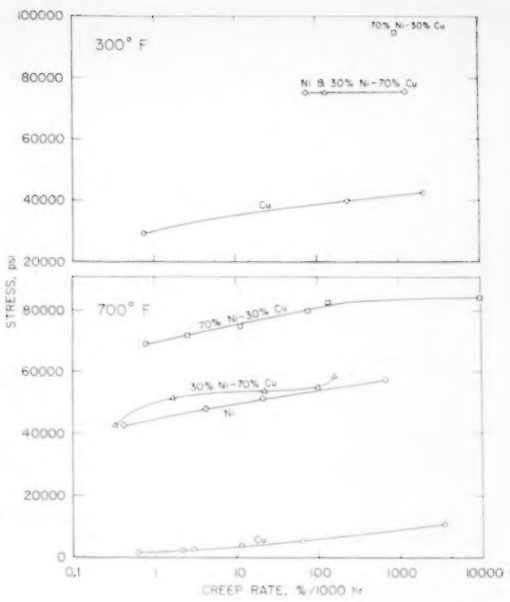


FIGURE 7. *Influence of stress on the average creep rate during the second stage at 300 and 700 °F.*

curves for each condition of the metal is similar (fig. 6A); however, at different temperatures the curves are dissimilar. At 300, 700, and 900 °F, the stress necessary to produce equal creep rates was increased by cold-drawing. The difference decreased with increase in temperature, and at 1,200 °F there was a coincidence of the curves for the annealed and cold-drawn metal. This is due, in part, to the fact that 1,200 °F is above the recrystallization temperature of the metal.

Attempts were made to ascertain whether creep data could be calculated from the results of short time tensile tests. Accordingly, the creep stress-tensile strength ratios at the different temperatures were determined and plotted as a function of the second stage creep rate for the 30 percent Ni–70 percent Cu alloy (fig. 6B). As the values of tensile strength [7] are those obtained at the respective temperatures, it is apparent that the creep stress-tensile strength ratio to produce equal creep rates decreases as the temperature is increased. However, the decrease in values is less at the fast creep rates than at the slow rates. Cold-drawing the metal appears to increase the ratio slightly at 700 and 900 °F whereas the reverse is true at 1,200 °F. The magnitude of the increase at 900 °F was significantly less than that previously shown for the nickel [9]. It is obvious from these results that no simple correlation exists between short-time tensile test data and creep data.

The effect of stress on the second stage creep rate of the cold-drawn metals is shown in figures 7 and 8. The curves for the nickel and the 30 percent Ni-70 percent Cu alloy are usually intermediate between the high values for the 70 percent Ni-30 percent Cu alloy and the low values for the copper. At 700 °F the stress necessary to produce equal creep

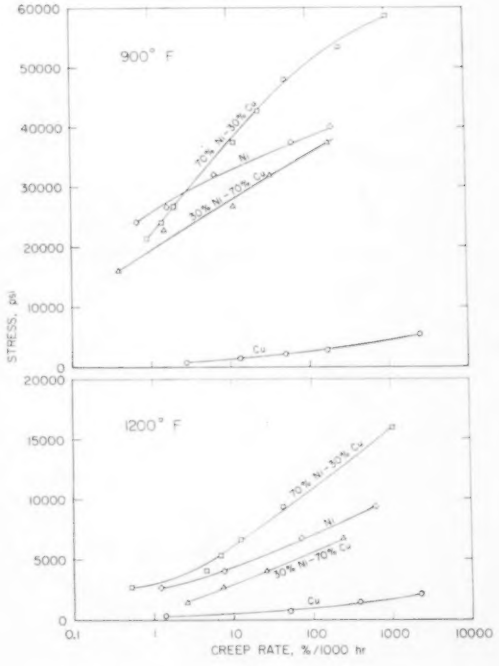


FIGURE 8. *Influence of stress on the average creep rate during the second stage at 900 and 1,200 °F.*

rates was slightly greater for the 30 percent Ni-70 percent Cu alloy than for the nickel, whereas, at 900 and 1,200 °F the reverse was observed.

The relation of creep stress-tensile strength ratio to the second stage creep rate of the cold-drawn metals indicated that, at all the temperatures used, this ratio was lowest for the copper. Although the ratios for the alloys at 900 and 1,200 °F appeared to be intermediate between the high values of the nickel and low values of the copper, they were significantly different at different creep rates. Furthermore, the values were more closely grouped at 1,200 than at 900 °F.

The relation between stress and temperature, to produce creep rates of 1 percent and 100 percent per 1,000 hr on the annealed and cold-drawn 30 percent Ni-70 percent Cu specimens, is shown in figure 9A. Strengthening due to cold-drawing is most pronounced at 300 °F and becomes less pronounced as the temperature is increased. At 1,200 °F, the values for the two conditions are effectively the same. Although the stress increase necessary to produce creep rates of 1 percent and 100 percent per 1,000 hr is small at 300 °F, appreciable increases are required at the higher temperatures. The spread in stress values, to produce different creep rates is greater at 900 than at 1,200 °F even though the percentage differences at 1,200 °F are greater.

When log stress-log creep rate values (not shown) for specimens are plotted, a linear relation can often result. The slope of the line $\Delta$ log stress/$\Delta$ log creep rate, at each temperature is designated "rate sensitivity" [14]. Generally, this value increases with increase in temperature as shown by the data for 30 percent Ni-70 percent Cu alloy specimens in figure 9B. Cold-drawing the metal appeared to increase the rate-sensitivity at 900 °F. In contrast, cold-drawing the nickel specimens caused a decrease in this property [9]. The relation of composition of the specimens to the rate sensitivity is shown in figure 10. With the exception of one value for the copper at 1,200 °F, the values for the copper are the highest. The rate sensitivity of the 30 percent Cu alloy was greater than that of the nickel. Prior cold-drawing appeared to cause an increase in some of the rate-sensitivity values and a decrease in others. This behavior indicates that no smooth relation exists between rate sensitivity and chemical composition.

The relation of composition to the stress necessary to produce equal creep rates at various temperatures of the cold-drawn metals is shown in figure 11. The slopes of the line segments indicate that the greatest increase in stress of the alloys above that of the base metals is obtained at 700 °F while the least is at 1,200 °F. The latter observation is due to the fact that this is above the recrystallization temperature of all the metals tested. It should also be observed that the slopes of the stress-composition line segments are also different at different creep rates.

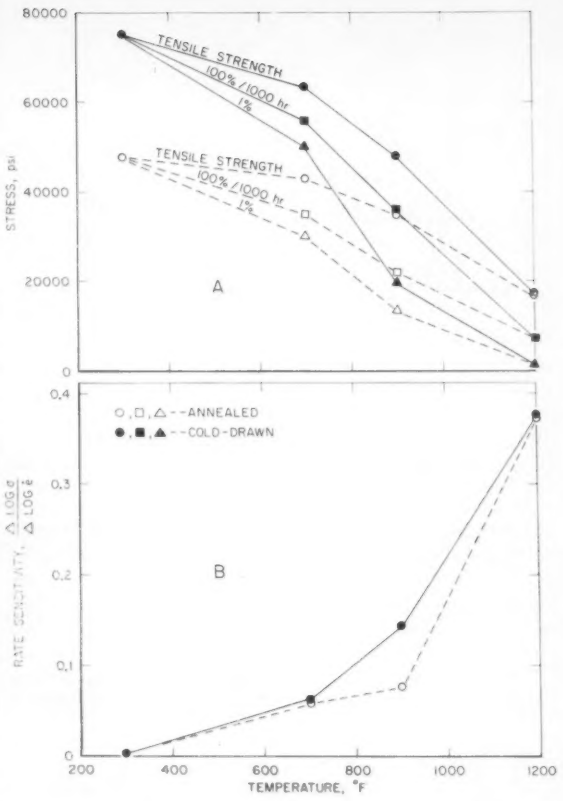


FIGURE 9. *Effect of temperature (A) on the tensile strength and the stress to produce different second stage creep rates and (B) on the rate sensitivity of the annealed and cold-drawn 30% Ni-70% Cu specimens.*

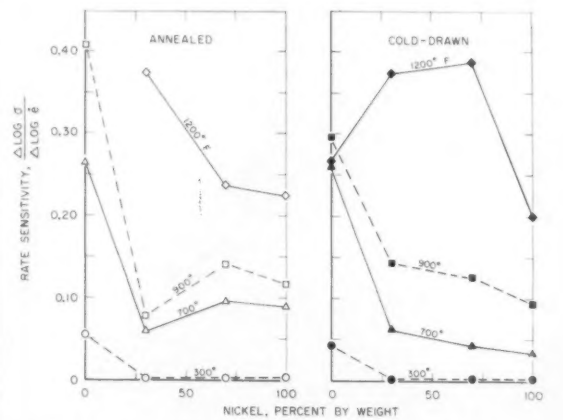


FIGURE 10. *Variation of rate sensitivity with nickel content of the annealed and cold-drawn specimens at different temperatures.*

($\sigma$ is the applied creep stress and $\dot{\epsilon}$ is the corresponding second stage creep rate.)

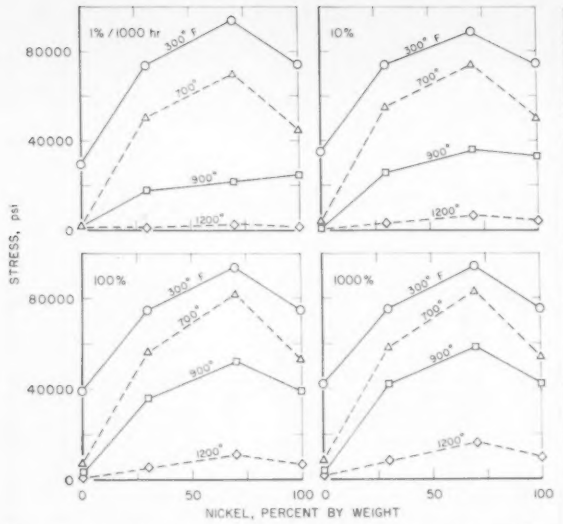


FIGURE 11. *Variation of stress with nickel content to produce equal second stage creep rates at different temperatures of the cold-drawn metals.*

### 3.3. Relations Between Test Conditions and Fracture Time

The relations of stress and second stage creep rate to fracture time, as influenced by temperature,

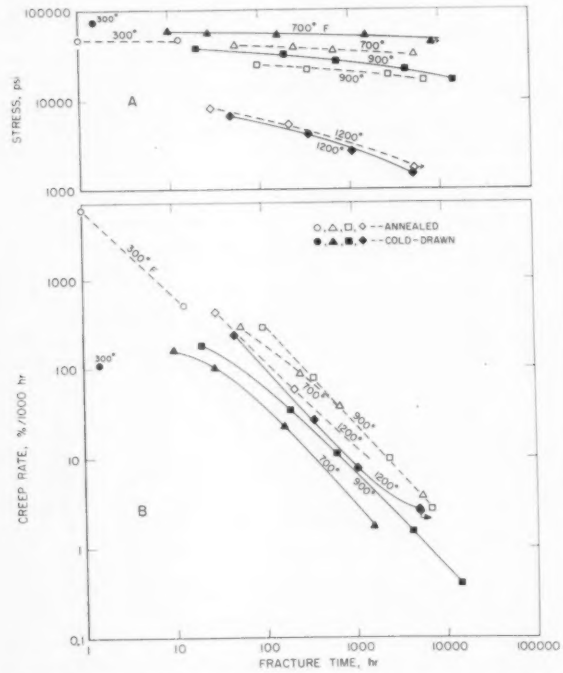


FIGURE 12. *Relation of stress and second stage creep rate to fracture time of the annealed and cold-drawn 30% Ni-70% Cu specimens.*

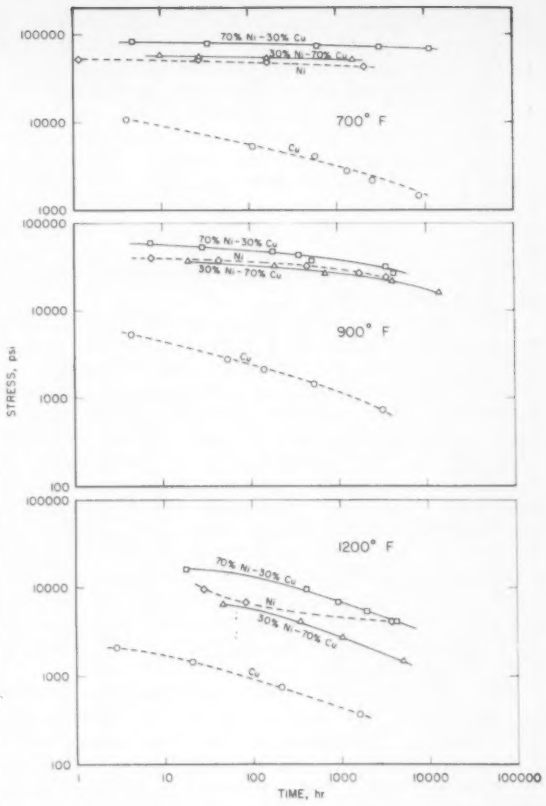


FIGURE 13. *Relation of stress to fracture time of cold-drawn specimens at different temperatures.*

cold-drawing, and composition, are shown in figures 12, 13, and 14. As illustrated in figure 12A, the stress necessary to cause fracture of 30 percent Ni-70 percent Cu specimens at any given time increases with decrease in test temperature, and with exception of the data at 1,200 °F, with cold-drawing. Strengthening due to cold-drawing is more pronounced as the temperature is decreased. The second stage creep rates necessary to produce fracture at equal times were generally greater for the annealed than for the cold-drawn metal, as shown by the data in figure 12B. As the temperature is increased, the creep rate necessary to cause fracture in any given time increases for the cold-drawn specimens; whereas no simple relation of this type was observed for the annealed specimens. The effect of stress on fracture time at 700, 900, and 1,200 °F of the cold-drawn metals is shown in figure 13. At each temperature, the values for the nickel and the 30 percent Ni-70 percent Cu specimens were intermediate between the low values of the copper and the high values of the 70 percent Ni-30 percent Cu alloy. The stress level of the 30 percent Ni alloy is slightly higher than that of the nickel at 700 °F; however, at 900 and 1,200 °F the opposite is

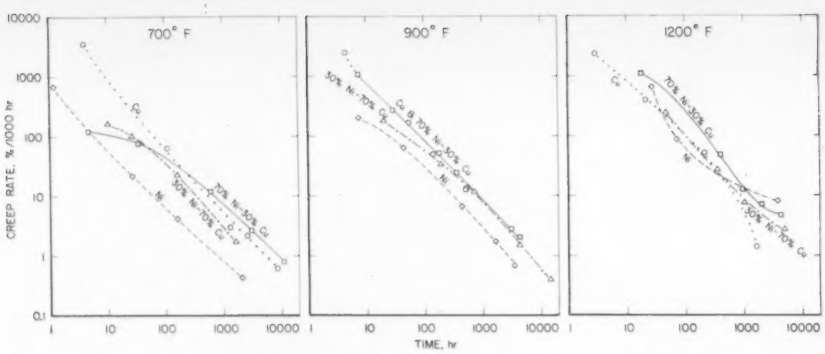


FIGURE 14. *Relation of second-stage creep rate to fracture time of cold-drawn specimens at different temperatures.*

true. The second stage creep rate-fracture time relations for the cold-drawn specimens are shown in figure 14. It is evident from the relative positions of the curves that no simple relation exists describing all of the variables involved. As the fracture time includes the total test time for each of the three stages of creep, apparently different types of microstructural changes occur which are dependent on the temperature, test time, and the creep rate. For different metals, the changes in structure during each of the stages are obviously different.

### 3.4. Relations of Temperature, Second Stage Creep Rate, and Composition to Ductility

Prior cold-drawing of the specimens tended to decrease the elongation and reduction of area values for specimens tested in creep below the recrystallization temperatures. Above the recrystallization temperatures, prior cold-drawing had no significant effect on the ductility. No consistent trends were observed on the relation between creep rate and elongation or reduction of area, at all temperatures, for the cold-drawn metal.

The elongation-creep rate values for the cold-drawn specimens (fig. 15) indicate that one curve could describe the limited amount of data obtained at 300 °F. The curves at 700 and 900 °F are another manifestation of the complexity of the mechanisms of deformation occurring at different rates and for different metals. At 1,200 °F, however, elongation values generally increase with increase in nickel content and no smooth relation between second stage creep rate and ductility could be established.

Although a single curve describes the relation of creep rate to the reduction of area values at 300 °F of the cold-drawn metals (fig. 16), the data obtained at 700, 900, and 1,200 °F indicate that the reduction of area increases with increase in nickel content of the specimens. However, the magnitude of the increase is affected by test temperature.

### 3.5. Relation of Creep Conditions to Structures

The effect of temperature on the tendency of the specimens tested at different rates, to contract locally (neck) is shown by the photographs of figures

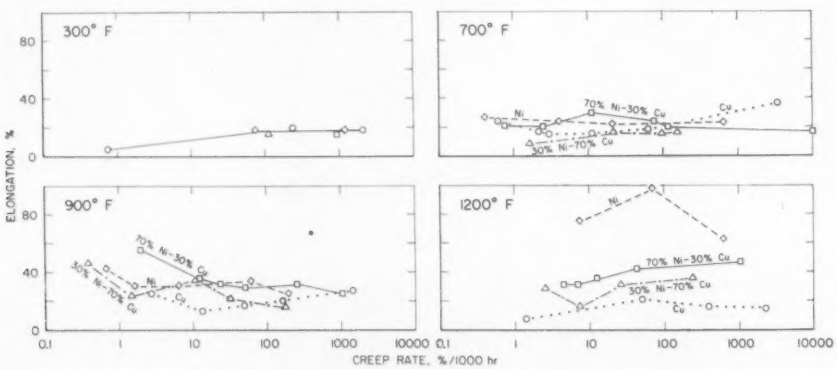


FIGURE 15. *Relation of second stage creep rate to elongation values of specimens at different temperatures.*

(Symbols used at 300 °F correspond to those used for the metals at 700, 900, and 1,200 °F.)

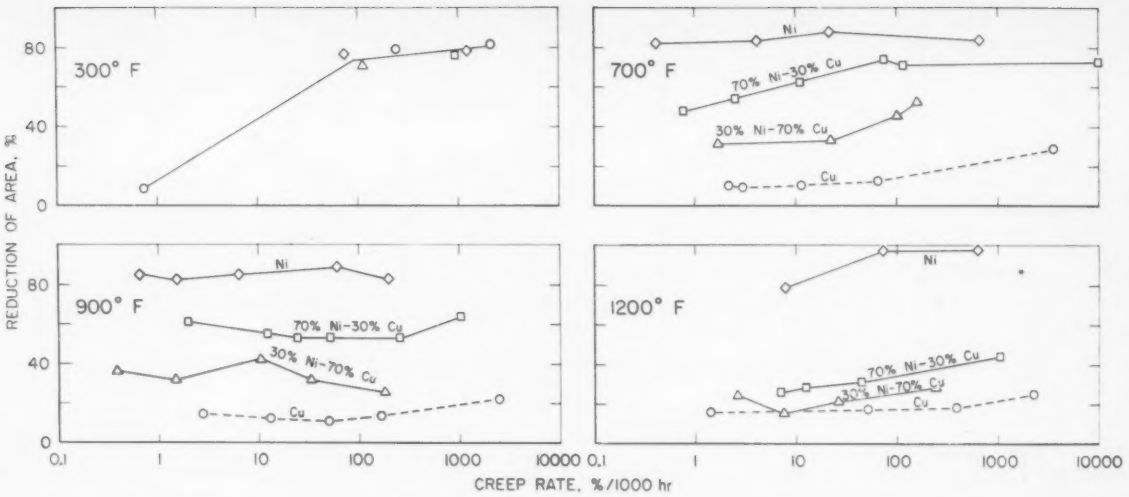


FIGURE 16. *Relation of second stage creep rate to reduction of area values of specimens at different temperatures.*

(Symbols used at 300 °F correspond to those used for the metals at 700, 900, and 1,200 °F.)

17 and 18. The necking of specimens of copper and of the nickel-copper alloys was more pronounced as the temperature was decreased and as the creep rate was increased. Surface cracks were also more evident in the specimens tested at high temperatures and low creep rates although their presence was sometimes obscured by oxide films on the surface (figs. 17G and 18, H and I). The surface cracking was associated with low ductility in the specimens, whereas this phenomenon was not observed for the cold-drawn nickel specimens [9].

It has been observed [2] that during the third stage of creep, lattice defects coalesce to form voids and cracks, some of which link up to form the main path of the fracture. Some of the cracks, that were discontinuous in the interior of the specimens used in the present investigation, are shown in figures 19 and 20. Round and elliptical cracks, generally associated with transcrystalline fracture are shown in A, B, C, and D of figures 19 and 20. Jagged cracks, the type associated with intercrystalline fracture, are more evident at the high temperatures and slow creep rates (longer fracture times), as shown in G, H, I of figures 19 and 20. A mixture of intercrystalline and transcrystalline cracking is illustrated by the photomicrographs in E and F of figures 19 and 20. The number of the cracks become less as the distance from the complete fracture becomes greater. Subsequent etching of these specimens showed definitely the existence of the different types of cracks in the specimens. Some of the etched specimens are shown in figure 21. These surfaces indicate that cracking exists even at a distance of 0.4-in. from complete fracture (fig. 21C, D, E, and F) although at the lower temperatures this occurrence was very limited (fig. 21A and B).

Extensive elongation of the grains, accompanied by very limited transcrystalline cracking, was evident in the cold-drawn 30 percent Ni-70 percent Cu specimens tested at 700 °F. A mixture of transcrystalline and intercrystalline cracks was observed for the specimen (fig. 21C) tested to fracture in 192 hr at 900 °F; whereas intercrystalline cracking, accompanied by recrystallization into small grains, predominated in the specimen tested at the same temperature for a long period of time (fig. 21D). Intercrystalline cracking, accompanied by recrystallization and the formation of equiaxed grains whose size increased with increase in test time, predominated at 1,200 °F (fig. 21E and F).

Subboundary structures in metals have been observed for many years [15]. The literature on the influence of creep on the formation of subgrains within the parent grains has recently been reviewed [9]. Subgrains, observed after fracture of cold-drawn copper and 30 percent Ni-70 percent Cu creep specimens, are shown in figure 22. The subgrain boundaries, evident for specimens strained at the lower temperatures, are apparently more effective barriers to the motion of dislocations than the subgrain boundaries existing at the higher temperatures. Some of the subgrains formed at the higher temperatures and long test times appeared to be larger than those formed at the lower temperatures. In general, the subgrain boundaries in the alloys appeared to be more distinct than those of the parent metals.

Some investigators have related the number of the etch figures to the number of dislocation sites. Triangular etch figures, developed by etching (etching time constant) the surface of the cold-drawn copper specimens used in the present investigation, are shown in figure 23. In general, it was observed

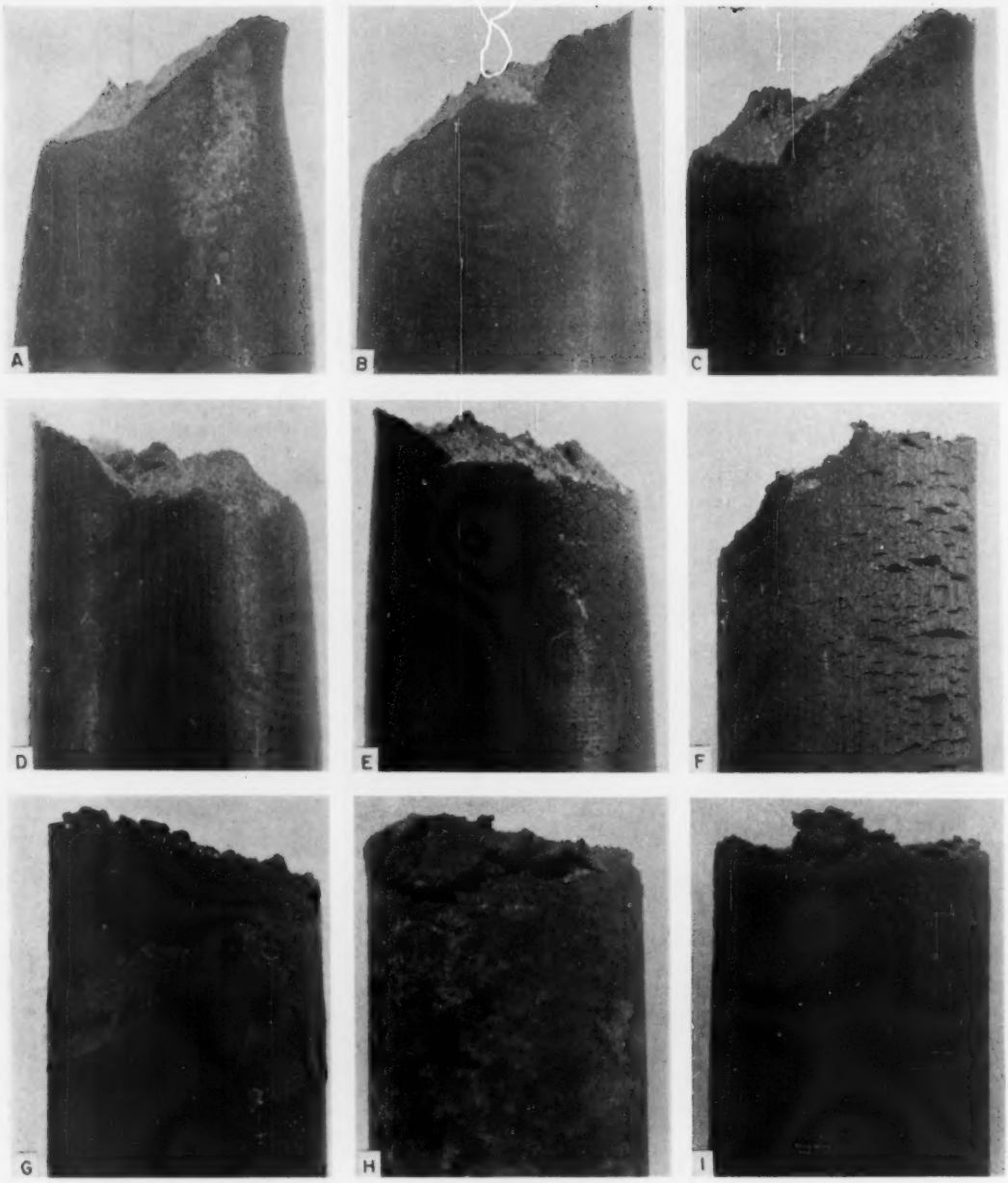


FIGURE 17. *Relation of temperature and second stage creep rate to the appearance of 30% Ni–70% Cu specimens tested to complete fracture.* ×4.

| Temperature | Creep rate, second stage | Temperature | Creep rate, second stage | Temperature | Creep rate, second stage |
|---|---|---|---|---|---|
| °F | %/1000 hr | °F | %/1000 hr | °F | %/1000 hr |
| A 700 | 160 | D 900 | 182 | G 1200 | 240 |
| B 700 | 22.3 | E 900 | 33.3 | H 1200 | 26.4 |
| C 700 | 1.7 | F 900 | 0.39 | I 1200 | 2.65 |

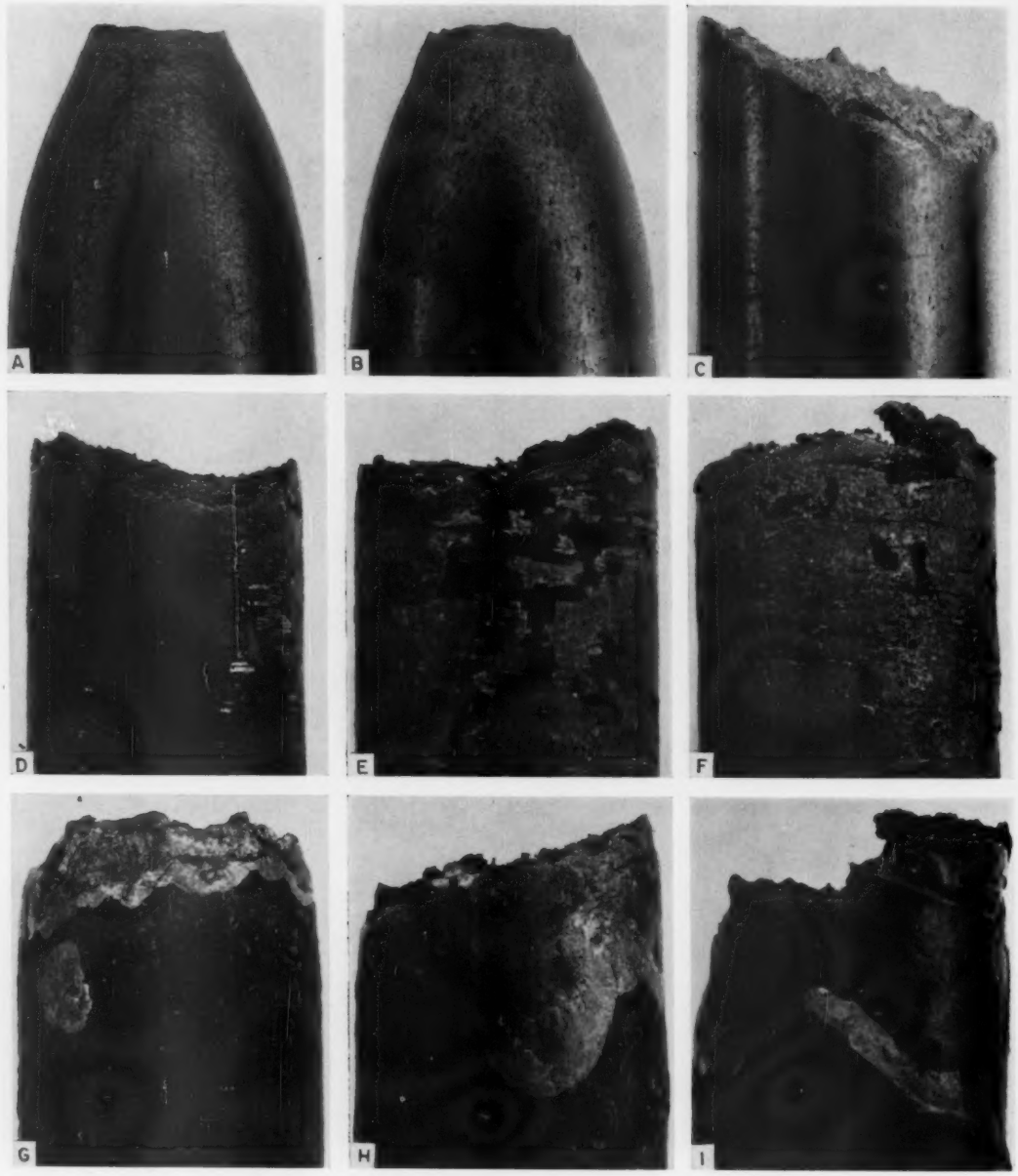


FIGURE 18. *Relation of temperature and second stage creep rate to the appearance of copper specimens tested to complete fracture.* ×4.

| Temperature | Creep rate, second stage | Temperature | Creep rate, second stage | Temperature | Creep rate, second stage |
|---|---|---|---|---|---|
| °F | %/1000 hr | °F | %/1000 hr | °F | %/1000 hr |
| A 300 | 2100 | D 700 | 3540 | G 1200 | 2300 |
| B 300 | 240 | E 700 | 11.6 | H 1200 | 50.5 |
| C 300 | 0.75 | F 700 | 0.62 | I 1200 | 1.4 |

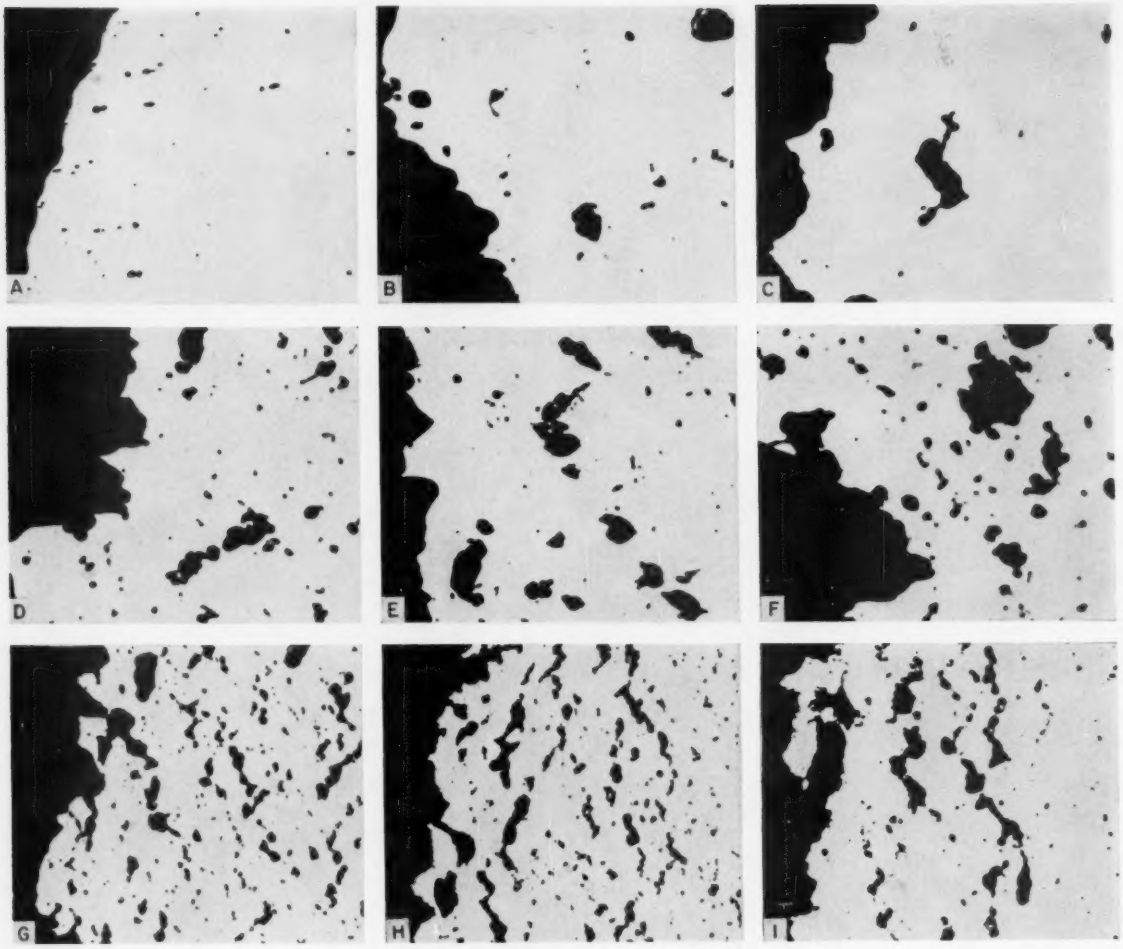


FIGURE 19. *Relation of temperature and fracture time to microstructures of 30% Ni–70% Cu specimens.*

Longitudinal sections, near axis, near fracture. Unetched, ×75

| Temperature | Fracture time | Temperature | Fracture time | Temperature | Fracture time |
|---|---|---|---|---|---|
| | °F hr | | °F hr | | °F hr |
| A | 300 1.5 | D | 900 20 | G | 1200 47.5 |
| B | 700 10 | E | 900 710 | H | 1200 355 |
| C | 700 1550 | F | 900 14044 | I | 1200 5002 |

that increasing the test temperature or decreasing the creep rate tended to increase the size and decrease the number of the etch figures. Furthermore, the etch figures were more evident within the grains than at the grain boundaries.

## 4. Summary

Creep tests were made in tension at 300, 700, 900, and 1,200 °F on specimens of copper, nickel, a 70 percent Ni-30 percent Cu alloy, and a 30 percent Ni–70 percent Cu alloy, initially cold-drawn to 40 percent reduction in area.

Conformance to the parabolic strain-time law was evident over limited ranges of stress, strain, and temperature.

Cold-drawing the metals, prior to testing below the recrystallization temperatures, tended: (1) to increase the stresses necessary to produce equal creep rates; (2) to displace the creep stress-fracture time curves to higher values of stress; (3) to displace the creep rate-fracture time curves to lower values of creep rate; (4) to decrease the elongation and reduction of area values; (5) and to change the rate sensitivity. Above the recrystallization tempera-

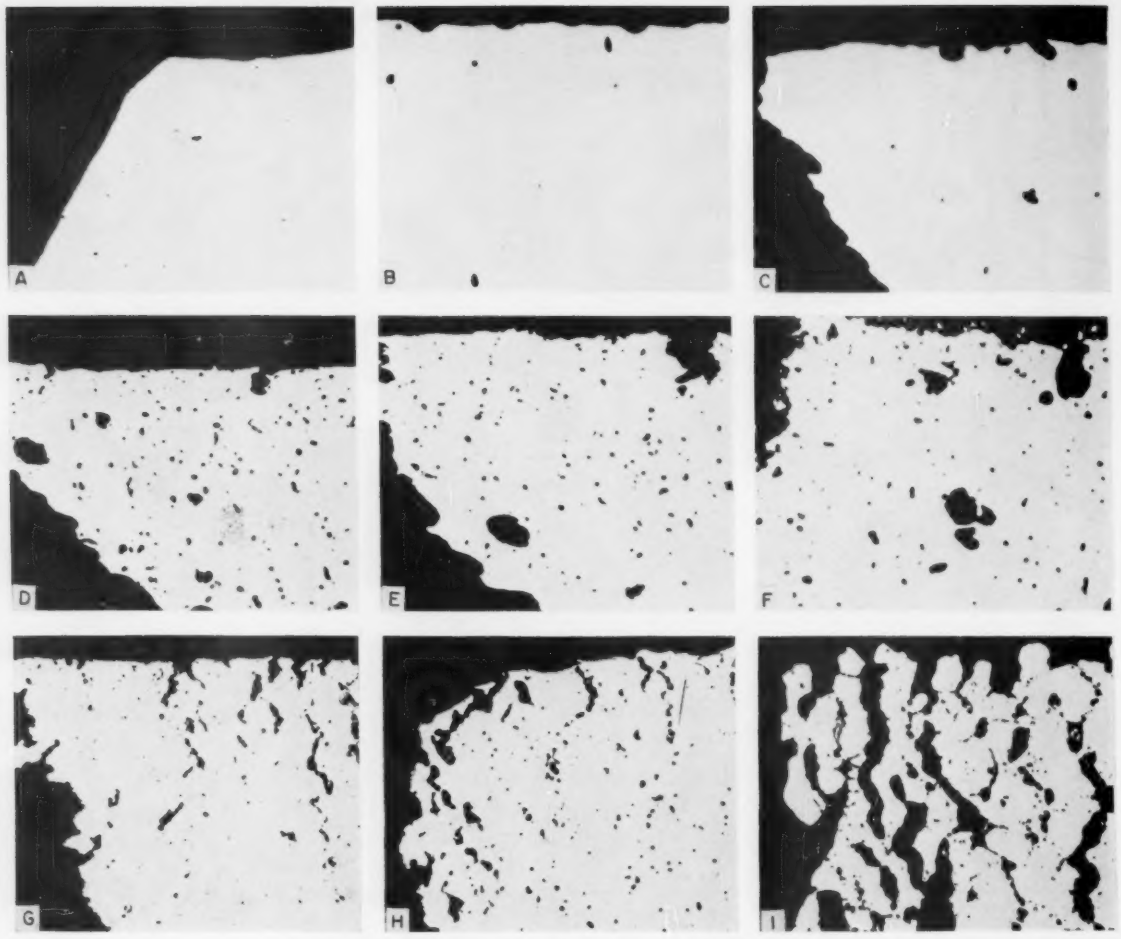


FIGURE 20. *Microstructures near surface near fracture of 30% Ni–70% Cu specimens tested at different temperatures and stresses. Unetched ×75.*

| Temperature | Fracture time | Temperature | Fracture time | Temperature | Fracture time |
|---|---|---|---|---|---|
| °F | *hr* | °F | *hr* | °F | *hr* |
| A 300 | 1.5 | D 900 | 20 | G 1200 | 47.5 |
| B 700 | 10 | E 900 | 710 | H 1200 | 355 |
| C 700 | 1550 | F 900 | 14044 | I 1200 | 5002 |

tures, the strength and ductility values were affected only slightly by prior cold-drawing.

The 70 percent Ni-30 percent Cu alloy generally showed the greatest resistance to creep and copper the least. The nickel was stronger than the 30 percent Ni-70 percent Cu alloy at 900 and 1,200 °F and weaker at 700 °F.

Strengthening of the alloys above that of the base metals was most marked at 700 °F and at the higher creep rates.

Although the rate sensitivities increased with increase in temperature, no smooth relation was shown between this property and chemical composition of the metals.

Reduction of area values obtained on specimens tested at 700, 900, and 1,200 °F and elongation values at 1,200 °F increased with increase in nickel content. No smooth relation was observed for elongation values at 700 and 900 °F. The ductility at 300 °F appeared to be independent of chemical composition.

The degree of necking of the specimens decreased and the tendency toward intercrystalline fracture increased with decrease in creep rate and, except the nickel, with increase in test temperature.

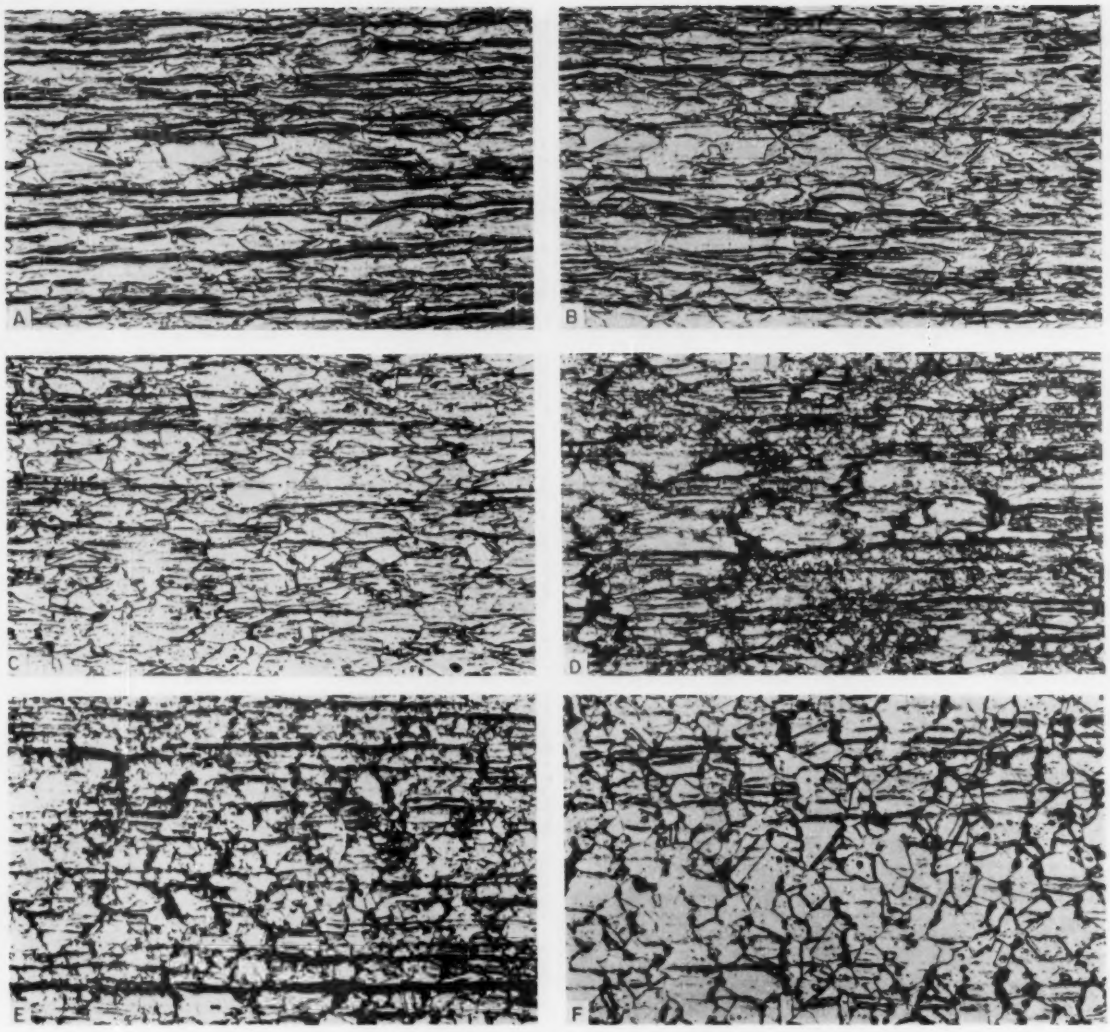


FIGURE 21. *Microstructures, near axis, approximately 0.4" from fracture of 30% Ni–70% Cu specimens.*

The point of fracture is to the left of each photomicrograph. Longitudinal sections, etched in 20 g $CrO_3$, 3.75 g $NH_4Cl$, 25 $cm^3$ $HNO_3$ (conc.), 25 $cm^3$ $H_2SO_4$ (conc.) and 450 $cm^3$ $H_2O$. × 100.

| Temperature | Fracture time | Temperature | Fracture time | Temperature | Fracture time |
|---|---|---|---|---|---|
| °F | *hr* | °F | *hr* | °F | *hr* |
| A 700 | 28 | C 900 | 192 | E 1200 | 47.5 |
| B 700 | 1550 | D 900 | 14044 | F 1200 | 1032 |

The largest subgrains with the most sharply defined boundaries were obtained for the specimens having the longest test times.

The size of the "etch figures" increased and their number decreased with increase in test temperature and with decrease in creep rate.

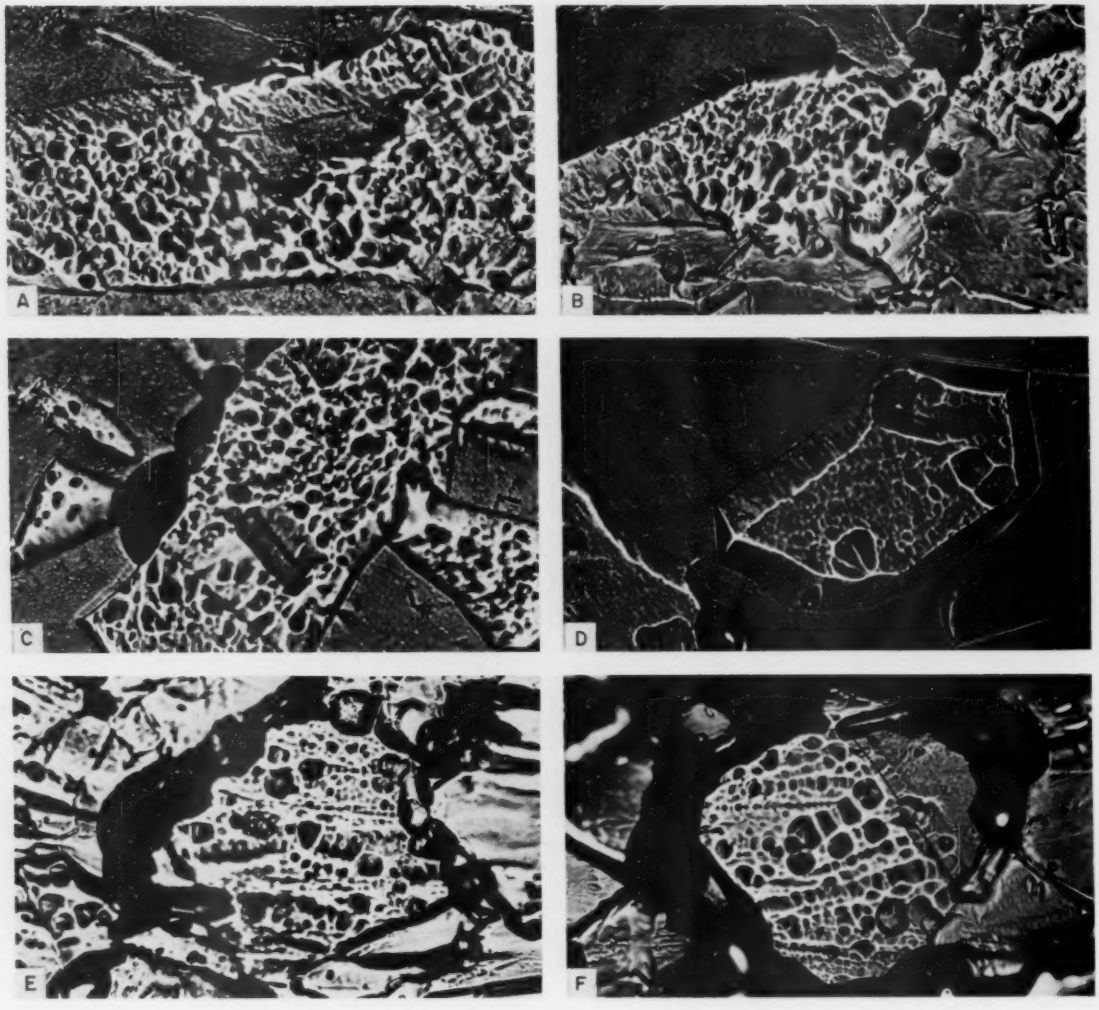


FIGURE 22. *Subgrains in specimens after fracture at different temperatures.*

Longitudinal sections A, B, C, D etched in equal parts $NH_4OH$, $H_2O_2$ (3%), and $H_2O$. E and F etched in 20 g $Cr\ O_3$, 3.75 g $NH_4Cl$, 25 $cm^3$ $HNO_3$ (conc.), 25 $cm^3$ $H_2SO_4$ (conc.) and 450 $cm^3$ $H_2O$.

| | Metal | Temperature | Fracture time | Magnification |
|---|---|---|---|---|
| | | °F | hr | |
| A | OFHC Cu | 300 | 1945 | ×1000 |
| B | do | 700 | 4 | ×1000 |
| C | do | 900 | 54.5 | ×1000 |
| D | do | 1200 | 1606 | ×1000 |
| E | 30% Ni–70% Cu | 1200 | 355 | ×500 |
| F | do | 1200 | 5002 | ×500 |

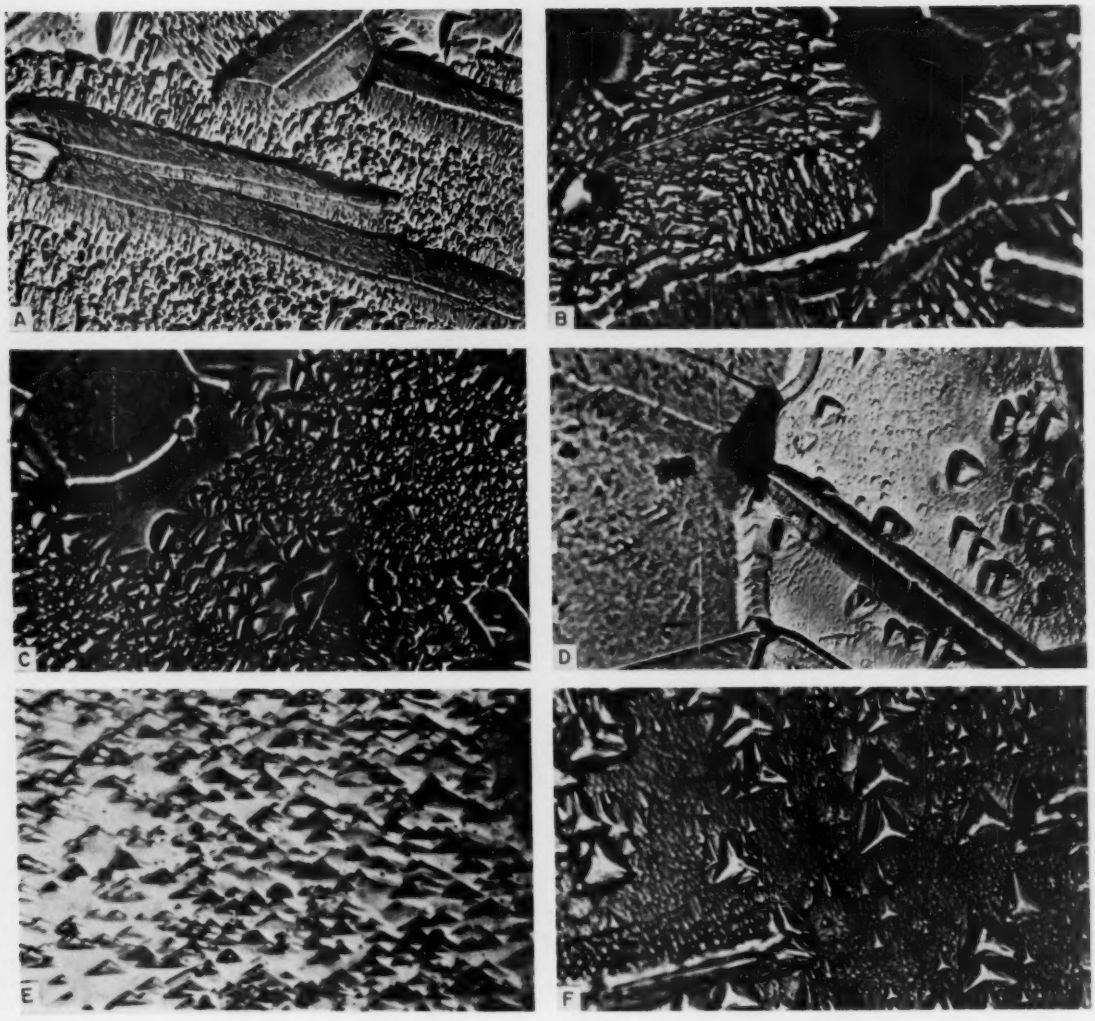


FIGURE 23. *Relation of temperature and second stage creep rate to the size and distribution of "etch figures" in* OFHC *copper specimens after fracture at different temperatures and stresses.*

Longitudinal sections, etched in equal parts $NH_4OH$, $H_2O_2$ (3%) and water. × 1000.

| | Temperature | Creep rate, second stage |
|---|---|---|
| | °F | %/1000 hr |
| A | 700 | 64 |
| B | 700 | 0.62 |
| C | 900 | 166 |
| D | 900 | 2.75 |
| E | 1200 | 2300 |
| F | 1200 | 1.4 |

## 5. References


[1] W. D. Jenkins and T. G. Digges, Creep of high-purity copper, J. Research NBS **45,** 153 (1950) RP2121.

[2] W. D. Jenkins and T. G. Digges, Creep of annealed and cold-drawn high-purity copper, J. Research NBS **47,** 272 (1951) RP2254.

[3] W. D. Jenkins and T. G. Digges, Effect of temperature on the tensile properties of high-purity nickel, J. Research NBS **48,** 313 (1952) RP2317.

[4] W. D. Jenkins and T. G. Digges, Influence of prior strain history on the tensile properties and structures of high-purity copper, J. Research NBS **49,** 167 (1952) RP2354.

[5] W. D. Jenkins, T. G. Digges, and C. R. Johnson, Creep of high-purity nickel, J. Research NBS **53,** 329 (1954) RP2551.

6] W. D. Jenkins, T. G. Digges, and C. R. Johnson, Effect of temperature on the tensile properties of a commercial and a high-purity 70-percent-nickel-30-percent-copper alloy, J. Research NBS **54,** 21 (1955) RP2561.

[7] W. D. Jenkins, T. G. Digges, and C. R. Johnson, Tensile properties of copper, nickel, and 70-percent-copper-30-percent-nickel and 30-percent-copper-70-percent-nickel alloys at high temperature, J. Research NBS **58,** 201 (1957) RP2753.

[8] W. D. Jenkins and C. R. Johnson, Creep of annealed nickel, copper, and two nickel-copper alloys, J. Research NBS **60.** 173 (1958) RP2836.

[9] W. D. Jenkins and C. R. Johnson, Creep of cold-drawn nickel, J. Research NBS **63C** (Eng. and Instr.) No. 1, 1 (1959).

[10] E. R. Parker and T. H. Hazlett, Principles of solution hardening, Seminar on Relation of Properties of Microstructure, Am. Soc. Metals **30,** (Cleveland, Ohio, 1953); Trans. ASME **46A,** (1954).

[11] Seminar on creep and recovery of metals, Trans. Am. Soc. Metals, **49A**. (1957).

[12] P. G. McVetty, Creep of metals at elevated temperatures. The hyperbolic-sine relation between stress and creep rate, Trans. Am. Soc. Mech. Engrs. **65,** 761 (1943).

[13] F. R. Larson and J. Miller, A time-temperature relationship for rupture and creep stresses, Trans. Am. Soc. Mech. Engrs. **74,** 765 (1952).

[14] J. D. Lubahn, Simultaneous aging and deformation in metals, Trans. AIME, **185,** 702 (1949).

[15] L. Northcott, Veining or sub-boundary structures, J. Iron and Steel Inst. (London) **162,** 267 (1932).


(Paper 66C1–88)

JOURNAL OF RESEARCH of the National Bureau of Standards—C. Engineering and Instrumentation
Vol. 66C, No. 1, January–March 1962

# Publications of the National Bureau of Standards*

## Selected Abstracts

**Physical entities and mathematical representation,** C. H. Page, *J. Research NBS 65B (Math. and Math. Phys.) No. 4 (Oct.–Dec. 1961) 70 cents.*
Certain basic postulates about physical observables yield the structure of their mathematical representation. Measure equations are contrasted with quantity equations, and measurement units with abstract units. The abstract vector spaces in which observables are represented comprise the core of dimensional analysis.
Systems of equations, units, and dimensions are discussed, along with comments on rationalization. The problem of assigning a dimension to angle is discussed, and a new proposal offered.

**Circumferentially uniform electroplating of tube bores,** J. F. Young and H. I. Salmon, *Plating* **48,** *No. 7, 783; 887–8 (July 1961).*
New procedures for plating the internal surface of tubes are described. Data are presented giving the degree of circumferential uniformity of thickness of deposits of chromium obtained with newly designed fixtures. The best procedure, in which a rotating anode was centered and insulated by a spirally wound rod of polyvinyl-chloride, resulted in deposits that deviated from uniformity by only 2 percent of the average thickness. The gun tubes used in this study had an inside diameter of 0.3 inch and a bore length of 20 inches.

**Residual losses in a guard-ring micrometer-electrode holder for solid-disk dielectric specimens,** A. H. Scott and W. P. Harris, *1960 Annual Report, Conference on Electrical Insulation, Natl. Acad. Sci.-Natl. Research Council, 11–17 (1961).*
A guard-ring micrometer-electrode holder especially designed for use in making dielectric measurements on solid-disk specimens of low-loss materials has been constructed. A method of determining the separation of the electrodes to $\pm 1$ micron, using ball reference gages, is described. Residual losses in the guard-ring holder, and also in the bridge standard capacitor used in the Schering bridge employed for the measurements, caused by losses in surface films on the electrodes and by series resistance in the leads, were accurately measured. It is shown that at frequencies from 100 cycles per second to 100 kilocycles per second these residual losses are not more than a few microradians. Using corrections thus obtained, the holder-bridge combination can be used to measure the losses of low-loss materials with greater accuracy than heretofore.

**Comparative *p*H measurements on papers by water extraction and glass electrode spot tests,** J. H. Flynn and L. E. Smith, *Tappi* **44,** *No. 3, 223–228 (March 1961).*
The *p*H of a large number of experimental and commercial papers was determined by the TAPPI T435 cold extraction method and a method in which glass-calomel electrodes were pressed against the surface of the papers, moistened with either distilled water or 0.1 *N* KCl.
The use of KCl instead of water gave better reproducibility, less time variation, and values, on an average, about 0.4 *p*H units lower.
Correlation between the spot tests and extraction *p*H's was rather poor, especially for papers of high extraction *p*H.
Few generalizations could be made concerning the effect of the types of pulps or added chemicals upon the *p*H values. It appears that other variables in the papermaking, blending, and pulping cause considerable variation in measured *p*H values of the paper.
Because of the complicated nature of the chemical and physical processes involved, none of the methods can be judged to be superior per se, but the spot test merits consideration in cases where a quick nondestructive method is needed.

**An analysis of errors in the calibration of electric instruments,** F. L. Hermach, *Communication and Electronics, 1–6 (May 1961).*
The often-stated rule of thumb that a standard must be "10 times as accurate as the instrument to be tested" is evaluated by an analysis of errors in tests of electrical instruments, and is illustrated by examples. If each standard is calibrated periodically and if corrections are applied so that determinate systematic errors are eliminated a much smaller ratio suffices. Such analyses, which are not difficult to make, should replace arbitrary accuracy ratios because of the economic and technical importance of correctly choosing standards, particularly in multiechelon systems of standardizing laboratories.

**Optical calibration of vibration pickups at small amplitudes,** V. A. Schmidt, S. Edelman, E. R. Smith, and E. Jones, *J. Acoust. Soc. Am.* **33,** *No. 6, 748–751 (June 1961).*
A photometric device for accurately measuring the amplitudes of sinusoidal vibrations is described. The device is designed for calibrating vibration pickups. The apparatus employs a Fizeau-type interferometer with a photomultiplier observing the fringe pattern. The method is applied to the measurement of vibrations throughout the audio and near ultrasonic frequency range with amplitudes ranging from 72 Å to 4400 Å. Extension to amplitudes as low as 5 Å can be made with some modification to the apparatus.

**Simple adiabatic demagnetization apparatus,** V. D. Arp and R. H. Kropschot, *Rev. Sci. Instr. Note* **32,** *217–218 (Feb. 1961).*
A simple and inexpensive adiabatic demagnetization apparatus which uses a superconducting solenoid and an appropriate paramagnetic salt is described. The solenoid is wound with niobium wire and produces three kilogauss. Dysprosium ethyl sulfate is chosen as the paramagnetic salt for its chemical stability, high heat capacity, and high magnetic susceptibility. Temperatures of the order of 0.1 °K can be attained.

**An interferometric instrument for the rapid measurement of small diameters,** D. H. Blackburn, *Rev. Sci. Instr.* **32,** *No. 2, 137 (Feb. 1961).*
An instrument was developed for the rapid and accurate measurement of small diameters. The operating procedure consists of placing the test fiber between two optically flat surfaces and, using the fiber as a fulcrum, adjusting the upper flat until the surfaces are parallel, utilizing the absence of interference fringes between the surfaces to indicate parallelism. Controlled tilting of the upper flat is obtained by adjusting, with a micrometer screw, a sliding wedge under a lever attached to the upper flat. Fiber diameter is a linear function of wedge position as indicated by micrometer screw setting.

**Low-temperature thermocouples.** *I. Gold-cobalt or constantan versus copper or "normal" silver,* R. L. Powell, M. D. Bunch, and R. J. Corruccini, *Cryogenics* **1,** *139–150 (Mar. 1961).*
An apparatus for calibrating thermocouples from 4° to 300 °K is described. The reference junctions are in a lower chamber kept at fixed temperatures by various boiling cryogenic fluids. The variable junctions are in a gas-filled upper chamber. The temperatures of the upper chamber are determined by a helium gas thermometer below 20 °K and by a calibrated platinum thermometer above that. The apparatus has been used to obtain a detailed calibration table of the thermoelectric power and potential difference for constantan, gold-cobalt (Au-2.1 At % Co), and "normal" silver (Ag-0.37 At % Au) versus copper. At low temperatures the gold-cobalt versus copper has a significantly larger thermoelectric power than does constantan versus copper (respectively 16 and 6$\mu$v/°K at 20 °K), but unfortunately it is also more inhomogeneous, so that uncertainties in temperature measurement are approxi-

mately the same. The "normal" silver has a very small thermoelectric power versus copper. Results are included of inhomogeneity, annealing, and long-time stability tests.

**A transistor frequency meter,** F. R. Bretemps and S. Saito, *Electronic Inds.* **19,** *No. 10, 196–190 (Oct. 1960).*
A transistor frequency meter is described which is used for checking signal generators. A 1 Mc crystal is used for comparison. Power is supplied by a single mercury cell and loudspeaker operation is obtained.

**Self-qualification of laboratories,** A. T. McPherson, *Instr. and Control Systems* **34,** *No. 7, 1265 (July 1961).*
A plan is presented whereby objective standards can be established to enable a calibration or testing laboratory to rate itself with regard to: (1) the qualifications of its staff, (2) the adequacy of its facilities and equipment for the work undertaken, and (3) its performance in the periodic measurement or testing of "unknown" reference samples. Under the plan, standards would be set up in the specific fields in which the interest would be sufficient to warrant the expense of a reference-sample program. The standards would be established by one or more central, nongovernmental agencies in which the laboratories, their customers, and independent scientific experts would be equally represented. The laboratories participating in the plan would be authorized to report or publish their qualifications on a standard form.

**Post office mechanization,** B. M. Levin, M. C. Stark, and P. C. Tosini, *Elec. Engr.* **80,** *105–110 (Feb. 1961).*
An approach to the mechanization of letter sorting called "codesorting" is presented. This approach utilizes a computer as an integral part of the system. The operational characteristics and requirements of the computer are emphasized.

**The precision measurement of transformer ratios,** R. D. Cutkosky and J. Q. Shields, *IRE Trans. Instrumentation* **I–9,** *No. 2, 243–250 (Sept. 1960).*
A procedure for measuring the voltage ratio between the two secondary windings of a three winding transformer is described. The application of this procedure to the calibration of transformers with ten-to-one ratios is discussed in detail. Explicit formulas are developed which correct for the finite lead impedances and load admittances associated with the measuring system, and yield a value for the open-circuit transformer ratio. Detailed calculations are presented for measurements performed on a given transformer with results believed to be accurate to a few parts in $10^9$.

**Electrodes for pH measurement,** R. G. Bates, *J. Electroanalytical Chem.* **3,** *93 (1961).*
The experimental *p*H value is defined in terms of a difference in the electromotive force or tension of a *p*H cell containing 1) the unkown" solution and 2) a standard solution of assigned *p*H. The *p*H cell consists of a reference electrode, a liquid junction, and an electrode whose potential is a function of *p*H. The potential or tension of the reference electrode, including that at the liquid junction, is assumed to remain unchanged while measurements (1) and (2) are being made and during the time interval between these measurements.
Although the glass electrode is the most common *p*H-responsive electrode, the hydrogen electrode, the quinhydrone electrode, and the antimony electrode all have their place in *p*H measurements. This paper describes these four indicator electrodes; discusses the advantages, limitations, and accuracy of each one; and summarizes the information needed for a selection of the best electrode for each special measuring situation.

**A precision RF attenuation calibration system,** C. M. Allred and C. C. Cook, *IRE Trans. Instrumentation* **I–9,** *No. 2, 268–274 (Sept. 1960).*
A new precision attenuation-calibrating system with greatly increased sensitivity, stability, and measurement range has been completed at the National Bureau of Standards, Boulder Laboratories. The increased stability and sensitivity are achieved by the use of a highly accurate piston attenuator and precision phase shifter combined into a null system. The extended attenuation measurement range has been obtained by using a new mode launching system which is excited by essentially a constant current source of very high magnitude. The padding necessary for correct impedance matching is kept at a minimum by use of a special non-interactive combining network.

**A vibrating sample magnetometer,** N. V. Frederick, *IRE Trans. Instrumentation* **I–9,** *No. 2, 194–196 (Sept. 1960).*
A vibrating sample magnetometer has been designed and constructed. The instrument combines the advantages of the techniques employed by Smith and Foner. The instrument employs the pickup coil and sample geometry of Smith's instrument and a vibration and measurement technique similar to that used by Foner. This combination of techniques makes unnecessary any modifications of the magnet employed and yet provides a system which is self-calibrating. The sample is mounted at the end of a Vycor" glass rod which is mounted in the plane of the magnet gap. The rod is vibrated in its gravest flexural mode. The vibration frequency and amplitude are controlled by feedback circuitry. The glass rod acts as a stable frequency source. The sample is vibrated parallel to the magnetic field and normal to the plane of the pickup coils which are mounted upon the magnet pole pieces. The voltage induced in the pickup coils is measured by a feedback amplifier-voltmeter which allows accuracy of approximately one percent.

**A standard current transformer and comparison method—A basis for establishing ratios of currents at audio frequencies,** B. L. Dunfee, *IRE Trans. Instrumentation* **I–9,** *No. 2, 231–236 (Sept. 1960).*
Prompted by recent demands of Science and Technology, the Electricity Division of the National Bureau of Standards has entered a program for the accurate measurement of ratio and phase angle of current transformers at frequencies up to 10 kc/s. The present paper describes a 1/1 Standard Transformer having very small errors, designed to operate up to 100 percent overload from 60 c/s to 10 kc/s, and the method used to establish its values to an accuracy of 5 ppm and 6 microradians. The 1/1 transformer and its assigned values of ratio and phase angles will serve as the basis for subsequent measurements and the evaluation of Standard Transformers of higher ratios.

**Comparison of four different methods of determining drying shrinkage of concrete masonry units,** J. O. Bryson and D. Watstein, *J. Am. Concrete Inst.* **58,** *No. 2, 163–184 (Aug. 1961).*
Four different procedures for determining the drying shrinkage of concrete masonry units were compared in order to determine their suitability as possible standard test methods. The test procedures differed mainly by the conditions under which the specimens were dried and were designated RT–50 (73° F and 50% R. H.), RT–30 (73° F and 30% R. H.), Modified British (122° F and 17% R. H.), and Rapid (220°–235° F). In addition to varying the drying conditions, the size and shape of test specimens were also varied. The specimens were whole block, face shells cut in half lengthwise, thin laminas removed from the block at right angles to the face shell, and "remnant" block remaining after removal of the thin laminas.
The drying-shrinkage test was performed using all four procedures on both autoclaved and low-pressure steam cured block of sand and gravel, cinders, expanded slag, expanded shale, and pumic aggregates.
Considering the RT–50 Method as a basis of comparison, the ratios of the results obtained with the RT–30 Method to those obtained with the RT–50 specimens ranged from 0.68 to 1.20 while for the Modified British procedure these ratios ranged from 0.92 to 1.35. For the Rapid Method, these ratios ranged from 1.22 to 3.82.
Considerable reduction in the time required for completion of the shrinkage test at room temperature was achieved by the use of a method developed at the NBS employing thin specimens.

**Static and dynamic calibrations of pressure measuring instruments at the National Bureau of Standards,** E. C. Lloyd and D. P. Johnson, *Automatic and Remote Control Proc. 1st Intern. Congress of IFAC, 274–280 (1960).*

Equipment developed or used at the National Bureau of Standards for pressure calibrations is described. For static calibrations this includes the controlled-clearance oil piston gage at high pressures, the air piston gage, the newly developed inclined air piston gage, and precision mercury columns. Use of a compact form of the tetrahedral anvil apparatus for investigation of polymorphic transitions to pressures above 100,000 atm is described. For dynamic pressure calibrations at pressures up to 3,500 atm a pressure-pulse generator of high amplitude accuracy is used, and for lower pressures the range of this equipment is overlapped by pressure pulses generated by a shock tube. The methods of use and the sources of error, and relative accuracies of these instruments are discussed.

**The NBS absolute gravity experiment,** D. R. Tate, *Proc. 2d Air Force Cambridge Research Center Military Geodesy Seminar, GRD Research Notes,* 40 (*Jan. 12-14, 1960*).

The experiment to measure the acceleration due to gravity at the National Bureau of Standards is described. The determination is made by measuring the average speed of a freely falling object over two different but related distances. The object falls within a vacuum case which is itself falling with approximately the acceleration of gravity thus avoiding some of the practical difficulties of handling the object in a vacuum. The time over the two distances is determined by a photoelectric sensing unit and two crystal-controlled electronic timers reading to one-tenth of a microsecond. Lengths are measured not as lengths on an object but as the distances the object must move to trigger the timers on and off.

**Computer for weather data acquisition,** P. Meissner, J. Cunningham, and C. Kettering, *Proc. Eastern Joint Computer Conf.* **18,** *No. 2.1, 57–66 (Dec. 1960).*

In order to meet a growing need for more rapid and detailed reporting of weather information, the U.S. Weather Bureau has been conducting an extensive program for the development of automatic weather stations. The National Bureau of Standards has had an opportunity to participate in this program and has developed a small, specialized computer for use as the control component in such a station. The computer is intended as a research tool for exploring the application of automatic data processing equipment to this type of problem. Basically, the computer must sample a number of weather-sensing instruments, suitably process the instrument data, and prepare outputs in the form of local displays and teletype messages. Since the machine is internally programmed, it will afford a wide latitude in the processing of input data including the simultaneous comparison of results obtained in different ways.

The design of a computer for this application was felt to be justified on the basis of a number of special requirements. Among these are:

1) parallel inputs from a number of separate sources,
2) multiple outputs in several forms,
3) concurrent operation of input, output, and data-processing functions,
4) extensive reference tables with special instructions for their use,
5) limited arithmetic capability,
6) three-digit word length,
7) computing speed need not be high.

**Location of the plane of best average definition for airplane camera lenses,** F. E. Washer and W. P. Tayman, *Photogrammetric Eng.* **26,** *No. 3, 475–488 (1960).*

The location of the plane of best average definition for lenses used in airplane mapping cameras is discussed. The effectiveness of the use of an average value of resolving power both as a means of locating the plane of best average definition and as a figure of merit in rating the optical performance of lenses and lens-camera combinations is investigated. Various methods of arriving at an average value of resolving power are described, such as area-weighted average resolution (AWAR), area and depth-of-focus weighted average resolution (ADWAR), and root mean square mean resolution $\sqrt{\overline{R_\delta T_\delta}}$. Location of the plane of best average definition by graphical analysis is given. A comparison of the various procedures using resolving power measurements obtained from four lenses with two emulsions are given. It is concluded that graphical analysis yields the most information and is simplest to use. Of the single-valued indices, such as AWAR, ADWAR, and $\sqrt{\overline{R_\delta T_\delta}}$, ADWAR is the best suited for locating the plane of best average definition. In using any of the indices as a rating factor, careful judgment is necessary if the rating is to be significant.

**Humidity standards,** A. Wexler, *Tappi* **44,** *No. 6, 180a (June 1961).*

This paper describes and discusses instruments which may serve as primary and secondary humidity standards, including a gravimetric hygrometer, now under development at the National Bureau of Standards, to serve as its basic reference for humidity measurements. The use of precision humidity generators for producing atmospheres of known humidity is outlined. Methods and techniques of obtaining fixed humidity points are given.

**A high-resolution ammonia-maser-spectrum analyzer,** J. A. Barnes and L. E. Heim, *IRE Trans. Instrumentation* **I–10,** *4–8 (June 1961).*

A quartz crystal oscillator was phase locked to an ammonia beam maser to give a sufficiently monochromatic signal to enable the measurement of power spectra of other crystal oscillators multiplied from 1458 to 145,800 times in frequency. The perturbing effects of amplifiers introduced in the early stages of multiplication were observed. It was found that for maximum purity, dc filaments on the oscillator and early stages of multiplication were essential. With this system it was possible to investigate sidebands and noise on various oscillators and determine which oscillators were most suited for precise frequency measurements with the National Bureau of Standards atomic frequency standards.

**Pulse voltage comparator measures height of positive or negative pulses,** O. B. Laug, *Electronics* **34,** *No. 36, 70–71 (Sept. 1961).*

A voltage comparator is described which responds to either positive or negative pulses of short duration by closing a relay. The comparator responds accurately to pulse widths of 50 nano sec. or greater and duty factors as low as $10^{-7}$. The basic circuit consists of two series triggered blocking oscillators coupled to a switching circuit driving a relay. The effect of temperature on the 1 volt threshold is compensated by forward biased diodes. The nominal threshold voltage is held within 0.5% from 0 to 50 °C for positive pulses.

**Digest of A general description of d-c digital voltmeters,** C. Stansbury, *AIEE Trans. Paper 61–721 (Apr. 1961).*

The widespread use of measurement transducers producing continuously varying voltage signals has led to extensive development of apparatus for the conversion of such signals to digital form. The term "digital voltmeter" is applied to the class of such converters having as primary function the direct visual indication of voltage in the form of decimal digits.

The advantages of digital voltmeters include feasibility of high accuracy superiority of reading characteristics, adaptability to code recording. Disadvantages include high cost and complexity and relatively low reliability compared to conventional scale-type instruments.

The paper describes the design features common to all types, and the various voltage-comparison mechanisms commonly employed. Performance characteristics are discussed, including accuracy considerations, coordination of resolution with accuracy and calibration.

It has been evident for some time that this field of instrumentation would benefit greatly from a degree of industrial standardization consistent with that existing for the older types of instrument. An ASA committee sponsored by AIEE, IRE, and NBS, has been organized for this purpose.

## Other NBS Publications

**Journal of Research 65A (Phys. and Chem.) No. 6 (Nov.-Dec. 1961). 70 cents.**

Comparison of lens response for sinusoidal and square-wave targets at several focal positions. S. H. Emara.

Wavelength shifts in $Hg^{198}$ as a function of temperature. S. H. Emara.

Variability of spectral tristimulus values. I. Nimeroff, J. R. Rosenblatt, and M. C. Dannemiller.

Extension of the Flory-Rehner theory of swelling to an anisotropic polymer system. S. D. Bruck.

Fiber structure-property relationships: a disulfide-crosslinked self-crimping polyamide. S. D. Bruck.

Acidity functions. Values of the quantity $p(a_{H}\gamma_{Cl})$ for buffer solutions from 0 to 95 °C. R. G. Bates and R. Gary.

2,3-0-Isopropylidene-α-D-lyxofuranose, the monoacetone-D-lyxose of Levene and Tipson. R. Schaffer.

Effect of perchloryl fluoride additions on the flame speed of methane. C. Halpern.

**Journal of Research 66A (Phys. and Chem.) No. 1 (Jan.-Feb. 1962). 70 cents.**

Absolute isotopic abundance of terrestrial silver. W. R. Shields, E. L. Garner, and V. H. Dibeler.

Temperature of a copper arc. C. H. Corliss.

Melting process and the equilibrium melting temperature of polychlorotrifluoroethylene. J. D. Hoffman and J. J. Weeks.

Tritium-labeled compounds VIII. Confirmation of the position of the tritium in D-glucose-6-t and D-glucitol-5-t. L. T.Sniegoski and H. S. Isbell.

Infrared absorption spectra in the study of mutarotational equilibria of monosaccharides. R.S. Tipson and H. S. Isbell.

Preparation of high purity trimethylborane. G. S. Ross, D. Enagonio, C. A. Hewitt, and A. R. Glasgow.

Reaction of several aminopyrimidines with formaldehyde. G. L. McLeod.

Acidic dissociation constant and related thermodynamic quantities for diethanolammonium ion in water from 0 to 50 °C. V. E. Bower, R. A. Robinson, and R. G. Bates.

Fiber structure-property relationships II: Macroscopic deformations of alkylene sulfide crosslinked polycaprolactam fibers. S. D. Bruck.

Ion transport across membranes: I. Definitions of membrane electromotive forces and of flows of electrolytic solutes. B. C. Duncan.

**Journal of Research 65B (Math. and Math. Phys.) No. 4 (Oct.-Dec. 1961). 75 cents.**

Physical entities and mathematical representation. C. H. Page. (See above abstract.)

On the range of a fleet of aircraft. A. J. Goldman.

Measurement of wave fronts without a reference standard: Part I. The wave-front-shearing interferometer. J. B. Saunders.

On the evaluation of the function $\Phi(\lambda)=\frac{1}{2\pi i}\int_{c-i\infty}^{c+i\infty} e^{u\ln u+\lambda u}du$ for real values of λ. W. Börsch-Supan.

Analyticity and probability properties of one-dimensional Brownian motion. A. Ghaffari.

Some higher order integral identities with application to bounding techniques. J. H. Bramble and B. E. Hubbard.

A priori bounds in the first boundary value problem in elasticity. J. H. Bramble and L. E. Payne.

**Journal of Research 66D (Radio Prop.) No. 1 (Jan.-Feb. 1962). 70 cents.**

A survey of the very wide band and frequency independent antennas—1945 to the present. J. D. Dyson.

Numerical investigation of the equivalent impedance of a wire grid parallel to the interface between two media. T. Larsen.

Current on and input impedance of a cylindrical antenna. Y. M. Chen and J. B. Keller.

Radar corner reflectors for linear or circular polarization. G. Latmiral and A. Sposito.

On the theroy of wave propagation through a concentrically stratified troposphere with a smooth profile. H. Bremmer.

On the propagation of VLF and ELF radio waves when the ionosphere is not sharply bounded. J. R. Wait.

Fields of electric dipoles in sea water—the earth-atmosphere-ionosphere problem. W. L. Anderson.

Reflection of electromagnetic waves from thin ionized gaseous layers. F. H. Northover.

Reflection and transmission of radio waves at a continuously stratified plasma with arbitrary magnetic induction. J. R. Johler and J. D. Harper, Jr.

On the diffraction of spherical radio waves by a finitely conducting spherical earth. L. C. Walters and J. R. Johler.

An approximate full wave solution for low frequency electromagnetic waves in an unbounded magneto-ionic medium. W. C. Hoffman.

VHF radio propagation data for the Cedar Rapids-Sterling, Anchorage-Barrow, and Fargo-Churchill test paths, April 1951 through June 1958. G. R. Sugar and K. W. Sullivan.

---

Capacities of stacks in sanitary drainage systems for buildings, R. W. Wyly and H. N. Eaton, NBS Mono. 31 (1961), 35 cents.

International practical temperature scale of 1948, text revision of 1960, H. F. Stimson, NBS Mono. 37 (1961), 10 cents.

Stopping powers for use with cavity chambers, NBS Handb. 79 (1961), 35 cents.

Hydraulic research in the United States, H. K. Middleton, NBS Mich. Publ. 238 (1961), $1.25.

Fractional factorial designs for experiments with factors at two and three levels, W. S. Connor and S. Young, NBS Applied Math. Series 58 (1961), 40 cents.

Quarterly radio noise data, March, April, May 1961, W. Q. Crichlow, R. T. Disney, and M. A. Jenkins, NBS Tech. Note 18–10 (PB151377–10) (1961) $1.50.

Mean electron density variations of the quiet ionosphere 4—June 1959, J. W. Wright, L. R. Wescott, and D. J. Brown, NBS Tech. Note 40–4 (PB151399–4) (1961) $1.50.

Mean electron density variations of the quiet ionosphere, No. 5—July 1959, J. W. Wright, L. R. Wescott, and D. J. Brown, NBS Tech. Note 40–5 (PB151399–5) (1961) $1.50.

An evaluation of Kacser's second order Born approximation to the bremsstrahlung differential cross section, G. S. Ofelt, NBS Tech. Note 81 (PB161582) (1961) 75 cents.

Collisions of liquid drops with liquids, O. G. Engel, NBS Tech. Note 89 (PB161590) (1961) $1.00.

Flux switching mechanisms in ferrite cores and their dependence on core geometry, G. W. Reimherr, NBS Tech. Note 90 (PB161591) (1961) $1.25.

Determination of the K fluorescence yield of argon by proportional-counter spectrometry, C. Godeau, NBS Tech. Note 91 (PB161592) (1961) 50 cents.

An experimental study of beta decay using the radiations from oriented nuclei, D. D. Hoppes, NBS Tech. Note 93 (PB161594) (1961) $1.50.

Bibliography on meteoric radio wave propagation, W. Nupen, NBS Tech. Note 94 (PB161595) (1961) $2.75.

On the climatology of ground-based radio ducts and associated fading regions, E. J. Dutton, NBS Tech. Note 96 (PB161597) (1961) $1.75.

The integrated starlight over the sky, L. R. Megill and F. E. Roach, NBS Tech. Note 106 (PB161607) (1961) $2.00.

A fixed frequency, 9.1 Gc, field intensity recording receiver with extremely narrow bandwidth, R. W. Hubbard and J. V. Cateora, NBS Tech. Note 107 (PB161608) (1961) 75 cents.

A compilation of the physical equilibria and related properties of the hydrogen-carbon monoxide system, D. E. Drayer and T. M. Flynn, NBS Tech. Note 108 (PB161609) (1961) $2.25.

A compilation of the physical equilibria and related properties of the hydrogen-helium system, D. E. Drayer and T. M. Flynn, NBS Tech. Note 109 (PB161610) (1961) $1.25.

A compilation of the physical equilibria and related properties of the hydrogen-nitrogen system, D. E. Drayer and T. M Flynn, NBS Tech. Note 110 (PB161611) (1961) $1.75.

Data reduction instrumentation for radio propagation research, W. E. Johnson, NBS Tech. Note 111 (PB161612) (1961) $1.00.

Load carrying capacity of gas-lubricated bearings with inherent orifice compensation using nitrogen and helium gas, H. Sixsmith, W. A. Wilson, and B. W. Birmingham, NBS Tech. Note 115 (PB161616) (1961) $1.00.

Vapor phase gamma-radiolysis of azomethane, L. J. Stief and P. Ausloos, J. Phys. Chem. **65,** 877–881 (1961).

Electron interferometer studies of iron whiskers, H. A. Fowler, L. Marton, J. A. Simpson, and J. A. Suddeth, J. Appl. Phys. **32,** No. 6, 1153 (June 1961).

Changes in dentures during storage in water and in service, J. B. Woelfel, G. C. Paffenbarger, and W. T. Sweeney, J. Am. Dental Assoc. **62,** No. 6, 643–657 (June 1961).

Solar disturbances and radio communication forecasts, J. F. Brockman, Sky and Telescope, **XXI,** No. 6, 322–326 (June 1961).

Dissociation constant of the protonated acid form of 2-Amino-2-(hydroxymethyl)-1, 3-propanediol [*tris*(hydroxymethyl)-aminomethane] and related thermodynamic quantities from 0 to 50°, R. G. Bates and H. B. Hetzer, J. Phys. Chem. **65,** 667–671 (1961).

Hyperfine structure and isotope shifts in the 2537-A line of mercury, W. G. Schweitzer, Jr., J. Opt. Soc. Am. **51,** No. 6, 692–693 (June 1961).

Long-distance one-hop $F_1$ propagation through the auroral zone, L. H. Tveten, J. Geophys. Research **66,** No. 6, 1683–1684 (June 1961).

Resonators for millimeter and submillimeter wavelengths, W. Culshaw, IRE Trans. Microwave Theory and Tech. **MTT-9,** No. 2, 135–144 (March 1961).

Paramagnetic substances for nuclear orientation, R. P. Hudson, Prog. in Cryogenics **3,** 99–127 (1961).

A five-attribute system of describing visual appearance, D. B. Judd, Am. Soc. Testing Materials Spec. Tech. Pub. No. 297 (1961).

Solar flare effects in the F region of the ionosphere, R. W. Knecht and K. Davies, Nature **190,** No. 4778, 797–798 (May 1961).

Age to indium resonance for D–D neutrons in heavy water, V. Spiegel, Jr., and A. C. B. Richardson, Nuclear Sci. and Eng. **10,** No. 1, 11–15 (1961).

Magnetic properties and optical absorption spectrum of K $ReCl_6$, J. C. Eisenstein, J. Chem. Phys. **34,** No. 5, 1628–1648 (May 1961).

Convective circulation in water induced by evaporation cooling, W. G. Spangenberg and W. R. Rowland, Phys. of Fluids **4,** No. 6, 743–750 (June 1961).

Photoionization heating in the F region of the atmosphere, D. C. Hunt and T. E. Van Zandt, J. Geophys. Research **66,** No. 6, 1673–1682 (June 1961).

Identification of fiber blends by infrared spectroscopy, M. K. Wharton and F. H. Forziati, Am. Dyestuff Rep. **50,** No. 14, 33–36 (July 1961).

Calculations of the neutron age in water and heavy water for D–D sources, J. W. Cooper, Nuclear Sci. and Eng. **10,** No. 1, 1–10 (May 1961).

Magnetic susceptibility of cerous magnesium Nitrate, R. P. Hudson and W. R. Hosler, Phys. Rev. **122,** No. 5, 1417–1420 (June 1961).

Use of gaussian orbitals for atoms-in-molecule calculations, M. Kraus, J. Chem. Phys. **34,** No. 2, 692–693 E (February 1961).

Measurement of minority carrier lifetime in SiC by a novel electroluminescent method, G. G. Harman and R. L. Raybold, J. Appl. Phys. **32,** No. 6, 1168–1169 (June 1961).

Absolute measurement of W for $Po^{210}$ alpha particles in air, nitrogen and carbon dioxide, Z. Bay, P. A. Newman, and H. H. Seliger, Radiation Research **14,** No. 5, 551–565 (May 1961).

The structure of the monoclinic form of sodium tetrametaphosphate tetrahydrate, H. M. Ondik, C. H. MacGillavry, and S. Block, Acta. Cryst. **14,** 555 (1961).

A comparison between theoretical and experimental data on phase velocity of VLF radio waves, J. R. Wait, Proc. IRE **49,** No. 6, 1089–1090 (June 1961).

A diffraction theory for LF sky-wave propagation, J. R. Wait, J. Geophys. Research **66,** No. 6, 1713–1724 (June 1961); An additional note, J. R. Wait and A. M. Conda, J. Geophys. Research **66,** No. 6, 1725–1729 (June 1961).

Mass spectrometric study of cyanogen and cyanoacatylenes, V. H. Dibeler, R. M. Reese, and J. L. Franklin, J. Am. Chem. Soc. **83,** 1813–1818 (1961).

Energy levels and magnetic dipole transitions in the $4p^4$ ground configuration of singly ionized atomic bromine (Br II), W. C. Martin and J. L. Tech, J. Opt. Soc. Am. **51,** No. 6, 591–594 (June 1961).

An improved structure determination for vinyl fluoride, D. R. Lide, Jr. and D. Christensen, Spectrochim. Acta **17,** 665–668 (1961).

Incoherent scattering by free electrons as a technique for studying the ionosphere and exosphere: Some observations and theoretical considerations, K. L. Bowles, pp. 223–243 of AGARDograph **42,** The upper atmosphere above *F*2-maximum. North Atlantic Treaty Organization, Advisory Group for Aeronautical Research and Development, Avionics Panel. Papers presented at the Symposium of the Ionospheric Research Committee, Paris, France, May 1959.

A *p*H standard for blood and other physiologic media, V. E. Bower, M. Paabo, and R. G. Bates, Clin. Chem. **7,** No. 3, 292 (June 1961).

Evidence on the laminar nature of the exosphere obtained by means of guided high-frequency wave propagation, R. M. Galley and W. F. Utlaut, Phys. Rev. Letters **6,** No. 11, 591–594 (June 1, 1961).

Comparison of the ionization produced in air by alpha particles near 5 mev and by beta particles, Z. Bay and P. A. Newman, Radiation Research **14,** No. 5, 566–572 (May 1961).

A century-old razor, S. J. Rosenberg, Metal Progress, 94–96 (1961).

Some applications of Hardy's formula in Brownian motion (Abstract), A. Ghaffari, Am. Math. Soc. Notices 8, No. 54, 238 (June 1961).

On the classical approximation in the statistical theory of mass spectra, H. M. Rosenstock, J. Chem. Phys. **34,** 2182 (1961).

Superconductivity of $Nb_3Sn$ in pulsed fields of 185 kilogauss, V. D. Arp, R. H. Kropschot, and J. H. Wilson, Phys. Rev. Letters **6,** No. 9, 452–453 (May 1961).

Proposed nomenclature for linear viscoelastic behavior, H. Leaderman and F. Schwarzl, Rheologica Acta, **1,** No. 4/6, 674–676 (1961).

FM and SSB radiotelephone tests on a VHF ionospheric scatter link during multipath conditions, IRE Trans. Commun. Systems **CS-8,** No. 3, 183–186 (Sept. 1960).

Matrix elements in the forbidden beta decay of $Ce^{139}$, D. D. Hoppes, E. Ambler, R. W. Hayward, and R. S. Kaeser, Phys. Rev. Letters **6,** 115–118 (1961).

The electromagnetic fields of horizontal dipole in the presence of a conducting half space, J. R. Wait, Can. J. Phys. **39,** No. 7, 1017–1028 (July 1961).

4-Nitrophenyl esters, carbonates, and bi-carbonates as leather fungicides, S. Dahl and A. M. Kaplan, J. Am. Leather Chemists Assoc. **55,** 480 (Sept. 1960).

The organization of international intercomparisons of radioactivity standards, with special reference to such measurements of NBS standards, L. M. Cavallo and W. B. Mann, Proc. 1959 Symp. Metrology Radioactive, IAEA, Vienna, 117 (1960).

The physical environment as affected by radiation, D. M. Gates, Proceedings of the 50th Anniversary Celebration of the University of Michigan Biological Station (1960).

Second revision American Dental Association specifications No. 4 for dental inlay casting wax, J. W. Stanford, K. V. Weigel, and J. W. Paffenbarger, J. Am. Dental Assoc. **62,** 45 (Jan. 1961).

The structure of B-type vibrational-rotational bands of an asymmetric rotor, H. C. Allen, Jr., Phil. Trans. Roy. Soc. of London, **Series A,** Mathematical and Physical Sciences, No. 1030, 253, 335 (1961).

Measurement of contrast in the aerial image, F. W. Rosberry, Photogrammetric Eng. 155–159 (March 1961).

Vapor-phase photolysis of formic acid, R. Gordon, Jr., and P. Ausloos, J. Chem. Phys. **65,** 1033 (1961).

Binary silicate glasses in the study of alkali-aggregate reaction, R. G. Pike, D. Hubbard, and E. S. Newman, Highway Research Board Bull. No. 275, 39–44 (1960).

Complex conductivity of some plasmas and semiconductors,

P. H. Fang, J. Appl. Research Soc. B (The Hague) **9,** 51 (1960).

Physical measurement-challenge to science and engineering, A. V. Astin, SPE J. **17,** No. 5, 455–458 (May 1961).

Dielectric properties of polyamides, A. J. Curtis, J. Chem. Phys. **34,** No. 5, 1849–1850 (May 1961).

Natural and synthetic rubbers: Review of test methods, F. J. Linnig, M. Tryon, and E. J. Parks, Anal. Chem. **33,** 127R (Apr. 1961).

Simple calculus for all-dielectric interference filters, K. D. Mielenz, J. Opt. Soc. Am. **50,** No. 10, 1014 (Oct. 1960).

Magnetic susceptibility of tetratonal titanium dioxide, F. E. Senftle, T. Pankey, and F. A. Grant, Phys. Rev. **120,** 820 (Nov. 1960).

Equipment and procedures for the evaluation of total hemispherical emittance, J. C. Richmond and W. N. Harrison, Bull. Am. Ceram. Soc. **39,** No. 11, 668 (Nov. 1960).

Limitations of radiosonde punch-card records for radiometeorological studies, B. R. Bean and B. A. Cahoon, J. Geophys. Research **66,** No. 1, 328–331 (Jan. 1961).

Evaluations of some oxide glasses for use as infrared materials, G. W. Cleek and T. G. Scuderi, Proc. Infrared Information Symp. **5,** No. 4 (Aug. 1960).

Improvement of some of the properties of sole leathers by impregnation with polymers, J. R. Kanagy, J. Am. Leather Chemists Assoc. **LVI,** No. 7, 322–342 (July 1961).

Studies on the flame-spraying of aluminum oxide, D. G. Moore, Metal Finishing J. **6,** No. 70, 397 (Oct. 1960).

Four-color achromats and superchromats, R. E. Stephens, J. Opt. Soc. Am. **50,** No. 10, 1016–1019 (Oct. 1960).

Bounds for determinants with positive diagonals, E. V. Haynsworth, Trans. Am. Math. Soc. **96,** 395–399 (1960).

Refining measurements by capacitance techniques, F. K. Harris and R. D. Cutkosky, ISA—J. Instr. Soc. Am. **8,** No. 2, 63–66 (Feb. 1961).

Standards for plastic pipe fittings, F. W. Reinhart, SPE J. **17,** 160 (Feb. 1961).

Comparison of observed tropospheric refraction with values computed from the surface refractivity, B. R. Bean, IRE Trans. Ant. Prop. AP–**9,** 415–416 (July 1961).

Studies of enviromental factors in a family-size underground shelter, P. R. Achenbach, F. J. J. Drapeau, and C. W. Phillips, Report OCDM–NBS–60–1 issued Office of Civil Defense Mobilization (Mar. 1961).

Phase-shift method for one-dimensional scattering, A. H. Khan, Am. J. Phys. **29,** 77 (1961).

Electric field distribution in a dense plasma, J. L. Jackson, Phys. Fluids **3,** 927–931 (1960).

The classical field theories, C. Truesdell and R. Toupin, Handb. der Physik, Springer, Berlin, **III,** No. 1, 226–793 (1960).

Standards development by ASTM committee D–20 on plastics, F. Reinhart, SPE J. **16,** 800 (Aug. 1960).

A nuclear magnetic resonance study of *syn-anti* isomerism in ketoximes, E. Lustig, J. Phys. Chem. **65,** 491 (1961).

Evaluating the freezing-and-thawing durability of concrete by laboratory tests in the U.S.A., H. T. Arni and R. L. Blaine, Preliminary Report on Symposium on Durability of Concrete of RILEM, Prague, Czechoslovakia, 218–231 (July 1961).

Spectroscopic standard samples of titanium and high-temperature alloys, R. E. Michaelis, J. Appl. Spectroscopy **15,** 7 (1961).

Analytical laboratory problems, J. Mandel, Trans. Metropolitan Conf. Am. Soc. Quality Control, 99–107 (Feb. 1960).

Some experimental aspects of nuclear orientation, E. Ambler, Proc. 10th Inter. Congress of Refrigeration, Copenhagen, Denmark, 1959, Progress in Refrigeration in Science and Technology, **I,** 195–198 (Pergamon Press, London, England, 1960).

Absorption spectrum and magnetic properties of osmium hexaflouride, J. C. Eisenstein, J. Chem. Phys. **34,** 310–318 (1961).

Rapid method for interpolating refractive index measuremets. O. N. Stavroudis and L. E. Sutton, J. Opt. Soc. Am. **51,** No. 3, 368–370 (Mar. 1961).

Effect of departures from local thermodynamic equilibrium on inferences on stellar atmospheric temperatures, R. N. Thomas, Book, Optical Spectrometric Measurements of High Temperatures, P. J. Dickerman, ed., 14–26 (University of Chicago Press, Chicago, Ill., 1961).

The retannage of chrome-tanned leather with vegetable tannins, J. R. Kanagy, J. Am. Leather Chemists Assoc. **LVI,** No. 6, 252–272 (June 1961).

Improved electron filter lens, J. A. Simpson and L. Marton, Rev. Sci. Instr. **32,** No. 7, 802–803 (July 1961).

X-ray diffraction study of acellular teleost bone, M. L. Moss and A. S. Posner, Nature **188,** 1037 (Dec. 1960).

Adsorption of polyesters and other polymers on glass and other substrates, R. R. Stromberg and G. M. Kline, Modern Plastics **38,** 123 (Apr. 1961), **38,** 241 (May 1961); Poliplastic **9,** 15 (Jan.-Feb. 1961).

Tunnel diode large-signal simulation study, S. B. Geller and P. A. Mantek, Proc. IRE **49,** No. 4, 803 (Apr. 1961).

Thermal degradation of organic polymers, S. L. Madorsky, Polymer Sci. **17,** No. 7, (July 1961).

Determination of carboxyl in cellulose—comparison of various methods, W. K. Wilson and J. Mandel, Tappi **44,** No. 2, 131 (1961).

A recalibration of NBS carbon-14 standards by Geiger-Muller and proportional gas counting, W. B. Mann, H. H. Seliger, W. F. Marlow, and R. W. Medlock, Rev. Sci. Instr. **31,** No. 7, 690 (1960).

The solar spectrum from 2635 to 2085 A, H. H. Malitson, J. D. Purcell, R. Tousey, and C. E. Moore, Astrophys. J. **132,** 746 (1960).

Winter thermal radiation studies in Yellowstone Park, D. M. Gates, Science **134,** 32–35 (July 7, 1961).

Vapor phase $\gamma$-radiolysis of acetone, L. J. Stief and P. Ausloos, J. Phys. Chem. **65,** 877 (1961).

Amine buffers for *p*H control, R. G. Bates, Ann. N. Y. Acad. Sci. **92,** 341 (1961).

Cryogenic adhesive properties of bisphenol-A epoxy resins, M. J. Hiza and P. L. Barrick, SPE Trans. **1,** 73–79 (Apr. 1961).

Resonance characteristics of a corrugated cylinder excited by a magnetic dipole, J. R. Wait and A. M. Conda, IRE Trans. Ant. Prop. AP–**9,** 330–333 (July 1961).

Infrared spectra of solid hydrocarbons at very low temperatures, J. J. Comeford and J. H. Gould, J. Mole Spectroscopy **5,** 474 (1960).

Recent work with compensated internal gas counters for the standardization of gaseous radionuclides, W. B. Mann, Proc. Symp. Metrology of Radioactive, IAEA, Vienna, 307 (1960).

Vanadium oxytrichloride [Vanadyl(V) chloride], R. B. Johannesen, Book, Inorganic Syntheses, E. G. Rochow, Editor-in-Chief (McGraw-Hill Book Co., New York, N.Y.), IV. Chapt. 5B, No. 38, 119–120 (1960).

Concerning the potential refractive index and the molecular refractivity, B. R. Bean and J. D. Horn, J. Meteorol. **18,** No. 3, 427–428 (June 1961).

Standard samples and related materials for spectrochemical analysis, R. E. Michaelis, Am. Soc. Testing Materials Spec. Tech. Publ. No. **58–D,** 116 (1960).

Aromatic fluorocarbons: Thermal stability and synthesis, L. A. Wall, Proc. 6th Joint Army-Navy-Air Force Elastomer Conf., Oct. 18–20, 1960, I. 150 (U.S. Army Quartermaster Research & Engineering Command, Natick, Mass.).

The Ionization constant of hydroxylamine, R. A. Robinson and V. E. Bower, J. Phys. Chem. **65,** 1279–1280 (1961).

The calculation of the energy levels of nearly symmetric rotors, S. C. Wait, Jr., J. Mol. Spectroscopy **6,** 276 (1960).

Multiple layer insulation for cryogenic applications, R. H. Kropschot, Cryogenics **1,** 171–177 (Mar. 1961).

Extinguishment effectiveness of some powered materials on hydrocarbon fires, T. G. Lee and A. F. Robertson, Fire Research Abstracts and Reviews, Natl. Acad. Sci.-Natl. Research Council Publ. 786 (June 1961).

Forty years of dental research at the National Bureau of Standards, W. T. Sweeney, Capital Chemist **10,** 228 (Oct. 1960).

A stainless steel for standard weights, S. J. Rosenberg and T. P. Royston, Materials Research & Standards (ASTM Bull.) **1,** No. 1, 21 (Jan. 1961).

Long-term working stress of thermoplastic pipe, F. W. Reinhart, SPE J. 751–754 (Aug. 1961).

NBS atomic frequency standards, R. C. Mockler and R. E. Beehler, Proc. 14th Annual Symp. Frequency Control, Atlantic City, N.J., May 31–June 3, 1960, p. 298–309 (Signal Corps. Eng. Laboratories, Fort Monmouth, N.J., 1961).

Microwave Zeeman effect of free hydroxyl radicals: $^2\Pi_{1/2}$ levels, H. E. Radford, Phys. Rev. **122,** 114 (1961).

A precision RF power transfer standards, P. A. Hudson, IRE Trans. Instrumentation **I–9,** 280–283 (Sept. 1960).

The fluorescence and phosphorescence of trifluoroacetone vapor, P. Ausloos and E. Murad, J. Am. Chem. Soc. **83,** 1327 (1961).

The morphology of sporadic E, E. K. Smith, Jr., Proc. XIIIth Gen. Assembly URSI (London, England, 1960), Natl. Acad. Sci.-Natl. Research Council Publ., Report No. 880, 218 (1961).

How to determine stack load limits, R. S. Wyly, Contractor, p. 19–20 (Aug. 15, 1961).

$\gamma$-Irradiation of liquid and solid oxygen, D. W. Brown and L. A. Wall, Phys. Chem. **65,** 915 (1961).

Testing of ball bearings with five different separator materials at 9200 RPM in liquid nitrogen, J. A. Brennan, W. A. Wilson, R. Radebaugh, and B. W. Birmingham, Am. Soc. Mech. Engrs. No. 61–LUBS–18, 1–8 (Apr. 1961).

The CRPL electron density profile program: Some features and early results, J. W. Wright, Proc. URSI-AGI Symp. (Brussels, Belgium, 1959), Book, Some Ionospheric Results Obtained During IGY, Ed. W. J. G. Beyon (Elsevier Publ. Co., Princeton, N.J.), 215 (1960).

Kinetic isotope effects in the reaction of methyl radicals with ethane, $-d_6$ and ethane-1, 1, 1-$d_3$, J. R. McNesby, J. Phys. Chem. **64,** No. 11, 1671 (Nov. 1960).

Theory of vibrational relaxation in liquids, R. Zwanzig, J. Chem. Phys. **34,** 1931–1935 (1961).

Nomenclature of carbohydrates, R. S. Tipson, J. Chem. Documentation **2,** No. 3, 3–7 (1961).

Determination of wax in paper, W. L. Marrow, Tappi **44,** No. 2, 120 (1961).

Mortar for cavity walls, C. C. Fishburn, Building Research Institute, 1960 Spring Conf. Program on Insulated Cavity Walls, Natl. Acad. Sci.-Nat. Research Council Publ. **793,** 37 (1960).

Variations of [OI] 5577 Å emission in the upper atmosphere, F. E. Roach, Ann. Geophys. **17,** 172–180 (Apr.–June 1961).

Continuously operating $He^3$ refrigerator for producing temperature down to ¼°K, E. Ambler and R. B. Dove, Rev. Sci. Instr. **32,** No. 6, 737–739 (June 1961).

Density fluctuations and heat conduction in a pure liquid, R. E. Nettleton, Phys. Fluids **4,** No. 1, 74 (Jan. 1961).

Low temperature properties of cerous magnesium nitrate, R. P. Hudson, R. S. Kaeser, and H. E. Radford, Proc. VIIth Intern. Conf. Low Temperature Physics, University of Toronto, Canada, pp.45–48 (1960).

The oxide films formed on copper single crystal surfaces in water II. Rate of growth at room temperature, J. Kruger, J. Electrochem. Soc. **108,** No. 6, 503 (June 1961).

A review of the hydraulics of circular sewers in accordance with the Manning formula, R. S. Wyly, Yearbook of Am. Soc. of Sanitary Engineering **38,** 154 (1960).

Line shape of ultraviolet absorption in solid noble gases, P. H. E. Meijer, J. Chem. Phys. **34,** 2078–2082 (1961).

Non-reciprocity and time-reversal in microwave circuits, H. A. Fowler, Academie royale de Belgique (Classe Des Sciences) **V–46,** No. 11, 963–977 (Dec. 1960).

A screening method for large information retrieval systems, R. T. Moore, Proc. Western Joint IRE-AIEE-ACM Computer Conf., Los Angeles, Calif. 6.3, 259–274 (1961).

Tchebycheff approximations by $ab^x+c$, J. R. Rice, J. Soc. Ind. Appl. Math. **8,** No. 4, 691–702 (1960).

Ionospheric "forward" scattering, D. K. Bailey, Proc. XIIIth Gen. Assembly of URSI (London, England, 1960), Natl. Acad. Sci.-Natl. Research Council Publ. Report No. 880, 281 (1961).

Apparatus for controlled slack quenching, N. L. Carwile, M. R. Meyerson, and S. J. Rosenberg, Materials Research and Standards (ASTM Bull.) **1,** No. 7, 532–536 (July 1961).

Exponential temperature dependence of Young's modulus for several oxides, J. B. Watchman, Jr., W. E. Tefft, D. G. Lam, Jr., and C. S. Apstein, Phys. Rev. **122,** 1754 (June 1961).

Electron spin resonance spectra of free-radical intermediates formed by reaction of polystyrene with atoms of hydrogen and deuterium, R. B. Ingalls and L. A. Wall, J. Chem. Phys. **35,** No. 1, 370–371 (July 1961).

The X- or gamma-ray energy absorption of transfer coefficient: Tabulations and discussion, R. T. Berger, Radiation Research **15,** No. 1, 1-29 (July 1961).

Reinhart, F. M., Twenty-year atmospheric corrosion investigation of zinc-coated and uncoated wire and wire products, Am. Soc. Testing Materials Spec. Tech. Publ. **290,** 1–141 (June 1961).

Time standards, A. G. McNish, Instr. and Control Systems **33,** 1340–1341 (Aug. 1960).

Adsorption of nitrogen and argon on mineralogical graphite and diamond at 77 and 90 °K, J. de Dios Lopez-Gonzalez, F. G. Carpenter, and V. R. Deitz, J. Phys. Chem **65,** No. 7, 1112–19 (July 1961).

Absorption of carbon dioxide by solutions of 2-amino-2-(hydroxymethyl)-1, 3-propanediol, R. G. Bates and H. B. Hetzer, Anal. Chem. **33,** No. 9, 1285 (Aug. 1961).

Stress-strain relationships in yarns subjected to rapid impact loading; Part 7. Stress-strain curves and breaking-energy data for textile yarns, J. C. Smith, P. J. Shouse, J. M. Blandford, and K. M. Towne, Textile Research J. **31,** No. 8, 721–734 (Aug. 1961).

V. Mutual interference between surfaces and satellite communication systems, B. Hartman, M. T. Decker, Chapt. 5, p. 111–157, Book, Frequency Allocations for Space Communications (Report of the Joint Tech. Adv. Comm. of IRE–EIA to the Federal Communications Commission, (Mar. 1961).

Quantum theory of interference effects in the mixing of light from phase-independent sources, U. Fano, Am. J. Phys. **29,** No. 8, 539–545 (August 1961).

Heats and volumes of mixing in several $C_{12}$ hydrocarbon systems, R. S. Jessup and C. L. Stanley, J. Chem. Eng. Data **6,** No. 3, 368–371 (July 1961).

Some observations of copper deposits on single crystals of copper, I. Giron and F. Ogburn, J. Electrochem. Soc. **108,** No. 9, 842–846 (Sept. 1961).

Binary oxide systems, H. R. Hoekstra and H. S. Parker, Chapt. 6, Sect. 6, p. 271–304, Book, $UO_2$, Properties and Nuclear Applications (U.S. Superintendent of Documents, Government Printing Office, Washington 25, D.C., Aug. 1961).

Wind resistance of asphalt shingle roofing, W. C. Cullen, Natl. Acad. Sci.-Natl. Research Council, 33–42 (1961).

Spectroscopic observations of the stratosphere and mesosphere D. M. Gates, Instr. Soc. Am. J. Conf. Preprint No. 2–NY60 (Sept. 1960).

Supercooling in the barnyard, C. P. Saylor, Capital Chemist **10,** No. 9, 292–293 (Dec. 1960).

Low-angle X-ray diffraction of crystalline nonoriented polyethylene and its relation to crystallization mechanisms, L. Mandelkern, A. S. Posner, A. F. Diorio, and D. E. Roberts, J. Appl. Phys. **32,** No. 8, 1509–1517 (Aug. 1961).

References to contemporary papers on acoustics, W. Koidan, Acoust. Soc. Am. **33,** No. 5, 705–716 (May 1961).

**Publications for which a price is indicated (except for Technical Notes) are available only from the Superintendent of Documents, U.S. Government Printing Office, Washington 25, D.C. (foreign postage, one-fourth additional). Technical Notes are available only from the Office of Technical Services, U.S. Department of Commerce, Washington 25, D.C. (Order by PB number.) Reprints from outside journals and the NBS Journal of Research may often be obtained directly from the authors.*



U.S. GOVERNMENT PRINTING OFFICE: 1962

UNIVERSITY MICROFILMS INC
EDITORIAL DEPARTMENT
313 NORTH FIRST ST
ANN ARBOR MICH
S.IR-C JUNE

UNITED STATES
GOVERNMENT PRINTING
DIVISION OF PUBLIC DOCU
WASHINGTON 25, D
OFFICIAL BUSINESS

NALTY FOR PRIVATE USE TO AVOID
PAYMENT OF POSTAGE, $300
(GPO)

JOURNAL OF RESEARCH of the National Bureau of Standards Vol. 66C, No. 1 January–March 1962
C. Engineering and Instrumentation

# Contents

| | Page |
|---|---|
| Reference tables for 40 percent iridium-60 percent rhodium versus iridium thermocouples. G. F. Blackburn and F. R. Caldwell. | 1 |
| A method for the self-calibration of attenuation-measuring systems. Robert L. Peck. | 13 |
| Special shielded resistor for high-voltage d-c measurements. J. H. Parks. | 19 |
| Voltage ratio measurements with a transformer capacitance bridge. Thomas L. Zapf. | 25 |
| Weight calibration schemes for two knife-edge direct-reading balances. H. E. Almer, L. B. Macurdy, H. S. Peiser, and E. A. Weck. | 33 |
| Tunnel diode large-signal equivalent circuit study and the solutions of its nonlinear differential equations. Sidney B. Geller and Paul A. Mantek. | 45 |
| A missile technique for the study of detonation waves. Fillmer W. Ruegg and William W. Dorsey. | 51 |
| Creep of cold-drawn nickel, copper, 70 percent nickel-30 percent copper, and 30 percent nickel-70 percent copper alloys. William D. Jenkins and William A. Willard. | 59 |
| Publications of the National Bureau of Standards. | 77 |

For sale by the Superintendent of Documents, U.S. Government Printing Office, Washington 25, D.C. Price 75 cents (single copy)
Subscription price: $2.25 a year; 50 cents additional for foreign mailing.
UNITED STATES GOVERNMENT PRINTING OFFICE, WASHINGTON : 1962